Dielectric and ultrasonic studies of polyethylene plaques and cable insulation

Fanggao, Chang

Award date:
1996

Awarding institution:
University of Bath

DIELECTRIC AND ULTRASONIC STUDIES OF POLYETHYLENE PLAQUES AND CABLE INSULATION

Submitted by Chang Fanggao
for the degree of PhD of the University of Bath
1996

COPYRIGHT

ProQuest LLC
789 East Eisenhower Parkway
P.O. Box 1346
Ann Arbor, MI 48106-1346

ACKNOWLEDGEMENTS

I would like to extend my thanks to all those who have helped me in the course of this work. In particular to Professor G. A. Saunders, without whose patient supervision and encouragement the production of this thesis would not have been possible. I would also like to thank BICC Cables Ltd. and National Grid Company for their financial support of this project, and Dr. R. N. Hampton, Dr. S. M. Moody and Ms M. Clarke of these companies for many instructive discussions during the period of this study.

I am indebted to the technical staff of School of Physics of Bath University for the assembly and maintenance of the equipment used in this work. Especially Mr. E. F. Lambson for constructing the transducers and much of the ultrasonic apparatus, Mrs. W. A. Lambson for cutting and polishing the samples and Mr. R. C. J. Draper for solving many technical problems. I am very grateful to all the research colleagues in the solid state group for many useful discussions and the harmonious atmosphere which makes the laboratory life so enjoyable.

I am especially indebted to my family for their understanding and continuous support which have encouraged me all the way through the course of this study.

ABSTRACT

The complex dielectric constants of crosslinked polyethylene plaques and cable insulations have been measured as functions of frequency, temperature and hydrostatic pressure. In addition, the elastic, anelastic and non-linear acoustic properties of thermoplastic and crosslinked polyethylenes as well as cable insulations have been obtained by measuring the temperature and pressure dependencies of the velocities and attenuation of 5 MHz longitudinal and shear ultrasonic waves propagated in these polymers. Analysis of the dielectric data evidences some impurities in the polyethylene samples, which result in the observed non-zero temperature and pressure derivatives of the polarizability. Both dielectric and ultrasonic measurements indicate that power cable insulations are not homogenous across the cable diameter. An extremely large temperature dependence of the longitudinal wave velocity $-(\partial V_L/\partial T)$ has been observed in the temperature range between the melting and glass transitions. This ultrasonic behaviour has been discussed in terms of the multiple scattering theory. The attenuation of longitudinal ultrasonic waves propagated in polyethylene is proportional to the temperature derivative of the ultrasonic wave velocity, which is consistent with a hysteresis absorption mechanism. The Arrhenius plot for the low frequency Dynamic Mechanical Thermal Analysis (DMTA) and ultrasonic data indicates that the relaxation processes can be described well by the Arrhenius relation over a frequency range from 1Hz to 5MHz. The longitudinal stiffness modulus C_L of polyethylene increases non-linearly with hydrostatic pressure. The dielectric and ultrasonic results, together with those obtained from DMTA measurements, have been used to investigate the electrical breakdown mechanism of these polyethylenes; the results are consistent with an electromechanical or an electronic breakdown following a local increase of temperature due to Joule heating at impurities as likely physical processes responsible for the a.c. breakdown strength of polyethylene.

CONTENTS

CHAPTER 1. INTRODUCTION

The electrical properties of cross-linked polyethylene, which is used as the insulation in some high voltage cables, are determined by its defect structure and interatomic binding forces. Although cross-linked polyethylenes are of great commercial importance, details of the processes involved in electrical conduction and breakdown remain uncertain. High frequency ultrasonic velocity and attenuation measurements provide a novel way of determining features of the structure and binding, which is achieved by characterising the mechanical properties, how they vary with temperature and under high pressure and how they differ between polyethylenes from diverse sources. The main purpose of the present work is to investigate the temperature and hydrostatic pressure dependences of the viscoelastic and dielectric properties of crosslinked polyethylene as well as cable insulations, and to develop a deeper understanding of the electrical breakdown behaviour and its relation to structural defects and impurities introduced into polyethylenes during production and treatment processes involved in cable manufacture.

A common feature of structure of polymers is that they are made of long molecular chains of covalently bonded atoms held together by weak van der Waals forces. Many polymers when cooled from the molten state form a disordered structure called the amorphous state in which the chains are arranged randomly. Polyethylene is semicrystalline: it contains both amorphous and crystalline regions. Many of the unusual and interesting properties of polyethylene arise from this complex structure. When the melt is cooled down it becomes more viscous; when the temperature has been reduced far enough, the material becomes rubbery and then eventually relatively hard. The glass transition temperature T_g is that at which the transformation from the rubbery to the harder phase takes place. A description of the general structure of polyethylene is given in Chapter 2, which also introduces a few elementary ideas associated with the present work.

One of the main objectives of the experimental work is to measure the longitudinal and shear ultrasonic wave velocities and attenuation as a function of temperature and pressure in polyethylenes including practical cable insulations. The experimental results

obtained provide extensive knowledge for polyethylenes of their technical properties, elastic stiffness, bulk modulus, anelastic and non-linear acoustic properties. Viscoelasticity is very important in describing the mechanical behaviour of polymers. Although it differs from classical elastic theory in a number of aspects, the main parameters characterizing the viscoelastic behaviour of polymers are still the elastic moduli and Poisson's ratio (Perepechko 1980). To study the viscoelastic properties using ultrasonic techniques, it is essential to establish the relationship between the elastic constants and the velocities of the ultrasonic waves propagated in the solid. Chapter 3 is concerned with the acoustical properties of polymers, with special regard to polyethylene. The acoustic investigations of polyethylene reported in the literature, the basic concepts of linear viscoelasticity, and three models which are normally used to describe the linear viscoelasticity, are reviewed. The effects of viscosity on the acoustic and elastic behaviour of polymers will be discussed in detail. The most commonly used technological elastic constants are related to the more general forms of these constants, which can be determined from measurements of velocities of acoustic waves propagated in the material.

In practice, epecially in the commercial cable industry, the fundamental electrical properties of polyethylene that need to be understood are the conductivity and the dielectric constant and how their behaviour with temperature and pressure relate to the structural, elastic and breakdown properties. An important part of the present work is to measure the temperature and pressure dependences of the dielectric properties of polyethylene using a HP impedance analyzer and a Model DS2560RL Dielectrometer. Chapter 4 gives a full description of the experimental techniques and apparatus which has been designed and constructed for this work. To test the measurement system and establish its reliability, the dielectric properties as a function of temperature and hydrostatic pressure, of poly(ethylene oxide) (PEO), a well studied semi-crystalline polymer, have been measured. However, the results obtained of the temperature and frequency dependences of the complex dielectric constant of PEO under hydrostatic pressure turned out to provide new understanding of the dielectric behaviour of this polymer. This new work is discussed in Chapter 5.

Chapter 6 presents the results of dielectric measurements on crosslinked polyethylene plaque samples as well as cable insulations. These results are analysed in terms of the macroscopic Clausius-Mossotti equation, providing experimental details of the effects of pressure and temperature on the dielectric constant and conductivity of polyethylene. The concentration of impurities in different polyethylenes is characterized by the temperature and pressure derivatives of the polarizability of each sample. One of the valuable features of making measurements as a function of pressure is that its application must have a dramatic effect on the free volume, the space which is not occupied by polymer molecules: the empty space between them. It has often been suggested that the electrical properties in polyethylene must be determined by the ability of charge carriers to hop across this intermolecular space. Breakdown itself must be associated with that space. It is obvious that measurements of the electrical properties under pressure should provide valuable insight into the problems associated with dielectric breakdown and conductivity in polyethylene.

A polymer manufactured by an industrial technique involving extrusion or a similar process could be anisotropic - this can be, and needs to be, assessed by measuring the dielectric constant and ultrasonic wave velocity and attenuation across and in the plane of manufacture. Cable insulations are expected to have a cylindrical symmetry which is likely to affect their electrical breakdown behaviour. For this purpose, efforts have been made to study the distribution of the complex dielectric constant and that of ultrasonic wave velocity across the cable section.

Because the network structure formed by crosslinking still exists above the crystalline melting point, crosslinked polyethylene has been widely used in making power cables which can operate at high temperatures. With the knowledge of the temperature and pressure dependences of the velocity and attenuation of ultrasonic waves propagated in crosslinked and thermoplastic polyethylene, the effects of crosslinking on the density, crystallinity, elastic constants and electrical breakdown strength can be studied. Comparing the ultrasonic results measured on samples crosslinked using different methods, the effects arising from different crosslinking mechanisms can be investigated.

An understanding of the way in which polyethylene changes its structure and elastic, anelastic and electrical properties as it is taken through T_g to the melting temperature region is of central importance because the amorphous region is crucial to breakdown strength. The onset of the glass transition of the amorphous materials at T_g is accompanied by a sharp change in the compressibility (or bulk modulus B), the heat capacity and thermal expansion coefficient. Therefore, the changes of structure, elastic and electrical properties at the glass transition, and other relaxation processes, are expected to have effects on polyethylene during application. The ultrasonic wave velocity and attenuation in polyethylene can be measured as a function of temperature right through the glass transition up to the melting point, which enables the elastic constants to be determined in this temperature region. The attenuation peaks occurring in this temperature range can be used to calculate the activation energy of the corresponding relaxation process, which provides useful information about the molecular motion in the polymer.

Ultrasonic wave velocity and attenuation measurements in polyethylene under hydrostatic pressure should provide much more information about the physics of the glass transition in polymers. Such measurements made as a function of temperature and pressure would make it possible to test the various models proposed for the mechanism of the glass transition and its effect on the structure of the amorphous region of polyethylene. It is believed that hydrostatic pressure has a considerable effect on the electrical conduction and electrical breakdown of low density polyethylene. To correlate the mechanical relaxation processes to the thermal and electrical properties of polyethylene, it is important to distinguish the effects arising from the amorphous materials and those from crystalline materials in the polymer. A convenient way to do this is to study the ultrasonic velocity and attenuation behaviour of polyethylene under pressure because the amorphous component in polyethylene is much more compressible than the crystalline phase. The non-linear acoustic and mechanical properties can then be studied. Because there is a large free volume in polyethylene at room temperature, its mechanical and electrical properties at very high pressure should

be quite different from those at atmospheric pressure. Chapter 7 presents and discusses the results obtained from the ultrasonic measurements.

The dynamic mechanical method assesses the mechanical properties of solids and viscoelastic liquids in terms of their dynamic moduli and damping. In particular, changes in these parameters can be studied as a function of temperature (Dynamic Mechanical Thermal Analysis-DMTA) and applied frequency. To enable a comparison between the ultrasonic behaviour and that observed at a much lower frequency, use has been made of the DMTA data, obtained from BICC workers, of two thermoplastic polyethylenes, which also lead to a calculation of the activation energies for the relaxation processes in these two polyethylenes. Characteristics found for the DMTA results are interlinked with those from the ultrasonic data in Chapter 8.

The central objective of the present work is to correlate the mechanical and dielectric properties of polyethylene to its electrical breakdown behaviour. It is generally observed that increasing the density of polyethylene improves the breakdown strength. The structural influence of increasing density is to increase the crystallinity and to decrease the amorphous content. Treeing is known to follow the inter-lamellae paths. A positive correlation also exists between Young's modulus and breakdown strength. Either increased Young's modulus, that is elastic stiffness, increases breakdown strength or, more likely, whatever increases Young's modulus also increases breakdown strength. Using a theoretical model, the electromechanical breakdown strength of polyethylene plaques and cable insulations have been estimated from the Young's moduli obtained from ultrasonic and DMTA measurements. In chapter 9, these results are compared with the a.c. breakdown data measured at 50 Hz at BICC and three electromechanical breakdown mechanisms are tested using the Young's modulus data. The local Joule heating at inclusions of dipolar impurities may be important in a.c. breakdown testing. The average rate of Joule heating is related to the frequency, dielectric loss and constant, as well as the concentration of the impurities. The correlation between the breakdown strength and the dielectric behaviour of polyethylene is also discussed in Chapter 9.

The last chapter, Chapter 10, serves as a summary of the whole thesis and the main conclusions drawn from the current study are presented.

CHAPTER 2. THE STRUCTURE OF POLYETHYLENE

2.1. Introduction

Common features of the structure of polymeric materials are long molecular chains of covalently bonded atoms, held together by relatively weak secondary van der Waals forces. Each polymer chain is made from a basic building block called a monomer whose structure is repeated many times in the chain. The average molecular weight of a polymer can be as high as 10^6 a.m.u. (Atomic mass unit) depending on the manufacturing process.

Many polymers, when cooled from the molten state, form a disordered structure, which is termed the amorphous state. Amorphous polymers are usually considered to be made of a random arrangement of molecules. Polymethylmethacrylate (PMMA) and ethylene propylene hexadiene terpolymer (EPDM) are examples of amorphous polymers. Some polymers, on the other hand, form crystalline structures as well as amorphous phases when they are cooled slowly from the melt. Polyethylene contains both amorphous and crystalline regions and so is sometimes referred to as being semi-crystalline. The mechanical properties of crystalline polymers are strongly affected by their crystallinity.

In addition to the molecular weight and its distribution, small variations in molecular structure, such as short chain branching and crosslinking, may improve or impair the thermal and mechanical properties of polymers considerably. Hindered rotation around the many single bonds in the chain structure can result in a relaxation process. This chapter is designed to give a brief review about the structure and some of the related properties of polyethylene in general.

2.2. Average molecular weight and molecular weight distribution

Polyethylene is, in principle at least, one of the simplest polymers, consisting of long chains of the $-CH_2$ repeat unit. It is an addition polymer, which is made by polymerizing the monomer ethylene $CH_2=CH_2$ to form the long chain polyethylene

$$[\text{-CH}_2\text{-CH}_2]_n.$$

In general, a polyethylene sample consists of molecular chains of varying lengths and can be normally described in terms of different types of average molecular weight: the number average $\overline{M}_n$ and the weight average $\overline{M}_w$ which can be determined respectively, by osmotic pressure and light-scattering measurements on dilute solutions of the polymers. The definitions are given by

$$\overline{M}_n = \frac{\sum N_i M_i}{\sum N_i} \quad \text{and} \quad \overline{M}_w = \frac{\sum (N_i M_i) M_i}{\sum N_i M_i} \tag{2.1}$$

where N_i is the number of molecules of molecular weight M_i and the summation is over all i molecular weights.

The most common commercial grades of polyethylene have a number average molecular weights of the order of 10,000-40,000 (corresponding to values of weight average molecular weight in the range 50,000-300,000).

The molecular weight distribution is important in determining flow properties. It may therefore affect the mechanical properties of a solid polymer indirectly by influencing the final physical state. Direct correlations of molecular weight to viscoelastic behaviour and brittle strength have also been obtained, and this is a developing area in polymer science.

2.3. Conformations of hydrocarbons

The term conformation refers to different three-dimensional spatial arrangements of molecules, which are altered by rotation about single bonds and do not involve any bond breaking to change them. In saturated hydrocarbon polymers, the carbon atoms are sp^3 hybridized and the angles between the C-C bonds are fixed normally at 109.5° degree. The lowest-energy chain conformation of polymers can be evaluated from considerations of the conformations of the n-butane molecule. As can be seen in Figure 2.1, the most favoured comformation for n-butane at normal temperatures is the so-called *trans* position but the *gauche* comformations, which have an energy of about

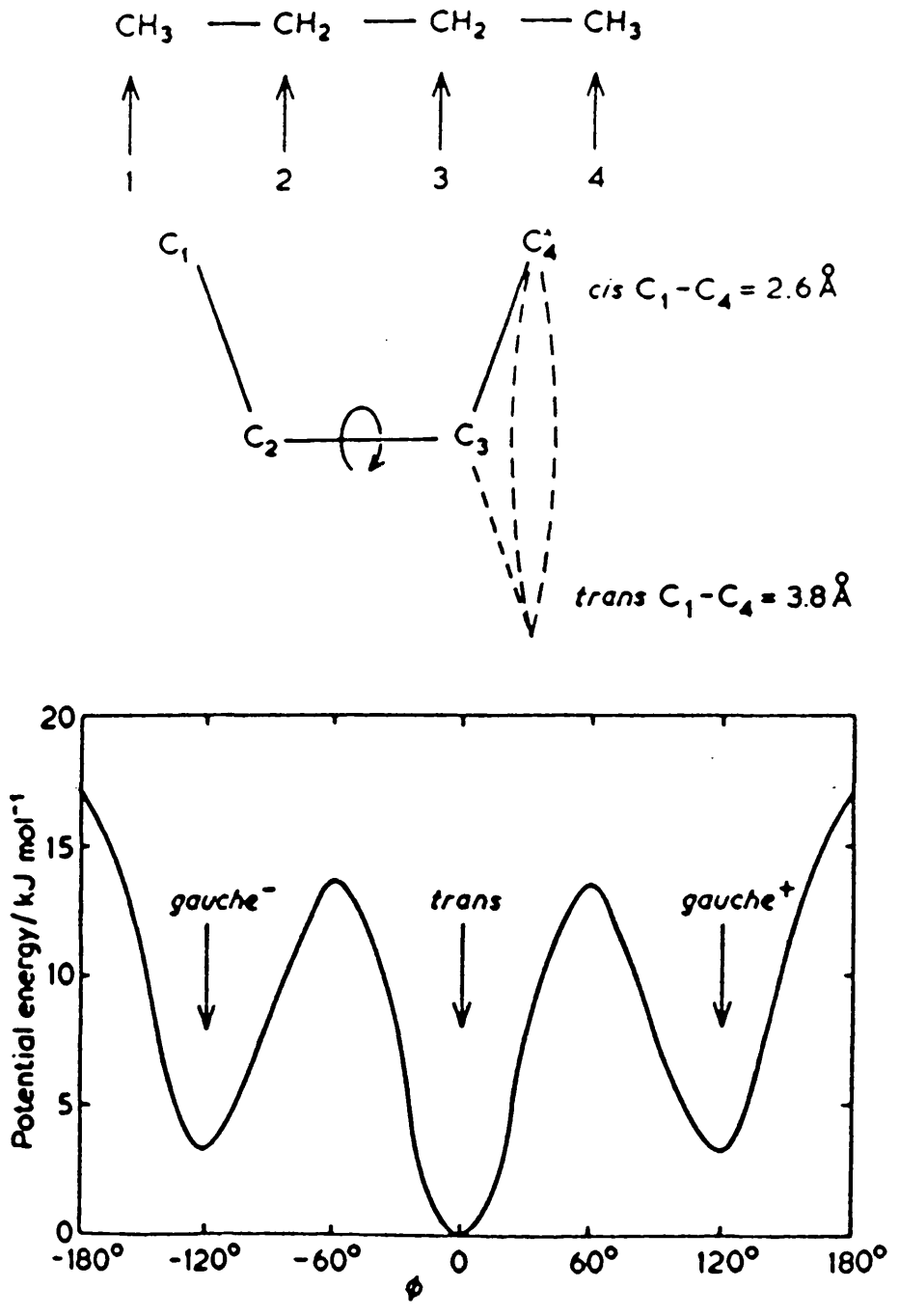

Figure 2.1 The different conformations of the n-butane molecule (upper) and the energy corresponding to these conformations as a function of ϕ (lower).

3.3kJ/mole higher than the *trans* position, are also found. Any other conformations are highly unlikely.

A series of all *trans* bonds produces the lowest-energy conformation in n-butane because of steric interactions; this can be extended to polyethylene where the most stable molecular conformation is the one with all *trans* bonds, i.e. the planar zig-zag. For bulk polyethylene at normal temperatures, however, there must be some *gauche* conformations present in the chains. To pass from one rotational isomeric form to another requires that an energy barrier be surmounted and this may give rise to a relaxation process at certain temperatures and frequencies.

2.4. Crystallinity

The most stable crystal structure of polyethylene is orthorhombic with a density ρ_c=997.2 Kg/m. A monoclinic structure ρ_c = 998.0 kg/m can also be formed by mechanical deformation of orthorhombic polyethylene. The two structures only differ in the way the molecules are packed in the unit cell. Single crystals of polyethylene are very small and bulk polyethylenes normally used commercially are all semicrystalline materials with various degrees of crystallinity. The degree of crystallinity is of great technological and practical importance. It can be defined as

$$\chi_c = W_c / W = \frac{\rho_c}{\rho}\left[\frac{\rho - \rho_a}{\rho_c - \rho_a}\right] \qquad (2.2)$$

where W is the mass of the sample, W_c the mass of crystalline material in the sample, ρ the density; the subscripts *c* and *a* represent the crystalline and amorphous states. For calculating the degree of crystallinity, the densities of the amorphous and crystalline phases can be taken as 855 and 1000 Kg/m^3 respectively.

2.5. Crosslinking

In general, crosslinking of a crystalline thermoplastic polymer has two distinct effects. Firstly, it interferes with the molecular packing, thereby reducing the level of crystallisation and consequently reducing the elastic modulus. The other effect is that it

produces permanent crosslinks between different chains and therefore increases the stiffness or the elastic modulus of the polymer. Hence, the mechanical properties of crosslinked crystalline polymers, such as polyethylene, can be very variable, depending mainly on the density of the crosslinks and the temperature of measurement. More importantly, because the network structure formed by crosslinking still exists above the crystalline melting point, crosslinked polyethylene has been used to make power cables, capable of resisting high temperatures.

Three main approaches are used for crosslinking polyethylene:

(1) Peroxide crosslinking;

(2) Radiation crosslinking;

(3) Vinyl silane crosslinking.

Peroxide methods are the most commonly used for crosslinking polyethylene. Peroxide-containing resins and compounds are extruded using conventional extruders at temperatures below that of the decomposition point of peroxide. Following extrusion onto the conductor, the compound is exposed in a continuous vulcanizer to high pressure steam. The high temperature causes the peroxide to decompose into reactive free radicals and pressure is required to prevent void formation. The peroxide-generated radicals react with the polyethylene by extracting a hydrogen atom from the polymer. This reaction forms a radical on the polymer chain, which in turn reacts with another polymer chain radical to form a crosslink.

The chemistry of radiation crosslinking is similar to that of the peroxide methods, except that high energy electrons, rather than peroxides, are used to extract hydrogen atoms from the carbon chain and generate the free radicals. After hydrogen extraction, the polymer radicals combine in the same manner to produce the crosslinked material. However, radiation is performed at ambient temperature and the most useful crosslinks occur in the amorphous regions of the polymer. Consequently, some subtle differences may be detected between radiation and peroxide crosslinked materials, where the latter are totally amorphous during the crosslinking step (Barlow 1991).

The vinyl silane crosslinking is sometimes called the "MONOSIL" method. The first stage of this crosslinking process involves the grafting of an easily hydrolysable vinyl silane onto the polyethylene chain, the site activation having been achieved with the aid of a small amount of peroxide. The compound is then extruded onto the conductor and the resulting product is exposed to hot water, which then hydrolyses the alkoxy groups to form a siloxane crosslink. The crosslinking reaction process is shown in Figure 2.2. The crosslinks made by vinyl silane crosslinking are different from those produced by radiation and peroxide methods with which permanent links are formed between carbon atoms. The long crosslinking bridge between the chains, made by the vinyl silane crosslinking, may affect the mechanical properties of the crosslinked polyethylene.

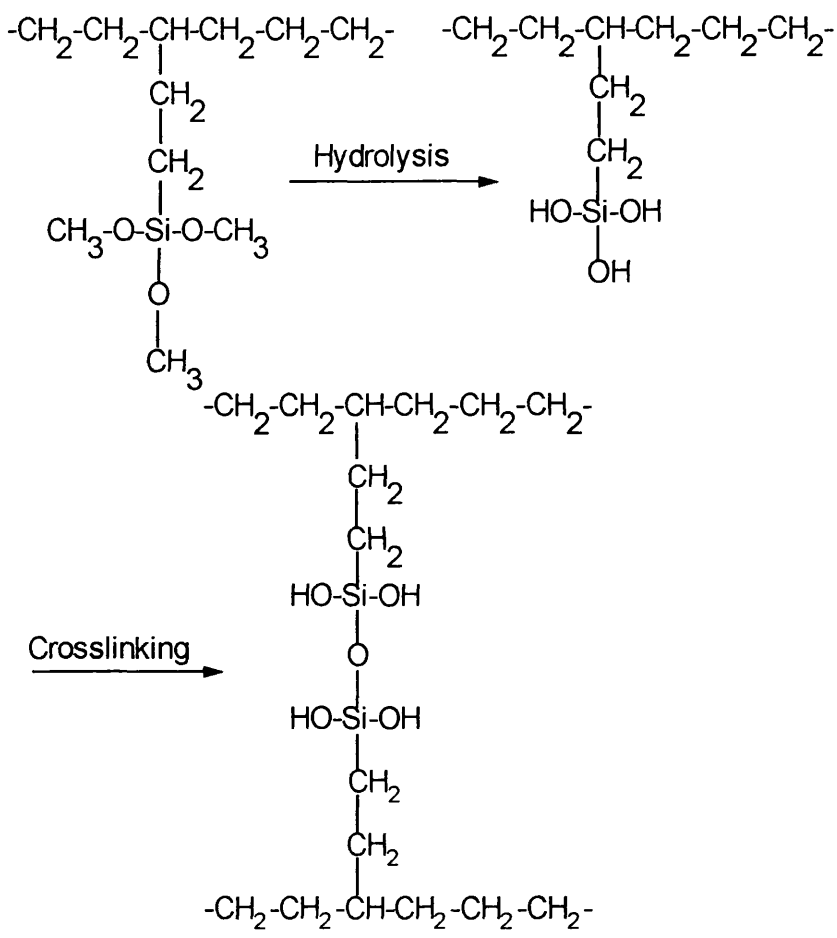

Figure 2.2 Simplified vinyl silane crosslinking mechanism.

CHAPTER 3. ACOUSTIC PROPERTIES OF POLYMERS

3.1. Introduction

Acoustic methods have long been used to determine the elastic and anelastic properties of solids. This approach has been extended to viscoelastic materials such as polymers, although they have quite different mechanical behaviour from those of normal elastic solids. In general other workers tend to apply the formulae established for the calculation of elastic constants from sound velocities for elastic materials to polymers without examining the effects of viscous damping and attenuation. Earlier acoustic studies on polymers, with polyethylene as the specific example, are first reviewed here in section 3.2. This is followed by a brief description of three mechanical models for linear viscoelastic materials. The effects of viscosity, based on the Voigt or Kelvin model, are discussed in detail in section 3.4. This discussion is restricted to solid isotropic polymers, because almost all of the bulk polymers are either amorphous or polycrystalline with random orientation.

3.2. Review of the acoustic investigations of polyethylene

Polyethylene (PE) was first discovered in the United Kingdom in 1939. Since then, it has been studied extensively by scientists from various disciplines. One reason for this is that polyethylene is one of the most widely used polymers in both industry and everyday life. From a scientific viewpoint, it has been of interest to physicists and chemists because of its relatively simple chemical structure as well as the wide range of well characterised samples which are available for study. A great deal of effort has been made to measure its mechanical properties. For technical design work, one needs to know the elastic and inelastic properties as a function of temperature, pressure and frequency.

Despite a number of acoustic investigations on polyethylene during the last forty years, the results and interpretation are far from complete. Polyethylene was examined by a dynamic method at low frequencies (a few Hz) by Schmieder and Wolf (1953), who determined the torsion modulus and damping for a wide range of temperatures. The

damping curve exhibits three peaks at -107°C, -5°C and 54°C. Sauer and Kline (1955), working in the frequency range of 200-2000Hz, obtained a rather flat plot of the resonance frequency versus temperature, without observing any sharp transition region. The measurements were soon extended to the ultrasonic range by Baccaredda and Butta (1956). Schuyer (1959) measured the sound velocity of polyethylene at 2 MHz using a pulse technique, with an accuracy of 1%. He established theoretically a relationship between the temperature coefficient of the longitudinal sound velocity V_L and the density ρ of polymers:

$$\frac{1}{V_L}\frac{dV_L}{dT} = \frac{A}{\rho}\frac{d\rho}{dT} - \frac{1}{(1-\sigma^2)}\frac{d\sigma}{dT} \tag{3.1}$$

which reduces to the Rama Rao (1940) empirical relationship:

$$\frac{1}{V_L}\frac{dV_L}{dT} = \frac{A}{\rho}\frac{d\rho}{dT} \tag{3.2}$$

if one assumes that the Poisson's ratio σ does not change with temperature. He found that the experimental results agree well with theory. A quite opposite result was obtained by Davidse et al (1962). They measured the sound velocity using a technique in which 2.7-10.9KHz longitudinal oscillations were generated electrodynamically in a thin bar specimen. Instead of an approximately cubic relation between sound velocity and density, suggested by Schuyer, they concluded that the variation of longitudinal wave velocity with density is a linear function. Later, the propagation constants of 12 MHz ultrasonic waves in melting and molten high density polyethylene were obtained (Eby 1964). Maxima in the internal friction were observed at -52°C, 60°C and 100-130°C. In an attempt to clarify the confusion in the velocity-density relationship, an ultrasonic interferometer was used by Levene, Pullen and Roberts (1965) to measure the velocity of 1.45 MHz longitudinal waves in polyethylene at 20°C. However, a plot of sound velocity against density does not show conclusively that the relationship is either linear or cubic. In 1966, Arnold and Guenther measured the velocity of longitudinal waves propagated in both high and low density polyethylene. The ultrasonic frequencies used were between 1 and 10 MHz and the temperature range covered was between room temperature and 100°C. Their results show a linear velocity-temperature relationship for the high density (964Kg/m^3) polyethylene and there seems to be a transition between 40-50°C in the low density (916Kg/m^3) sample.

It is difficult to derive a velocity-density relation from their results, but the data do show disagreements with the linear function suggested by Davidse et al (1962). Arnold and Guenther then argued that the velocity measured in a thin rod by Davidse et al could not be compared with the bulk longitudinal wave velocity that they obtained. The temperature dependences of the 1MHz shear wave velocity for the same high and low density samples of polyethylene have been reported (James and Guenther 1967). In addition to a linear velocity-temperature relationship, a large difference in velocity (by a factor of 2), corresponding to a density change of about 5%, was found.

Although there had been several investigations on the absorption of ultrasound in polyethylene (Waterman 1963, Eby 1964, Crissman et al. 1964 and Krupskaya 1968), the first systematic study of sound absorption in polymers at ultrasonic frequencies was reported by Hartmann and Jarzynski (1972). Ultrasonic absorption measurements were made in polyethylene and also in PMMA and polyethylene oxide (PEO) as a function of frequency, temperature and strain. The temperature range was from room temperature to about 130°C. The mechanism responsible for the hysteretical absorption in polymers was postulated to be the trapping of the polymer in one of many local metastable potential-energy minima. This mechanism led to the prediction that the absorption should be a linearly decreasing function of volume. Folds (1972) measured the longitudinal sound wave velocity of 16 plastics, including a low- and a high-density polyethylene, two low-sound-velocity elastomers, and three types of syntactic foam at a frequency of 500 kHz in a temperature range of 0-30°C. A very good correlation between attenuation and the thermal coefficient of the sound velocity was observed in these measurements. Further ultrasonic attenuation measurements on polyethylene were reported over a frequency range of 0.1 to 1 GHz by North, Pethrick and Phillips (1977). Attenuation in polyethylene at 233 and 296K was found to be proportional to the square of the frequency and this behaviour was ascribed to scattering by domains (crystallites) of different modulus.

Early ultrasonic work on polyethylene was focused mainly on high temperature properties. It was not until 1972 that the first low temperature, (down to helium temperatures), ultrasonic study on a high density polyethylene was reported by

Perepechko and Sorokin (1972, 1973). Using the pulse-phase method, they measured the velocities of 1-5 MHz longitudinal and shear waves in polyethylene from 4.2 to 240K. Transitions at 120K and 180K were observed in the temperature dependence of the velocity of longitudinal waves. The velocity levelled off and became temperature independent below 120K. These transitions shifted to 90K and 170K respectively for the shear wave. Considering the low temperature behaviour of polyethylene, the results obtained by Perepechko and Sorokin contrast with the low frequency (1 to 3 Hz) torsion pendulum measurements of Papir and Baer (1971) in which two loss peaks were observed at 48K and 20K, indicating that polyethylene is not viscoelstically inactive at helium temperatures (as suggested by Perepechko and Sorokin).

Measurement of the velocity of both longitudinal and shear waves enables one to calculate the elastic constants. The bulk, shear and Young's moduli, as well as the Poisson's ratio, of a high density polyethylene at room temperature were obtained by Hartmann and Jarzynski (1974). A more systematic ultrasonic study of polyethylene was reported by Adachi et al (1981). They measured the longitudinal wave velocity and attenuation of several polyethylene samples between 100 and 350K and found a kink at about 210K in the velocity curves as well as a corresponding attenuation peak. The temperature dependence of the longitudinal wave velocity outside the relaxation region was observed to be consistent with Schuyer's (1959) relation. On the other hand, a linear correlation of the velocity with density was also obtained for different polyethylene samples. Further evidence favouring the linear velocity and density relationship came from Pich's work (1984) in which a 3 MHz longitudinal wave velocity was determined as a function of density in 35 samples of polyethylene. It was suggested that the velocity of sound at 20°C was linearly related to density. In his recent work, the same author measured the specific volume, storage modulus and loss modulus by propagating 2.5 MHz ultrasonic waves in high and low density polyethylenes under a pressure of 225 bars (Pich, 1989). The temperature range was between 20-180°C and the heating rate is 2°C/min. The results show that Rao's law, equation (3.2), is correct, at least at high temperatures, where the samples are more or less liquid. To resolve the apparent contradiction of the velocity-density relationship, Pich analyzed theoretically longitudinal and shear wave velocities in polyethylene using

a model developed by Sornette (1989) and concluded that the propagation of sound in polyethylene is very sensitive to the microstructural geometry of the different phases. The velocity and the attenuation reflect the microscopic details of the structure and in certain circumstances the velocity and density relation may be approximately linear.

In the past three decades, the use of static high pressure measurements as a tool for studying the structure, morphology and properties of bulk polymers has led to a considerable advance in the understanding of the physics of these synthetic materials. Yet, surprisingly, ultrasonic measurements as a function of pressure, which is a non-destructive and very accurate technique, are seldom made in polymers.

From the brief review presented already, one can see that, although there are extensive ultrasonic studies on polyethylene in the polymer literature, there is only sparse systematic data available, especially at low temperatures and high pressures. Some ultrasonic studies only measured the velocity but not the attenuation, while in other the attenuation has been measured but not the velocity. Some measurements are of the velocity and attenuation of the longitudinal waves but not of the shear waves. Moreover, all the measurements were carried out with large temperature intervals and important effects could be missed in some temperature ranges.

3.3. The linear viscoelastic behaviour of polymers

According to Hooke's law for an ideal elastic solid, stress is always directly proportional to strain for small deformations but is independent of the rate of the strain. The mechanical behaviour of ideal viscous liquids, on the other hand, is normally described by Newton's law:

$$\sigma = \eta \frac{d\varepsilon}{dt} \qquad (3.3).$$

Here the stress σ is always proportional to the rate of strain, $d\varepsilon/dt$, but independent of the strain ε itself. Real materials have properties which are intermediate between those of an elastic solid and a viscous liquid. It is for this intermediate state of materials that the word "viscoelasticity" is used. Two main deviations of viscoelastic materials from ideal elastic solid can be distinguished. First, when a "finite" strain, which may be

referred to as "infinitesimal" in the case of ideal elastic solids, is imposed on a viscoelastic solid, a more complicated non-linear stress-strain relation is normally obtained instead of Hooke's law. Second, it is assumed in the Hooke's law that the strain occurs immediately on applying a load, and on releasing the load the material immediately returns to its original dimensions. Time does not enter into the stress-strain relationship and both of them are time independent. However, this elastic behaviour does not hold for viscoelastic materials such as polymers. Even in the assumed elastic region (infinitesimal strain), there are time-dependent processes (for example stress relaxation and creep) occurring, and these produce effects such as energy dissipation, and the mechanical damping of acoustic vibrations.

The relations between stress and strain and their time dependence are in general described by a "constitutive equation" (Ferry 1970). If strains and rate of strain are finite, the constitutive equation is non-linear and may be quite complicated. However, if they are infinitesimal, the constitutive equation is a simple linear function, which gives rise to the concept of "linear viscoelasticity". In a linear viscoelastic solid the ratio of stress and strain is a function of time or frequency alone but not of the stress and strain.

Polymers belong to that class of solids whose stress-strain behaviour should be described as viscoelastic. If one takes the standard Maxwell element as a model (Figure 3.1 (a)), the stress-strain relation for viscoelastic solids is deduced (Nielsen 1965):

$$\sigma = K\eta(1-e^{-E\varepsilon/K\eta}) \tag{3.4}$$

where σ is the stress, K is the rate of the strain, η is the viscosity of the polymer, E is the modulus, and ε is the strain. By expanding the exponential and ignoring the terms higher than first order, equation (3.4) reduces to the well-known relationship

$$\sigma = E\varepsilon \tag{3.5}$$

which assumes very low stress and strain levels. Thus, the mechanical performance of a linear viscoelastic material is describable by Hooke's law to a first approximation.

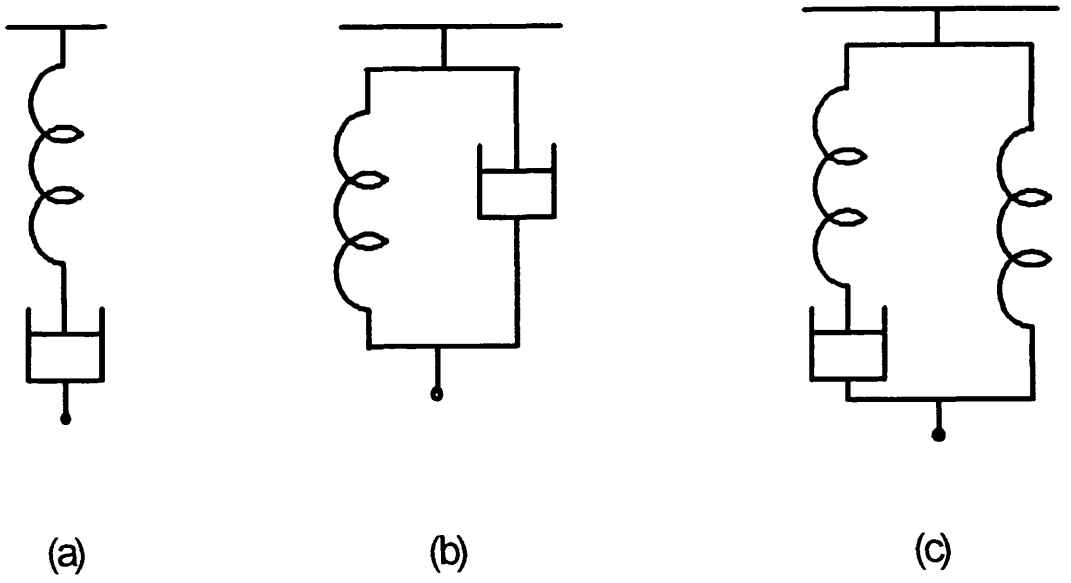

Figure 3.1 Spring and dashpot models of viscoelastic behaviour: (a) Maxwell; (b) Voigt and (c) Standard linear solid.

where

$$\sigma_1 = \sigma_{xx}, \sigma_2 = \sigma_{yy}, \sigma_3 = \sigma_{zz}$$

$$\sigma_4 = \sigma_{yz} = \sigma_{zy}$$

$$\sigma_5 = \sigma_{xz} = \sigma_{zx}$$

$$\sigma_6 = \sigma_{xy} = \sigma_{yx} \tag{3.11}$$

3.4.2. Strain

In an unstrained medium, one may establish a Cartesian coordinate system with position vector $\vec{r} = \vec{r}(x, y, z)$. When the material is strained, each point moves to a new position. For a general point with initial position vector $\vec{r}$, the position vector after deformation is given by

$$\vec{r'} = \vec{r} + \vec{u} \tag{3.12}$$

where $\vec{u}$ is the displacement vector which is a function of the original position vector $\vec{r}$ and time t. To measure the deformation of the material, strain is defined as

$$\varepsilon_{ij} = \frac{1}{2}\left(\frac{\partial u_i}{\partial r_j} + \frac{\partial u_j}{\partial r_i} + \frac{\partial u_k}{\partial r_i}\frac{\partial u_k}{\partial r_j}\right) \tag{3.13}$$

where $i,j,k = x,y,z$ and the summation over repeated subscripts is assumed.

For most rigid materials, the displacement gradient must be kept below the range 10^{-4} to 10^{-3} if permanent deformation or fracture is to be avoided. For displacement derivatives much smaller than this, the quadratic terms in equation (3.13) are negligible and a linear strain-displacement relation is obtained:

$$\varepsilon_{ij} = \frac{1}{2}\left(\frac{\partial u_i}{\partial r_j} + \frac{\partial u_j}{\partial r_i}\right) \tag{3.14}$$

with $i,j = x,y,z$. In some materials such as rubbers, however, displacement gradients greater than unity are easily achieved. Hence it is often necessary to use non-linear form strain (3.13) rather than the linear form (3.14) when dealing with rubber elasticity.

Typically, ultrasonic measurements are made in the strain range from 10^{-9} to 10^{-6} (Fava 1980). Hence, the linear strain-displacement relation, equation (3.14), can be used to describe the strain field generated by ultrasonic waves in polymers.

The strain [ε] is a symmetric second rank tensor in which only six of the nine components given by equation (3.14) are independent. Therefore instead of a nine-element square matrix, it may be written as a six-element column matrix:

$$\begin{bmatrix} \varepsilon_1 \\ \varepsilon_2 \\ \varepsilon_3 \\ \varepsilon_4 \\ \varepsilon_5 \\ \varepsilon_6 \end{bmatrix} \tag{3.15}$$

where

$$\varepsilon_1 = \varepsilon_{xx} = \frac{\partial u_x}{\partial x}$$

$$\varepsilon_2 = \varepsilon_{yy} = \frac{\partial u_y}{\partial y}$$

$$\varepsilon_3 = \varepsilon_{zz} = \frac{\partial u_z}{\partial z}$$

$$\varepsilon_4 = 2\varepsilon_{yz} = 2\varepsilon_{zy} = \frac{\partial u_y}{\partial z} + \frac{\partial u_z}{\partial y}$$

$$\varepsilon_5 = 2\varepsilon_{xz} = 2\varepsilon_{zx} = \frac{\partial u_x}{\partial z} + \frac{\partial u_z}{\partial x}$$

$$\varepsilon_6 = 2\varepsilon_{xy} = 2\varepsilon_{yx} = \frac{\partial u_x}{\partial y} + \frac{\partial u_y}{\partial x} \tag{3.16}$$

3.4.3. Hooke's law and the isotropic condition

The generalised form of Hooke's law may be written as

$$\sigma_I = c_{IJ}\varepsilon_J \tag{3.17}$$

where I,J = 1,2,3,4,5,6 and summation over the repeated subscripts is assumed. The c_{IJ} represent a fourth rank tensor, c_{ijkl}, whose components are called elastic or stiffness constants. The Voigt notation with

$$\begin{array}{cccccccc} I & (J) & 1 & 2 & 3 & 4 & 5 & 6 \\ ij & (kl) & xx & yy & zz & yz & xz & xy \end{array} \tag{3.18}$$

has been used here. The maximum number of independent elastic constants for any medium is 21 in the most general case (Huntington 1958). This number can be reduced further by the symmetry operations of the respective crystal classes. For an isotropic elastic medium only two elastic constants are independent and Hooke's law is reduced to

$$\begin{bmatrix} \sigma_1 \\ \sigma_2 \\ \sigma_3 \\ \sigma_4 \\ \sigma_5 \\ \sigma_6 \end{bmatrix} = \begin{bmatrix} c_{11} & c_{12} & c_{12} & 0 & 0 & 0 \\ c_{12} & c_{11} & c_{12} & 0 & 0 & 0 \\ c_{12} & c_{12} & c_{11} & 0 & 0 & 0 \\ 0 & 0 & 0 & c_{44} & 0 & 0 \\ 0 & 0 & 0 & 0 & c_{44} & 0 \\ 0 & 0 & 0 & 0 & 0 & c_{44} \end{bmatrix} \begin{bmatrix} \varepsilon_1 \\ \varepsilon_2 \\ \varepsilon_3 \\ \varepsilon_4 \\ \varepsilon_5 \\ \varepsilon_6 \end{bmatrix} \tag{3.19}$$

with

$$c_{12} = c_{11} - 2c_{44} \tag{3.20}$$

3.4.4. Generalised stress-strain relation in the Voigt or Kelvin model

Ideal elastic materials, which can be described by Hooke's law, do not have any energy losses when they are deformed; acoustic waves propagated in such a material would be completely undamped. However such kind of materials do not exist in nature. To investigate the acoustic damping and attenuation in viscoelastic polymers, the Hooke's law equation (3.17) can be modified by using the Voigt or Kelvin model. A more general stress-strain relation than equation (3.6) may be given by

$$\sigma_I = c_{IJ}\varepsilon_J + \eta_{IJ}\frac{\partial \varepsilon_J}{\partial t} \tag{3.21}$$

where subscripts I,J can be 1,2,3,4,5 or 6 and summation over repeated I or J is assumed. It can be shown that the 6×6 viscosity matrix in equation (3.21) has the same general form as the stiffness matrix [c] (Auld 1973). For an isotropic medium

$$[\eta]=\begin{bmatrix} \eta_{11} & \eta_{12} & \eta_{12} & 0 & 0 & 0 \\ \eta_{12} & \eta_{11} & \eta_{12} & 0 & 0 & 0 \\ \eta_{12} & \eta_{12} & \eta_{11} & 0 & 0 & 0 \\ 0 & 0 & 0 & \eta_{44} & 0 & 0 \\ 0 & 0 & 0 & 0 & \eta_{44} & 0 \\ 0 & 0 & 0 & 0 & 0 & \eta_{44} \end{bmatrix} \tag{3.22}$$

with

$$\eta_{12} = \eta_{11} - 2\eta_{44} \tag{3.23}$$

It follows from equation (3.21) that

$$\begin{aligned} \sigma_1 &= \left(c_{11} + \eta_{11}\frac{\partial}{\partial t}\right)\varepsilon_1 + \left(c_{12} + \eta_{12}\frac{\partial}{\partial t}\right)\varepsilon_2 + \left(c_{12} + \eta_{12}\frac{\partial}{\partial t}\right)\varepsilon_3 \\ \sigma_2 &= \left(c_{12} + \eta_{12}\frac{\partial}{\partial t}\right)\varepsilon_1 + \left(c_{11} + \eta_{11}\frac{\partial}{\partial t}\right)\varepsilon_2 + \left(c_{12} + \eta_{12}\frac{\partial}{\partial t}\right)\varepsilon_3 \\ \sigma_3 &= \left(c_{12} + \eta_{12}\frac{\partial}{\partial t}\right)\varepsilon_1 + \left(c_{12} + \eta_{12}\frac{\partial}{\partial t}\right)\varepsilon_2 + \left(c_{11} + \eta_{11}\frac{\partial}{\partial t}\right)\varepsilon_3 \\ \sigma_4 &= \left(c_{44} + \eta_{44}\frac{\partial}{\partial t}\right)\varepsilon_4 \\ \sigma_5 &= \left(c_{44} + \eta_{44}\frac{\partial}{\partial t}\right)\varepsilon_5 \\ \sigma_6 &= \left(c_{44} + \eta_{44}\frac{\partial}{\partial t}\right)\varepsilon_6 \end{aligned} \tag{3.24}$$

3.4.5. Velocity and attenuation of acoustic plane waves propagating in an isotropic linear viscoelastic material

The equation of motion for a stress wave propagating in a vibrating medium is given by

$$\frac{\partial}{\partial r_j}\sigma_{ij} = \rho\frac{\partial^2 u_i}{\partial t^2} \qquad i,j = x,y,z \tag{3.25}$$

Considering an x-polarised, y-propagating shear wave in an attenuating medium, the particle displacement field takes the form

$$\vec{u} = \hat{x}e^{-\alpha y}e^{i(\omega t - ky)} \tag{3.26}$$

and the corresponding strain field is

$$\varepsilon_{xy} = \frac{1}{2}\frac{\partial u_x}{\partial y} = -i\frac{(k - i\alpha)}{2} e^{i\omega t} e^{-i(k-i\alpha)y} \tag{3.27}$$

The stress field, according to equation (3.24), is then given by

$$\sigma_6 = \sigma_{xy} = -i(k - i\alpha)(c_{44} + i\omega\eta_{44}) e^{i\omega t} e^{-i(k-i\alpha)y} \tag{3.28}$$

The equation of motion (3.25) in this case reduces to

$$\frac{\partial}{\partial y}\sigma_{xy} = \rho\frac{\partial^2}{\partial t^2} u_x \tag{3.29}$$

Substitution of (3.26) and (3.28) into (3.29) finally yields

$$k^2 - \alpha^2 = \frac{\rho}{c_{44}} \frac{\omega^2}{\left[1 + \left(\omega\eta_{44} / c_{44}\right)^2\right]} \tag{3.30}$$

$$2\alpha k = \frac{\rho}{c_{44}} \frac{\omega^3 \eta_{44} / c_{44}}{\left[1 + \left(\omega\eta_{44} / c_{44}\right)^2\right]} \tag{3.31}$$

For most solids the viscosity coefficient is sufficiently small so that

$$\left(\frac{\omega\eta_{44}}{c_{44}}\right)^2 << 1 \tag{3.32}$$

Equations (3.30) and (3.31) can be further reduced to

$$\alpha^2 = \frac{\omega^4}{4}\frac{\rho}{c_{44}}\left(\frac{\eta_{44}}{c_{44}}\right)^2 \tag{3.33}$$

and

$$k^2 = \frac{\rho\omega^2}{c_{44}}\left[1 + \frac{3}{4}\left(\frac{\omega\eta_{44}}{c_{44}}\right)^2\right]^{-1} \tag{3.34}$$

Because the wave number $k = 2\pi / \lambda$ and the phase velocity is ω / k, the elastic constant is therefore written as

$$c_{44} = \rho V_S^2\left[1 + \frac{3}{4}\left(\frac{\omega\eta_{44}}{c_{44}}\right)^2\right]^{-1} \tag{3.35}$$

where V_S is the phase velocity of shear waves.

Similarly, for longitudinal acoustic waves propagating in a lossy isotropic solids one has

$$c_{11} = \rho V_L^2 \left[1 + \frac{3}{4} \left(\frac{\omega \eta_{11}}{c_{11}} \right)^2 \right]^{-1} \tag{3.36}$$

and

$$\alpha = \frac{\omega^2}{2} \sqrt{\frac{\rho}{c_{11}}} \left(\frac{\eta_{11}}{c_{11}} \right) \tag{3.37}$$

where V_L is the phase velocity of longitudinal acoustic waves.

According to (3.35) and (3.36), the effect of introducing viscous damping is to make the elastic constants smaller than those which could be expected from an ideal elastic solid. From (3.33) and (3.37), the attenuation factor, α, is proportional to the square of the frequency. Here the unit of the attenuation factor is neper per meter. To estimate the viscosity constants, equation (3.33) can be rewritten as

$$\alpha = 4.343 \sqrt{\frac{\rho}{c_{44}}} \left(\frac{\eta_{44}}{c_{44}} \right) \omega^2 \tag{3.38}$$

in dB/meter. As an example for polyethylene, one can take

$$\rho = 1000 kg/m^3, \quad c_{44} = 2 \times 10^9 Pa, \quad \omega = 3 \times 10^7 rad/s, \quad \alpha = 4500 dB/m$$

Equation (3.38) then gives

$$\eta_{44} \approx 4.5 Nsm^{-2}$$

thus

$$\left(\frac{\omega \eta_{44}}{c_{44}} \right)^2 \leq 5 \times 10^{-3}$$

and equation (3.35) can be written approximately as

$$c_{44} = \rho V_s^2 \tag{3.39}$$

which is equivalent to that for elastic solids.

Although the viscosity of polymers is much larger than that for normal solids (Auld 1973), the effect of viscous damping is still so small that it falls within the experimental error and can therefore be neglected in calculating the elastic constants from acoustic velocities. Similar arguments can apply to the longitudinal wave and show that the

effect of viscosity is negligible. Thus the second order elastic constants, components of the fourth rank tensor, may be calculated from measurements of the longitudinal and shear wave ultrasound velocities. The viscosity constants of polymers can then be calculated using the attenuation data.

3.4.6. Adiabatic Poisson's ratio, bulk and Young's moduli for isotropic solids

Having seen that the effects of viscous damping can be neglected in calculating the second order elastic constants which are components of the fourth rank tensor, it is important to notice that all the elastic constants obtained from ultrasonic measurements are effectively ***adiabatic*** rather than ***isothermal***. Throughout this thesis, all the moduli are taken to be adiabatic unless stated otherwise.

The longitudinal modulus c_{11} and shear modulus c_{44} for an isotropic solid can now be determined by measuring the ultrasound velocities. Another important constant is Young's modulus which is defined as the ratio of the uniaxial stress exerted on a thin rod to the resulting strain in the same direction. Since all other stresses vanish, the Hooke's law, equation (3.19) reduces to:

$$\begin{aligned} \sigma_1 &= c_{11}\varepsilon_1 + c_{12}\varepsilon_2 + c_{12}\varepsilon_3 \\ 0 &= c_{12}\varepsilon_1 + c_{11}\varepsilon_2 + c_{12}\varepsilon_3 \\ 0 &= c_{12}\varepsilon_1 + c_{12}\varepsilon_2 + c_{11}\varepsilon_3 \end{aligned} \tag{3.40}$$

in this case and the Poisson's ratio

$$-\varepsilon_2/\varepsilon_1 = \frac{c_{12}}{c_{11}+c_{12}} = \frac{c_{11}-2c_{44}}{2(c_{11}-c_{44})} \tag{3.41}$$

Young's modulus can now be given by

$$E = \frac{\sigma_1}{\varepsilon_1} = \frac{c_{44}(3c_{11}-4c_{44})}{c_{11}-c_{44}} \tag{3.42}$$

The bulk modulus B is defined for materials under hydrostatic pressure as the ratio of the applied pressure to the negative dilatation. The dilation is given by

$$\frac{\Delta V}{V} = \varepsilon_1 + \varepsilon_2 + \varepsilon_3 = 3\varepsilon_1 \tag{3.43}$$

For the isotropic case one obtains

$$B = -V\frac{dP}{dV} = \frac{\sigma_1}{3\varepsilon_1} = c_{11} - \frac{4c_{44}}{3} \tag{3.44}$$

CHAPTER 4. EXPERIMENTAL TECHNIQUES

4.1. Introduction

In an isotropic solid, such as the polymers studied here, two types of ultrasonic waves can be propagated. One is a longitudinal wave in which the particles vibrate along the direction of propagation. The other is a shear wave, where the vibration is perpendicular to the direction of propagation. These two types of waves propagate independently of each other.

Associated with each of the two modes of propagation, there is a velocity and an attenuation. Thus, four parameters are required to specify the ultrasonic properties of an isotropic solid: the longitudinal and shear velocity, the longitudinal and shear attenuation. These four parameters generally vary with the measurement frequency as well as temperature and pressure. A complete description of the ultrasonic properties of a solid in the long wavelength limit requires measurement to be made of all these variables over a suitable temperature and pressure range. In this work, pulse echo techniques have been used to measure the ultrasonic velocities and attenuations of polymers. Two temperature controlling systems, for working at low and high temperatures respectively, as well as a pressure rig are used to change the temperature and pressure of these polymers.

The term ultrasonic normally implies frequences higher than that which can be heard by the human ear: above about 20 kHz. A 5 MHz measurement frequency is used in this work. At such a high frequency, the elastic constants determined from ultrasonic measurements are essentially adiabatic and may be quite different from those determined at very low frequencies, which are, isothermal to some extent. It is useful to compare the results obtained at high frequencies with those obtained at much lower frequencies as this may be helpful for understanding the nature of the relaxation processes which normally cause attenuation peaks and anomalous velocity changes in the ultrasonic measurements. To achieve this purpose Dynamic Mechanical Thermal Analysis (DMTA) has also been carried in a frequency range of 1 to 10 Hz.

One of the primary objectives of this project is to investigate the correlation between the mechanical and electrical properties of polyethylene and its effect on the breakdown behaviour of commercial cable insulation. Mechanical relaxations in polymers and glasses are often coupled with dielectric relaxation process. The dielectric properties of a material are usually characterised by the permittivity or dielectric constant and the dielectric loss. Dielectric spectroscopy is based on the interaction of electromagnetic radiation with the electric dipole moments of the material. To correlate the mechanical and electrical properties, measurements have been made of the complex dielectric constant as functions of frequency, temperature and hydrostatic pressure. In the following sections of this chapter, the techniques and equipment used will be described.

4.2. The ultrasonic pulse overlap technique

4.2.1. Velocity measurement

To determine the velocity of ultrasonic waves, and hence the elastic constants of polymers, it is necessary to measure the transit time of an ultrasonic wave propagating through a suitably prepared specimen. This has been done by using the pulse echo overlap technique, which allows changes in the transit time to be measured to an accuracy of 1 part in 10^5. The pulse echo overlap method using the double ended technique was first reported by May (1958). Later, a single-transducer modification was used by Papadakis (1964 and 1967) to measure the transit time between any pair of echoes in a pulse echo pattern. A block diagram of the arrangement of the apparatus used in this work is shown in Figure 4.1. The dotted lines indicate that equipment which is needed only for the measurement of the attenuation as discussed in section 4.2.2. The high resolution oscillator (MATEC 110) can generate pulses (Figure 4.2(1)) with frequencies which are highly stable, typically to better than 1 part in 10^7 per day. In order to be able to trigger the r.f. pulses generated by the MATEC 6600, the frequency of the MATEC 110 oscillator must be reduced by a factor of 10 or 100 and this is achieved using the MATEC 122B decade divider as shown in Figure 4.2(2). The high voltage r.f. pulse generator (MATEC 6600) produces a short duration, high

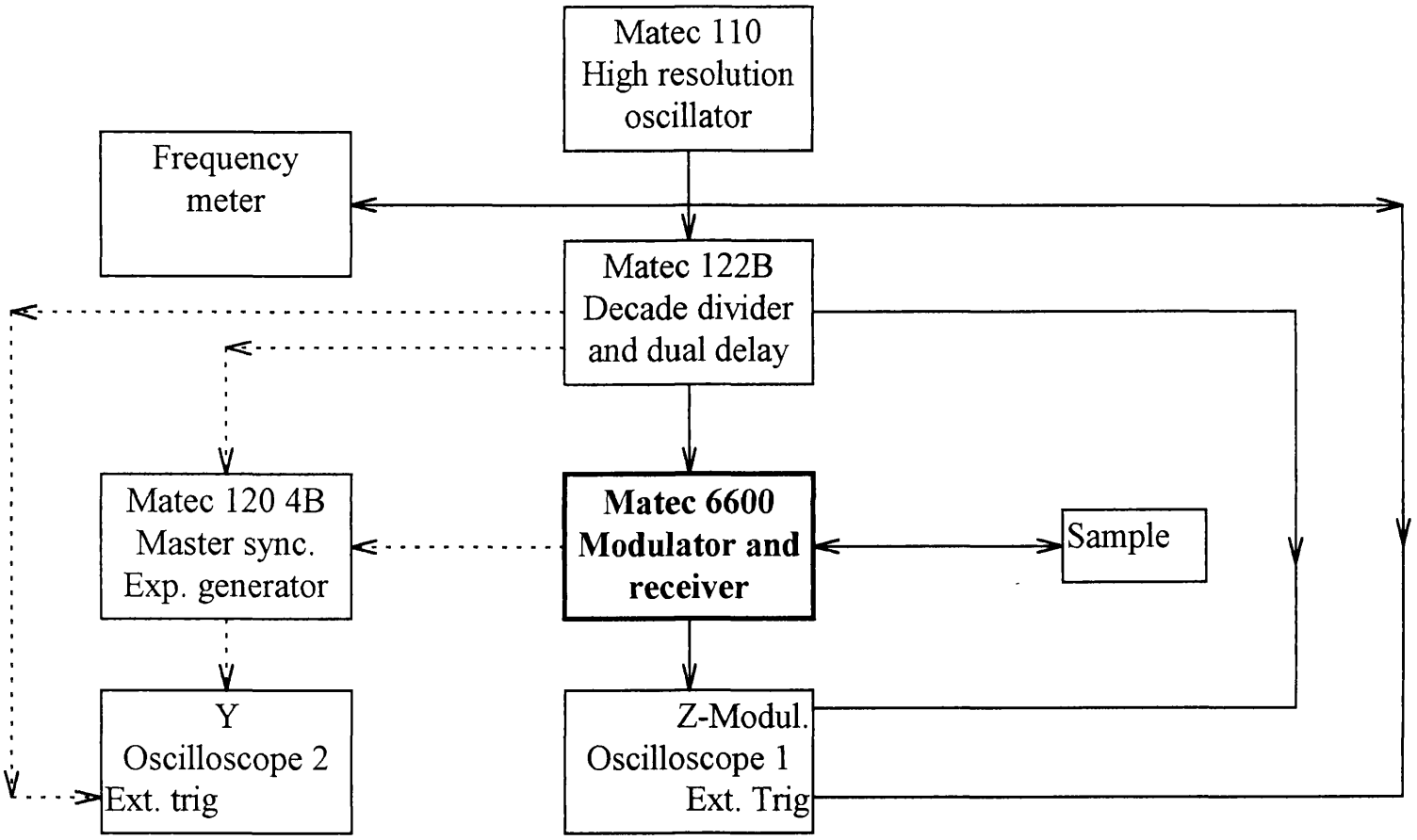

Figure 4.1. Block diagram of the pulse echo overlap apparatus.

(1) Master sync. from high resolution oscillator

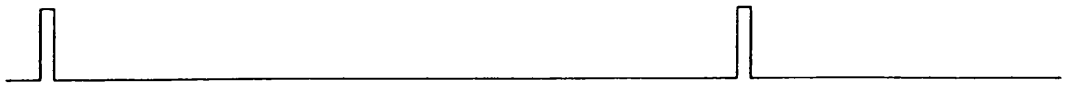

(2) Divided sync (÷10)

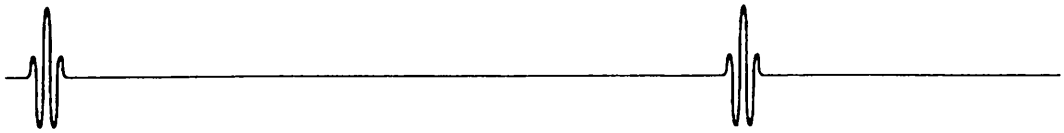

(3) Radio frequency (r.f.) pulses to transducer

(4) Radio frequency echoes

(5) Z modulation – intensification of echoes 1 and 2

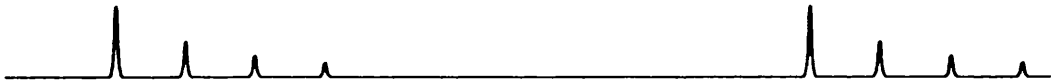

(6) Video out

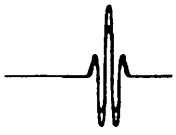

(7) Overlap of echoes 1 and 2

Figure 4.2 Signals at various points in the pulse echo overlap system.

voltage r.f. pulse when triggered. This pulse is typically about 3 microseconds long and about 1000 volts maximum amplitude (Figure 4.2(3)). When this pulse is applied to a transducer mounted on a sample, a train of ultrasonic echoes is produced (Figure 4.2(4)). Details of the transducers will be discussed in section 4.2.3. To enable a complete set of echoes to be observed the r.f. pulse generator has to be triggered at a sufficiently low frequency (below 1000 pps) using the output from the decade divider (MATEC 122B). Two echoes in the train are selected to be intensified (Z modulation, Figure 4.2(5)) using the strobe generator on the MATEC 122B. The oscilloscope is triggered using pulses from the MATEC 110 high resolution oscillator.

The frequency of the oscillator is adjusted until it is approximately the same as the reciprocal of the time delay between the two selected echoes. The brightness of the oscilloscope is then reduced until only the intensified echoes are visible. Adjustment of the oscilloscope timebase then enables the two echoes to be displayed alternately on the screen. Fine tuning of the oscillator will bring the r.f. cycles within the echo envelopes into coincidence (Figure 4.2(7)). The frequency counter displays the oscilloscope triggering frequency, which is used to determine the velocity of ultrasound propagating in the sample. An integral multiple m of this frequency also produces the overlap, since an echo then appears for every m^{th} sweep. The real time delay t between the two echoes is then m times the reciprocal of the overlap frequency.

4.2.2. Attenuation measurements

Acoustic attenuation can be measured, as well as velocity, by using the pulse echo method. However, an additional piece of equipment is required, which is shown by the dotted lines in Figure 4.1. The initial pulse from the transducer loses energy during its passage through the sample as a result of a variety of absorption and/or scattering processes. It is also reflected at each air-sample interface, where it can be shown from acoustic matching calculations that almost all of the energy of the pulse is reflected and only a very small amount is transmitted. The passage of the pulse therefore produces an exponential decay pattern, as shown in figure 4.2(6), and the decrease in amplitude of the echoes is a measure of the attenuation of the stress wave in the sample.

Several different techniques can be used to determine the attenuation. Among these, the exponential method has been most commonly used. A calibrated exponential generator (MATEC 1204B) is used to produce an exponentially decaying curve and this is displayed on the oscilloscope together with the pulse echo train shown in Figure 4.2(6). The exponential curve is adjusted so that it fits exactly to the echo pattern and the attenuation is then read directly from the calibrated dial on the MATEC 1204B.

4.2.3. Transducers

Transducers are used as both transmitters and receivers of mechanical vibrations, converting electrical energy to acoustic energy and vice versa. For ultrasonic applications, two types of piezoelectric transducer are most commonly used. The first type is a crystalline piezoelectric transducer and is fabricated from a material such as quartz. Quartz is inherently piezoelectric, with properties determined by its crystallographic structure. Other types of transducers are made from artificial piezoelectric ceramic materials such as lead-zirconium-titanate (PZT).

The crystallographic axes of quartz are illustrated in Figure 4.3, together with the most frequently used plate orientations (cuts). Transducers for the generation of longitudinal waves are made from X-cut quartz; that is they are cut with their plane comprising the Y and Z crystallographic axes, and the X axis is normal to the plane. Transducers for the generation of shear waves are made from Y cut plates which have the Y axis normal to the plane.

Ceramic piezoelectric elements are fabricated from polycrystalline ferroelectric materials which are initially isotropic. The local regions ("domains") within the material exhibit electrical polarisation, but the orientations of adjacent domains in a plate of such a material are random. Consequently, there is no net polarisation and the plate is at best weakly piezoelectric. A preferred orientation for the domains is achieved by raising the temperature of the plate above the Curie point for the ceramic and imposing a large dc electric field; this is the process of poling. The applied electric field causes a large fraction of the domains to align themselves parallel to the field. The resulting net

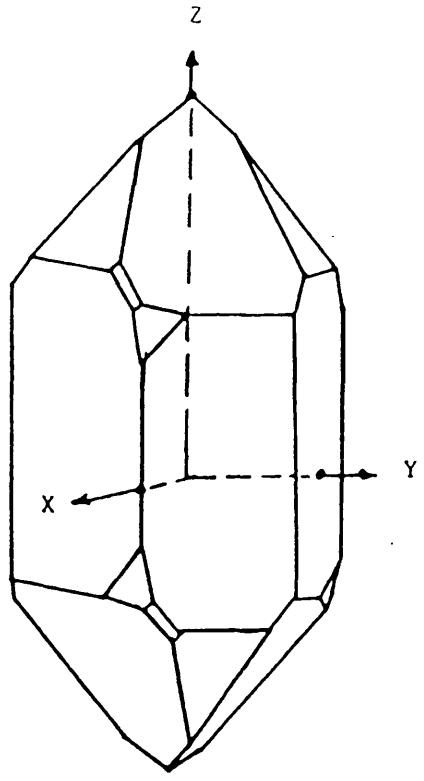

Quartz crystal.

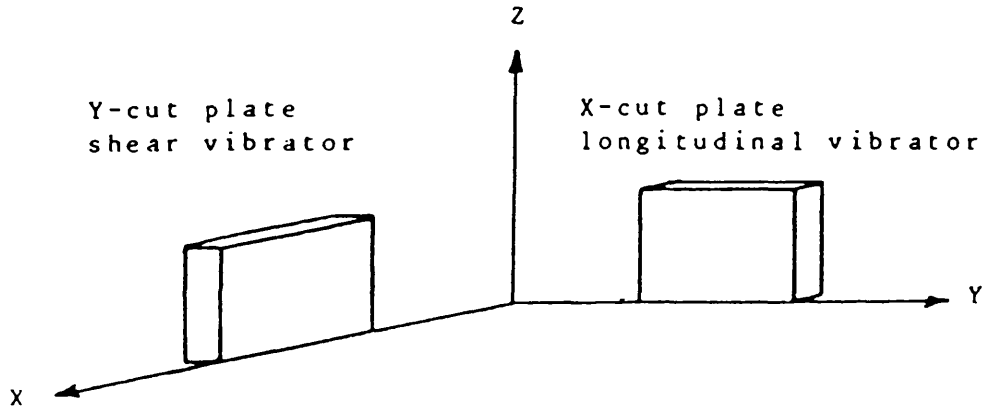

Figure 4.3 Quartz crystal and pure mode transducer cuts.

polarisation is maintained if the ceramic is cooled before it is removed from the poling field. The direction of poling is conventionally designated as the Z axis. Figure 4.4 shows that ceramic plates can be operated in thickness expander or thickness shear modes depending on the orientation of the plate relative to the axis of polarisation.

To choose the best transducers for a particular application, first the duration of the pulses used for the measurement must be carefully considered. The number of wavelengths in the pulse must be less than the distance between two reflecting surfaces. This requirement can be met either by reducing the pulse width or increasing the sample thickness. In the present work, the ultrasonic attenuation in the polymers is so high that the thickness of the specimen has to be thin to get a good echo train. Therefore, the pulses used must be short. However, the extent of the high frequency spectrum of the modulating signal is inversely proportional to the pulse duration (Naunton, 1961). The shorter the pulse, the greater the bandwidth required for the transducer to pass an undistorted signal. One method commonly used to achieve a broadband transducer is bonding a well matched material to the back of the piezoelectric plate. This backing material is fabricated to exhibit very high ultrasonic attenuation and thus to appear as an infinite transmission line representing a purely resistive mechanical load. Hence, piezoelectric materials exhibiting large electromechanical coupling coefficients are necessary to achieve adequate sensitivity over a broad frequency range.

It has been found that normal quartz transducers do not give ultrasonic signals strong enough for the measurements of sound wave velocities and attenuation in polyethylene at the vicinity of room temperature. PZT ceramic plates have much larger transmission constant (a parameter indicates the efficiency of transmitting ultrasonic energy) and electromechanical coupling coefficient than quartz, but the echo-trains obtained using PZT plain plates are always more noisy and distorted. To measure the temperature and hydrostatic pressure dependences of ultrasonic wave velocity and attenuation of polyethylene, special transducers have been manufactured by backing poled piezoelectric PZT ceramic plates, which are 5.5 mm in diameter and 0.44 mm thick corresponding to a resonance frequency of 5 MHz, with aluminium loaded epoxy resin

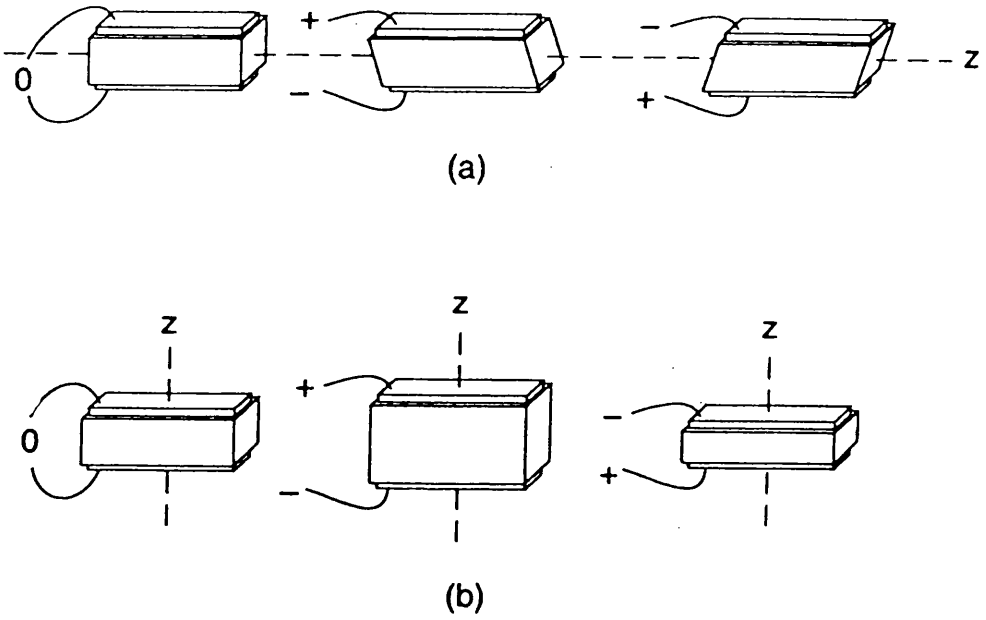

Figure 4.4 Mechanical displacements relative to the poling axis z in ferroelectric ceramics for two modes: (a) the thickness shear mode with transverse orientation is poled perpendicular to the applied field; (b) the thickness expander mode with longitudinal orientation is poled parallel to the applied field.

(Figure 4.5). The backing has the effect of "spoiling the Q" of the mechanical resonance of the piezoelectric plate and thus increasing the bandwidth. In addition, it suppresses the oscillatory output by preventing unwanted acoustic waves from returning to the transducer. The output of the transducer is a maximum at its resonant frequency, but it can be operated below its resonant frequency without too much loss in output. A piece of copper wire is soldered to the back of the PZT plate to act as one electrical lead. The ground is the silver paint coating of the sample which presses against the front face of the transducer.

A model M110H, 5 MHz industrial transducer has also been used to measure the sound velocity at room temperature (about 20°C).

4.2.4. Transducer-polymer sample bonding

To enable the acoustic energy generated by the transducer to be transmitted into the specimen, it is necessary to bond the transducer to the specimen using a coupling material which produces a minimum energy loss. A number of viscous liquids have been tested on the different polymers:

1. Ultragel II. This is an industrial ultrasound couplant with reputably excellent bonding between -35°C and 150°C.
2. ZGHT High Temperature Coupling Paste.
3. Resin 276-V9.
4. Nonaq Stopcock Grease.

The essential requirements for a good bond are:

(a) The thickness must be uniform and should be a small fraction of the ultrasonic wavelength; usually the seal thickness is of the order of 10^{-6}m.

(b) The bond characteristics should not vary appreciably over the temperature range of measurements.

(c) Clean conditions are needed.

(d) The bonding agent should not interact chemically with either the sample or the transducer.

The best bonding material tested is Nonaq Stopcock Grease (manufactured by the Fisher Scientific Co.), which provides satisfactory bonds below room temperature and

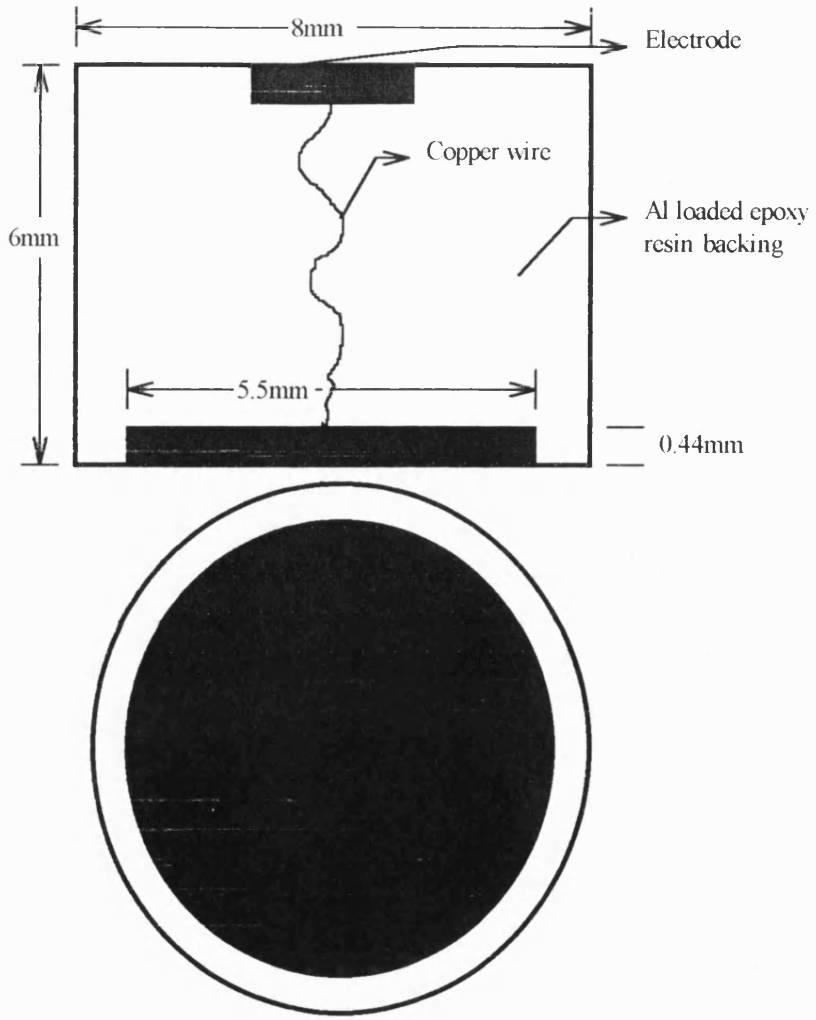

Figure 4.5 Schematic diagram of the PZT transducer made in "house".

also at temperatures as high as 130°C. It is necessary to avoid moisture which interacts with Nonaq and can cause problems especially at low temperatures. For high temperature measurements, Resin 276-V9 (made by Du Pont UK Ltd) makes a useful bond for both longitudinal and shear waves. The general procedure for bonding consists of polishing the polymer samples to have the faces flat and parallel to better than 10^{-3} radians. This is achieved by using a Logitech PM2 Precision Polishing Machine with a PP5 jig and then making a thin and uniform layer of the appropriate bonding material after cleaning the sample and the transducer with acetone. A good bond shows an exponential decay of the echo train displayed on the oscilloscope screen.

4.3. Tensor Post-Processing and Single Pulse Demodulator: MBS-8000 ultrasonic system

In addition to the pulse-overlap method, a new ultrasonic technique has also been used to carry out the work on polyethylene. This new technique uses a Matec MBS-8000 DSP measurement system which includes an MBS-8050 frequency agile toneburst pulse/receiver system, digitisation hardware, an 80486 IBM compatible computer, a Marconi 10kHz-1 GHz AM/FM signal generator and a 100 MHz Hitachi oscilloscope and Matec's DSP measurement software. In this system, the measurement of attenuation and transit time is based on pulse-echo technique similar to that used in earlier work. After generating a single pulse, the transducer receives a series of echoes, each of which is separated from the last by twice the time-of-flight through the sample. The amplitude of these pulses decays exponentially with the number of passes through the medium. Because of the dispersive nature of the material, the wave shape changes from echo to echo. The received pulse is a delayed copy of the original transmitted pulse, which is blurred by the dispersion of the material and the reflection of the rear wall which is normally not a perfect reflector.

Instead of the overlap method used in the old Matec ultrasonic equipment, the MBS-8000 system uses a so-called Tensor Post-Processing technique to determine the transit time and the attenuation of ultrasound in a material. A blur model is used by the Tensor Post-Processor as a Single Pulse Demodulator. The Demodulator treats the second echo as the reflection and/or dispersion function blurred by the transmitted wave and uses the first echo as a reference against which the second received echo is demodulated. The sequence of operation required to determine time-of-flight of an ultrasonic pulse is:

1. Transmit a pulse.
2. Capture the first and second echo.
3. Use the first pulse as a reference for demodulation of the second echo to obtain the reflection and dispersion function.
4. Calculate the time-of-flight as the time of strongest reflection (time of largest positive value of reflection/dispersion function).

Because the dispersion waveform is of the order of several nanoseconds and the width of the front and rear wall reflection functions is even shorter in duration, the tensor post-processing technique yields a very accurate estimate of time-of-flight with possibly picosecond resolution. An additional advantage of this technique is that it enables computer control of the measurement. However, the new technique works only with materials from which good echo-train can be obtained.

4.4. Apparatus for dielectric measurements

4.4.1 HP 4192A LF impedance analyser

A Hewlett Packard 4192A LF impedance analyser capable of carrying out a.c. measurements over the frequency range of 5Hz to 13MHz has been used to measure the conductance G and susceptance B of polyethylene thin films. The impedance analyser provides an a.c. voltage of constant magnitude and compares it with the phase and magnitude of the resultant current. In order to minimise the experimental error, especially at high frequencies, it is necessary to adopt the so-called four terminal pair

configuration. This negates the possible mutual inductance and high frequency pick-up effects of the measurement leads. This system allows the application of a bias voltage to the sample to enable any features of the resulting profiles corresponding to electrode effects to be identified.

The real and imaginary parts of the complex dielectric constant are calculated from

$$\varepsilon' = \frac{d}{A\varepsilon_o}\frac{B}{\omega} \tag{4.1}$$

and

$$\varepsilon'' = \frac{d}{A\varepsilon_o}\frac{G}{\omega} \tag{4.2}$$

respectively, here d is the thickness and A the area of the sample.

In general, the accuracy of the measured G and B values depends on the oscillator voltage (OSC) level of the synthesiser, the admittance range and the dissipation factor D=|G/B|, as well as the measurement frequency used. In order to minimise the measurement error, a high oscillator voltage level should be used. The available range of the OSC level for the HP impedance analyser is from 5mV to 1.1V. In the current work, the OSC level has been set to 1 volt for all the measurements, which would effectively reduce the error to a minimum as far as the OSC level is concerned. In the frequency window between 400Hz and 1MHz, the measurement accuracy is frequency independent. Therefore the measurement error for G and B is only associated with the quality factor and the measurement range, which varies with sample and operating frequency. For crosslinked polyethylene, measurements show that the susceptance B and conductance G are too small to be measured below 1kHz using this equipment and the quality factor D is much less than 0.1 above this frequency. Typical measurement accuracy (ΔB) of susceptance B (and conductance G) for crosslinked polyethylene S188/S299/94 has been calculated at selected frequencies and is given in Table 4.1. The measurement accuracy for other crosslinked polyethylenes is expected to have the same order.

Table 4.1. The accuracy ΔB and the relative error ΔB/B of the susceptance of crosslinked polyethylene at selected frequencies.

F	1kHz	10kHz	100kHz	1MHz
ΔB (/ohm)	3.5×10^{-9}	8.0×10^{-9}	6.0×10^{-8}	5.5×10^{-7}
ΔB/B	1.4%	0.3%	0.2%	0.2%

The relative error of the dielectric constant ε′ can be calculated as

$$\left|\frac{\Delta\varepsilon'}{\varepsilon'}\right| = \left|\frac{\Delta d}{d}\right| + \left|\frac{\Delta A}{A}\right| + \left|\frac{\Delta B}{B}\right| \tag{4.3}$$

where d is the thickness and A the area of the sample. For crosslinked polyethylene sample S188/S299/94, $\left|\frac{\Delta\varepsilon'}{\varepsilon'}\right|$ has been estimated as 3.5%. The main error arises from the thickness and area measurements, which can be minimised by increasing the dimensions of the sample. In many cases, however, it is not realistic to have a sample with a large area. Nevertheless, one should not be discouraged by this relatively large error introduced by dimension measurements. In most circumstances, as in the current work, the only important quantity is the relative change of the dielectric constant with temperature and pressure rather than the dielectric constant itself. The error arising from the dimension measurement is small and can be neglected. Another type of error related with the dimensions of the sample is the edge effect of the capacitor. This effect is equivalent to an extra capacitor connected parallel with the sample, resulting in an increase in the measured dielectric constant. Usually the sample area is much larger than the thickness and the error arising from the distribution of the electrical field near the edge of the electrodes should not be significant. In the following discussion of the dielectric constant, only the error arising from the susceptance will be considered.

Two methods have been used to make electrodes: (1) coating the samples with silver paint and (2) vacuum evaporating silver and gold on the sample. Preliminary tests at room temperature have showed that the results are independent of bias voltage,

indicating a good electrical contact between the electrode and the sample. The dielectric constant measured using silver and gold electrodes is similar to that of the silverdag coated samples.

To measure the dielectric constants of polyethylene above the melting point, it is necessary to use PTFE coaxial cables, which can stand much higher temperatures than the standard one metre measurement cable supplied by Hewlett Packard. Efforts have been made to reduce the error at high frequencies by adjusting the length of the PTFE cables. To enable low temperature electrical measurements down to 10K using the helium cryostat, a sample holder has been constructed and a special cable configuration has been used.

To enable more convenient and efficient data processing, the operating computer program of the HP impedance analyser, which was originally written in BBC basic, has been transferred from the Archimedes to an IBM compatible PC by rewriting it in Quick Basic. Moreover, a routine has been included in the new program to allow the computer to obtain the pressure data automatically. The program reads the resistance of the manganin wire coil from the DVM, calculates the value of pressure, prints it on the screen and then saves it on the disk. Recording the resistance data by hand and then re-entering them into the computer to calculate the pressure is not only time consuming but more likely to introduce unnecessary errors. Another main modification on the controlling software is that the program has been extended to allow an automatic dielectric measurements down to 10K using the helium cryostat together with the Lakeshore temperature controller.

To ensure the reliability of the measurements of the temperature and hydrostatic pressure dependences of the dielectric behaviour of polyethylene, the whole system has been tested extensively on a semicrystalline polymer: polyethylene oxide, whose dielectric properties are relatively easier to measure than those of polyethylene. Satisfactory results, interesting in themselves, have been obtained on this polymer using the system.

4.4.2 Dielectric Spectrometer and the Chelsea Dielectric Interface.

To extend the dielectric measurements to lower frequency range (down to 10^{-3} Hz), a Model DS2560RL Dielectric Spectrometer made by Dielectric Instrumentation has been used. The characteristic feature of this dielectric measurement system is the utilisation of a Chelsea Dielectric Interface as the front-end of the frequency response analyser. The function of the Chelsea Dielectric Interface is two-fold: to act as a high impedance buffer between the sample and the frequency response analyser, and to facilate the measurement of the current flowing through the dielectric sample.

4.5. Cryostats and temperature measurements

To make ultrasonic measurements at low temperatures a Cryophysics Model 22C cryodyne refrigeration system has been used. This system consists of a Model SC compressor, a Model 22 Cold Head, a temperature controller and associated interconnecting lines. The operation of this refrigerator is analogous to that of a common domestic refrigerator, except that helium gas rather than freon gas is used as the working fluid. The helium gas is compressed and the heat of compression is removed by heat exchangers. When the gas is allowed to expand, its cooling results in a lowering of the temperature. To obtain the very low temperatures produced by this cryostat, it is necessary to have highly efficient heat exchangers. This is achieved by means of a regenerator which is able to extract heat from the incoming gas, store it, and then release it to the exhaust stream. A regenerator is a reversing-flow heat exchanger through which the helium passes alternately in either direction. It is packed with a material of high surface area, high specific heat, and low thermal conductivity, that will readily accept or give up heat to the helium depending on whether the helium is at a higher or a lower temperature. A schematic diagram of the refrigerator system, showing the direction of flow of the helium is given in Figure 4.6, and a detailed diagram of the Model 22 Cold Head is in Figure 4.7. In normal refrigerators the compressions and expansions are carried out with a piston assembly. In the model 22 system a double ended cylinder is used together with an elongated piston made from a material of low thermal conductivity. The pressures above and below the piston are

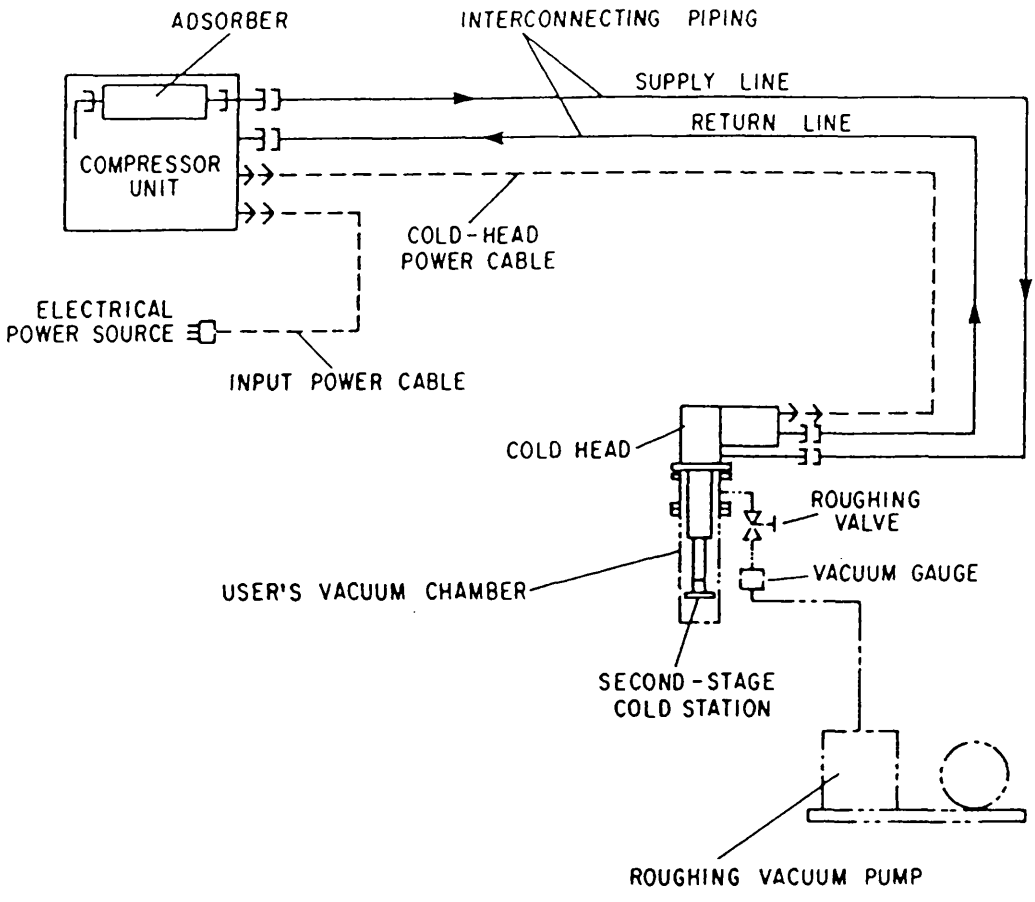

Figure 4.6 A schematic diagram of Cryophysics Model 22C cryodyne refrigeration system used to cool the sample to 10K.

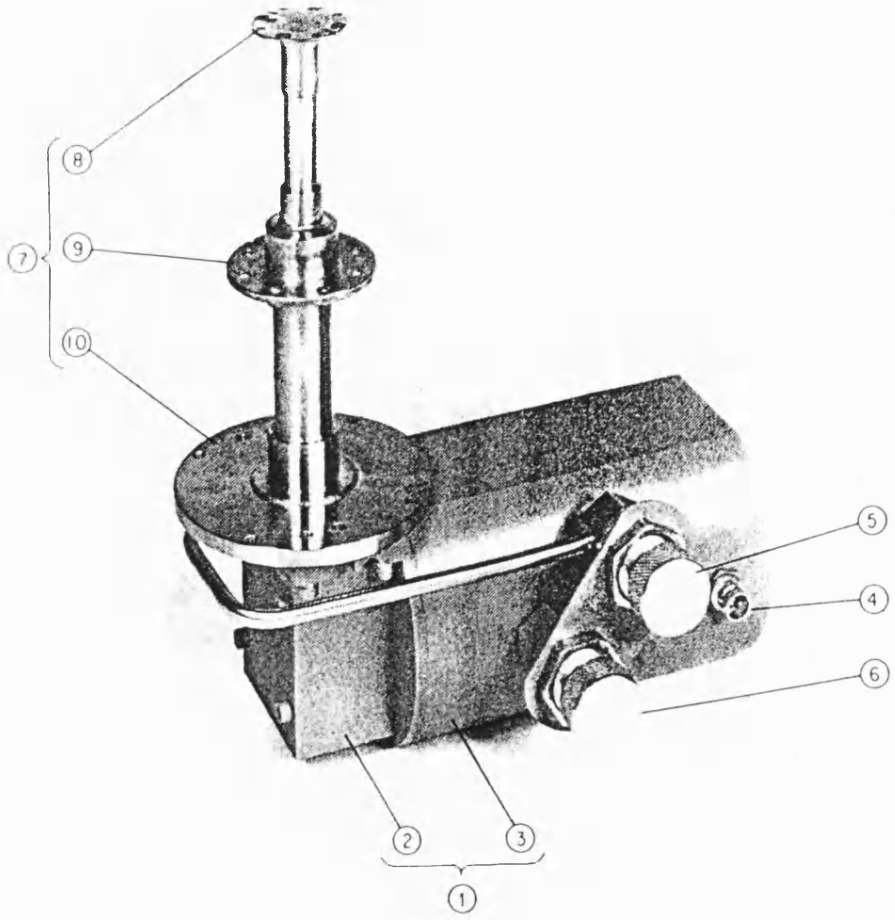

Figure 4.7 A photograph of the Model 22 cold head in the refrigeration system: 1. Drive Unit; 2. Crankcase (houses the drive mechanism); 3. Drive Motor; 4. Power Connector; 5. Gas-Supply Connector; 6. Gas-Return Connector; 7. Cylinder; 8. Second-Stage Cold Station; 9. First-Stage Cold Station and 10. Top Flange.

substantially equal and the piston is called a "displacer," because it effectively moves gas from one end of the cylinder to the other. The regenerator is placed inside the displacer to avoid unnecessary piping and to minimise heat losses. During operation, high pressure helium from the compressor enters the cold head at the helium supply connector, and flows through the displacer-regenerator assembly, crankcase and motor housing before exiting through the helium gas return connector and returning to the compressor. Helium expansion in the displacer-refrigerator assembly provides cooling at the cold head. The cold head, see Figure 4.7, is divided into a first and second stage cold station. The first cold station can produce temperatures between 60 and 120K while the second cold station reaches 10 to 20K depending on the operating conditions. Helium returning from the cold head enters the compressor and is recycled.

A coil heater with a resistance of 25Ω is fixed on the cold head cylinder. A Model DT-470-CU-12A diode temperature sensor is mounted on the second-stage cold station which also acts as a sample holder. Both the heater and sensor are connected to a Model DRC-91C temperature controller (manufactured by Lake Shore Cryotronics, Inc.). A rotary pump, together with a diffusion pump, is used to produce adequate vacuum isolation for the cold head and related components. This is necessary for temperature control and satisfactory cooldown.

After the sample is installed, the vacuum chamber is rough-pumped down to 5×10^{-2} torr or better. Then the roughing valve is closed prior to starting cooldown of the refrigerator. To acquire proper helium supply static pressure, the helium pressure gauge on the back of the compressor is checked and the readings are kept within the range of 220 to 230 psig (1515 to 1585 bar). With the temperature controller, the sensor and the heater, the temperature can be stabilised and measured to an accuracy of 0.1K in the range of 10 to 300K.

The model 22C Cryodyne system is only suitable for use below room temperature. For high temperature measurements, the sample (in its holder) is put into a closed aluminium tube which is immersed in an oil bath controlled thermostatically to about ±0.5°C. The oil used is Dow-Corning DC 200/20cs silicone fluid which can be heated

up to 230°C. A stirrer is used to allow good mixing and ensure isothermal conditions. The temperature is read to an accuracy of ±0.5°C using a type K nickel-chromium/nickel-aluminium thermocouple mounted near the specimen.

To ensure that the sample temperature is uniform, the temperature is changed very slowly, typically ten minutes being allowed between measurements due to the low thermal conductivity of the polymers.

4.6. The hydrostatic pressure apparatus

The pressure rig, which has been adapted to measure the effects of pressure on the ultrasonic properties of polymers, is shown in figure 4.8. It consists of a cylinder and two pistons, which are made from EN26 nickel alloy carbon steel, and a hydraulic pressure pump, which can provide a hydrostatic pressure up to 2.5 kbar in the cell. The sample holder and a manganin wire coil, which acts as a pressure gauge, are fixed to the top piston. Several electrical lead-throughs are arranged radially around the piston to enable connections from inside the cell to the measurement equipment. The manganin wire has a linear resistance-pressure relationship with a pressure coefficient of 2.4×10^{-6} bar^{-1} and a temperature coefficient of 1.0×10^{-7} $°C^{-1}$. A NiCr/NiAl thermocouple is mounted near the sample to measure the temperature to an accuracy of ±0.2°C. The pressure is transmitted by "Dow Corning" 200/1000 cs silicone fluid which can work in a temperature range of -30°C to 230°C without freezing or igniting. Rubber "O" rings and PTFE delta rings, with an internal diameter of 22.23 mm, have been used as seals between the cylinder wall and the pistons. The black VIT (viton) "O" rings, made from fluoroelastomer, which is a copolymer of vinylidene fluoride and hexafluo-propylene (Edwards High Vacuum, U.K.), provide satisfactory sealing below 200°C. The delta rings work at higher temperatures. Pressure is created and transmitted to the sample when the top piston is pressed downwards. An alarm device is connected to the top piston to prevent crushing of the sample due to a leak in the seals. A "Thurlby" 1905a Intelligent Multimeter (Thurlby Electronics Ltd.), with a sensitivity of 1mΩ, is used to measure the electrical resistance of the manganin coil

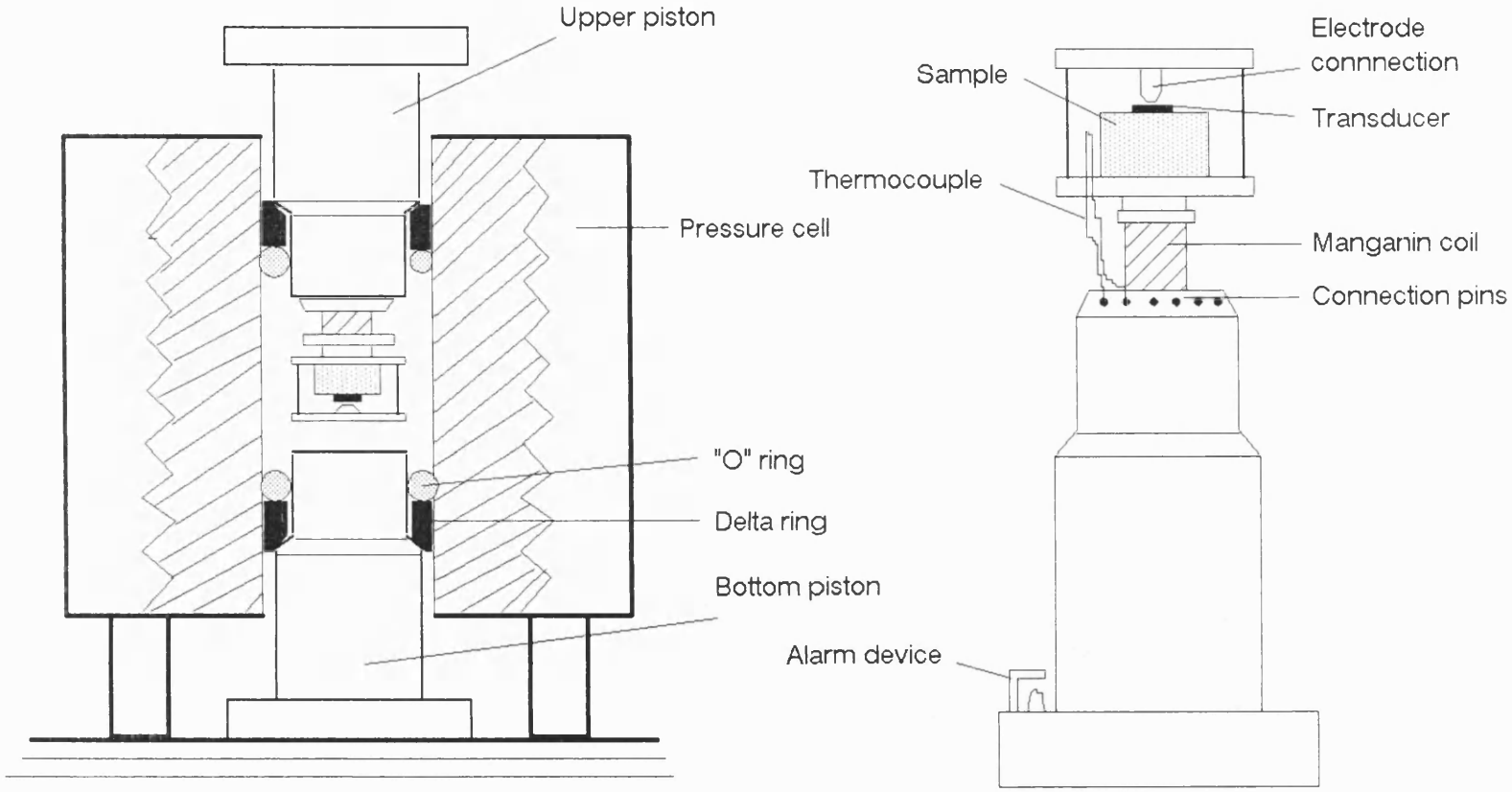

Figure 4.8 Diagram of hydrostatic pressure cell and sample holder.

under pressure. The pressure data are converted from resistance to pressure by the relation:

$$P=(R/R_o-1)/2.4\times10^{-3} \text{ (kbar)}$$

where R and R_o are the resistance under arbitrary pressure P and initial pressure P_o respectively.

4.7. Dynamic Mechanical Thermal Analysis (DMTA) technique

As stated in Chapter 1, the Introduction chapter, the purpose of including the DMTA data is to provide a complementary study at much lower frequencies than that obtained from the ultrasonic investigations. In the DMTA technique, a sinusoidal stress is applied to the sample. If the solid was perfectly elastic, then the resultant strain would be in phase with the applied stress. Conversely, if the solid was completely viscous, the strain would lag the stress by an angle of 90°. In all real solids, the loss angle is less than 90° and the resultant strain will lag behind the stress by some angle δ. The magnitude of the loss angle is dependent upon the amount of the internal motion occurring in the same frequency range as the imposed stress. All the data are collected and presented as the temperature dependence of:

(i) the storage modulus E'(G')=(amplitude of in phase stress component)/(strain amplitude);

(ii) the loss modulus E"(G")=(amplitude of out of phase stress component)/(strain amplitude);

(iii) the tangent of the loss angle tanδ=E"/E'.

Here E and G represent the modulus corresponding to the bending and shear mode respectively. The system used in this work is manufactured by Polymer Laboratories Limited. It consists of a mechanical spectrometer head and a micro-processor control unit. The driving frequency of the vibrator can be selected to be 0.033, 0.1, 0.33, 1.0, 3.0, 10, 30 and 90 Hz. The sample modulus and loss tanδ are obtained as a function of temperature at a fixed frequency. In operation, the DMTA imposes a sinusoidal stress on polyethylene samples, which have been cut as rectangular sheets approximately 12 mm long, 8 mm wide and 2 mm in thickness, in the bending mode. The temperature is controlled within 2°C of the indicated temperature for scan rates up to 5°C/min, by

using heater windings surrounding the sample enclosure and a cooling jacket situated just outside the heater windings. The working temperature range is -150°C to 300°C with a linearity of ±0.5°C. A scan rate of 3°C/min has been used for all the measurements on polyethylene.

CHAPTER 5. TEMPERATURE AND FREQUENCY DEPENDENCES OF THE COMPLEX DIELECTRIC CONSTANT OF POLY(ETHYLENE OXIDE) (PEO) UNDER HYDROSTATIC PRESSURE

5.1. Introduction

Due to its potential application in high energy density solid state batteries the temperature dependence of the dielectric properties of poly(ethylene oxide) (PEO) have been studied extensively (Connor, Read and Williams 1964, Ishida, Matsuo and Takayanagi 1965, Arisawa, Tsuge and Wada 1965, Porter and Boyd 1971, Fontanella *et al.* 1983, Wintersgill *et al.* 1985, Fontanella *et al.* 1985, Vincent 1987, Bruce and Vincent 1993). The frequency response of the dielectric constant is dominated by a low frequency dispersion, whose physical origin has long been in question (Arisawa, Tsuge and Wada 1965, Porter and Boyd 1971). The glass transition relaxation process has been studied over a wide frequency and temperature range up through the crystalline melting point and into the melt (Connor, Read and Williams 1964, Porter and Boyd 1971). The α_a peak, which is a feature of the temperature dependence of the dielectric loss, unexpectedly could not be found over the frequency range 10-10^5 Hz at any chosen temperature (Wintersgill *et al.* 1985, Fontanella *et al.* 1985). Although the effect of pressure on the dielectric properties of complexed PEO has been widely studied (Fontanella *et al.* 1983, Chadwick, Strange and Worboys 1983), it seems that there has only been one such examination (Fontanella *et al.* 1985) of the host polymer PEO.

In general, dielectric relaxation processes observed in polymers have been interpreted in terms of motional modes of polar groups in long chain molecules. At temperatures well above the glass transition temperature T_g, the motion of long chain molecules occurs as a result of the co-operative movement of segments of the chain. The rate of segmental motion can be estimated from the relaxation time of the dielectric relaxation process associated with the micro-Brownian motion of the main chain, the so-called α_a-relaxation. This rate can be thought of as a function of the free volume fraction,

which varies not only with temperature but also with applied pressure. Determination of the pressure dependence of the dielectric relaxation process is a useful approach to checking the applicability of the free volume concept to segmental motion in polymers.

Originally, PEO, as a well studied semi-crystalline polymer, was chosen to test the dielectric measurement system. The testing results, however, turned out to provide new understanding of the dielectric behaviour of this polymer. Hence the temperature and frequency dependences of the complex dielectric constant of PEO under hydrostatic pressure are presented here. The physical origin of the low frequency dispersion and the effect of pressure on the dielectric behaviour of the glass transition in PEO are discussed.

5.2. The frequency dependence of the dielectric constant and dielectric loss

The frequency (f) dependences of the dielectric constant ε' and loss ε'' of PEO samples of 600,000 molecular weight have been measured at different temperatures and the results are shown in figure 5.1. At room temperature (292 K) the dielectric constant has a value of 39 at 100 Hz but only 5.2 at 1 MHz. The graph shows that log ε' decreases almost linearly with log (f) in the frequency range of 100 to 5 kHz, and remains at an almost constant value at higher frequencies. The plot of log ε'' against log (f) is almost linear with slight changes of slope at about 10 kHz and 100 kHz (figure 5.1(b)). This frequency response of the dielectric constant of PEO is similar to that reported by Arisawa, Tsuge and Wada (1965) and Porter and Boyd (1971), although the dielectric constant they show graphically is slightly smaller at the high frequency end.

The strong low frequency dispersion which characterises the frequency dependence of the dielectric constant of PEO (Figure 5.1(a)) has never been understood. Arisawa *et al.* (1965) found that at low frequencies the plot of log ε'' versus log (f) was almost linear with a gradient of -1. They believed that this behaviour was due to the d.c. conductivity, which becomes important at low frequencies. By subtracting the loss

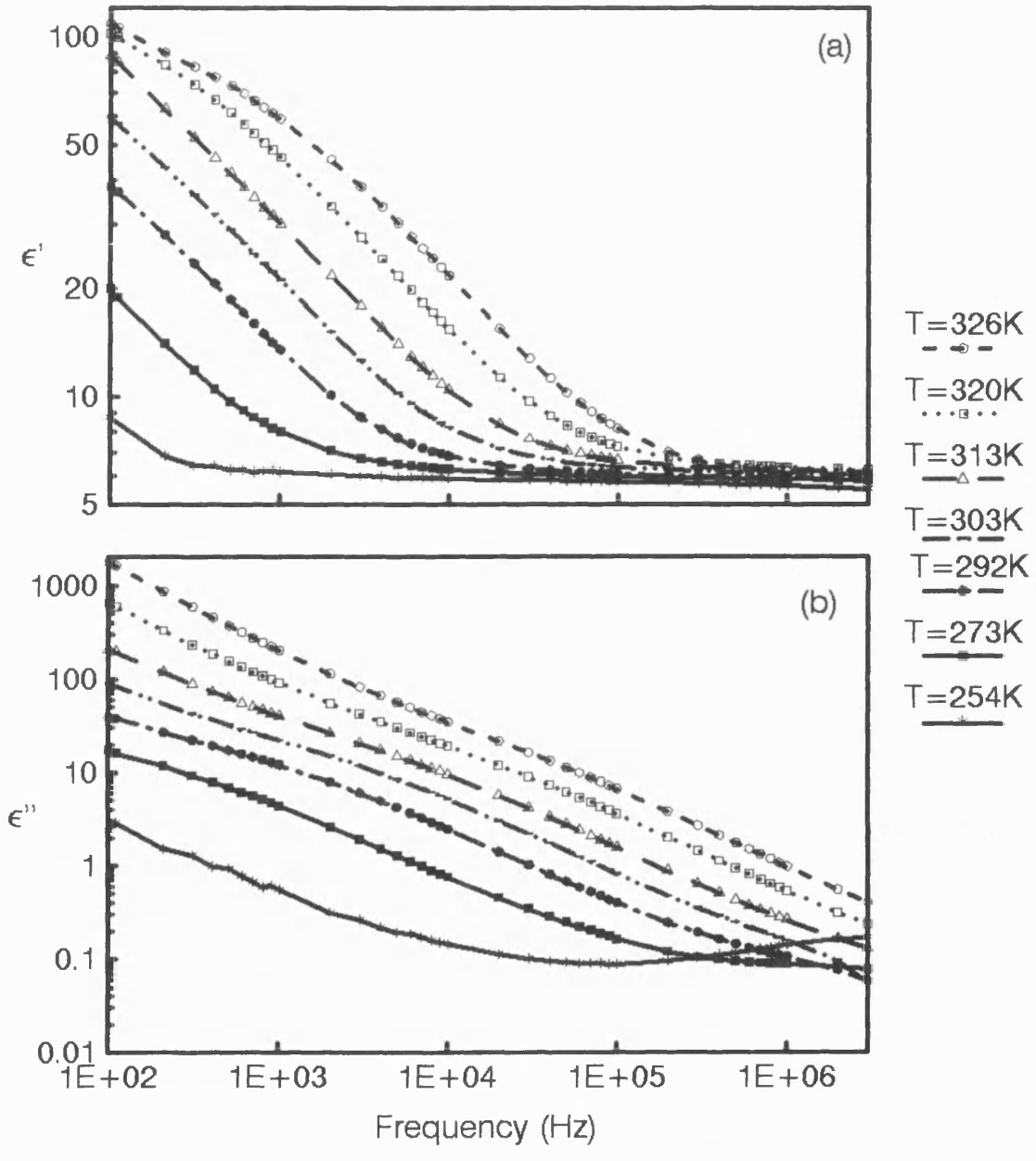

Figure 5.1. Frequency dependence of dielectric constant ϵ' (a) and loss ϵ'' (b) of PEO at selected temperatures.

arising from the d.c. conductivity from the total loss, a loss peak was obtained. From the location of this peak (200 Hz at 15 $^{\circ}C$), they concluded that it corresponded to the a relaxation observed in mechanical studies on solid PEO and therefore labelled it as the α dielectric dispersion. Similar data were obtained later by Porter and Boyd (1971) but they were not able to find any loss peak even after the contribution of the d.c. conductivity had been subtracted from the dielectric loss. This caused them to believe that, if a low frequency α dispersion did exist, it could not be resolved from the low frequency loss data. They argued that the big increase in the dielectric constant was much too large to be ascribed to a dipole-orientation relaxation process.

In general, four possible mechanisms may contribute to the low frequency dielectric behaviour of polymers:

(1) The effect of the electrode interface. Characteristically there is an apparent increase in the dielectric constant at low frequencies (Blythe 1979). Since no difference has been detected in the dielectric constant by applying different bias voltages, the contribution of this effect must be negligibly small and can therefore be ignored.

(2) The effect of d.c. conductivity. Polymers in principle also transport charge under the influence of an electric field, even for a good insulator: they have a bulk resistance which contributes to the measured dielectric properties, behaving as if in parallel with the sample capacitance. Unlike the resistive component due to the dipolar relaxation (or the frequency-dependent hopping conductivity $\sigma(\omega)$), the resistance due to this source is independent of frequency. This d.c. conductivity contributes only to the dielectric loss which becomes infinite at zero frequency and is unimportant at very high frequencies (Hill *et al.* 1969, Boyd 1980).

(3) The dipole-orientation relaxation process. This process normally involves a rapid increase in dielectric constant and a dielectric loss peak as the measurement frequency is reduced. In the case of PEO ε' increases as $f \rightarrow 0$, which suggests a possible low frequency dielectric relaxation, but there is no sign of a corresponding loss peak (Figure 5.1). To isolate any possible low frequency loss peak, the contribution of the d.c. conduction must be subtracted from the total loss. The zero-frequency intercept on the real axis of the admittance profile gives the d.c. conductance G_0. The d.c. conductivity is then obtained from

$$\sigma = G_0 d / A \tag{5.1}$$

where d is the thickness and A is the area of the sample. The d.c. conductivity of PEO has been measured here as 4.3×10^{-8} $ohm^{-1}m^{-1}$ at 292 K, which is fairly close to that reported for the samples of PEO with similar molecular weight (Wintersgill *et al.*1985, Fontanella *et al.* 1985, Bailey and Koleske 1976). When the contribution of the d.c. conductivity is subtracted, a dielectric loss curve is obtained (Figure 5.2), which still does not show any sign of a loss peak. Instead, both dielectric constant and loss have almost the same value below 1 kHz and increase as the frequency is lowered. Therefore, it is difficult to ascribe the low frequency dispersion to a simple orientation relaxation process.

(4) The effect of charge carriers. Charge carriers not only enable d.c. conduction but also make a contribution to the dielectric polarisation (Jonscher 1983). The dielectric effects of free charge carriers, such as electrons, only become significant at frequencies of the order of the reciprocal collision time, which falls in the 10-100 GHz range. In the frequency range used in this work, effects of free carriers are negligible and only the localised charge carriers, which are ions, may contribute to dielectric polarisation. This conduction mechanism probably gives rise to the low frequency dielectric behaviour. If a diffusive transport mechanism is assumed, it can be shown (Jonscher 1983) that the complex dielectric constant obeys the relationship

$$\varepsilon(\omega) \propto (1-i)\omega^{-1/2} \tag{5.2}$$

Equation (5.2) has two important implications: (1) the real and imaginary parts are equal and there is no sign of any loss peak, (2) the real and the imaginary components increase indefinitely as frequency is lowered. It can be seen from Figure 5.2 that the experimental data at 292K obey these requirements quite well below 1 kHz. These results provide strong evidence that the low frequency dispersion of PEO arises mainly from the localised charge carrier conduction, which is characterised by a diffusive ion transport mechanism. The slope of both the log ε' and log ε'' against log (f) at low frequencies is about -1/3 instead of the -1/2 predicted by the theory. It is also noted that at high temperatures near the melting point of PEO the ε' curve in Figure 5.1(a) is flattening out at low frequencies. These observations suggest that there may be more than one transport mechanism present at low frequencies.

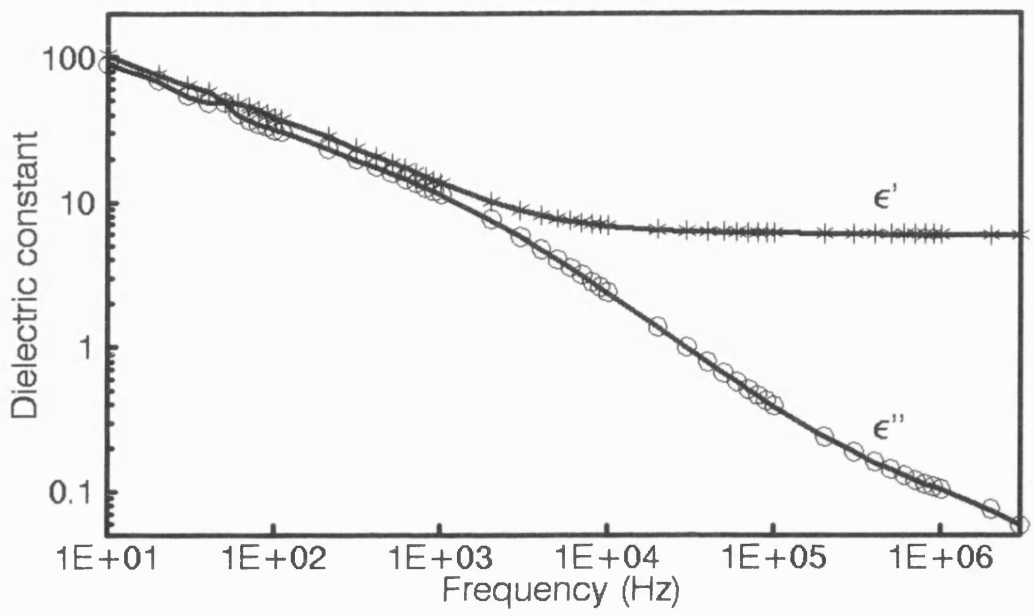

Figure 5.2. Frequency dependencies of the dielectric constant ϵ' and loss ϵ'' of PEO at 292K. The contribution of the d.c. conducitvity σ has been subtracted from the dielectric loss. Note that ϵ' and ϵ'' approach each other below about 1kHz and continue to increase as the frequency is reduced further, as predicted by the diffusive transport mechanism of the localized charge carriers.

Another slightly different model, the conduction relaxation model (Macedo, Moynihan and Bose 1972) can also lead to a low frequency dispersion in ε′, arising from the long range ionic diffusion process. By introducing a distribution of conduction relaxation times, this model predicts a constant ε′ at lowest frequencies, which seems consistent with the low frequency behaviour of PEO at high temperatures. Due to lack of sufficiently low frequency data, we are not going to discuss these models further in detail, but to conclude that the diffusive transport of ions is dominant in the low frequency conductivity and consequently leads to the low frequency dispersion of the dielectric constant of PEO .

To highlight further the physical origin of the low frequency dispersion of PEO, the frequency dependence of the dielectric constant ε' in Figure 5.1(a) has been normalised to 254 K to form a master curve (Figure 5.3(a)). If the log frequency shift obtained from the displacement of the reference point in Figure 5.3 is plotted against 1/T, a linear relationship between the two (Figure 5.3(b)) is seen to exist; the straight line, which is a least-square fit, has a gradient of -3.2×10^{3}. This leads to the empirical relationship:

$$\log f - \log f_0 = 3.2\times10^{3}\left[\frac{1}{T_0}-\frac{1}{T}\right] \tag{5.3}$$

Hence, for the low frequency dielectric relaxation concerned, the relaxation time can be expressed as

$$\ln\tau = 7.4\times10^{3}/T + C \tag{5.4}$$

where C is a constant. Equation (5.4) has an Arrhenius form:

$$\ln\tau = \frac{\Delta U}{RT} + C \tag{5.5}$$

which would correspond to a relaxation model based on thermal activation over a potential-energy barrier. By comparing equation (5.4) with equation (5.5), the activation energy for this relaxation process is obtained as:

$$\Delta U = 6.2\times10^{4}\text{J/mole.}$$

The gradient of the dielectric loss curves at the high frequency end changes from negative to positive as the temperature is reduced (Figure 5.1(b)). This indicates the onset of another relaxation process. Corresponding to this increase of the gradient, the

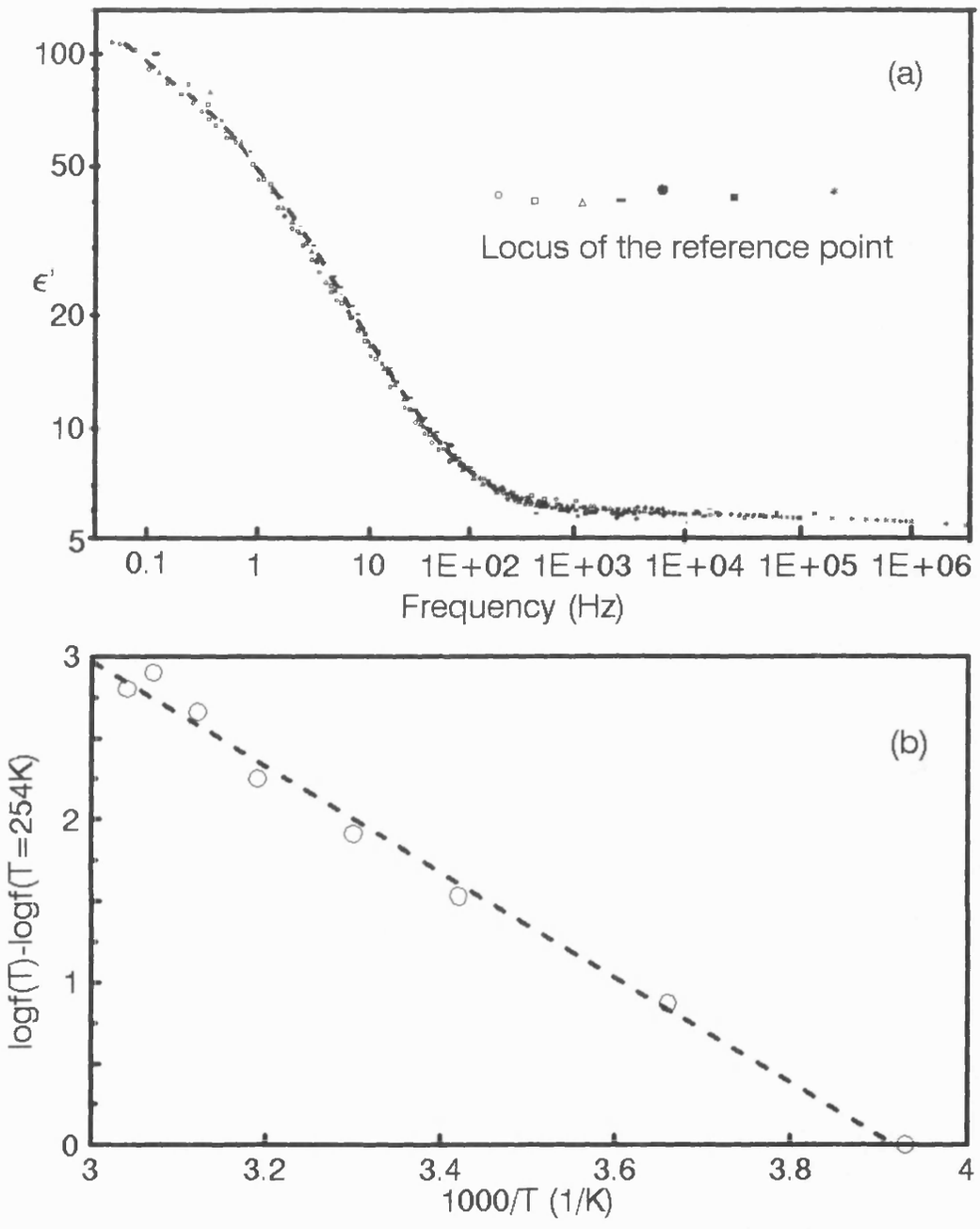

Figure 5.3. The master curve (a) constructed by normalising the frequency dependence of the dielectric constant ϵ' in Figure 1(a) to 254K, and (b) the temperature dependence of the shifting factor used to construct the master curve.

dielectric constant begins to fall as temperature is decreased (Figures 5.1(a) and 5.6(a)). As will be seen in the next section, this high frequency relaxation is the same as that indicated by the large peak observed at about 240 K in the temperature dependence data and can be readily related to the glass-rubber transition.

5.3. Temperature dependence of the dielectric constant and dielectric loss

The temperature dependences of the dielectric constant and dielectric loss of PEO at selected frequencies are given in Figure 5.4. The dielectric constant increases smoothly with temperature until about 240 K, where it increases much faster than at low temperatures and forms a step. Corresponding to this step, there is a peak in the dielectric loss (Figure 5.4(b)). The magnitude of this peak decreases dramatically as the measurement frequency is lowered. The position of the peak and the step shift to higher temperatures as the measuring frequency is increased. It is also noted that the dielectric loss at 100 kHz is greater than that at 1 MHz between 120 K and 210 K (Figure 5.4(b)). This suggests that there may be a broad relaxation peak in this temperature range, appearing when the measurement frequency is reduced.

The relaxation peaks (at 240 K for 1 MHz and at 235 K for 100 kHz) in the temperature dependence of the dielectric loss (Figure 5.4(b)) are consistent with those reported by Ishida *et al.* (1965), and Wintersgill *et al.* (Fontanella *et al.* 1983, Wintersgill *et al.* 1985, Fontanella *et al.* 1985). Ishida *et al.* have labelled this absorption peak as the α_a absorption, while it is denoted as β-relaxation by McCrum *et al.* (1967). To avoid any further confusion, it will be labelled as α_a-relaxation in the following discussion.

The α_a-relaxation is almost certainly due to the micro-Brownian motions of the chain (glass-rubber relaxation) in the non-crystalline regions of the polymer (McCrum *et al.* 1967)]. If log (f) is plotted against $1/T_{max}$, the data obtained agrees well with those measured by Connor *et al.* (1964) on a PEO sample of molecular weight 8.4×10^5, which is close to that (6×10^5) of the sample studied in this work. From the log (f)

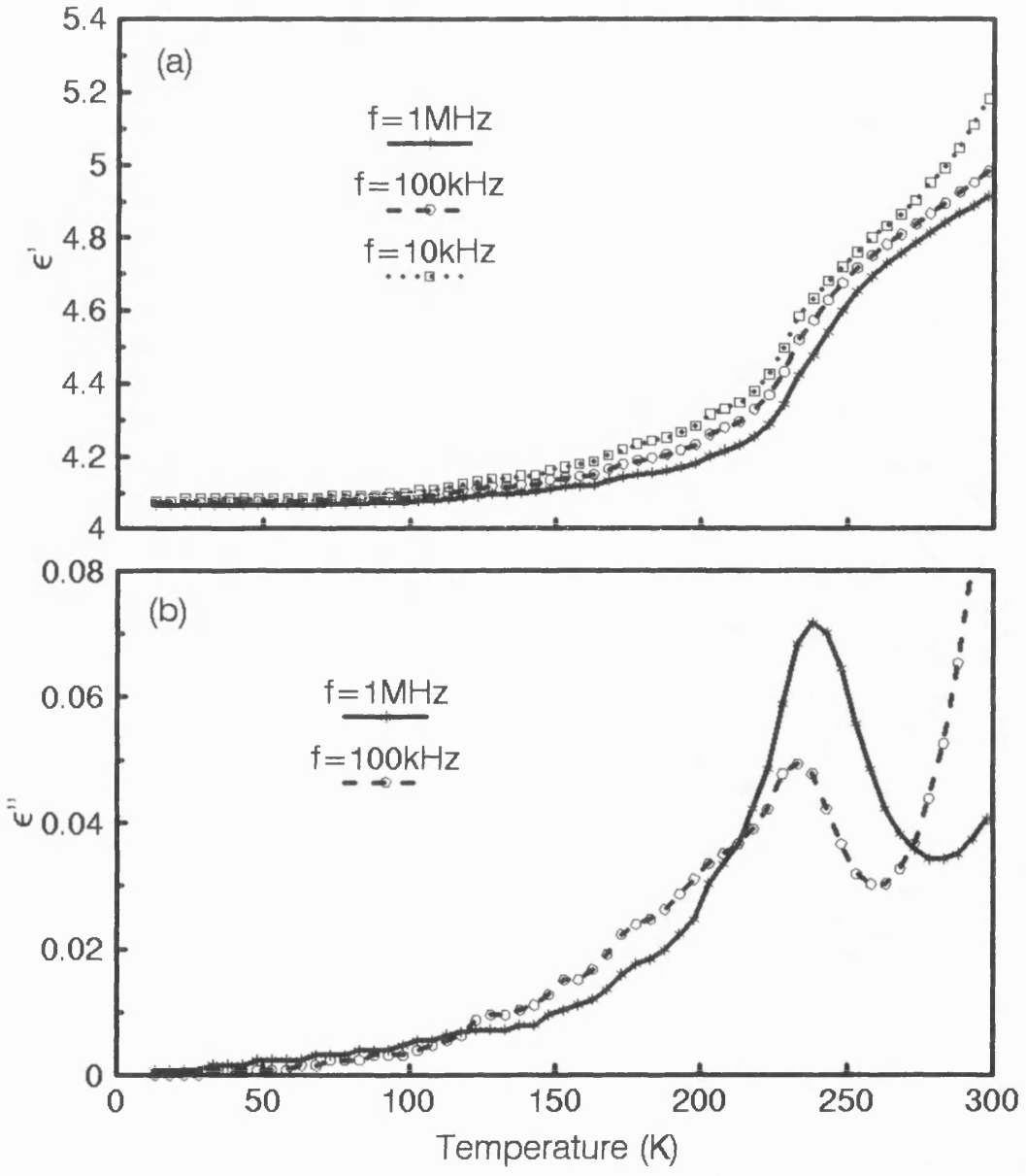

Figure 5.4. Temperature dependence of dielectric constant ϵ' (a) and loss ϵ'' (b) at selected frequencies.

versus $1/T$ plot, it is expected that at about 10 MHz in the frequency dependence of the dielectric loss at 254 K there will be a loss peak which is associated with the glass transition process. This is true (Figure 5.1(b)).

Normally, for a certain measurement frequency the α_a-peak appears at a higher temperature than the γ-peak and for a certain temperature, the α_a-relaxation tends to appear at lower frequencies than the γ-relaxation (Hedvig 1977). This is so at low temperatures, but the γ-relaxation moves rapidly into the α_a-region as the temperature is raised. At about 240 K the two relaxation processes overlap each other, forming a mixed relaxation peak in the frequency range 5 to 7 MHz in the frequency dependence of the loss curve. Alternatively, if the measurement frequency is between 5 and 7 MHz, one cannot distinguish the two peaks in the temperature dependence of the loss curve. This explains why there is no γ-peak in Figure 5.4(b). The broadening of the α_a-peak at 100 kHz at the low temperature side, and the relatively larger value of loss at this frequency in the temperature range between 120 K and 210 K, must be a consequence of the separation of these two peaks when the measurement frequency is reduced. At temperatures above 250 K, the α_a-peak tends to appear at higher frequencies than the γ-peak, and these two peaks are practically indistinguishable in the frequency dependence of the dielectric loss. The high frequency loss peak evidenced in Figures 5.1(b) and Figure 5.6(b) is most likely to arise from a mixture of the α_a- and γ-peak.

The variation of the magnitude of the loss peak with frequency (or temperature) can be explained by considering that the peak at 240 K for the 1 MHz data is a mixture of α_a- and γ peaks. As the measurement frequency is reduced, the γ-peak moves more quickly towards low temperature than the α_a-peak does, so that the two peaks tend to separate, decreasing the magnitude of the mixed peak.

5.4.The effect of hydrostatic pressure on the frequency dependence of the dielectric constant and dielectric loss of PEO

5.4.1. The experimental results.

The frequency dependences of the dielectric constant and dielectric loss have been measured at pressures up to 0.25 GPa at selected temperatures. Figure 5.5 shows the results obtained at room temperature. Although the application of hydrostatic pressure does not change the dielectric constant much at high frequencies (Figure 5.5(a)), its effect is enormous at low frequencies: the whole curve shifts towards lower frequency as the pressure is increased. The dielectric loss curve shows similar behaviour to that of the dielectric constant, the whole curve moves towards lower frequencies when the sample is stressed. An interesting feature of the dielectric loss appears at high frequencies, where the slope of the curves gets smaller with increasing pressure and all the curves converge to one point at 3 MHz (Figure 5.5(b)). As the temperature is reduced, this point of intersection moves towards lower frequencies and the curves begin to show positive gradients at the high frequency end (Figure 5.6(b)). Applying pressure moves the intersection point further to lower frequencies and eventually a broad peak appears at about 1 MHz (Figure 5.6(b)). Corresponding to this peak, the dielectric constant drops rapidly (Figure 5.6(a)), which suggests that a relaxation process is occurring.

5.4.2. The low frequency dispersion.

Applying hydrostatic pressure to PEO at room temperature changes the frequency response of the dielectric constant; the logarithmic plots of the dielectric constant versus frequency shift to lower frequencies without changing shape (Figure 5.5(a)). The application of hydrostatic pressure has the same effect as decreasing the temperature. To study the effect of pressure on the low frequency dispersion, the data at different pressures in Figure 5.5(a) have been normalised to atmospheric pressure (P=0 GPa) to form the master curve shown in Figure 5.7(a). All the data obtained from six sets of measurements carried out at different pressures join satisfactorily into a single curve, showing that the shape of the frequency response remains invariant under the effect of both temperature and hydrostatic pressure. Increase of pressure slows

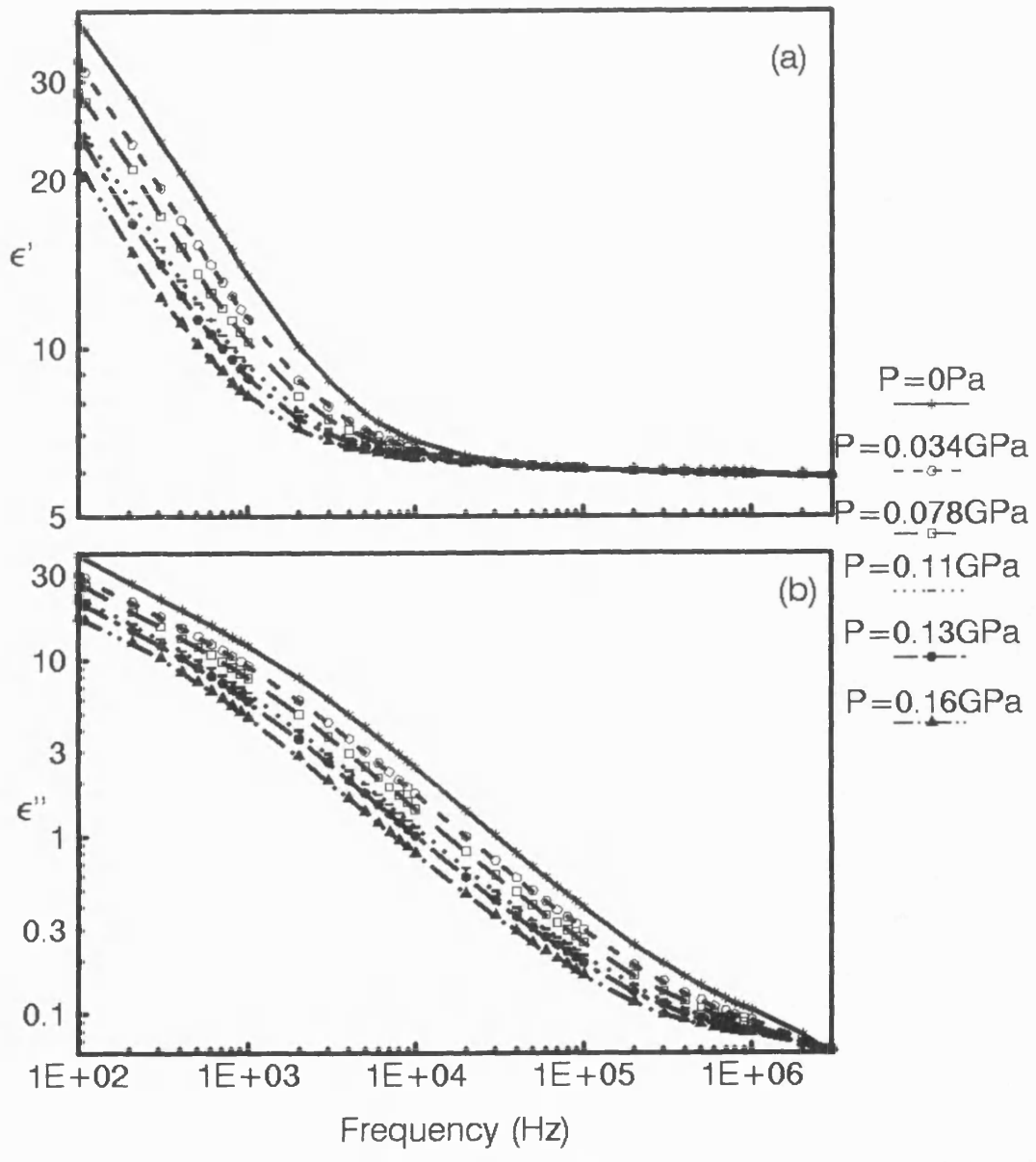

Figure 5.5. Frequency dependence of the dielectric constant ϵ' (a) and and loss ϵ'' (b) of PEO at selected pressures at 292K.

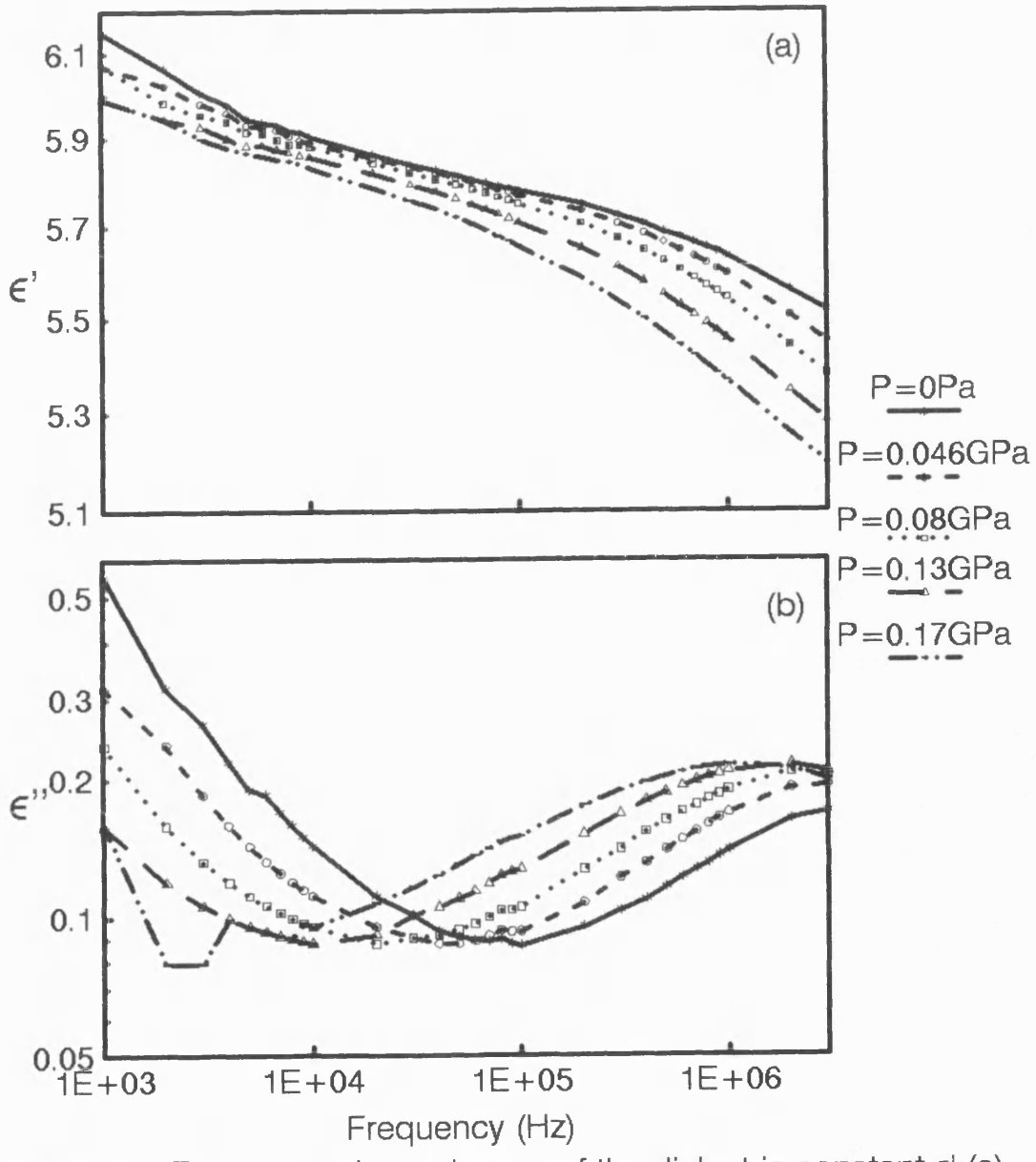

Figure 5.6. Frequency dependences of the dielectric constant ϵ' (a) and loss ϵ'' (b) of PEO at selected pressures at 254K.

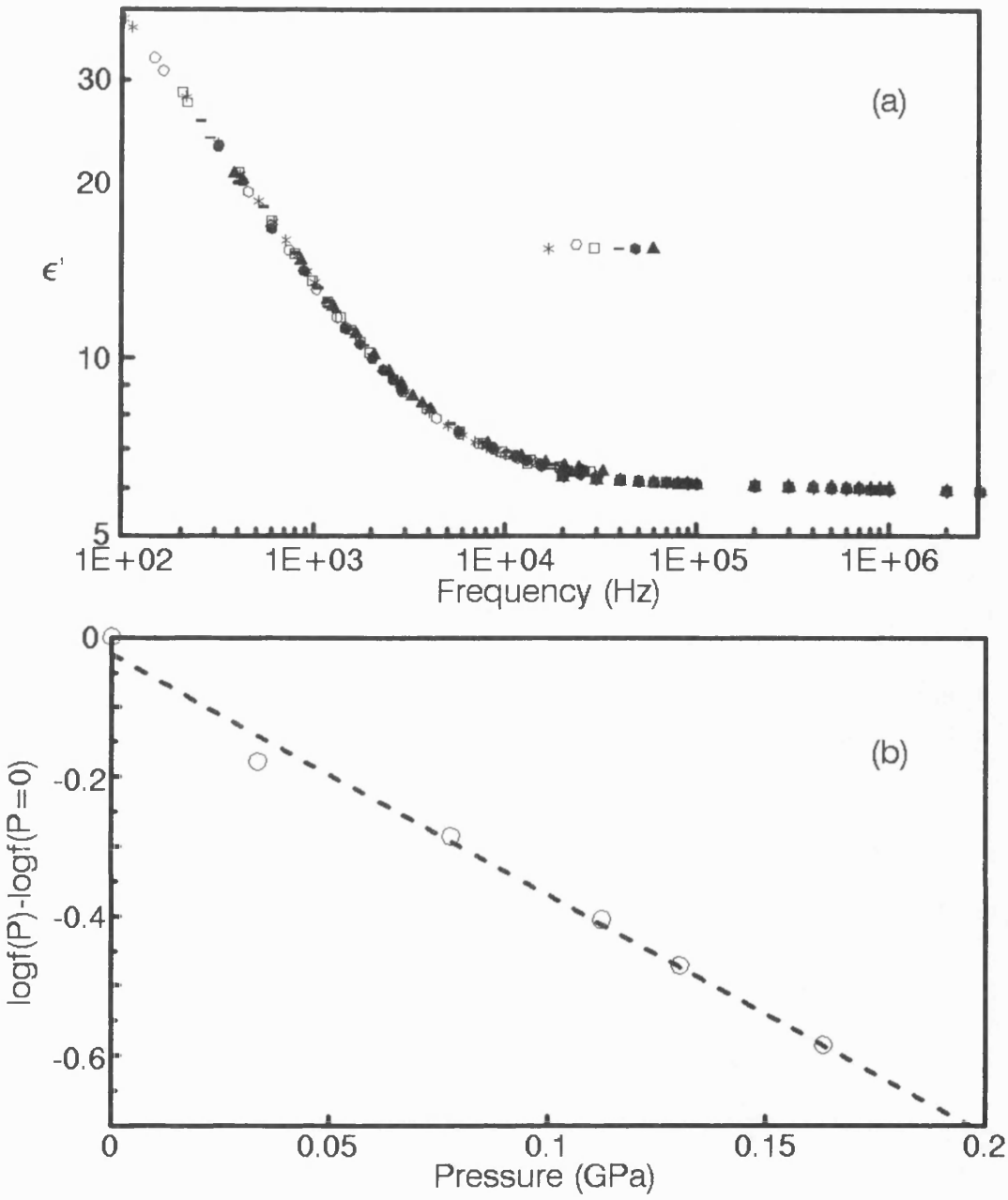

Figure 5.7. The master curve (a) constructed by normalising the frequency dependence of the dielectric constant ϵ' in Figure 5(a) to atmospheric pressure, and (b) the temperature dependence of the shifting factor used to construct the master curve.

down the rate process without affecting the shape of the spectra. The effects of an increase in pressure are nullified by an increase of temperature. The shifting factors in log frequency, determined from the trace of the reference point, are given in Figure 5.7(b) as a function of pressure. The shifting factor is proportional to the pressure; the straight line of slope -3.4×10^{-9}/Pa in Figure 5.7(b) is the least-square fit to the 292 K data. Therefore, for the low frequency relaxation process,

$$\log f - \log f_0 = -3.4\times10^{-9}(P - P_0) \tag{5.6}$$

and the corresponding relaxation time can be given as

$$\ln\tau = 7.9\times10^{-9}P + C_2 \tag{5.7}$$

where C_2 is a constant. Supposing that increase pressure from P_0 to P results in a shift in log(f) which can be nullified by increasing the temperature from T_0 to T, comparison of equations (5.6) and (5.3) gives

$$3.2\times10^{3}\left[\frac{1}{T_0}-\frac{1}{T}\right] = 3.4\times10^{-9}(P - P_0)$$

and this leads to

$$(\partial T/\partial P)_f = 3.4/3.2\times10^{-12}T^2 \approx 10^{-7}\,K/Pa$$

at 292 K.

The activation volume ΔV can be obtained directly from the pressure dependence of the relaxation time τ (Saito *et al.* 1968):

$$\Delta V = RT\left[\partial(\ln\tau)/\partial P\right]_T \tag{5.8}$$

where R is gas constant. The activation volume of the low frequency relaxation of PEO at 292 K has been calculated as $\Delta V = 1.9\times10^{-5}m^3/mole$. Taking the density of PEO (Bartolotta *et al.* 1991) as 1240 kg/m^3, the molar volume of the monomer unit is obtained as V_m= 3.5×10^{-5} m^3/mole. This leads to a ratio of activation volume to molar volume $\Delta V/V_m \approx 0.5$. This result suggests that the low frequency dispersion involves only small atomic groups with a size less than that of a monomer.

5.4.3. The rubber-glass transition.

In the temperature dependence of dielectric loss (Figure 5.4(b)), the α_a-relaxation peak is observed at 240 K at a measurement frequency of 1 MHz. In order to see this peak appear at 1 MHz in the frequency dependence of the loss, the temperature must be reduced to 240 K. From Figure 5.6(b), we can conclude that the application of a pressure of 0.17 GPa is equivalent to a 14 K decrease in temperature. The value of $(\partial T_g / \partial P)_f$ is then estimated as 0.8×10^{-7} K/Pa which is very close to that calculated for the low frequency dispersion process ($\sim10^{-7}$ K/Pa). This result is in excellent agreement with the value $0.878\sim0.918\times10^{-7}$ K/Pa found for the glass transition in PEO by Wintersgill *et al.* (1985). This suggests that the high frequency loss peak, revealed by application of pressure, arises mainly from the glass transition relaxation; the contribution of the γ-relaxation, if present, is not important. That the pressure has almost the same effects on both the low and high frequency relaxation processes indicates that the low frequency ionic conductivity may be associated with the glass transition to some extent.

The thermodynamic phase transition behaviour suggests that the rubber-glass transition might be regarded as a second-order phase transition, which requires

$$\partial T / \partial P = \Delta k / \Delta\alpha \tag{5.9}$$

and

$$\partial T / \partial P = TV\Delta\alpha / \Delta C_P \tag{5.10}$$

where Δ represents the difference between the properties above and below the transition and k, α, V, T, C_p are compressibility, thermal expansion coefficient, volume, temperature and heat capacity respectively. In fact, equation (5.9) can be regarded as a consequence of the free-volume theory. A basic hypothesis of this theory is that the free volume is constant up to T_g and then increases linearly with increasing temperature. The fractional free volume can therefore be written as

$$f = \mathrm{v}_f / \mathrm{v} = f_g + \alpha_f (T - T_g) \tag{5.11}$$

where f_g is the fractional free volume at the glass transition T_g, v is the total macroscopic volume and α_f is the coefficient of expansion of the free volume. This leads to the relation

$$\partial T / \partial P = k_f / \alpha_f \tag{5.12}$$

where k_f is free volume compressibility and α_f is the free volume expansion coefficient, which is equivalent to equation (5.9).

Bartolotta *et al.* (1991) have measured the temperature dependence of the dynamic modulus in PEO with a molecular weight of 6×10^5 at 30 Hz. From their data the difference between the compressibility of PEO above and below the glass transition can be calculated as $\Delta\kappa=4.6\times10^{-10}$/Pa. The thermal expansion coefficient of PEO at room temperature is 2.0×10^{-4}/K (Bartolotta *et al.* 1991). Thus the right side of equation (5.9) can be estimated as 4.6×10^{-6} K/Pa, which is much larger than the value of $\partial T_g / \partial P$ of 0.8×10^{-7} K/Pa obtained for the glass transition of PEO. Similarly, taking the glass transition temperature T=213 K, $\Delta\alpha=2\times10^{-4}$/K, ρ=1240 kg/m^3 and $\Delta C_p \approx 100$ Jkg^{-1}K^{-1}, the right side of equation (5.10) is given by

$$TV\Delta\alpha / \Delta C_P = \frac{T\Delta\alpha}{\rho\Delta C_P} \approx 3.4\times10^{-7} K / Pa \tag{5.13}$$

which is closer to the measured $\partial T_g/\partial P$.

The above results are consistent with those observed at the glass transition of a number of polymers (O'Reilly 1962) and glasses (Elliot 1990). In general, equation (5.10) is usually obeyed within experimental error but the values of $\Delta\kappa/\Delta\alpha$ are appreciably higher than those of $\partial T / \partial P$ at the glass transition. Therefore on this evidence it appears that the glass transition is not a simple second-order phase transition; the free-volume theory, although having been very successful in interpreting the well known WLF equation, needs more justification as an approach to describing the glass transition behaviour of polymers under pressure.

The activation volume for this relaxation at 254 K is calculated as

$$\Delta V = RT\left[\partial(\ln\tau)/\partial P\right]_T = 28\times10^{-5} \text{ m}^3\text{/mol.}$$

This value is ten times larger than that for the gamma relaxation (Wintersgill *et al.* 1985) as can be expected for a large scale segmental motion at the glass transition.

5.5. Conclusions about the dielectric properties of PEO

In summary, the following central conclusions have been reached:

(1) The values of the dielectric constant and the conductivity of PEO are strongly dependent on the frequency, temperature and pressure.

(2) Below 1 kHz log ε" has almost the same value as that of the log ε' and increases linearly with decreasing log frequency, after the contribution of the d.c. conductivity has been subtracted from the total loss. There is no sign of any loss peak which can be related to the low frequency dispersion. This dielectric behaviour is consistent with the predictions of a theoretical model (Jonscher 1983) in which the low frequency dispersion is described as a consequence of the diffusive transport of the localised charge carrier, rather than an α relaxation as reported previously.

(3) Master curves have been constructed from the pressure and temperature dependence of the dielectric constant data, and $(\partial T/\partial P)_f$ has been determined as 10^{-7} K/Pa. The activation energy and the activation volume for this dispersion relaxation process have also been obtained as 6.2×10^4 J/mole and 1.9×10^{-5} m^3/mole respectively.

(4) The application of hydrostatic pressure enables the α_a-loss peak of PEO to be observed near room temperature in a frequency range which is accessible using the equipment available to us. $(\partial T/\partial P)_f$ has been obtained as 0.8×10^{-7} K/Pa which agrees well with that reported previously. The activation volume of the α_a-relaxation is calculated as 2.8×10^{-5} m^3/mole which is much larger than that for the γ-relaxation, as can be expected from the activation process of large scale segmental molecular motion at the glass transition. It has been found that the glass transition of PEO cannot simply be regarded as a second order phase transition. The free volume model does not interpret the effect of pressure on the glass transition in a completely satisfactory fashion.

CHAPTER 6. TEMPERATURE, FREQUENCY AND HYDROSTATIC PRESSURE DEPENDENCES OF DIELECTRIC PROPERTIES OF POLYETHYLENE AND POLYETHYLENE CABLE INSULATION

6.1. The dielectric constant and loss of crosslinked polyethylene at room temperature

The dimensions of the samples, the dielectric constants and the dielectric losses of crosslinked polyethylenes, measured at room temperature at 10kHz, are given in Table 6.1. The values of the thickness have been obtained by averaging ten readings across the sample area (A). The dielectric constants of polyethylenes S185/P6/94 and P42 are the same while those of polyethylene P40 and S188/S299/94 are larger (Table 6.1). The dielectric losses of these polyethylenes are zero within the experimental error.

Table 6.1. Sample dimension and the dielectric constant ε' and loss ε'' measured at 10kHz for crosslinked polyethylenes at room temperature.

Sample	Thickness (mm)	Area (cm^2)	ε'	ε''
S185/P6/94	0.251±0.001	3×3	2.274±0.005	<0.003
S186/P40/94	0.208±0.001	3.871	2.313±0.005	<0.003
S187/P42/94	0.194±0.001	3.871	2.274±0.005	<0.003
S188/S299/94	0.254±0.001	2×2.5	2.296±0.005	<0.003

6.2. The frequency and temperature dependence of the dielectric constant and loss of crosslinked polyethylene and polyethylene cable insulation

The dielectric constant and the dielectric loss of the four crosslinked polyethylene plaque specimens have been measured as functions of frequency and temperature from 290K to 403K. The results are given in Figures 6.1 to 6.8. The dielectric constant decreases slightly as the measurement frequency is increased (Figures 6.1, 6.3, 6.5 and 6.7). For example, it changes from 2.301 at 1 kHz to 2.286 at 4 MHz for sample S299 at room temperature and from 2.278 at 1 kHz to 2.269 at 4 MHz for sample P6. The values of the dielectric loss are near zero for all the samples in this frequency range and have therefore not been presented here.

The temperature dependence of the dielectric constant of the crosslinked polyethylenes is shown in Figures 6.2, 6.4, 6.6 and 6.8. It can be seen that polyethylene P6 has a similar dielectric behaviour to that of polyethylene S299 (Figures 6.2 and 6.8). The dielectric constant decreases just above room temperature and then tends to level off until 350K, where a sharp drop is observed (Figures 6.2 and 6.8). The dielectric constant of P40 and P42 near room temperature (Figures 6.4 and 6.6) decreases **smoothly** with temperature up to about 380K and then drops sharply until 390K, where it tends to change with the same gradient as that below 380K; this behaviour is somewhat different from those of P6 and S299. The dispersion of the dielectric constant becomes smaller as the temperature is increased. No notable effects of temperature on the dielectric loss of these polyethylenes have been observed.

The frequency dependences (10^{-2}-10^{5} Hz) of the dielectric constant and loss of crosslinked polyethylene P6, S299, P40 and P42 at room temperature and atmospheric pressure are shown in Figure 6.9. These data have been obtained using the Model DS2560RL Dielectric Spectrometer (DS), which can cover a very wide range of frequency. The dispersion in the dielectric constant of these polyethylenes observed using the HP unit has been confirmed: the dielectric constant decreases with increasing frequency. The dielectric constant and loss for the four samples measured at 10 kHz

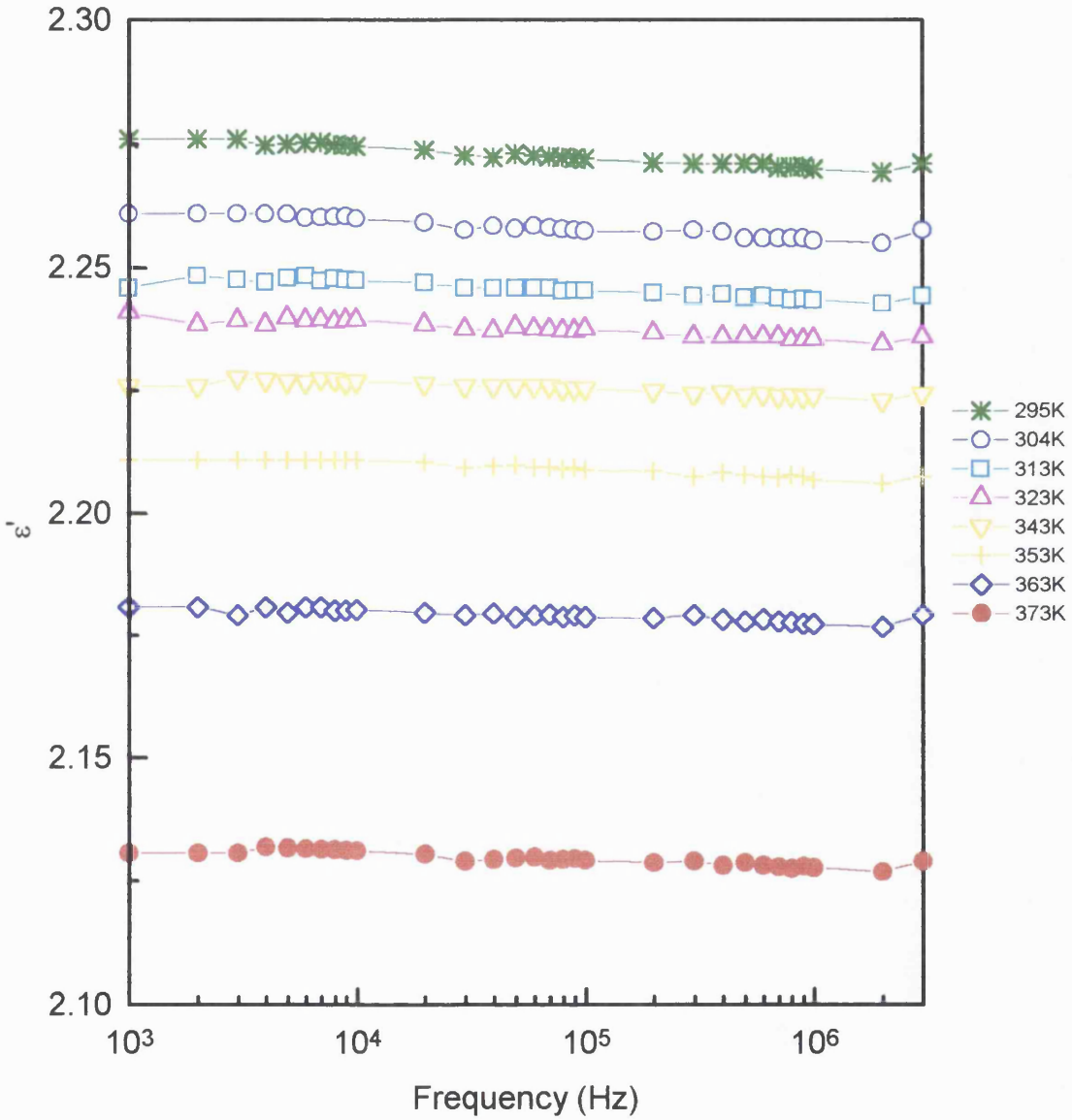

Figure 6.1. Frequency dependence of dielectric constant of crosslinked polyethylene (S185/P6/94) at selected temperatures.

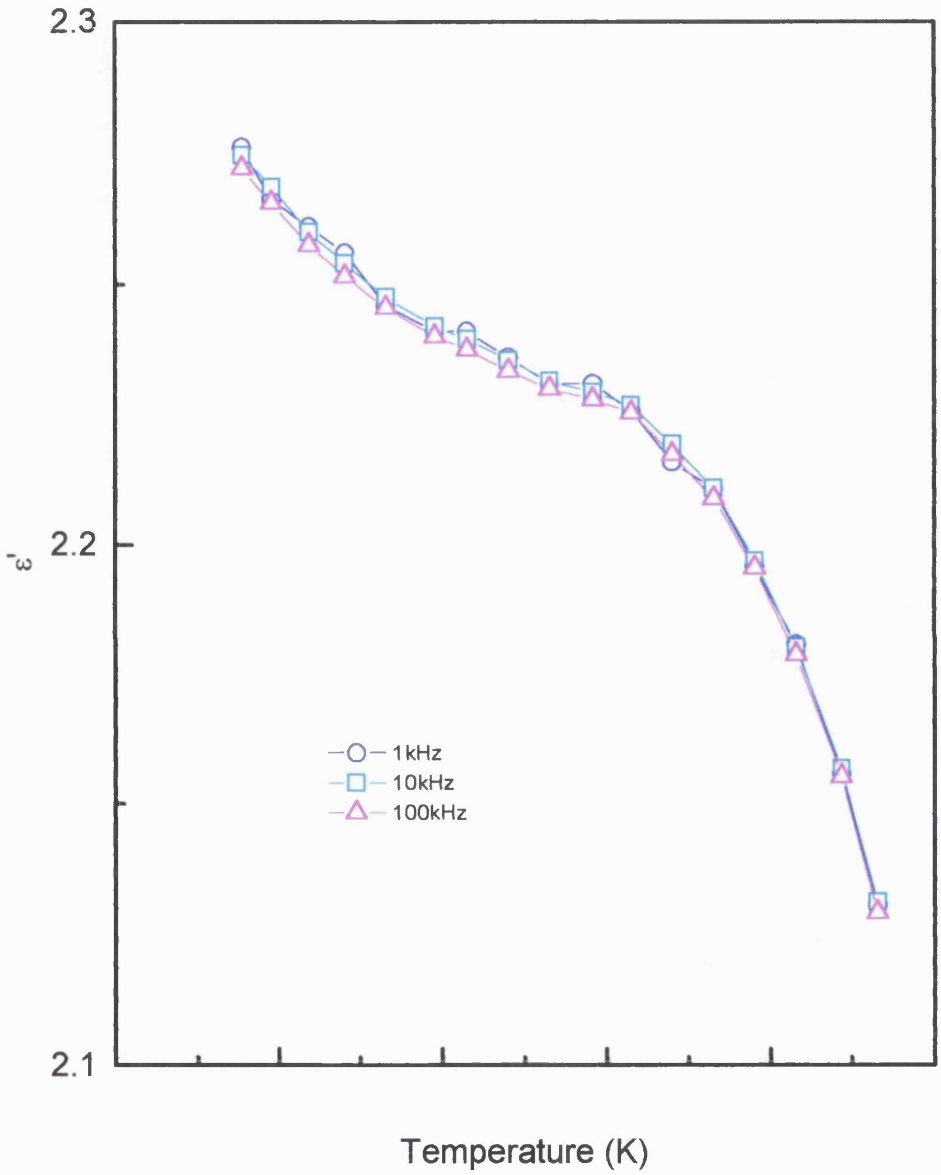

Figure 6.2. Temperature dependence of dielectric constant of crosslinked polyethylene (S185/P6/94) at selected frequencies.

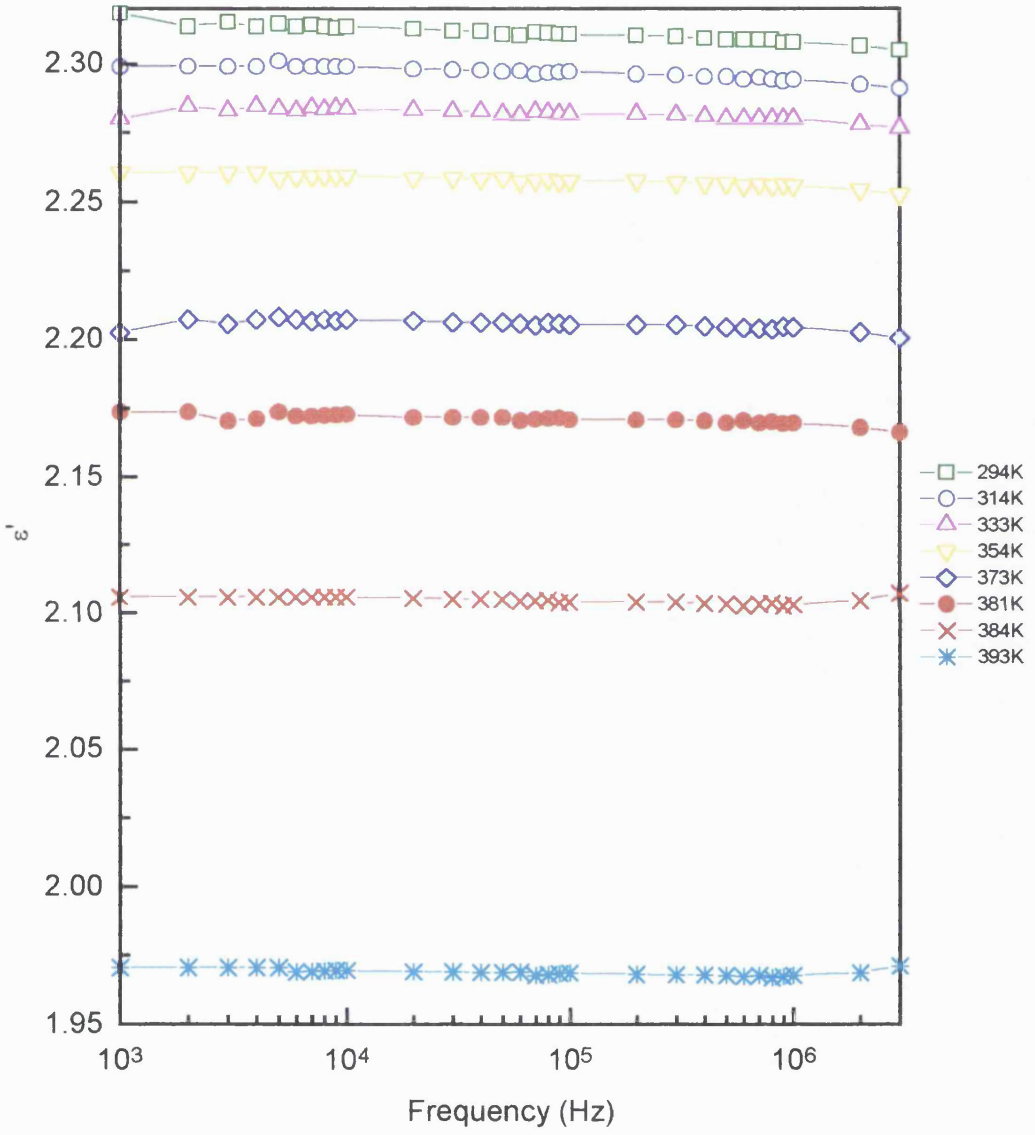

Figure 6.3. Frequency dependence of dielectric constant of crosslinked polyethylene (S186/P40/94) at selected temperatures.

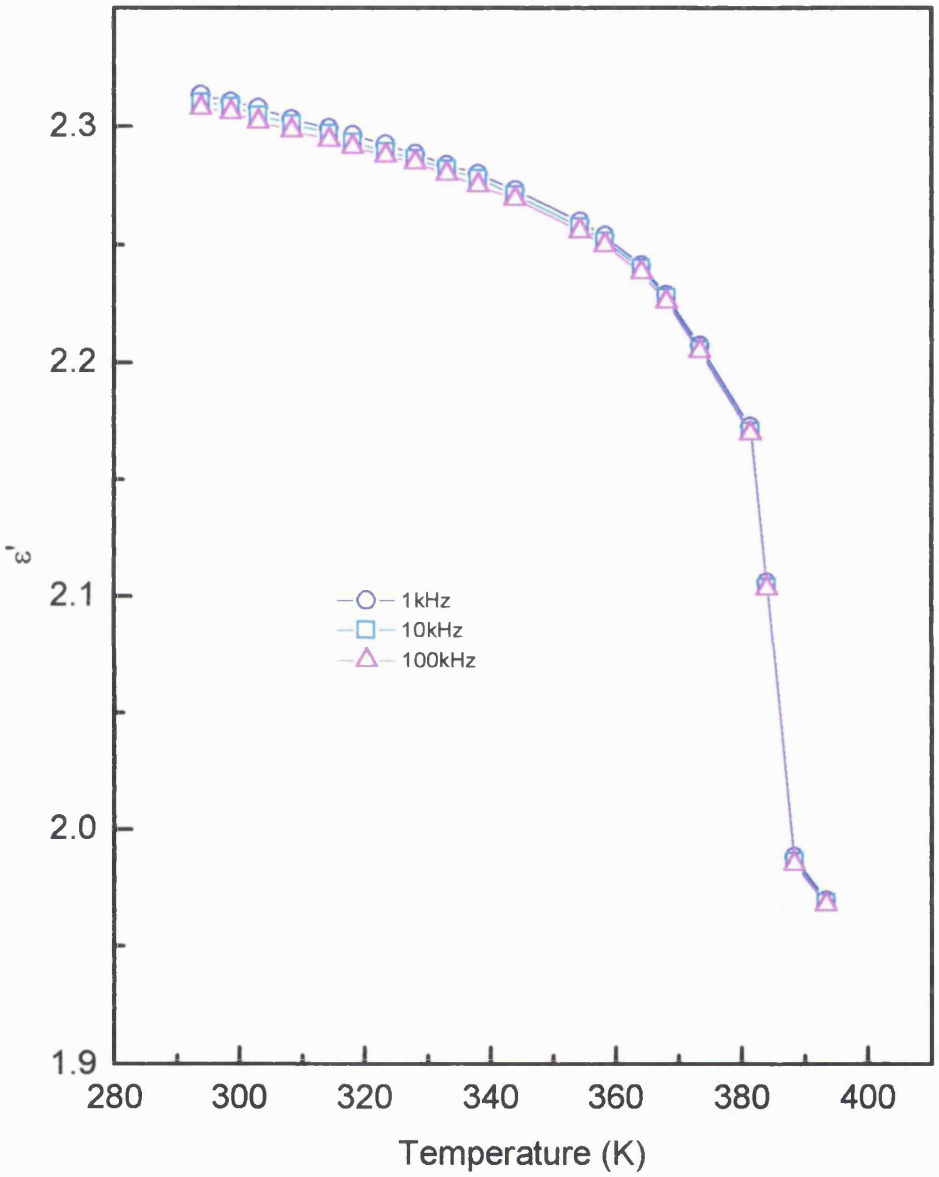

Figure 6.4. Temperature dependence of dielectric constant of crosslinked polyethylene (S186/P40/94) at selected frequencies.

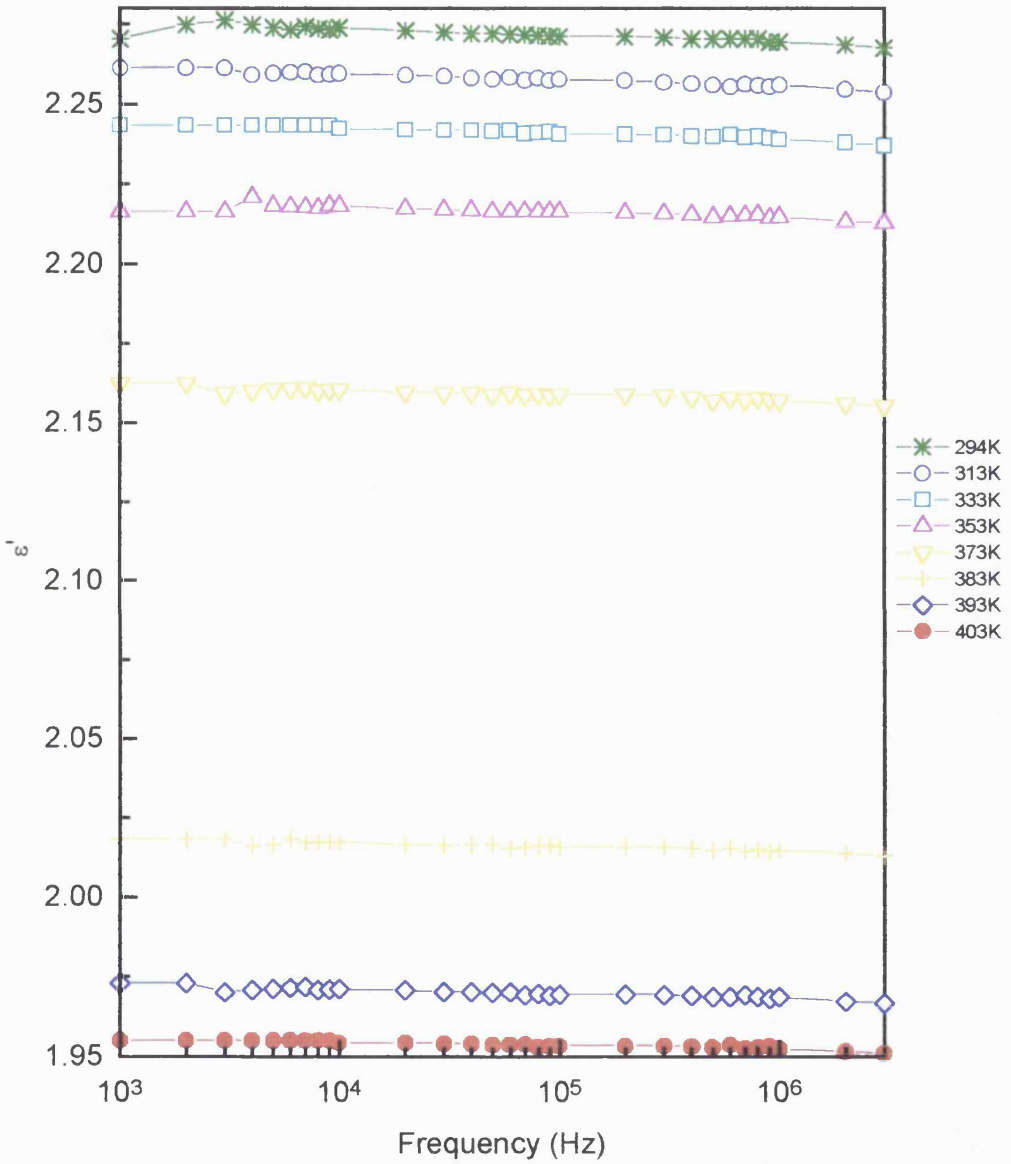

Figure 6.5. Frequency dependence of dielectric constant of crosslinked polyethylene (S187/P42/94) at selected temperatures.

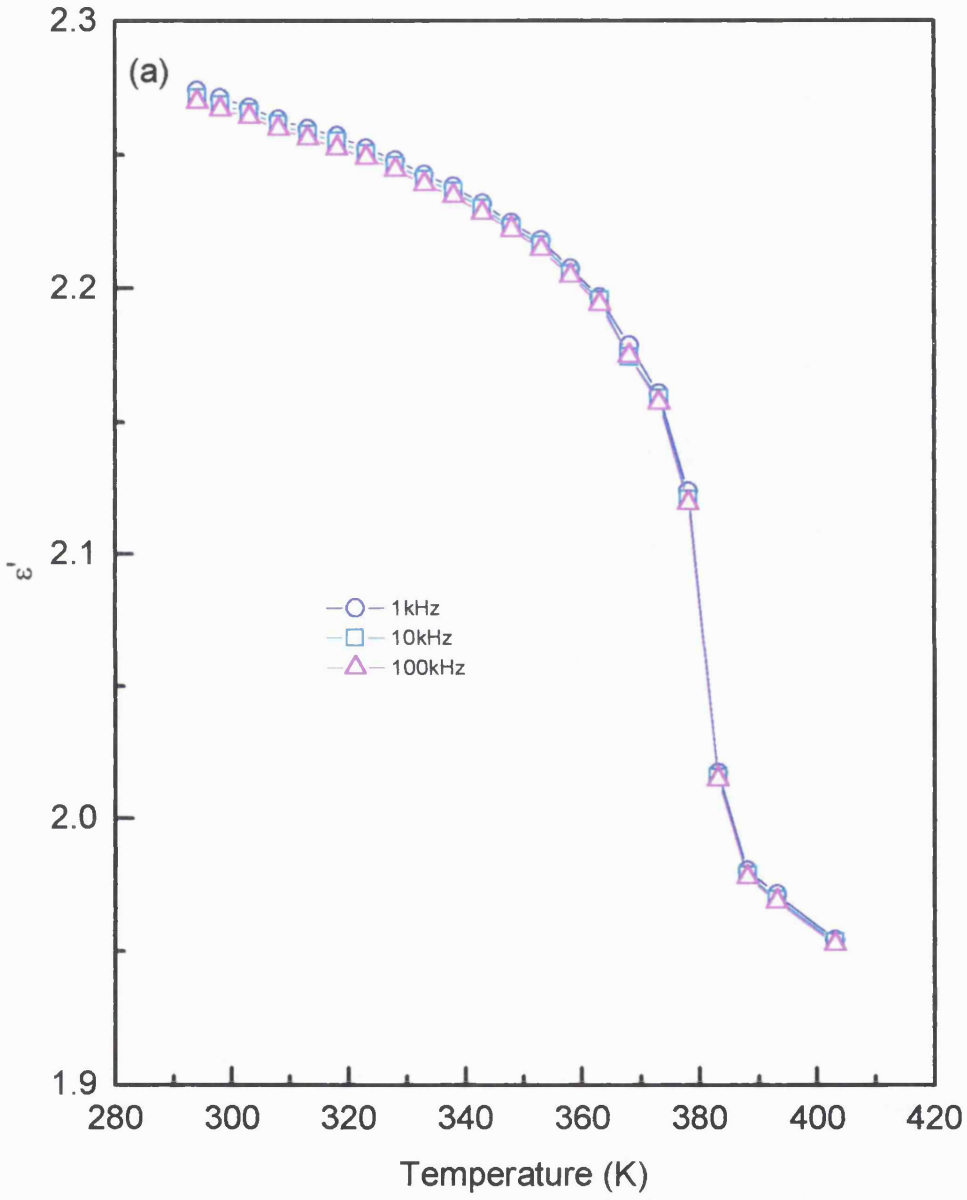

Figure 6.6. Temperature dependence of dielectric constant of crosslinked polyethylene (S187/P42/94) at selected frequencies.

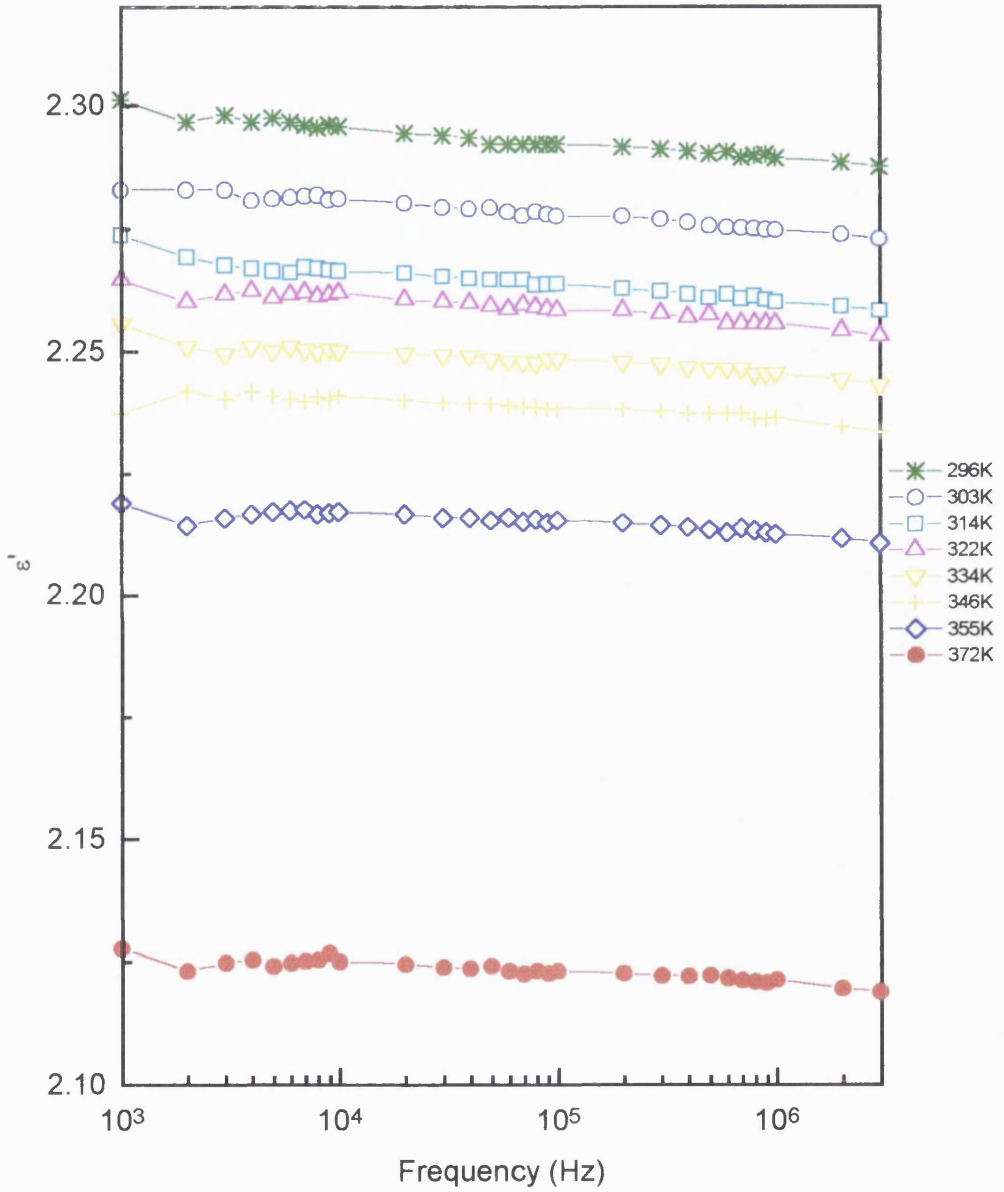

Figure 6.7. Frequency dependence of dielectric constant of crosslinked polyethylene (S188/S299/94) at selected temperatures.

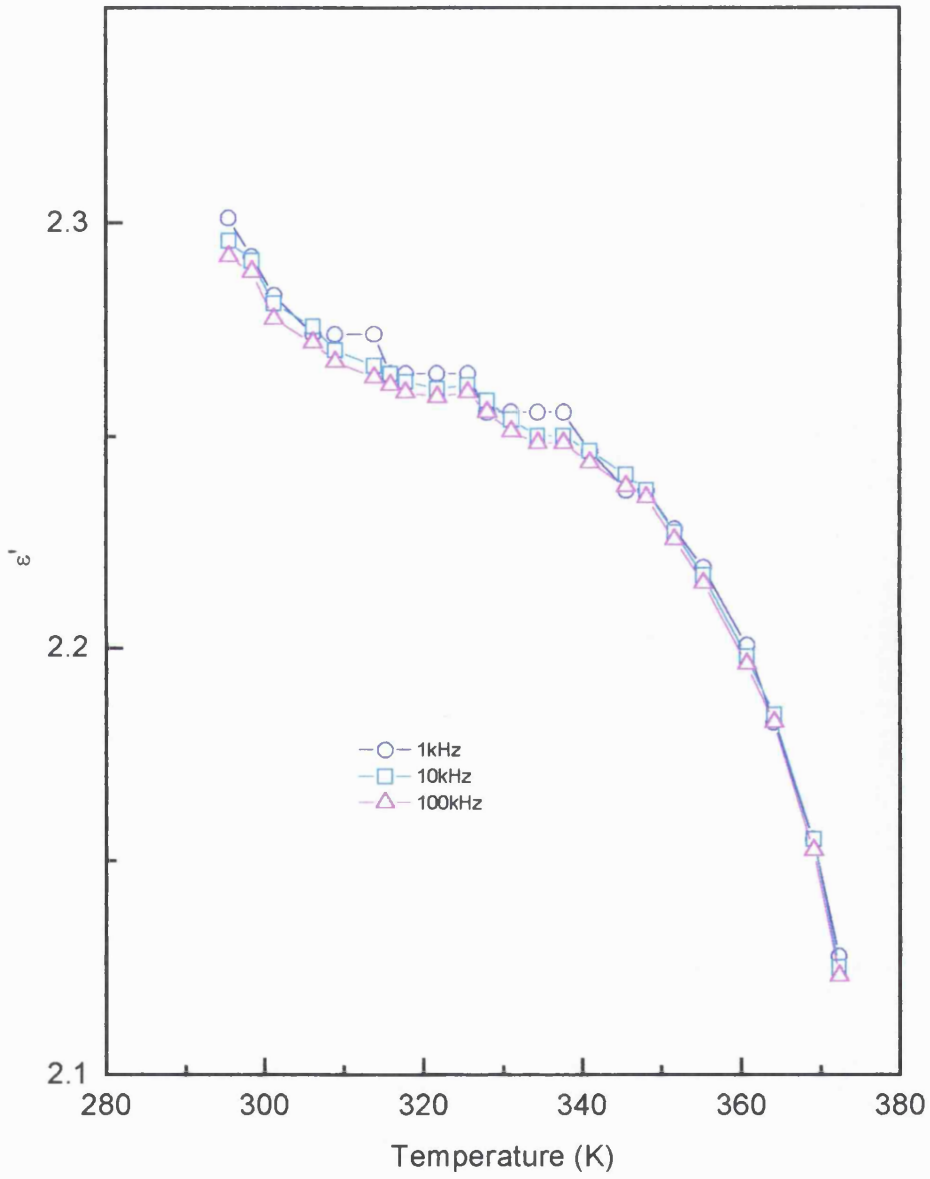

Figure 6.8. Temperature dependence of dielectric constant of crosslinked polyethylene (S188/S299/94) at selected frequencies.

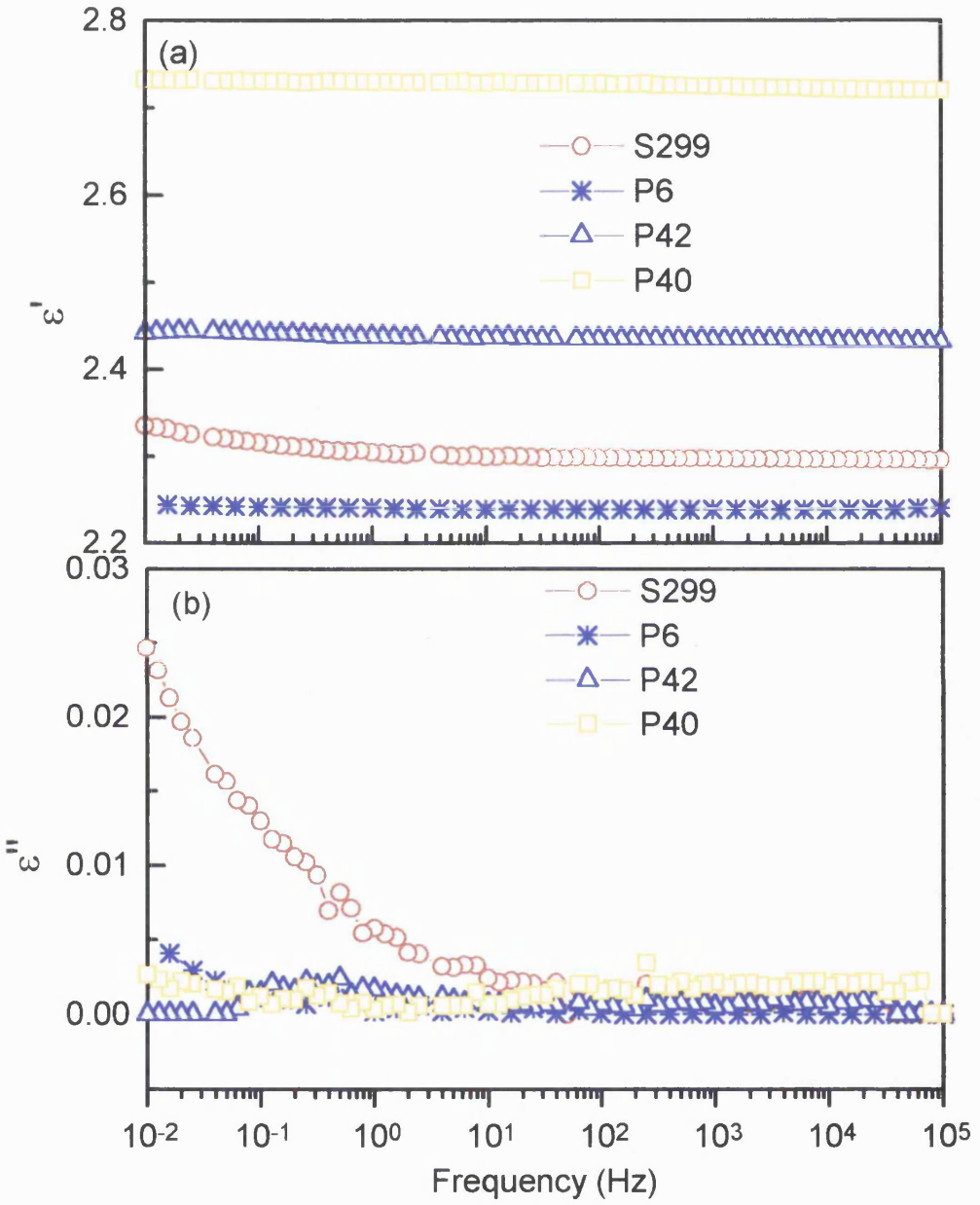

Figure 6.9. Frequency dependence of real (a), and imaginary (b) part of the permittivity for crosslinked polyethylene S299 (circles), P6 (stars), P42 (triangles) and P40 (squares) at room temperature.

are given in Table 6.2, together with those obtained using the HP Impedance Analyzer (HP) for comparison.

Table 6.2. Dielectric constant ε′ and loss ε″ of polyethylenes at room temperature and atmospheric pressure measured at 10kHz.

Sample	ε′ (DS)	ε′ (HP)	ε″ (DS)	ε″ (HP)
S299	2.767	2.296	0.001	<0.003
P6	2.238	2.274	0.000	<0.003
P40	2.721	2.313	0.002	<0.003
P42	2.433	2.274	0.000	<0.003

It is noted that for the two sets of data, the dielectric constant of polyethylene S299 is similar to that of P40, while that of P42 is similar to that of P6. The values of the dielectric constant of polyethylene S299, P40 and P42 obtained using the Dielectric Spectrometer (DS) are much larger than that (~2.3) conventionally accepted, while those measured using the HP impedance analyser are more accurate. This discrepancy may arise from the two-terminal method used in the DS system.

A remarkable dispersion at low frequencies in the dielectric constant of polyethylene S299 has been observed, together with a corresponding increase in the dielectric loss (Figure 6.9). Early dielectric measurements showed that the dielectric constants of polyethylene are frequency independent, which is consistent with its non-polar structure. The dispersion observed in the frequency dependence of the dielectric constant and loss of crosslinked polyethylenes indicates that there must be some impurities in these polymer specimens. One possibility is that the additives incorporated in the process of crosslinking create a small number of electrical dipole moments. Depending on the method and the extent of the crosslinking, the dielectric constant can be rather different from sample to sample, even if the base material is the same.

The dielectric constant ε' and the dielectric loss ε'' of a polyethylene cable insulation (C23) have been measured as functions of frequency and temperature from 290K to 410K. The electrodes have been made by silver paint coating as well as with silver evaporated on both sides of the sample. The results are shown in Figures 6.10 and 6.11.

Compared with the plaque polyethylene samples reported on above (Table 6.1), the cable sample has a higher dielectric constant at room temperature (2.5 compared with 2.3). The temperature dependence of the dielectric constant of this cable sample (Figure 6.11) is similar to that of polyethylene P40 and P42, except that the drop starting at 380K is much larger and sharper. At this drop the dielectric constant decreases more than 30% to a value of 1.65. The dielectric loss is near zero within the experimental error.

To study the difference in dielectric properties across the cable section, two samples were cut from the inner and outer parts of a cable section, as shown below. It has been found that the dielectric constant of the sample cut from the outer part of the cable section is larger than that of the inner sample, while the dielectric loss remains near zero for both of them (Table 6.3). The measurement has been repeated on three pairs of samples cut from three polyethylene sheets and the trend is reproducible. The fact that there are differences in dielectric constant across the cable cross-section may have important technological ramifications.

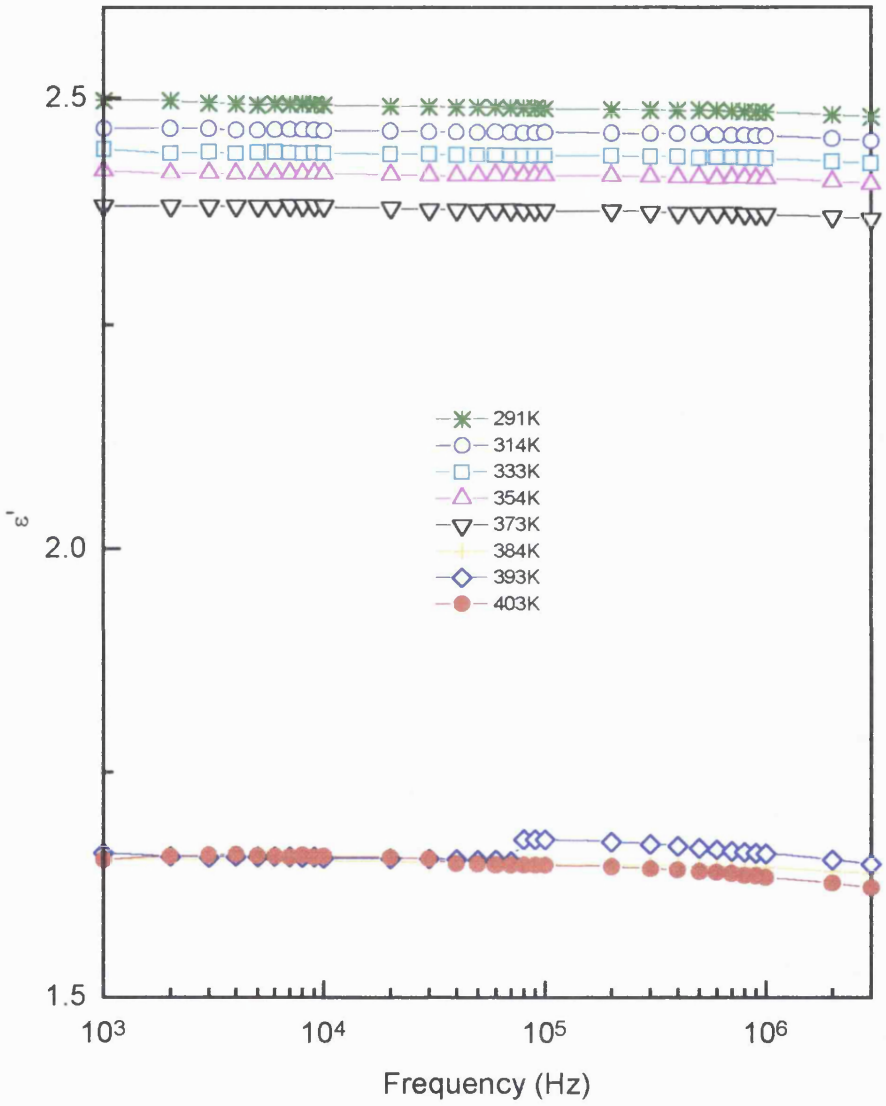

Figure 6.10. Frequency dependence of dielectric constant of crosslinked polyethylene cable sample(S260/C23/94) at selected temperatures.

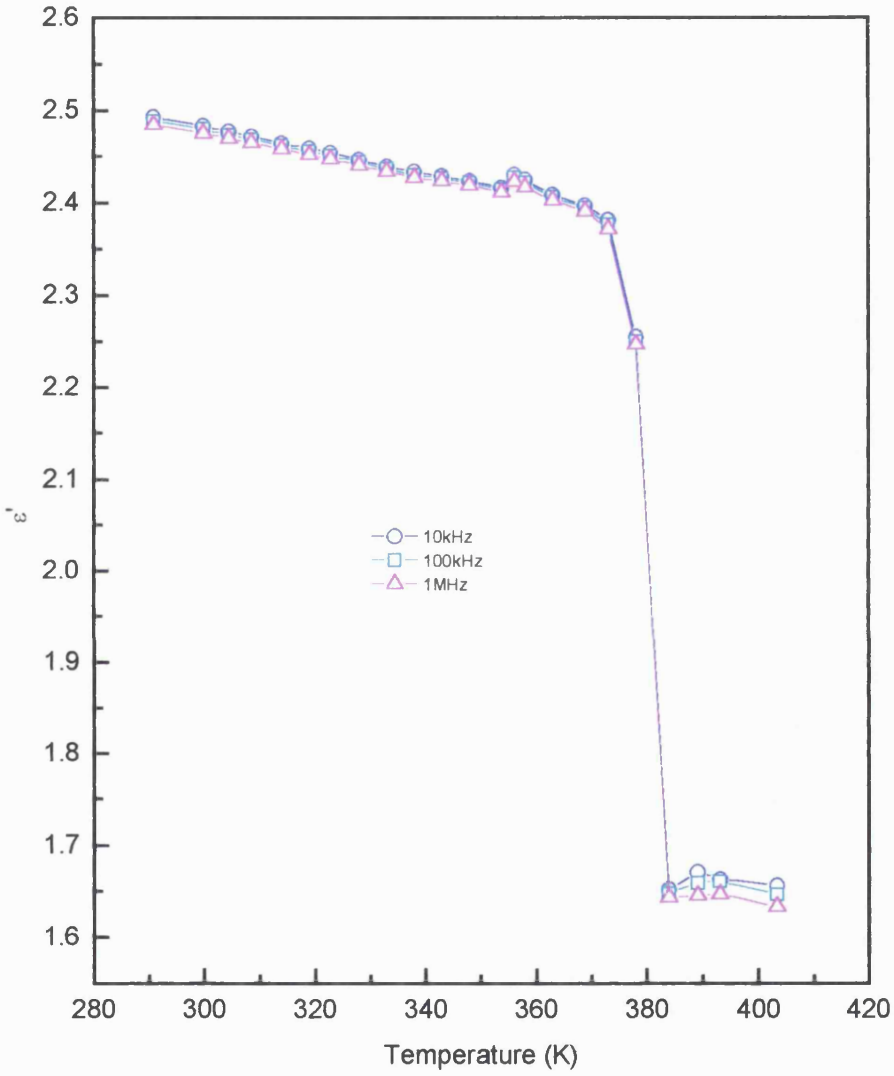

Figure 6.11. Temperature dependence of dielectric constant of crosslinked polyethylene cable sample (S260/C23/94) at selected frequencies.

Table 6.3. The distribution of dielectric constant ε' across the cable section.

Sample	Outer	Inner
1	2.71	2.59
2	2.51	2.46
3	2.51	2.42

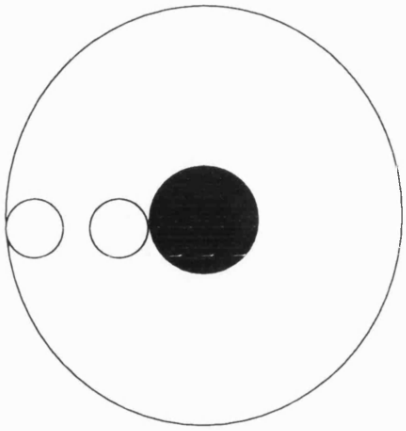

6.3. The effect of hydrostatic pressure on the dielectric constant of crosslinked polyethylene and polyethlene cable insulation

Hydrostatic pressure dependences of the dielectric constants of crosslinked polyethylenes S299, P6, P42 and two cable insulations C51 and C56 have been measured at selected frequencies and temperatures. The results are shown in Figures 6.12 to 6.17. Gold and silver electrodes, evaporated on polyethylene films typically 0.2mm thick and 15mm in diameter, have been used. Measurements of the pressure effect on the dielectric loss have proved to be more difficult due to the relatively low resistivity of the transmitting silicone fluid ($\sim 10^{12}\Omega$m, while for polyethylene the value of resistivity is 10^{14}-$10^{18}\Omega$m).

The dielectric constant has been observed to increase nonlinearly with pressure: the gradient becomes smaller at higher pressures. The data obtained with both increasing and decreasing pressure fall nicely on the same smooth curve, indicating no hysteresis in the pressure cycles (Figures 6.13 and 6.14). The solid lines are the least square quadratic fits to the data. The correlation parameter and the pressure derivatives of the dielectric constant for these polyethylenes are given in Table 6.4. The hydrostatic pressure dependence of the dielectric constant shows very little variation with change in measurement frequency (Figures 6.12 and 6.13). The shape of the curve for the dielectric constant of P6 versus pressure remains essentially the same as temperature

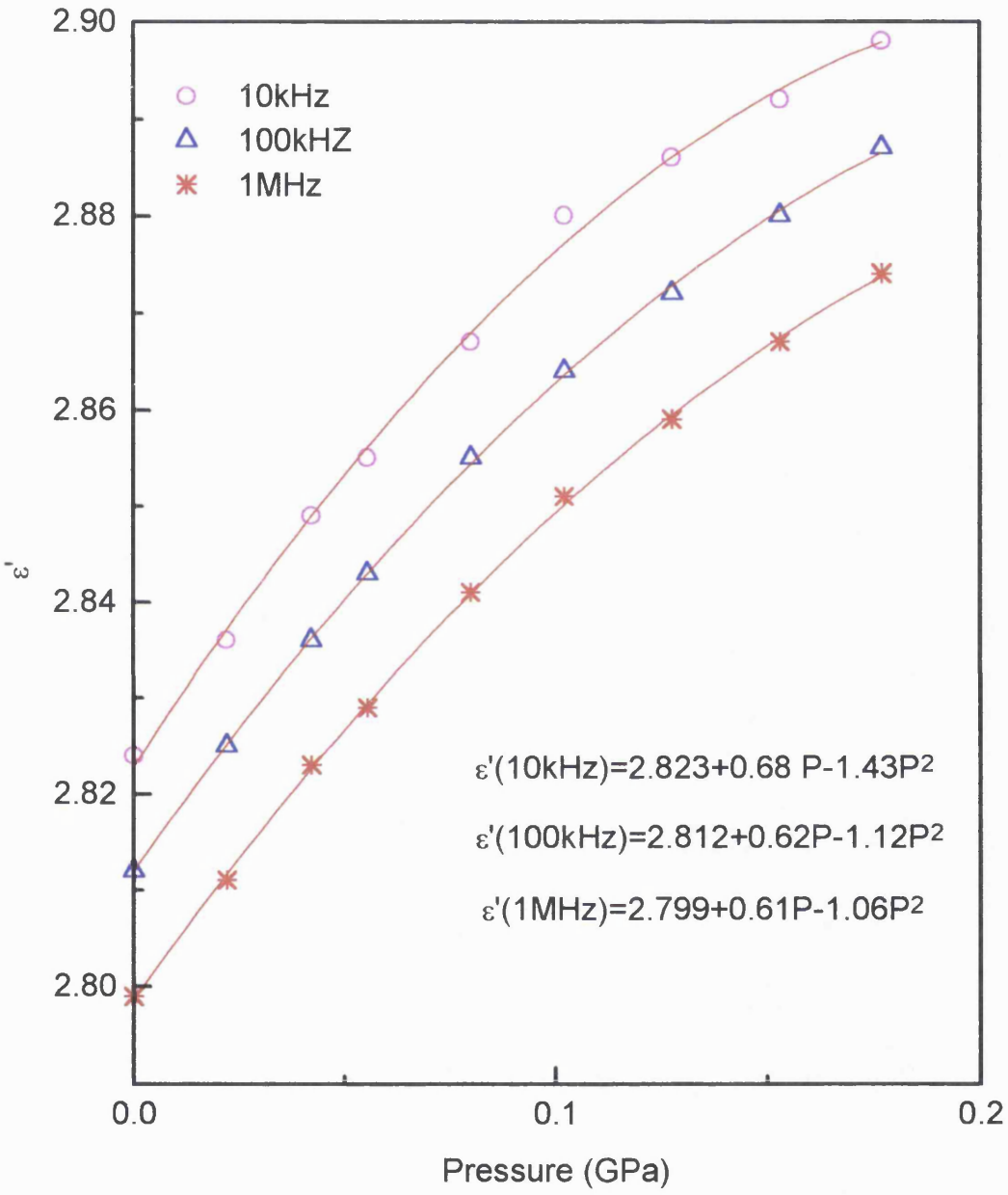

Figure 6.12. Pressure dependence of dielectric constant of crosslinked polyethylene S188/S299/94 at 292K measured at selected frequencies. The solid lines are least square fits to the data.

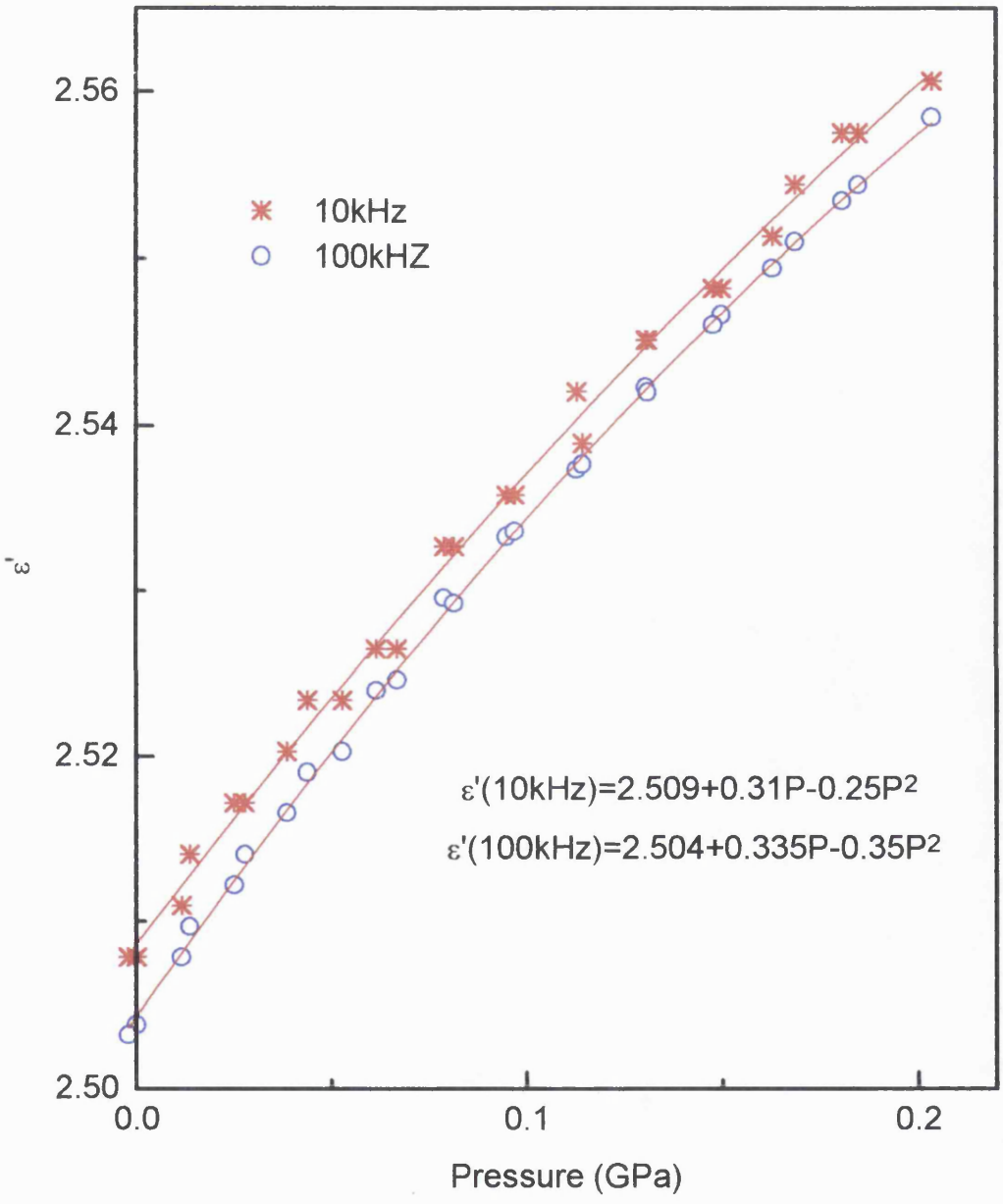

Figure 6.13. Pressure dependence of dielectric constant of crosslinked polyethylene P6 at 294K measured at selected frequencies. The solid lines are least square fits to the data.

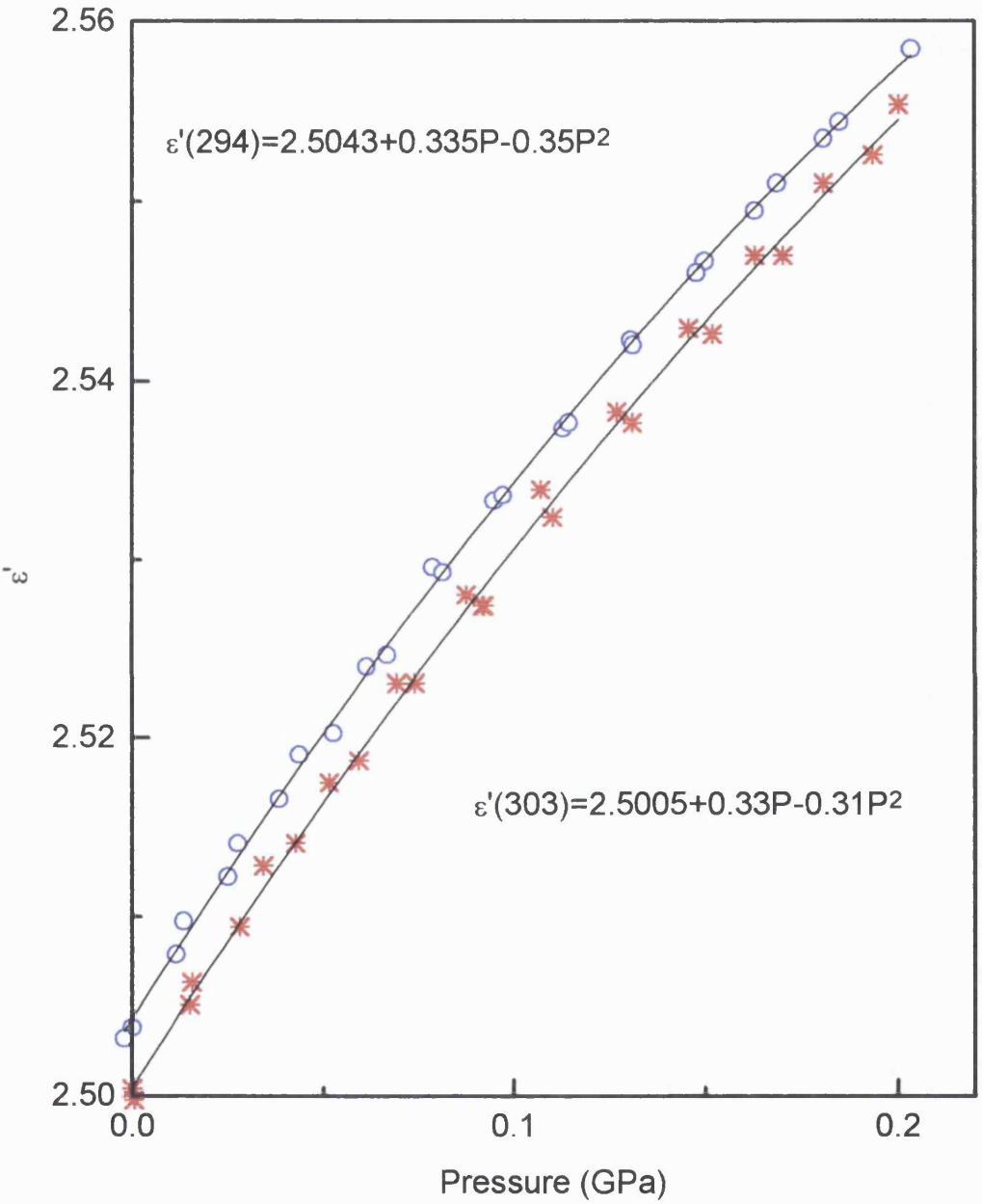

Figure 6.14. Pressure dependence of dielectric constant of crosslinked polyethylene P6 at 294K (open circles) and 303K (stars) measured at 100kHz. Solid lines are the least square fits to the data.

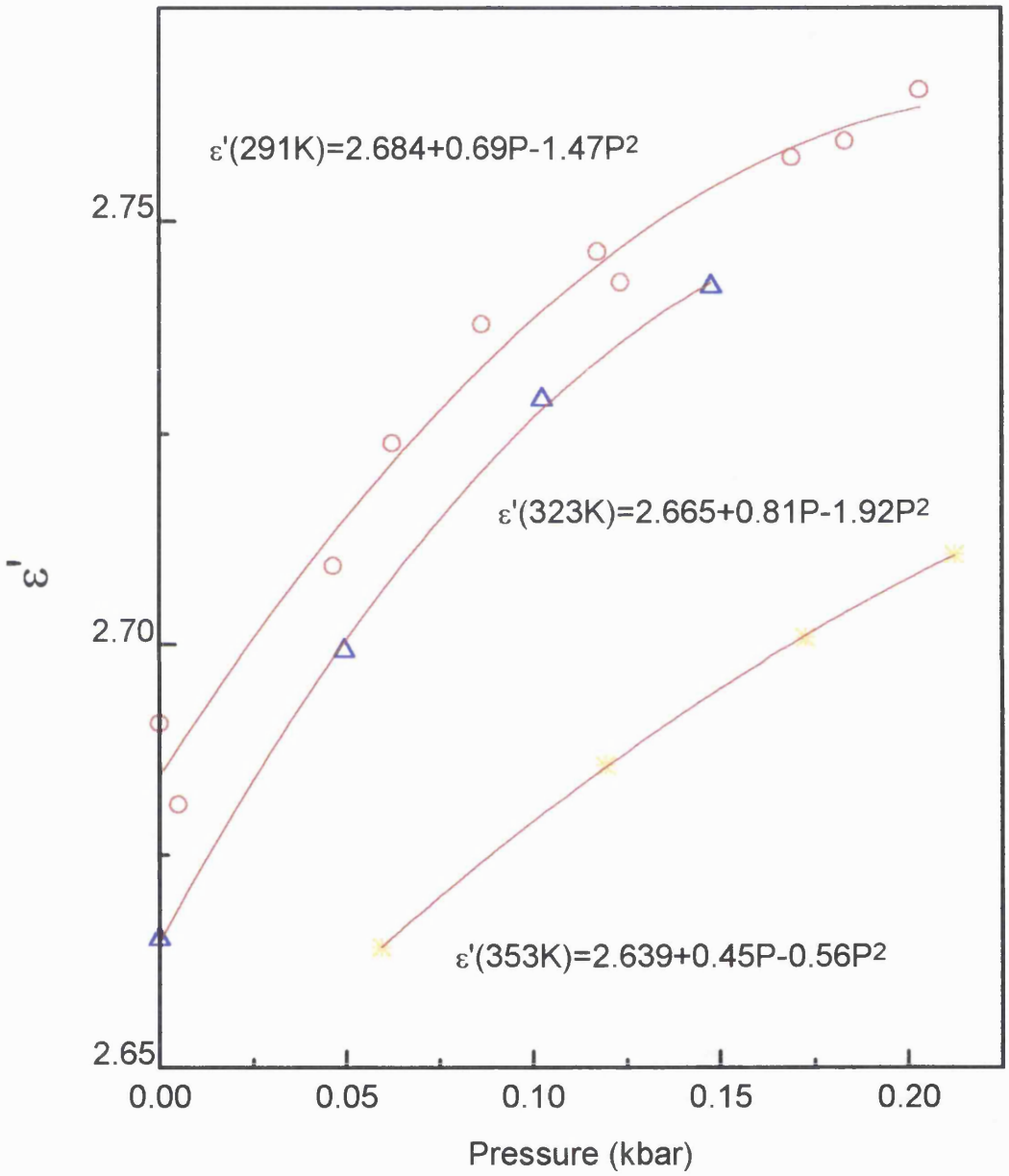

Figure 6.15. Pressure dependence of dielectric constant ε' of polyethylene P42 at 291K (circles), 323K (triangles) and 353K (stars) measured at 10kHz.

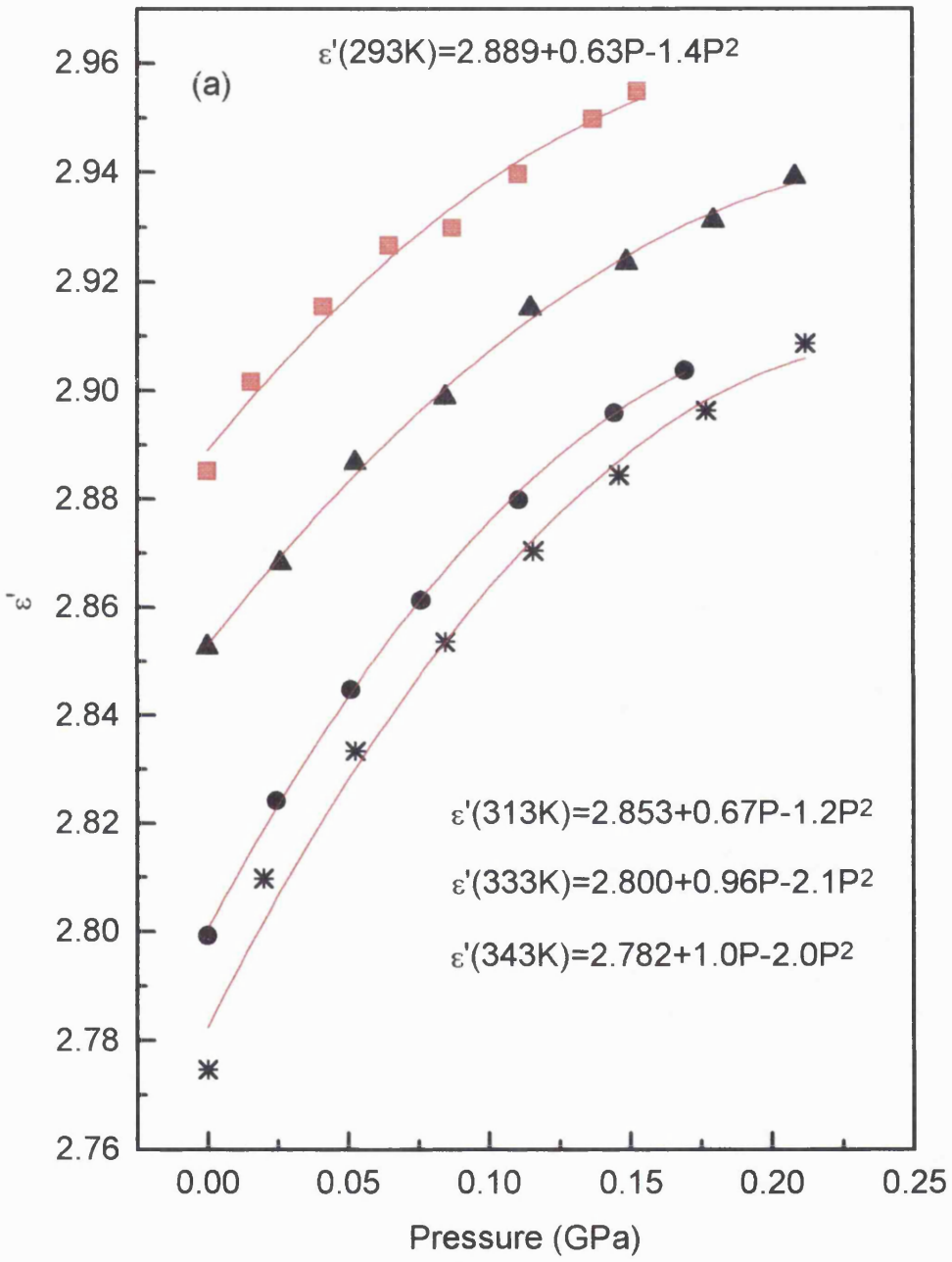

Figure 6.16. Pressure dependence of the dielectric constant of C51 at 293K (squares), 313K (triangles), 333K (circles) and 343K (stars) measured at 10kHz.

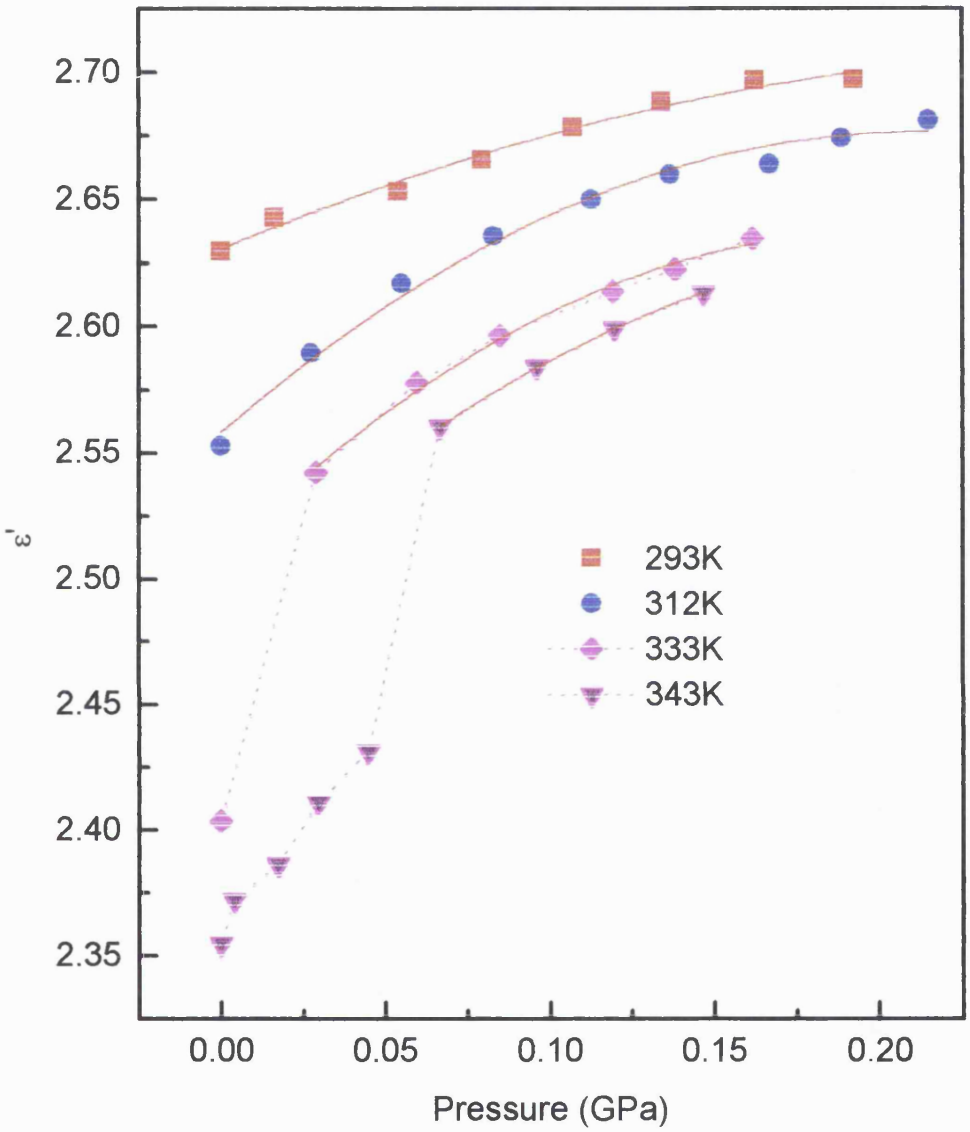

Figure 6.17. Pressure dependence of dielectric constant at 10,000Hz for C56 at selected temperatures. The solid lines are the least square fits to the data.

increases from 294K to 303K (Figure 6.14). There is, however, a strong temperature effect on the pressure dependence of the dielectric constant of P42 (Figure 6.15).

The magnitude of the dielectric constant measured in the pressure experiments (Figures 6.12, 6.13 and 6.15) tends to be larger than that determined previously (Table 6.1). This discrepancy arises from the edge-effect of the smaller samples used in the pressure measurements and has nothing to do with the silicone oil in the pressure cell; the dielectric constant of a polyethylene sample measured outside the pressure cell is the same as that measured with the same sample in the cell. As the dielectric constant of the silicone fluid (~2.2) is roughly the same as that of the polyethylene (~2.3), the edge-effects can easily be corrected for by considering a relatively larger effective electrode area.

Table 6.4. The pressure derivatives of the dielectric constant obtained from the least square fits of the pressure dependence data for polyethylenes at selected temperatures and frequencies (f). R is the correlation parameter of the fits.

Sample	T (K)	f (kHz)	R	$(\partial\varepsilon'/\partial P)_{P=0}$ (Pa^{-1})	$(\partial^2\varepsilon'/\partial P^2)$ (Pa^{-2})
S299 (XLPE)	292	10	0.9987	6.8×10^{-10}	-2.86×10^{-18}
		100	0.9998	6.2×10^{-10}	-2.24×10^{-18}
		1000	0.9998	6.1×10^{-10}	-2.12×10^{-18}
P6 (XLPE)	294	10	0.9982	3.1×10^{-10}	-0.50×10^{-18}
		100	0.9996	3.4×10^{-10}	-0.70×10^{-18}
	303	100	0.9988	3.3×10^{-10}	-0.62×10^{-18}
P42 (XLPE)	291	10	0.9897	6.9×10^{-10}	-2.94×10^{-18}
	323	10	0.9996	8.1×10^{-10}	-3.84×10^{-18}
	353	10	1	4.5×10^{-10}	-1.12×10^{-18}
C51 (cable)	293	10	0.9924	6.3×10^{-10}	-2.8×10^{-18}
	313	10	0.9986	6.7×10^{-10}	-2.4×10^{-18}
	333	10	0.9997	9.6×10^{-10}	-4.2×10^{-18}
	343	10	0.9946	10×10^{-10}	-4.0×10^{-18}
C56 (cable)	293	10	0.9937	5.4×10^{-10}	-3.6×10^{-18}
	312	10	0.9949	11.2×10^{-10}	-10.4×10^{-18}
	333	10	0.9970	26×10^{-10}	-12.4×10^{-18}
	343	10	1	23.8×10^{-10}	-9.92×10^{-18}

6.4. Discussion of the results obtained from the dielectric measurements

Certain aspects of the dielectric constant and loss can be understood on the basis of the Clausius-Mosotti equation (Ku and Liepins 1987)

$$\frac{\varepsilon'-1}{\varepsilon'+2}\frac{M}{\rho}=\frac{N\alpha}{3\varepsilon_o} \tag{6.1}$$

where ε' is the dielectric constant, N is Avogadro's constant (6.024×10^{23}), M is the molecular weight, ρ is the density, $\varepsilon_o=8.85\times10^{-12}$ Fm^{-1}. The Clausius-Mosotti equation does not hold for all polymers but should apply only to nonpolar or weakly polar polymers such as polyethylene (Chen and Liepins 1987). The molecular polarizability α can be considered to arise from two sources: (i) an electronic polarizability α_e, which is not temperature dependent, (ii) a dipole polarizability α_d due to orientation of permanent electrical dipole moments. Hence

$$\alpha=\alpha_e+\alpha_d \tag{6.2}$$

According to a simple theory due to Debye, the second contribution is given by

$$\alpha_d=\frac{\mu^2}{3kT} \tag{6.3}$$

where μ is the dipole moment, k is Boltzmann's constant, and T is the temperature in K.

In polyethylene the dipole polarization might arise from three sources: (i) CH bond moments, (ii) C=C bond moments, (iii) impurity moments. CH moments are small ($\sim1.3\times10^{-30}$C·m) and because of the molecular structure of polyethylene, the electric moments of CH bond tend to cancel. The double bonds may make the molecules somewhat polar but such moments are also small ($\sim1.0\times10^{-30}$C·m) and will certainly be present, although in a very small concentration. Dipole moments arising from an impurity may have a large effect on the dielectric behaviour of the polymer, depending on the properties of the impurity. For example, even slightly oxidized polyethylene may have quite different dielectric properties (Boyd 1985). Although it is generally believed that impurities make a negligible contribution to the dielectric constant in normal

electrical quality, pure polyethylene, that does not seem to be true for the materials under study here. This will be established in what follows.

The temperature dependence of the dielectric constant of polyethylene can be used to calculate the molecular polarizability of polyethylene and to investigate the validity of applying the Clausius-Mosotti equation (6.1). Taking P42 as an example, we have $\varepsilon'=2.274$, $\rho=917 kg/m^3$ at room temperature and the weight average molecular weight $M_w=1.009\times10^5$. Consequently the molecular polarizability of P42 is obtained from equation (6.1) as 1.446×10^{-30} m^3. Similar calculations have been carried out for polyethylene P40, P6 and S299 and the results are given in Table 6.5.

Table 6.5. The molecular polarisability α of crosslinked polyethylenes.

Sample	ε'	ρ (kg/m^3)	M_w	α (m^3)
S185/P6/94	2.274	919	102550	1.466×10^{-30}
S186/P40/94	2.313	921	92800	1.352×10^{-30}
S187/P42/94	2.274	917	100900	1.446×10^{-30}
S188/S299/94	2.296	917	101500	1.472×10^{-30}

The molecular polarisability of these polyethylenes is twice as large as that for a single CH chemical bond (0.65×10^{-30} m^3), and lies between the polarisability of a C=C bond (1.66×10^{-30} m^3) and that of a C=O bond (1.2×10^{-30} m^3). In general, orientational polarisability is much larger than the induced electronic polarisability (Jonscher 1983). The ability of the bond moments to follow the electrical field is severely restricted in a solid, making the effect of the orientational polarization much smaller than would be expected from the free bond moments. The results in Table 6.5 suggest that the C=C bond is likely to make some contributions to the observed polarizability of these polyethylenes.

If the orientational polarization of the permanent dipole moments in polyethylene were to be negligible and the electronic polarisability to be independent of temperature, then

the following form of the Clausius-Mosotti equation relationship should be followed at high temperatures:

$$\rho(T) = \rho_o \frac{\varepsilon'(T) - 1}{\varepsilon'(T) + 2} \bullet \frac{\varepsilon_o' + 2}{\varepsilon_o' - 1} \tag{6.4}$$

where ρ_o and ε'_o are the density and dielectric constant at a reference temperature. Using equation (6.4), the densities of four crosslinked polyethylenes have been calculated and the results are given in Figure 6.18, where crosslinked polyethylene P3+G17 is the same material as S188/S299/94 and P16+G17 is the same as S185/P6/94. The sample descriptions and nomenclature can be found in Appendix 1. These densities are compared in this Figure with data provided by the manufacturers. It can be seen that the calculated density is nearly the same as that measured directly in the vicinity of room temperature. However, the difference between the two becomes significant at higher temperatures, which suggests that the polarisability of polyethylene does not remain constant as temperature increases. Equation (6.4) can be rewritten as

$$\rho(T) = \rho_o \frac{\alpha_o}{\alpha(T)} \frac{\varepsilon'(T) - 1}{\varepsilon'(T) + 2} \bullet \frac{\varepsilon_o' + 2}{\varepsilon_o' - 1} \tag{6.5}.$$

To study further the temperature behaviour of the dielectric properties of polyethylene, the temperature dependence of the polarizability α for the four samples has been determined from equation (6.1) using the measured density and dielectric constant data. The results are shown in Figure 6.19. The polarizabilities α of these crosslinked polyethylenes are strongly temperature dependent. This strong temperature dependence would be expected to relate to α_d since it would be consistent with an orientational polarisation process. For polyethylene P40 and P42, the polarizability increases almost linearly with temperature below 380K, where a sudden drop has been observed. However, the polarizability for polyethylene P3+G17 and P16+G17, has quite different temperature behaviour from that of P40 and P42. The calculated α for P3+G17 and P16+G17 decreases with temperature at first and then begins to increase linearly with temperature until 350K, above which it gradually turns over (Figure 6.19).

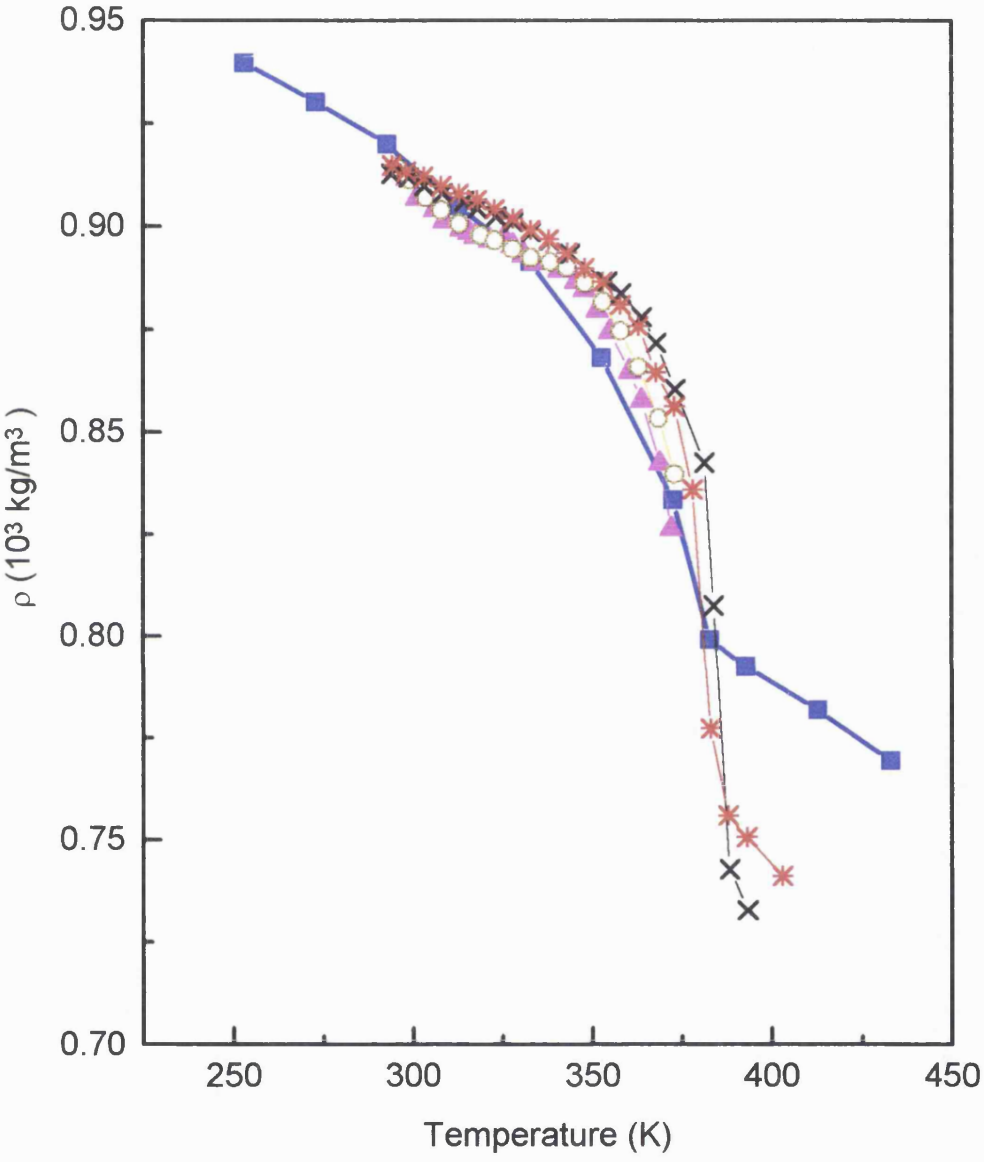

Figure 6.18. Temperature dependence of density for crosslinked polyethylenes: measured directly (squares), calculated for P3+G17 (triangles), P16+G17 circles), P40 (crosses) and P42 (stars).

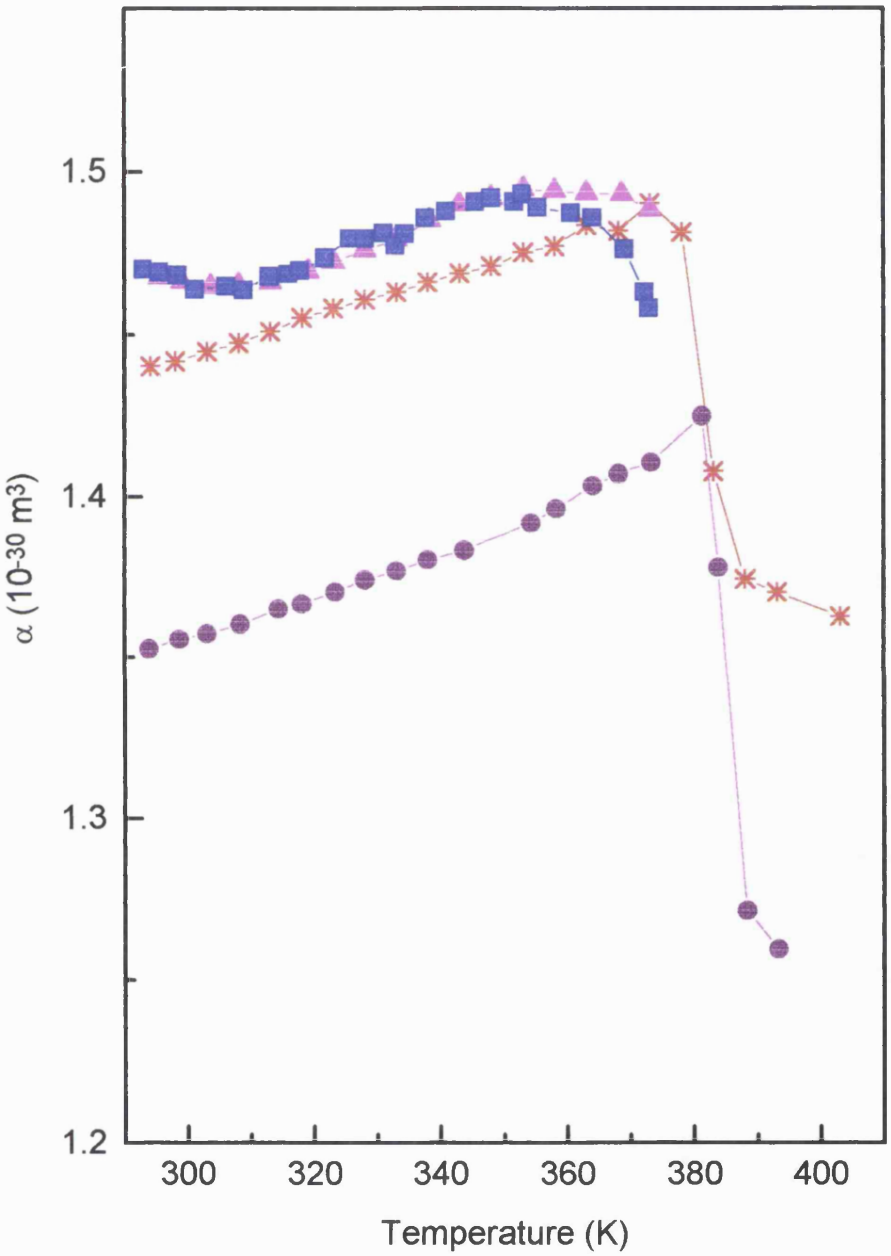

Figure 6.19. Temperature dependence of the polarizability of crosslinked polyethylene P3+G17 (squares), P16+G17 (triangles), P40 (circles) and P42 (stars).

It is not surprising that the features observed in the temperature dependence of the polarizability for crosslinked polyethylene cannot be ascribed to the simple Debye theory, equation (6.3). In Debye's model the interaction between the dipoles are completely ignored and all the polar molecules are assumed to be floating freely in a dielectrically inert non-polar fluid. The effect of increasing temperature, according to this model, is simply to increase the thermal motion of the molecules, making them more difficult to line up along the electrical field. Consequently the polarisability would be smaller at high temperatures (Equation (6.3)). However, the polarisability of a solid depends not only on the thermal vibration but also on the interaction force of the molecules. The force restricting free dipole rotation gets much weaker as the free volume of polyethylene increases at higher temperatures, resulting in a larger polarizability. The real temperature dependence of polarizability of a solid relies on which mechanism is dominant. The results in Figure 6.19 suggest that the polarisability of crosslinked polyethylene below the melting point (380K) arises mainly from the 'defects' or impurities related dipoles in the crystalline region, where the dominant effect of increasing temperature is to reduce the strong intermolecular forces of the crystals. In the vicinity of melting, the polarizability due to the dipoles related with the crystalline structure decreases sharply. The dielectric behaviour of these polyethylenes above the melting point is consistent with the Debye theory, since the intermolecular force then becomes much smaller.

It is interesting to note that the polarizability of polyethylene P3+G17 and P16+G17 has an anomalous decrease with increasing temperature in the vicinity of room temperature (Figure 6.19). An anomalous thermal contraction, instead of expansion, has been observed for crosslinked polyethylene P6+G17 in the vicinity of room temperature (Figure 6.20(b)). Dielectric breakdown and X-ray measurements on the thermoplastic version of this polyethylene also show an anomalous increase in dielectric strength and crystallinity in this temperature range (Figure 6.20). The results obtained from several different experimental techniques evidence a possible correlation of the polarisability, crystallinity, thermal expansion and breakdown strength of crosslinked polyethylene, which needs to be investigated more intensively.

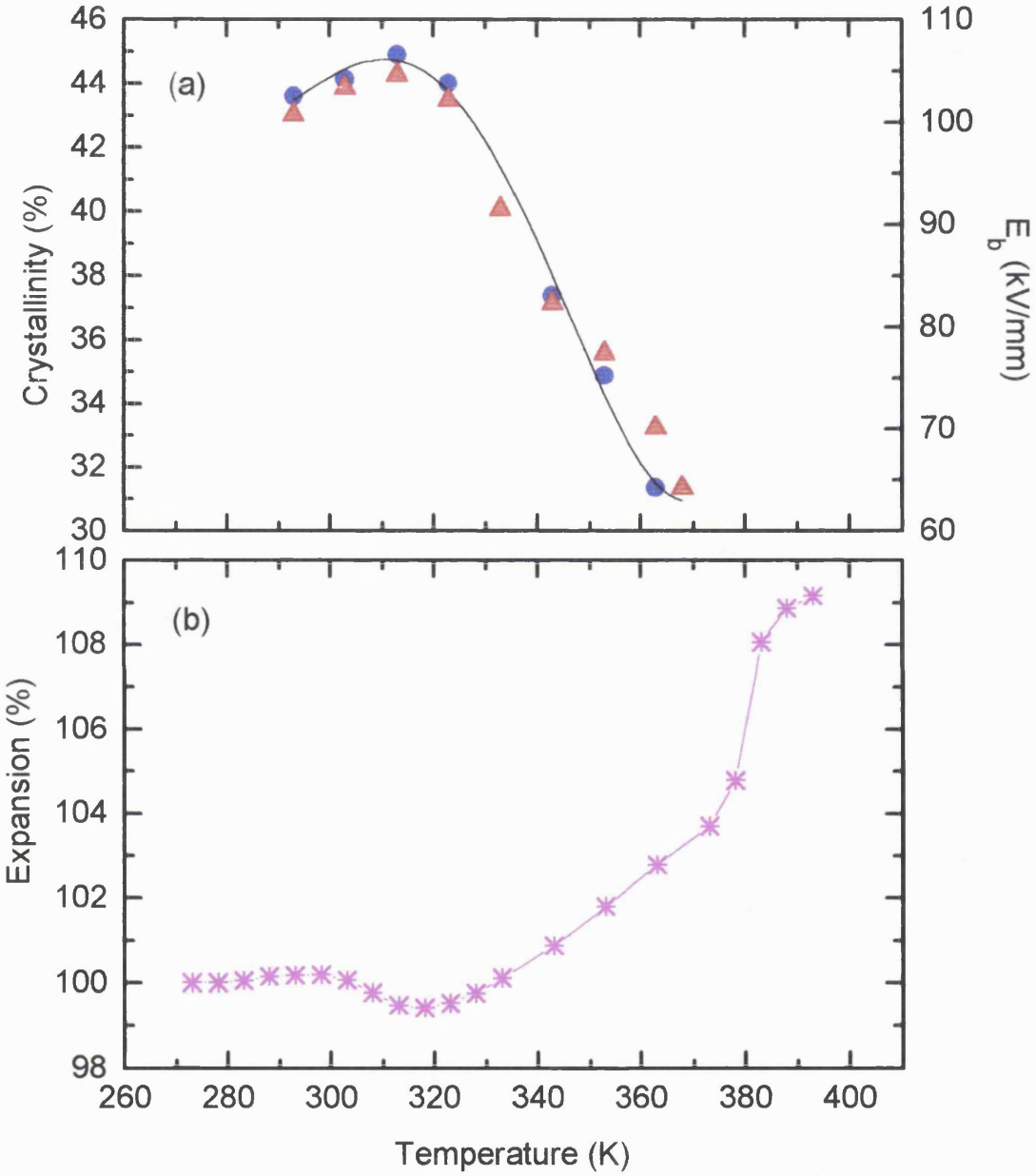

Figure 6.20. Temperature dependence of (a) the crystallinity (circles) and beakdown strength (triangles) for thermoplastic polyethylene P16, and (b) the linear thermal expansion for crosslinked polyethylene P16+G17.

The temperature and pressure dependence of the dielectric constant is often discussed in terms of the so-called Havinga equation (Bosman and Havinga 1963, Havinga 1961). Differentiating Equation (6.1) with respect to the temperature gives

$$\frac{1}{(\varepsilon'-1)(\varepsilon'+2)}\left[\frac{\partial\varepsilon'}{\partial T}\right]_P = A+B+C \qquad (6.6).$$

Here the first term, $A = -(1/3V)(\partial V/\partial T)_P$, is the coefficient of linear thermal expansion, which takes into account the effect of the decrease in the number of polarisable particles in a given volume as the temperature rises. The second term, B, can be written as $-A(\partial \ln\alpha/\partial \ln V)_T$. This measures the effect of the change of the polarisability of a fixed number of particles as the available volume increases with temperature. The term $C = (\partial\ln\alpha/\partial T)_V/3$ measures the contribution from the change of polarisability due to variation of temperature at constant volume. In fact, the last two terms together measure the effect of temperature on the polarizability α at constant pressure:

$$B+C=\frac{1}{3}\left[\frac{\partial\alpha}{\partial T}\right]_P \qquad (6.7)$$

In the restrictive circumstance that the orientational polarisability is zero and the electronic polarizability is temperature independent, $(\partial\alpha/\partial T)_P=0$ and equation (6.6) becomes

$$\beta = -\frac{3}{(\varepsilon'-1)(\varepsilon'+2)}\left[\frac{\partial\varepsilon'}{\partial T}\right]_P \qquad (6.8)$$

where $\beta=(1/V)(\partial V/\partial T)_P$ is the volume thermal expansion coefficient. The measured temperature derivatives of the dielectric constant for five crosslinked polyethylene samples are shown in Figures 6.21 to 6.25. The volume thermal expansion coefficient calculated using equation (6.8), together with that measured directly, is given in Table 6.6 for the five polyethylenes at selected temperatures.

It can be seen from the results given in Table 6.6 that the calculated data for P40 and P42 at room temperature fall within the range of measured thermal expansion, while those for P6 and S299 are notably larger than the measured thermal expansion coefficient. At 393K the calculated volume thermal expansion of crosslinked polyethylene P40 and P42 is not far from that directly measured. The difference between the measured and the calculated values of the thermal expansion corresponds

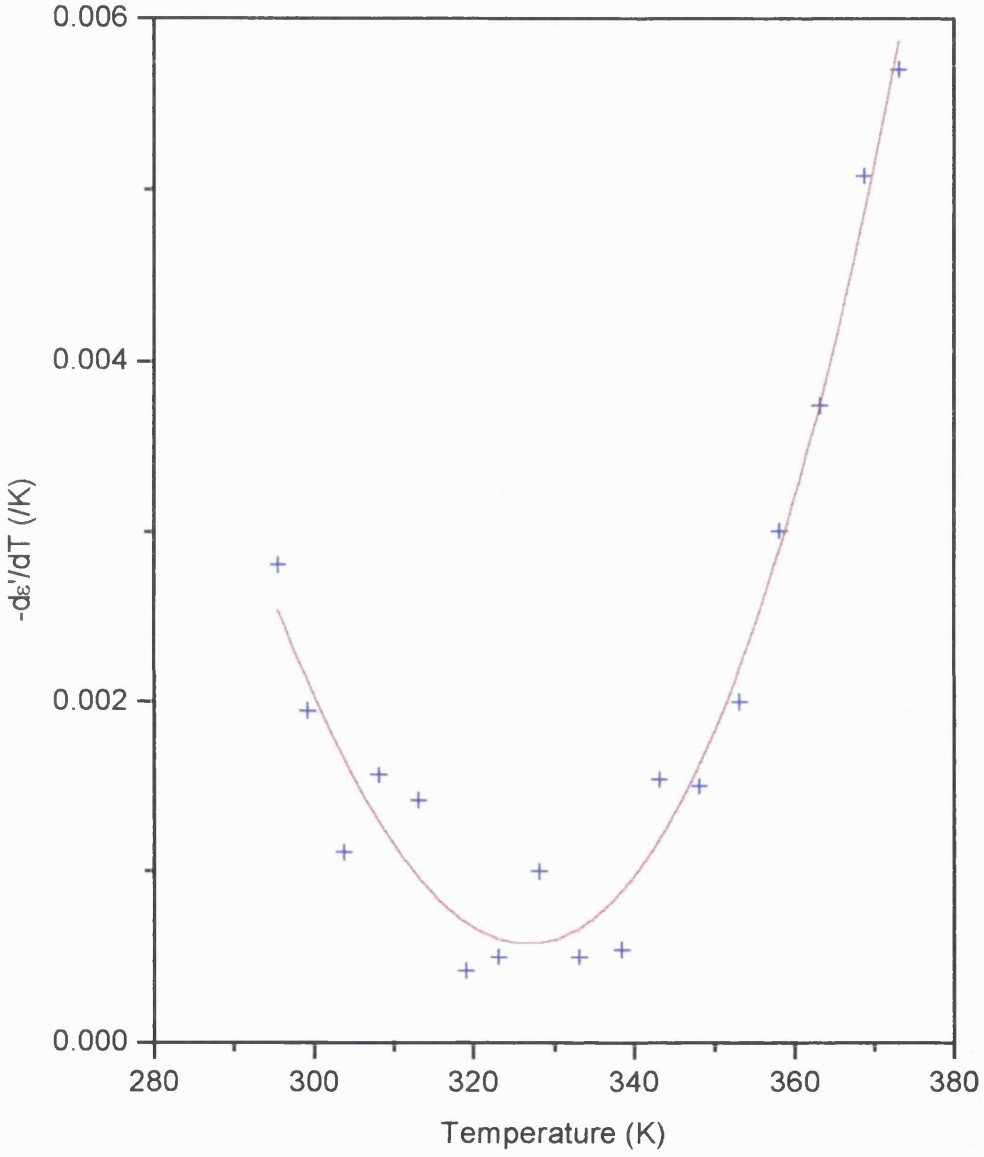

Figure 6.21. Temperature derivative of the dielectric constant of crosslinked polyethylene S185/P6/94. The solid line is the polynomial fit to the data.

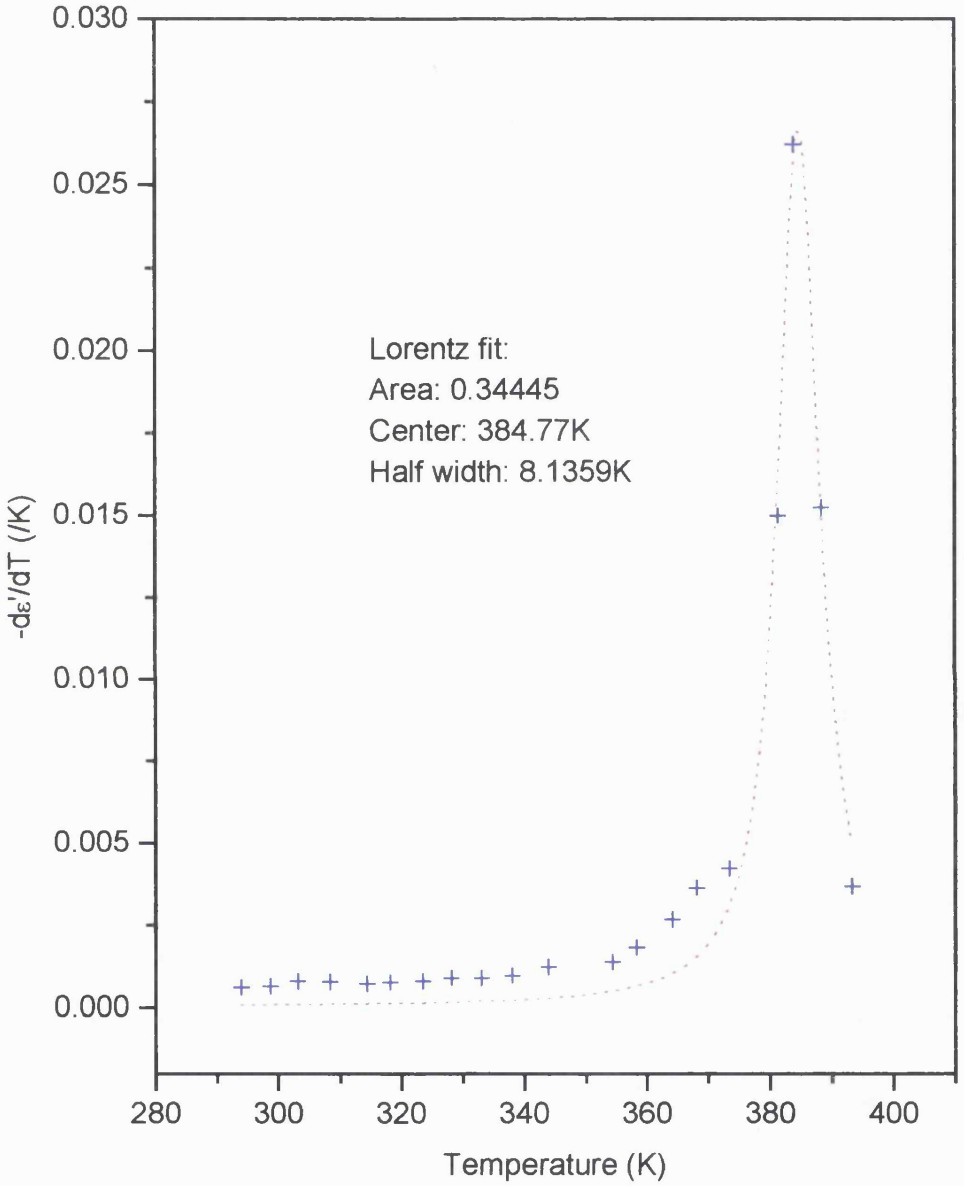

Figure 6.22. Temperature derivative of the dielectric constant of crosslinked polyethylene S186/P40/94. The dotted line is the Lorentz fit to the data.

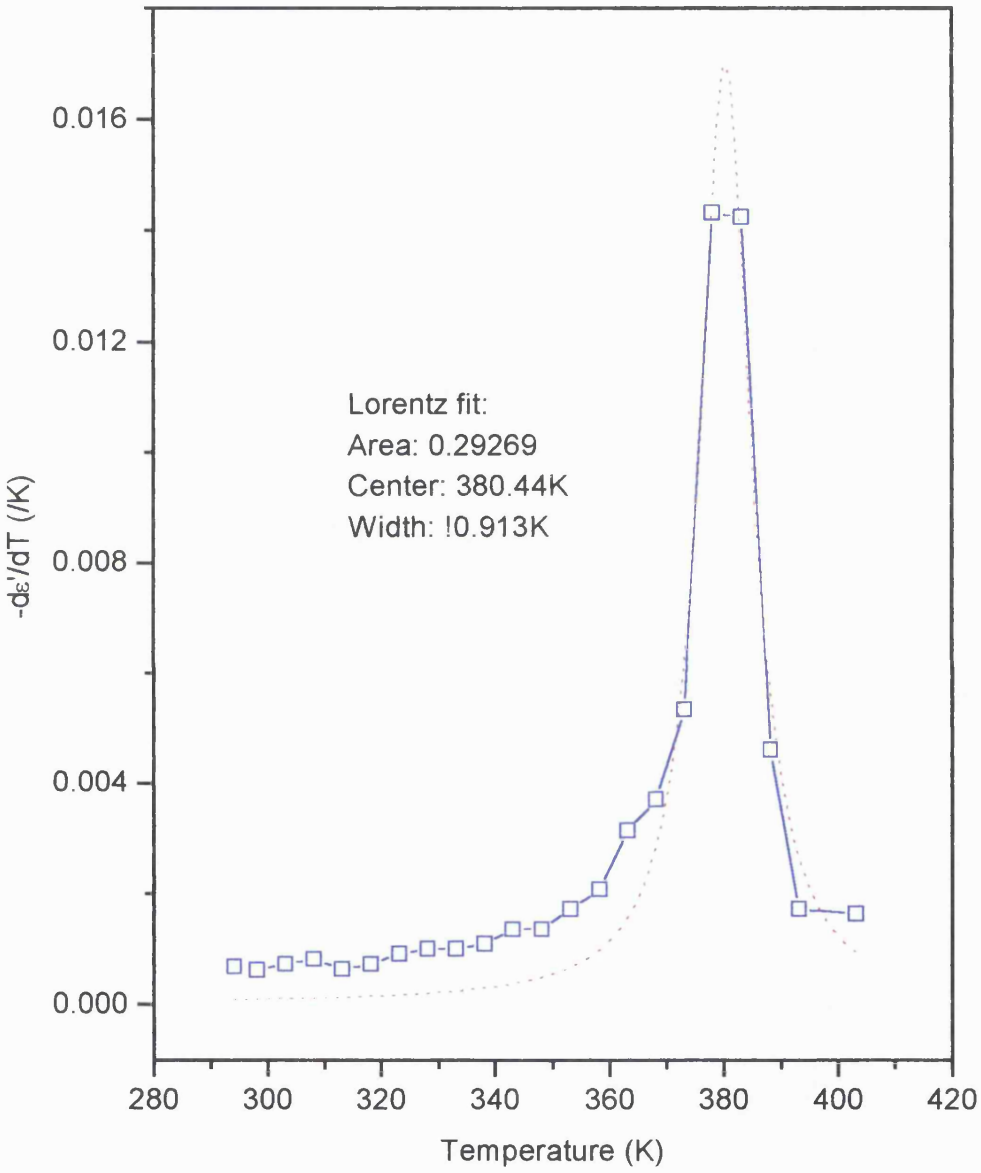

Figure 6.23. Temperature derivative of the dielectric constant of crosslinked polyethylene S187/P42/94. The dotted line is the Lorentz fit to the data.

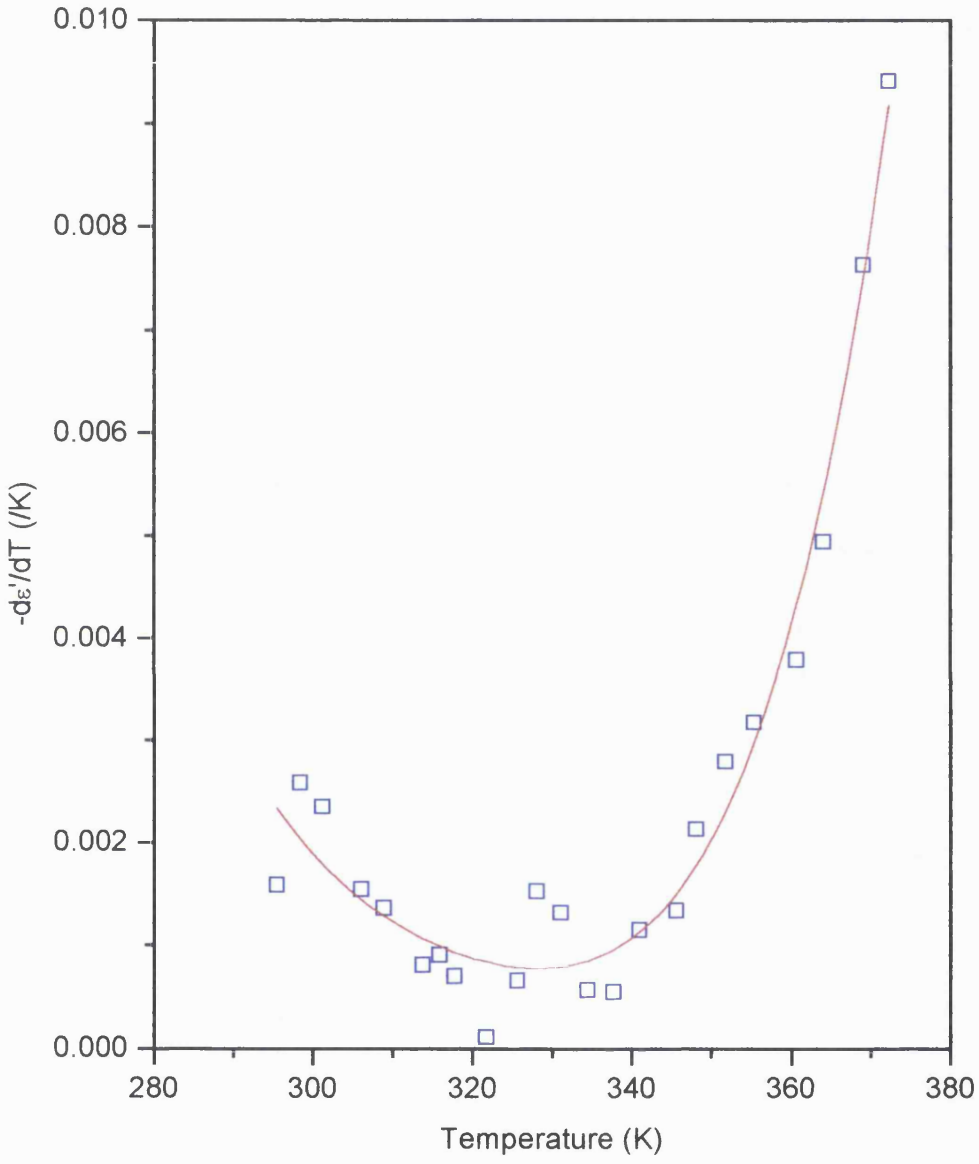

Figure 6.24. Temperature derivative of the dielectric constant of crosslinked polyethylene S188/S299/94. The solid line is the polynomial fit to the data.

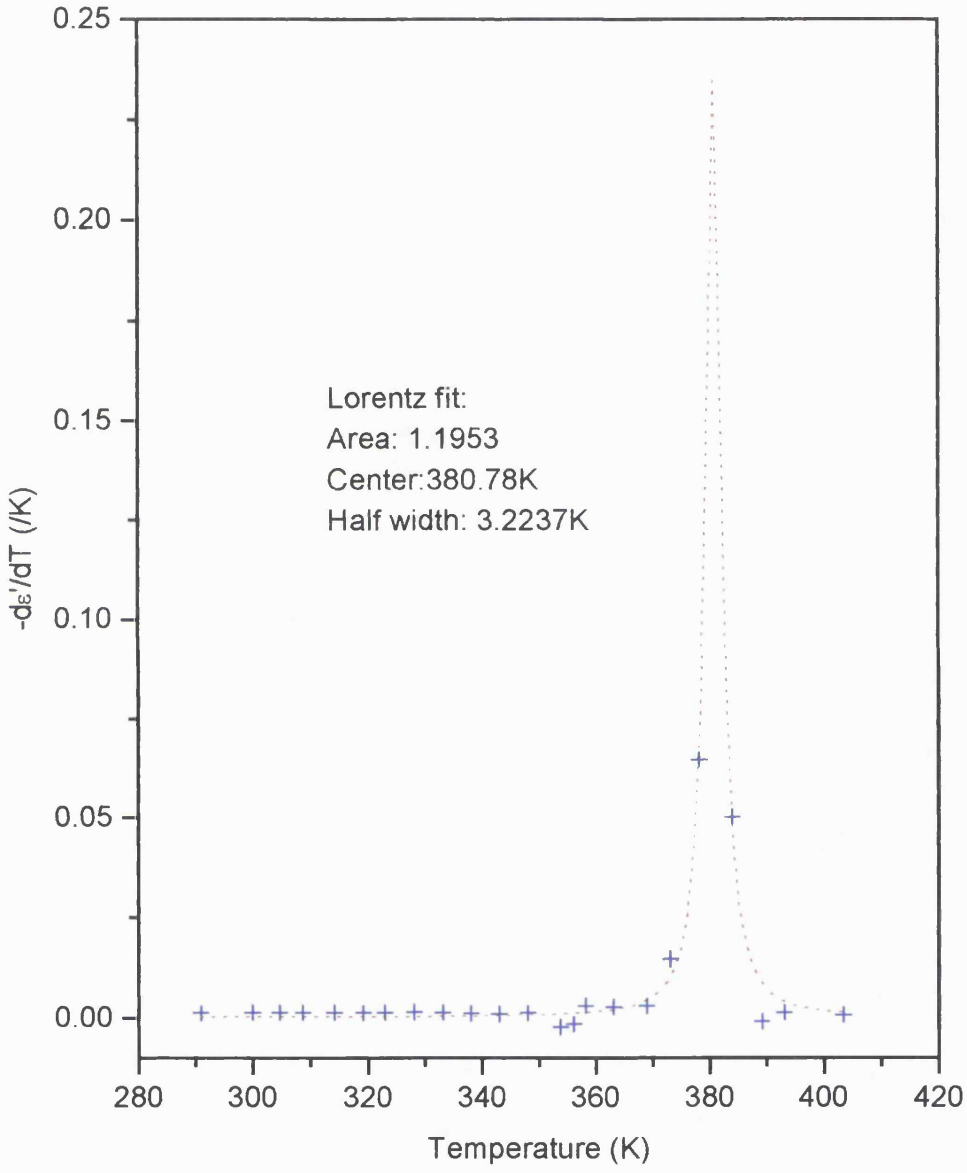

Figure 6.25. Temperature derivative of the dielectric constant of crosslinked polyethylene cable sample S260/C23/94. The dotted line is the Lorentz fit to the data.

to the contribution from terms B and C in equation (6.6). To distinguish these two terms, the pressure dependences of the dielectric constant are needed.

Table 6.6. The temperature derivative of the dielectric constant $-\partial\varepsilon/\partial T$ and the volume thermal expansion coefficient β for polyethylenes at selected temperatures. The subscripts c and m denote calculated and measured data respectively.

Sample	$-\partial\varepsilon/\partial T$ (10^{-4}/K)		β_c (10^{-4}/K)	β_m (10^{-4}/K)	β_c (10^{-4}/K)	β_m (10^{-4}/K)
	294 K	393K	294K		393K	
S185/P6/94	28.2		15.4	4.55		17.82
S186/P40/94	6.0	36.6	3.2	4.71	19.4	17.58
S187/P42/94	6.7	17.1	3.7	4.38	9.4	15.69
S188/S299/94	15.9		8.5	4.55		
S260/C23/94	11.1	13.1	5.0	4.55	5.9	

Differentiating Equation (6.1) with respect to pressure gives

$$\frac{1}{(\varepsilon'-1)(\varepsilon'+2)}\frac{\partial\varepsilon'}{\partial P} = (A+B)\frac{(\partial \ln V/\partial P)}{(\partial \ln V/\partial T)} \tag{6.9}$$

where $-(\partial \ln V/\partial P)=\kappa$ is the compressibility of the material, which has been obtained from the ultrasonic measurements. Equation (6.9) enables the calculation of $(A+B)$ from the pressure derivatives of the real permittivity. Substituting the value of $(A+B)$ into equation (6.6) then gives the value for term C. The terms in equations (6.6) and (6.9) thus calculated for three crosslinked polyethylenes and a cable sample at room temperature and atmospheric pressure are shown in Table 6.7 under the subtitle of *Havinga analysis.*

To analyze the pressure dependence of the dielectric constant data, Gibbs and Jarman (1963) used another method, which is based on the equation:

$$\frac{\partial \ln\varepsilon'}{\partial P} = \frac{(\varepsilon'-1)(\varepsilon'+2)}{3\varepsilon'}\left[\frac{\partial \ln\alpha}{\partial P} - \frac{\partial \ln V}{\partial P}\right] \tag{6.10}$$

Table 6.7. The results of the analysis of the dielectric data for polyethylene samples using the methods of Bosman-Havinga (Bosman and Havinga 1963), and Gibbs-Jarman. The thermal expansion data for XLP3 and XLP16 has been obtained by averaging the values for P40 and P42 at 293K, and that for C56 has been taken as the same as that for XLP16.

Terms in the equations	unit	XLP3	XLP16	XLP42	C56
$\varepsilon'_{P=0}$		2.296	2.274	2.274	2.3
$(\varepsilon'+2)(\varepsilon'-1)$		5.568	5.445	5.445	5.59
Havinga analysis					
$\partial\varepsilon'/\partial T/(\varepsilon'+2)(\varepsilon'-1)$	$10^{-4}K^{-1}$	-2.83	-5.13	-1.23	-7.16
$\partial\varepsilon'/\partial P/(\varepsilon'+2)(\varepsilon'-1)$	$10^{-10}Pa^{-1}$	1.11	0.55	1.27	0.66
$\partial \ln V/\partial T$	$10^{-4}K^{-1}$	4.55	4.55	4.71	4.55
$\partial \ln V/\partial P$	$10^{-10}Pa^{-1}$	-3.6	-3.8	-3.7	-4.1
A+B	$10^{-4}K^{-1}$	-1.40	-0.66	-1.62	-0.73
A	$10^{-4}K^{-1}$	-1.52	-1.52	-1.57	-1.52
B	$10^{-4}K^{-1}$	0.12	0.86	-0.05	0.79
C	$10^{-4}K^{-1}$	-1.43	-4.47	0.39	-6.43
$\partial \ln\alpha/\partial \ln V$		0.08	0.57	-0.03	0.52
Gibbs analysis					
$\partial \ln\varepsilon'/\partial P$	$10^{-10}Pa^{-1}$	2.7	1.3	3.0	1.6
$(\varepsilon'+2)(\varepsilon'-1)/3\varepsilon'$		0.808	0.798	0.798	0.81
$\partial \ln V/\partial P$	$10^{-10}Pa^{-1}$	-3.6	-3.8	-3.7	-4.1
$\partial \ln\alpha/\partial P$	$10^{-10}Pa^{-1}$	-0.26	-2.17	0.059	-2.12
$\partial \ln\alpha/\partial \ln V$		0.07	0.57	-0.02	0.52

This equation is essentially the same as equation (6.9). The main purpose of the *Havinga analysis*, equations (6.6) and (6.9), is to study the effect of temperature (terms A, B and C), while *Gibbs* approach aims purely at the effect of pressure. A useful quantity, which can be extracted from both analyses, is (Hampton et al. 1989):

$$\frac{\partial \ln \alpha}{\partial \ln V} = -B / A = \frac{\partial \ln \alpha / \partial P}{\partial \ln V / \partial P} \qquad (6.11).$$

This quantity enables assessment of the overall agreement between the two different methods of analysis of the same data. In Table 6.7 the results obtained using Gibbs-Hill approach have also been presented. The measurement frequency is 100 kHz for P6 and S299, and 10 kHz for P42 and C56. The pressure dependence of the dielectric constant for these polyethylenes is essentially frequency independent in the frequency range studied.

It can be seen from Table 6.7 that the quantity $\partial \ln\alpha/\partial \ln V$, obtained using two methods of analysis, agrees well, although the Havinga analysis involves temperature dependence data while Gibbs method deals with only the pressure dependence data. The agreement between the two methods indicates the reliability of experimental data measured dielectrically and ultrasonically.

The results in Table 6.7 show that samples XLP3, XLP16 and C56 have different dielectric behaviour from that of polyethylene XLP42, for which both the temperature and pressure derivatives of the polarizability are positive rather than negative - as found for the other three samples. The polarizability for crosslinked polyethylenes XLP3, XLP16 and cable insulation C56 decreases with pressure. In general, increasing pressure would decrease the free volume of the polymer, restricting the rotation of the dipoles and consequently reducing the polarizability. The small positive value $(\partial \ln\alpha/\partial P)_T$ for P42 does not mean anything physical because its value falls within the experimental error. This negligible $(\partial \ln\alpha/\partial P)_T$ and relatively small $(\partial \ln\alpha/\partial T)_P$ suggest that the impurity level in polyethylene P42 is small compared with those in the other three polyethylenes. The characteristics found in the temperature and pressure dependences of the dielectric constant of this polymer P42 arise mainly from the

change in density as the temperature and pressure are increased. However, for the other three polyethylenes, $(\partial \ln\alpha/\partial T)_P$ and $(\partial \ln\alpha/\partial P)_T$ make much larger contributions to the temperature and pressure derivatives of the dielectric constant, indicating that an appreciable amount of impurities exist in these polyethylenes. Among the four samples studied, the samples C56 and XLP16 show a much stronger temperature dependence, as well as pressure dependence, of polarizability than those of the others.

Normally, the polarizability of a solid would be expected to increase with temperature because the intermolecular force which restricts the rotation of dipoles would become much weaker. The negative value found for $(\partial \ln\alpha/\partial T)_P=B+C$ for XLP3, XLP16 and C56 is probably due to the anomalous thermal contraction observed on XLP16 around room temperature (Figure 6.20(b)). The contraction may be associated with increase the crystallinity and make it more difficult for the dipoles to rotate, resulting in a decrease in polarizability as temperature rises.

The relationship between the effects of pressure and temperature.

It is interesting to note that the changes in the real permittivity induced by the hydrostatic pressure (~20% for pressure 0-0.2GPa) are enormous compared with those produced by increasing temperature (~6% for temperature 295K-370K,). Study of the effects of hydrostatic pressure on the permittivity of crosslinked polyethylene should provide a key towards understanding more about the nature of the free volume and its influence on the dielectric behaviour of the polymer.

The dielectric constant of polyethylene can in general be expressed as a function of temperature T, pressure P and volume v. If we assume that the dielectric properties of a polymer are mainly determined by its free volume, the temperature and pressure derivatives of the dielectric constant can be written as

$$\left[\frac{\partial \varepsilon'}{\partial T}\right]_P = \left[\frac{\partial \varepsilon'}{\partial v}\right]_{T,P}\left[\frac{\partial v}{\partial T}\right]_P \tag{6.12}$$

$$\left[\frac{\partial \varepsilon'}{\partial P}\right]_T = \left[\frac{\partial \varepsilon'}{\partial v}\right]_{P,T}\left[\frac{\partial v}{\partial P}\right]_T \tag{6.13}$$

It follows that

$$-\left(\frac{\partial \varepsilon'}{\partial T}\right)_P \Big/ \left(\frac{\partial \varepsilon'}{\partial P}\right)_T = -\left(\frac{\partial v}{\partial T}\right)_P \Big/ \left(\frac{\partial v}{\partial P}\right)_T = \beta B = \left(\frac{\partial P}{\partial T}\right)_v \qquad (6.14)$$

Using equation (6.14) and the experimental values of $(\partial\varepsilon'/\partial T)_P$ and $(\partial\varepsilon'/\partial P)_T$, the $(\partial P/\partial T)_v$ for crosslinked polyethylene P6, S299 and P42 at atmospheric pressure and room temperature have been calculated. The results are given in Table 6.8, together with those obtained from ultrasonic data for comparison.

Table 6.8. The pressure and temperature derivatives of the dielectric constant and the value of $(\partial P/\partial T)_v$ for polyethylenes at room temperature and atmospheric pressure.

Sample	$(\partial\varepsilon'/\partial P)_T$ (Pa^{-1})	$(\partial\varepsilon'/\partial T)_P$ (K^{-1})	$(\partial P/\partial T)_v$[(a)] (K/Pa)	$(\partial P/\partial T)_v$[(b)] (K/Pa)
P6	3.1×10^{-10}	-28.2×10^{-4}	9.1×10^{6}	1.6×10^{6}
S299	6.2×10^{-10}	-15.9×10^{-4}	2.6×10^{6}	1.9×10^{6}
P42	6.9×10^{-10}	-6.7×10^{-4}	1.0×10^{6}	1.2×10^{6}

(a) Determined dielectrically.

(b) Determined ultrasonically.

For the three polyethylenes, the value of $(\partial P/\partial T)_v$, measured using the ultrasonic method, has the same order of magnitude as that obtained from the dielectric data. This is consistent with a strong correlation between the ultrasonic and electrical properties of crosslinked polyethylene. The large intermolecular volume (or free volume), responsible for the large pressure derivative of ultrasonic wave velocity, $(\partial V_L/\partial P)_T$, must play an important role in determining the dielectric behaviour of the material.

The dielectric behaviour of cable insulation.

The dielectric behaviour of polyethylene cable sample (Figures 6.10, 6.11, 6.16, 6.17 and 6.25) is notably different from that of the plaque polyethylene samples. The dielectric constant of cable polyethylene (~2.5) is larger than the normally accepted

value (~2.3 or less). The temperature dependence of the dielectric constant is almost linear below the melting point where a much sharper drop than that of the plaque samples has been observed (Figure 6.11). The Lorentz fit ($F(x) = (2Aw/\pi)/(w^2+4(x-x_c)^2)$), where A is area, w is the width of the peak and x_c the center of the peak.) of the $-\partial\varepsilon/\partial T$ for cable polyethylene (Figure 6.25) shows a much narrower peak width (~3K) at the melting point than the corresponding peak widths of 8K for P40 and 11K for P42 (Figures 6.22 and 6.23). The loss peak at melting is a unique characteristic of the cable insulation (Figure 6.10(b)).

An interesting feature of the dielectric response of polyethylene cable insulation is that the outer layer of the cable has a larger dielectric constant than the inner part (Table 6.3). As will be discussed later in Chapter 7, the ultrasonic wave velocity shows a similar distribution across the cable section. Both the dielectric and ultrasonic results suggest that there may be a density difference across the cable section, the outer part having a higher density than the inner part. The ultrasonic measurement substantiates the dielectric data and is consistent with the correlation between the mechanical and electrical properties of the polymer.

Although it is still difficult at this stage to understand all the dielectric features mentioned above, it is instructive to point out the possible effects on the dielectric breakdown properties of the polyethylene cable insulation. Because the dielectric constant of the outer layer of the cable insulation is larger than that of the inner layer, the dielectric breakdown strength of the outer layer is likely to be less than the inner layer (see the following discussion on electromechanical breakdown). Therefore the dielectric properties of the outer part of the polyethylene cable insulation may play a more important role than those of the inner part in the electromechanical breakdown process. However, the measurement of ultrasonic wave velocity indicates that the outer part of the cable also has a larger value of Young's modulus so that the dielectric response of real cable could be much more complicated.

CHAPTER 7. TEMPERATURE AND HYDROSTATIC PRESSURE DEPENDENCES OF ULTRASONIC WAVE VELOCITY AND ATTENUATION IN POLYETHYLENE AND POLYETHYLENE CABLE INSULATIONS

7.1. The characterization of samples at room temperature using ultrasonic velocity and density measurements

To characterize the various polyethylene (PE) samples supplied by BICC Cables Limited, room temperature measurements have been made of the velocity of longitudinal ultrasonic waves at 5MHz. In addition the density of each sample has been measured using the Archimedes method with acetone as the floatation liquid. Taken together the ultrasonic velocity and density data enable calculation of the characteristic acoustic impedance (ρV_L) and the longitudinal stiffness modulus (ρV_L^2) for low density polyethylenes (LDPE), low density polyethylene with additives (LDPE+a), electronic beam radiation crosslinked polyethylene (EBXLPE) and peroxide crosslinked polyethylene (XLPE). The results are given in Table 7.1. Among the polyethylene samples studied, HFDE 4201 EC is the crosslinked version of HFDQ 4201 EC, P3+G17, P16+G17, P40 and P42 are the crosslinked version of P3, P16, P61 and P64 respectively. C56 was cut from the cable insulation made from crosslinked polyethylene P16+G17 (see Appendix 1 for detailed sample descriptions and nomenclature). The molecular weights of the thermoplastic polyethylenes (except HFDQ4201 EC) are given in Table 7.2. The molecular weight for the corresponding crosslinked polyethylenes is expected to be the same.

Table 7.1. The density ρ, longitudinal wave velocity V_L, characteristic impedance ρV_L and longitudinal stiffness modulus ρV_L^2 of polyethylenes at room temperature.

	Sample		ρ (kg/m^3)	V_L (m/s)	ρV_L (kg/m^2s)	ρV_L^2 (GPa)
1	HFDQ4201EC	LDPE	914	2118	1.94×10^6	4.10
2	HFDE4201EC	EBXLPE	924	1950	1.80×10^6	3.51
3	P3	LDPE	919	2025	1.86×10^6	3.77
4	P3+G16	LDPE+a	915	1995	1.83×10^6	3.64
5	P3+G17	XLPE	914	1959	1.79×10^6	3.51
6	P16	LDPE	920	2040	1.88×10^6	3.83
7	P16+G16	LDPE+a	920	2000	1.84×10^6	3.68
8	P16+G17	XLPE	914	1976	1.80×10^6	3.57
9	C56	CABLE	917	1979	1.81×10^6	3.59
10	P61	LDPE	924	2044	1.89×10^6	3.86
11	P40	XLPE	921	1995	1.84×10^6	3.67
12	P64	LDPE	921	2021	1.86×10^6	3.76
13	P42	XLPE	916	1980	1.81×10^6	3.59
14	P2	LDPE	930	2147	2.00×10^6	4.29
15	C23	CABLE	917	1996	1.83×10^6	3.65
16	C51	CABLE	921	1987	1.83×10^6	3.64

Table 7.2. The weight average molecular weight M_w, the number average molecular weight M_n and the polydispersity M_w/M_n of some polyethylene samples studied in this work.

Sample	M_w	M_n	Polydispersity
P2	80700	17050	4.73
P3	101500	16850	6.02
P16	102550	15150	6.77
P61	92800	16400	5.66
P64	100900	15200	6.64

There are considerable differences in ultrasound wave velocity from sample to sample, although they are all basically low density polyethylenes. The longitudinal ultrasonic wave velocity varies between 1950m/s and 2147m/s. Clearly, the ultrasonic properties are much influenced by the manufacturing process.

The effect of electron beam (EB) crosslinking is to increase the density, while that of the peroxide crosslinking is to decrease the density. The difference in density resulting from these two crosslinking methods may arise from the fact that most of the crosslinks generated by EB radiation occur in amorphous region, which tend to enhance the interaction of the molecules, reduce the mobility of the polymer chains, while peroxide crosslinks take place uniformly in the amorphous region as well as crystalline region. The decrease in crystallinity seems to be dominant in the peroxide crosslinking process. In general, for polymers high density tends to be correlated with greater velocity. However, as can be seen in Table 7.1, this is not always true for polyethylenes. Both the longitudinal wave velocity and the stiffness modulus for the crosslinked samples are smaller than those of the corresponding thermoplastic polyethylenes. The characteristic acoustic impedances are found to be of the same order for all samples. This indicates that the loss in transmission of a stress wave across an interface between the polymers is rather small.

Comparing the results for samples 3 and 4, as well as samples 6 and 7 in Table 7.1, it is clear that the effect of the antioxidant itself is to reduce the velocity, the characteristic impedance and the modulus of the polyethylenes.

7.2. The temperature dependence of the ultrasonic wave velocity and attenuation of polyethylene

The ultrasonic wave velocity in a polymer depends primarily on the intermolecular potential, which is related to the intermolecular separation and hence to the polymer density. Ultrasonic attenuation is expected to depend mainly on relaxation processes. To follow the changes in physical properties of polyethylene with temperature, measurements of ultrasonic sound wave velocity and attenuation have been made on 16 polyethylene samples in the temperature range of 10K to 403K. The velocity, attenuation and stiffness modulus of longitudinal ultrasonic waves propagated in these polyethylenes at selected temperatures are given in Tables 7.3, 7.4 and 7.5. Some of the results are also shown graphically in Figures 7.1 to 7.13.

Table 7.3. The velocity V_L (m/s) of longitudinal ultrasonic waves propagated in polyethylene samples at selected temperatures. The sample descriptions and nomenclature can be found in Appendix 1.

Sample	300K	323K	343K	363K
HFDQ4201EC	2030	1801	1601	
P3	2088	1847	1654	1480
P16	2102	1872	1704	1533
P61	2075	1869	1709	1556
P64	2110	1917	1766	1619
P2	2145	1974	1831	1675
P3+G16	2122	1856	1670	1490
P16+G16	2123	1875	1685	1509
HFDE4201EC	2077	1856	1698	1522
P3+G17	2099	1851	1682	1492
P16+G17	2076	1858	1682	1498
P40	2074	1843	1676	1492
P42	2059	1829	1649	1471
C51	2017	1796	1635	1476
C56	1974	1798	1653	1506

Table 7.4. The attenuation α (dB/cm) of longitudinal ultrasonic waves propagated in polyethylene samples at selected temperatures. The sample descriptions and nomenclature can be found in Appendix 1.

Sample	300K	323K	343K	363K
HFDQ4201EC	26.6	36.2	28.2	
P3	31.8	35.2	30.0	25.9
P16	32.7	31.7	27.4	22.2
P61	28.2	29.8	26.6	24.0
P64	28.5	28.7	25.2	26.3
P3+G16	32.0	31.6	31.6	27.6
P16+G16	37.4	31.3	31.9	26.4
HFDE4201EC	26.8	25.5	29.5	18.8
P3+G17	32.8	36.8	27.6	20.0
P16+G17	34.4	46.8	26.6	22.3
P40	26.9	28.6	23.8	18.9
P42	25.6	27.2	21.9	16.3
C51	26.0	24.2	18.8	12.8
C56	21.4	21.0	15.6	9.9

Table 7.5. The longitudinal stiffness C_{11} (GPa) of polyethylene samples at selected temperatures. The density ρ of the sample at room temperature has been used in the calculation of C_{11}. The sample descriptions and nomenclature can be found in Appendix 1.

Sample	300K	323K	343K	363K	ρ (kg/m^3)
HFDQ4201EC	3.77	2.96	2.34		914
P3	4.01	3.14	2.51	2.01	919
P16	4.06	3.22	2.67	2.16	920
P61	3.98	3.23	2.7	2.24	924
P64	4.11	3.38	2.87	2.41	921
P2	4.29	3.63	3.12	2.61	930
P3+G16	4.12	3.15	2.55	2.03	915
P16+G16	4.15	3.23	2.61	2.09	920
HFDE4201EC	3.99	3.18	2.66	2.14	924
P3+G17	4.03	3.13	2.59	2.03	914
P16+G17	3.94	3.15	2.59	2.05	914
P40	3.96	3.13	2.59	2.05	921
P42	3.88	3.06	2.5	1.98	916
C51	3.75	2.97	2.46	2.01	921
C56	3.57	2.96	2.51	2.08	917

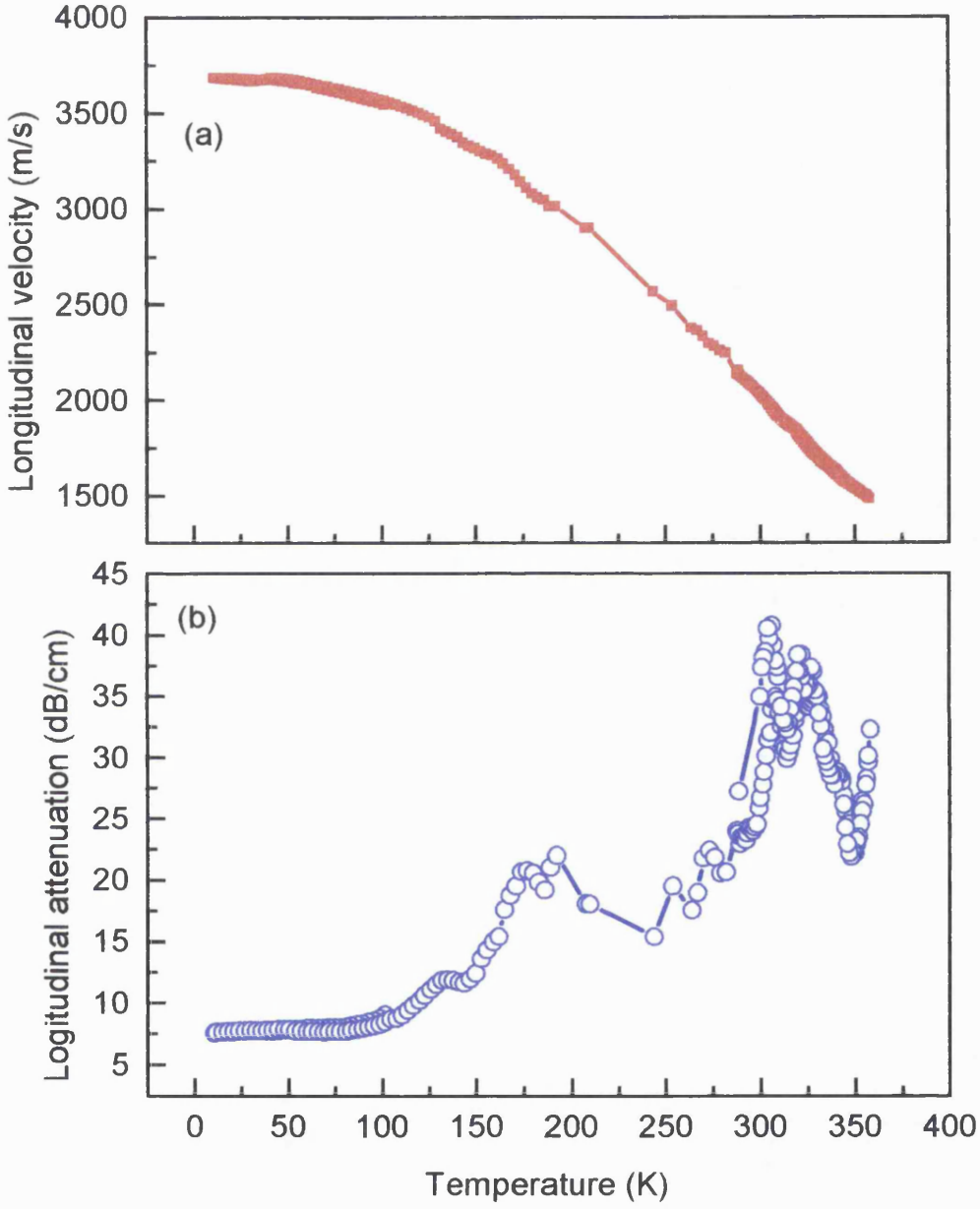

Figure 7.1 The temperature dependence of the velocity (a) and attenuation (b) of longitudinal ultrasonic waves propagated in low density polyethylene HFDQ 4201.

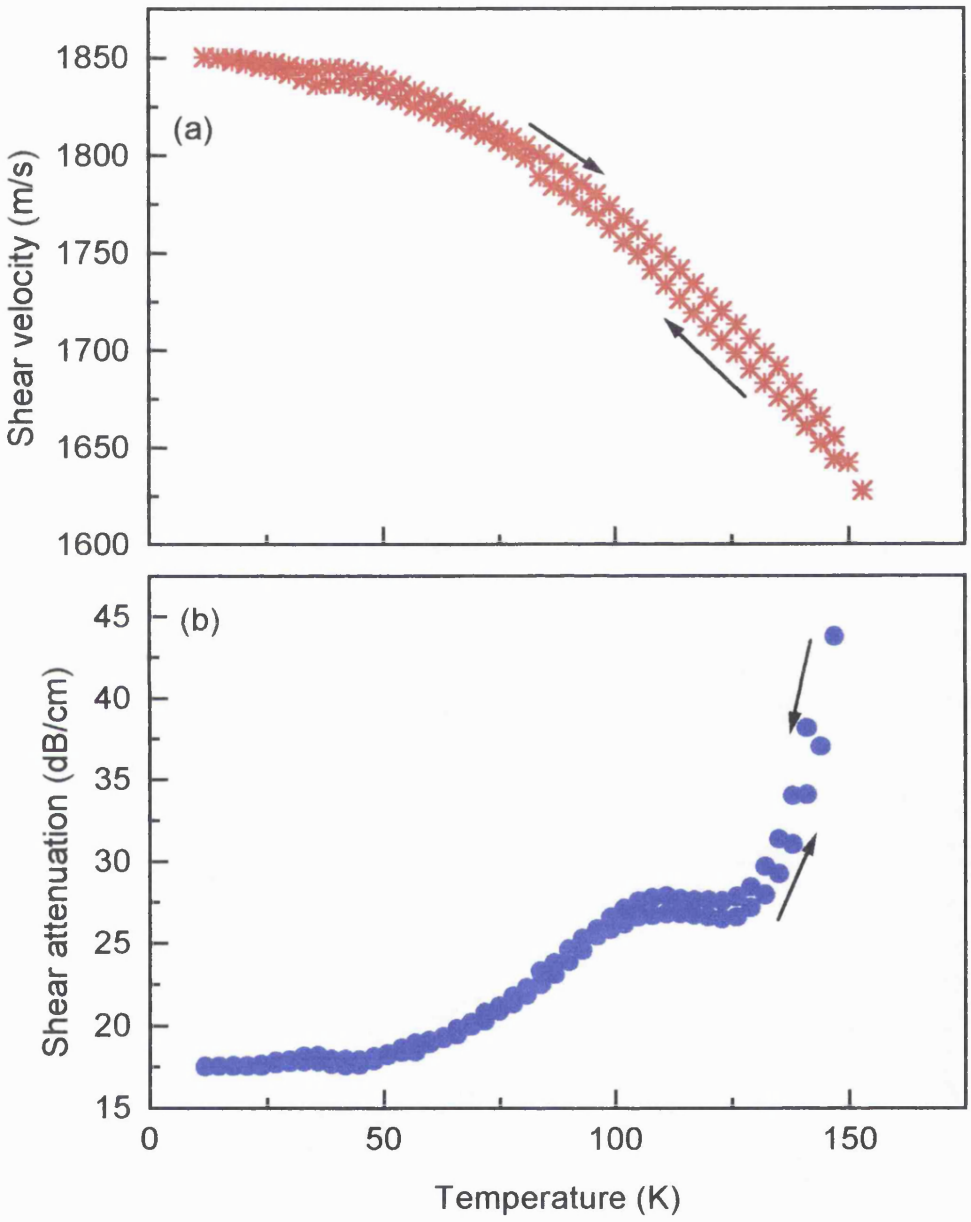

Figure 7.2 The temperature dependence of the velocity (a) and attenuation (b) of shear ultrasonic waves propagated in low density polyethylene HFDQ 4201 with decreasing and increasing temperature.

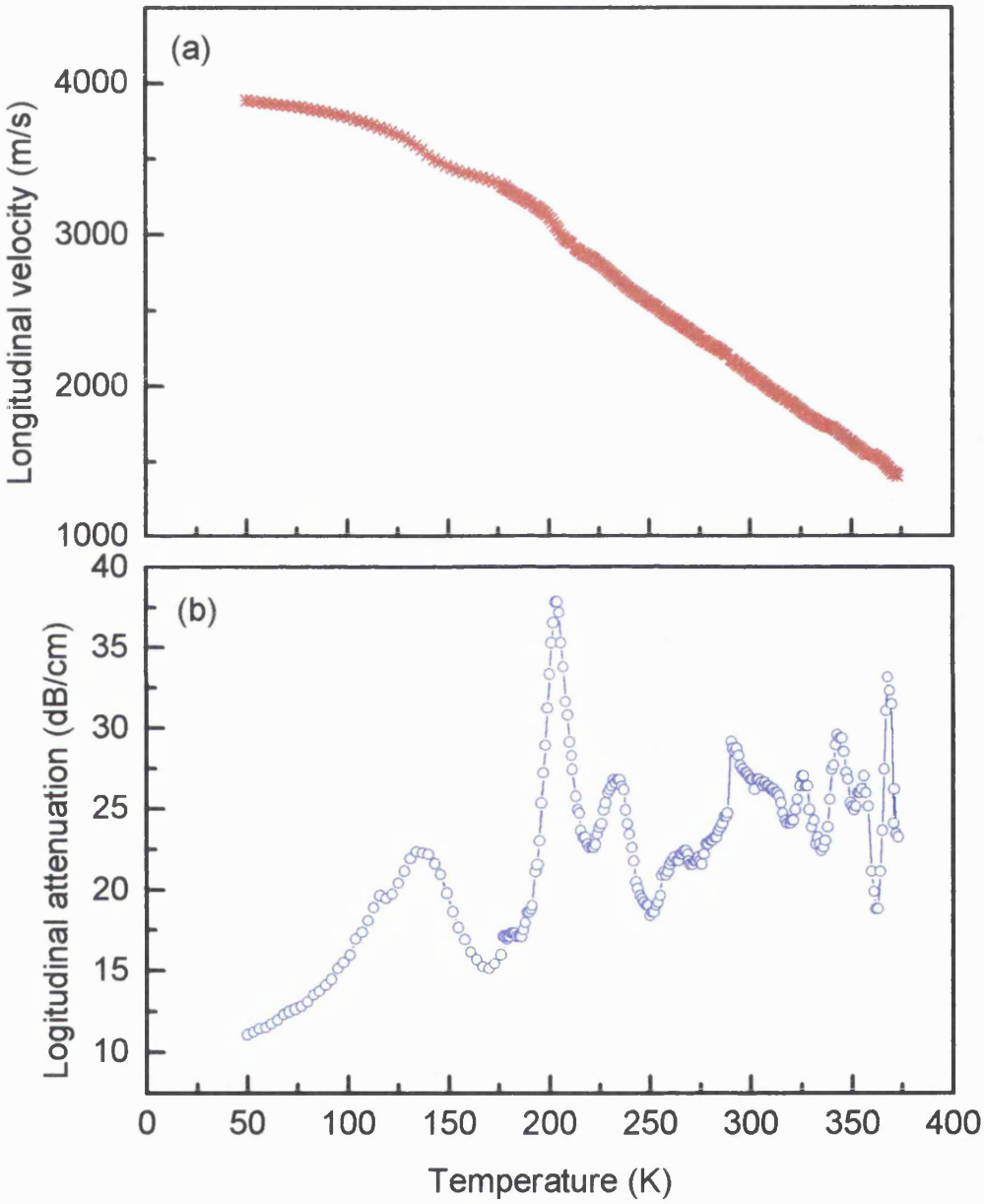

Figure 7.3 The temperature dependence of the velocity (a) and attenuation (b) of longitudinal ultrasonic waves propagated in crosslinked polyethylene HFDE 4201.

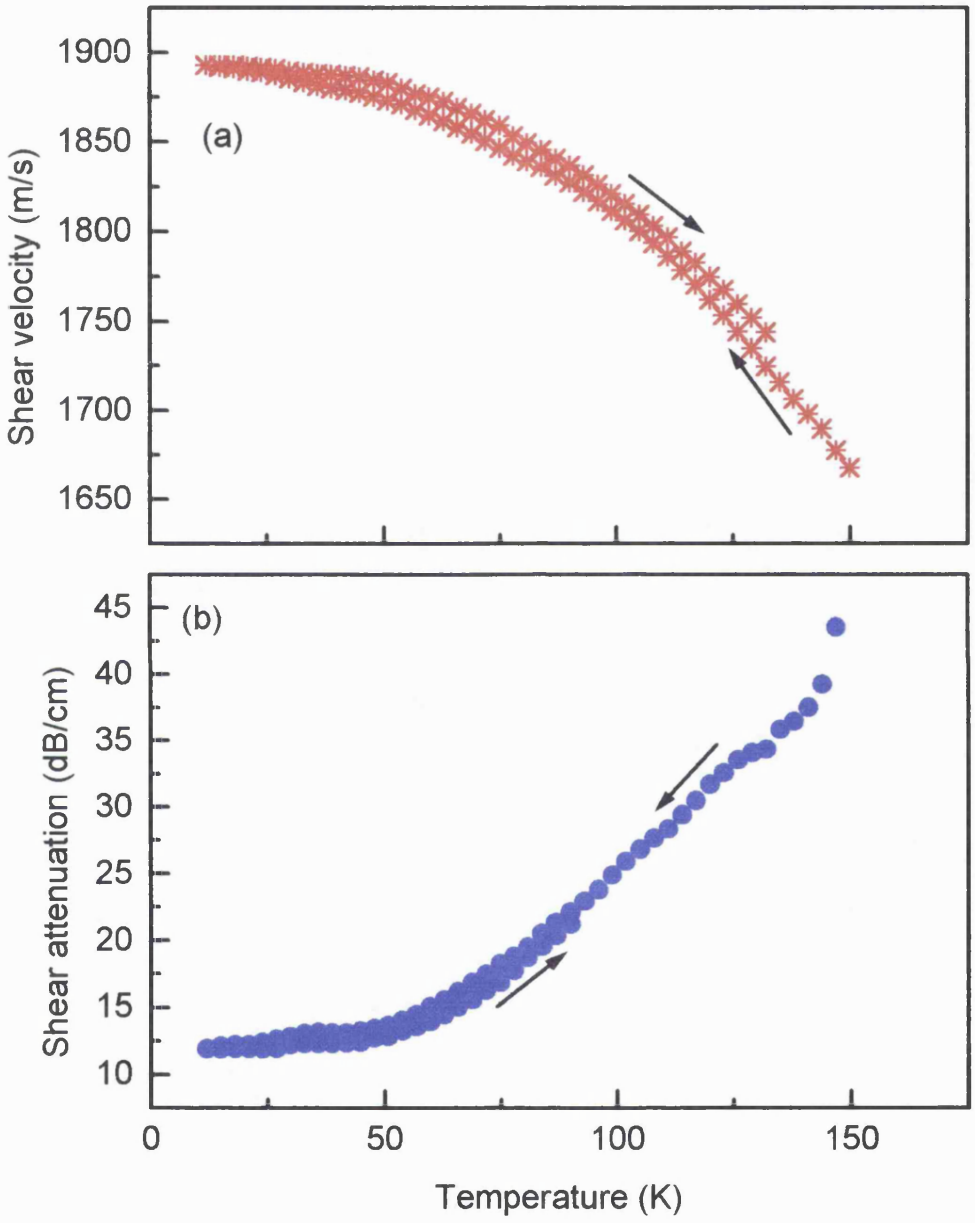

Figure 7.4 The temperature dependence of the velocity (a) and attenuation (b) of shear ultrasonic waves propagated in crosslinked polyethylene HFDE 4201 with increasing and decreasing temperature.

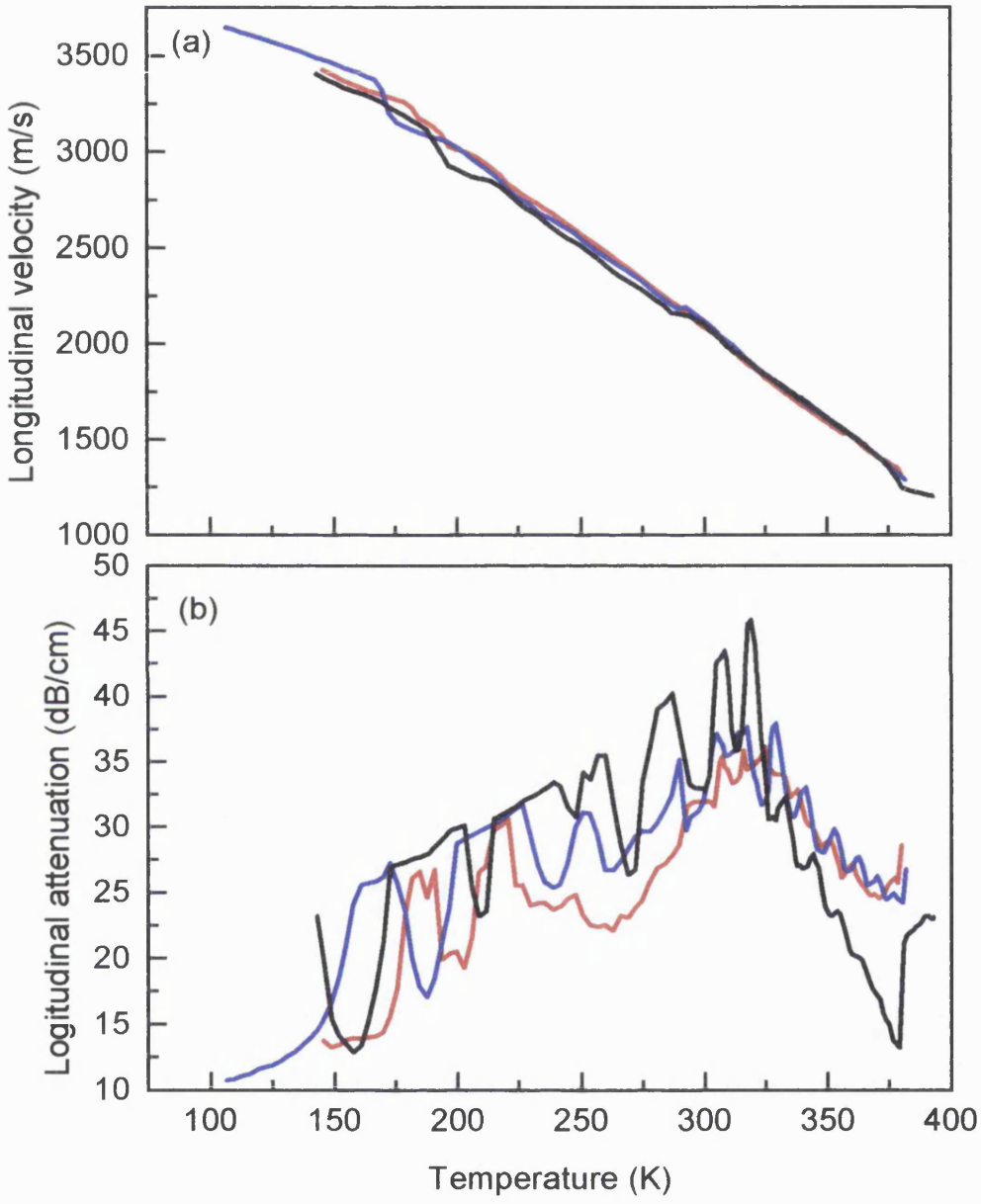

Figure 7.5 The temperature dependence of the velocity (a) and attenuation (b) of longitudinal ultrasonic waves propagated in low density polyethylene P3 (red), P3 with additives (blue) and crosslinked polyethylene P3+G17 (black).

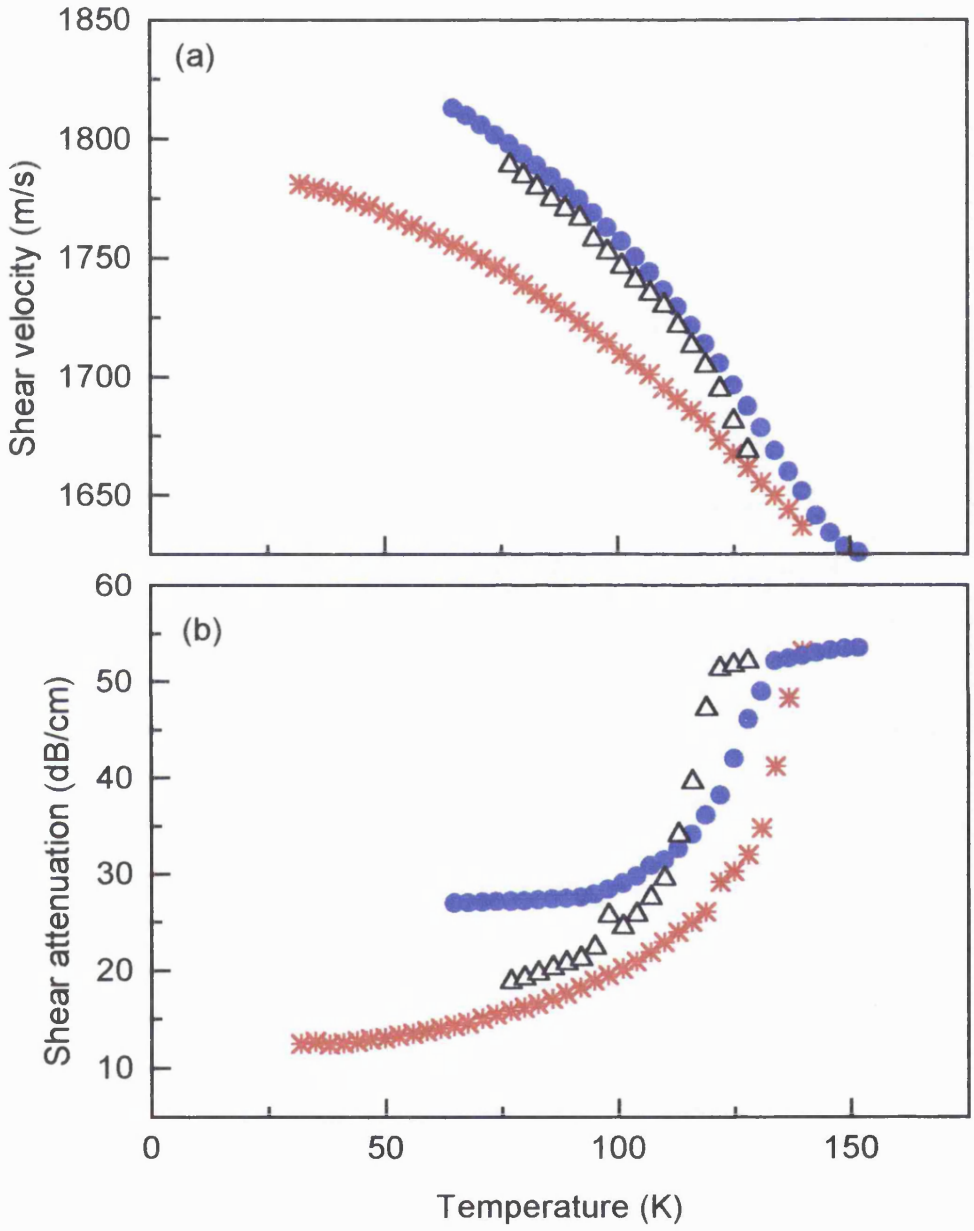

Figure 7.6 The temperature dependence of the velocity (a) and attenuation (b) of shear ultrasonic waves propagated in low density polyethylene P3 (red stars), P3 with additives (blue circles) and crosslinked polyethylene P3+G17 (black triangles).

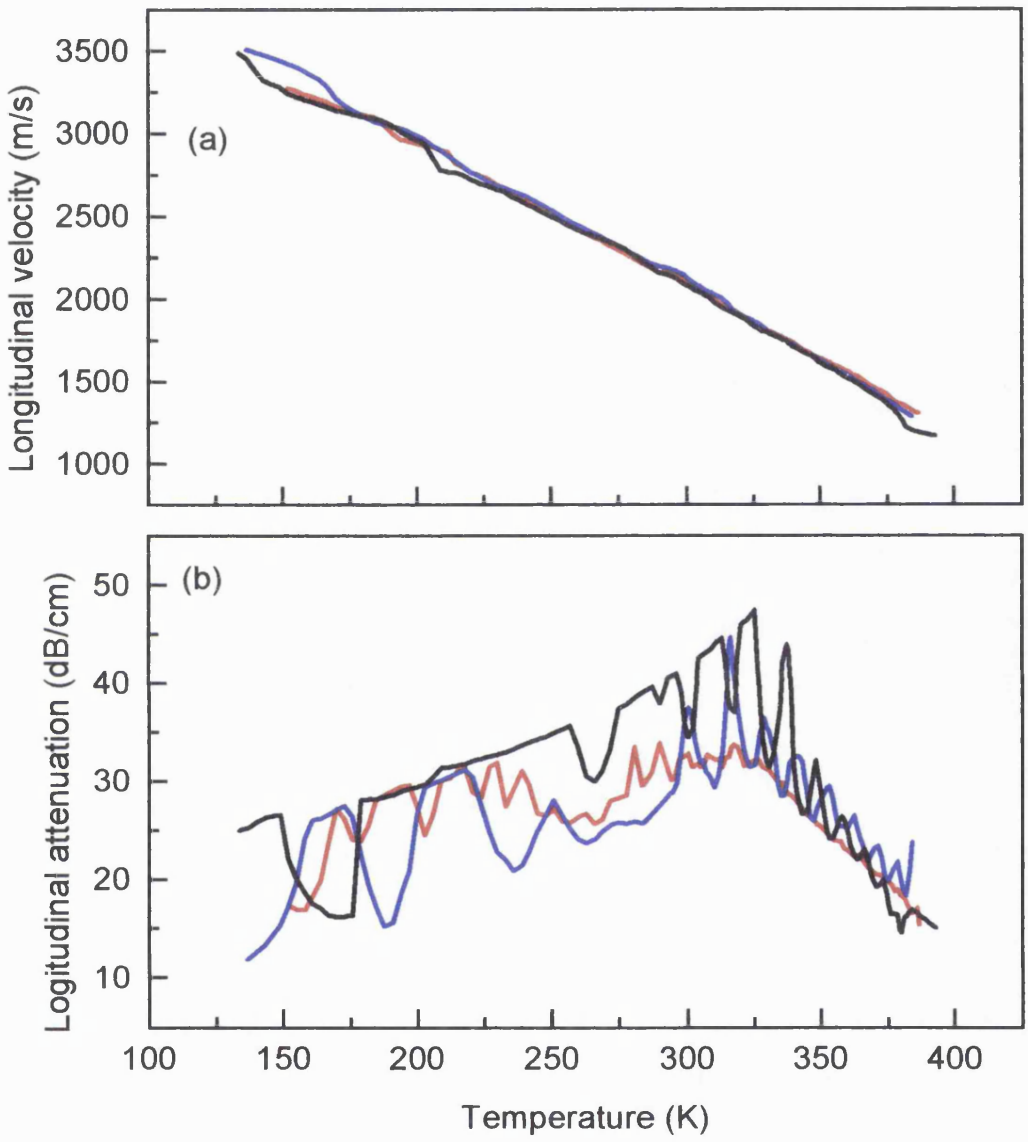

Figure 7.7 The temperature dependence of the velocity (a) and attenuation (b) of longitudinal ultrasonic waves propagated in low density polyethylene P16 (red), P16 with additives (blue), crosslinked polyethylene P16+G17 (black) and cable sample C56 (brown).

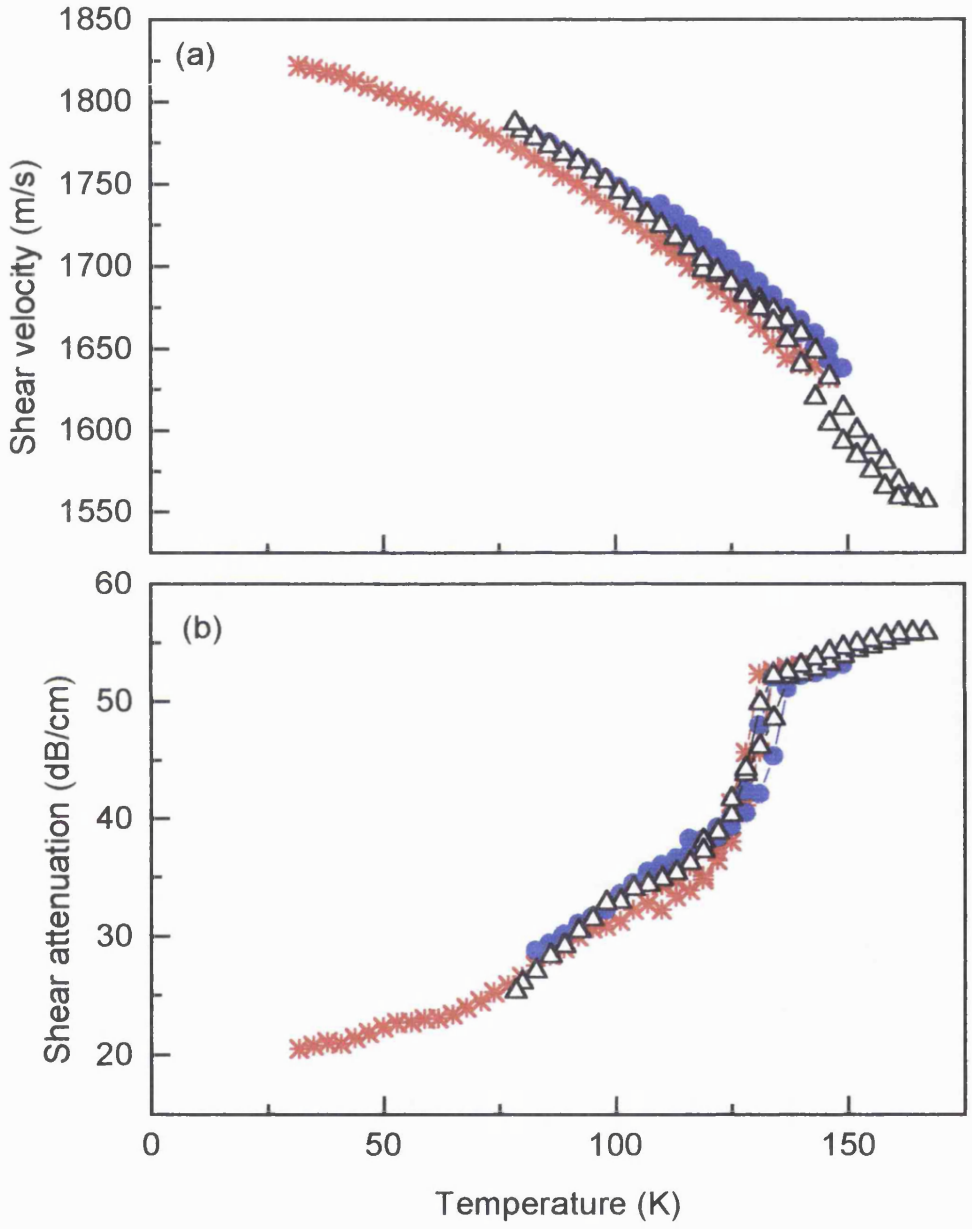

Figure 7.8 The temperature dependence of the velocity (a) and attenuation (b) of shear ultrasonic waves propagated in low density polyethylene P16 (red stars), P16 with additives (blue circles) and crosslinked polyethylene P16+G17 (black triangles).

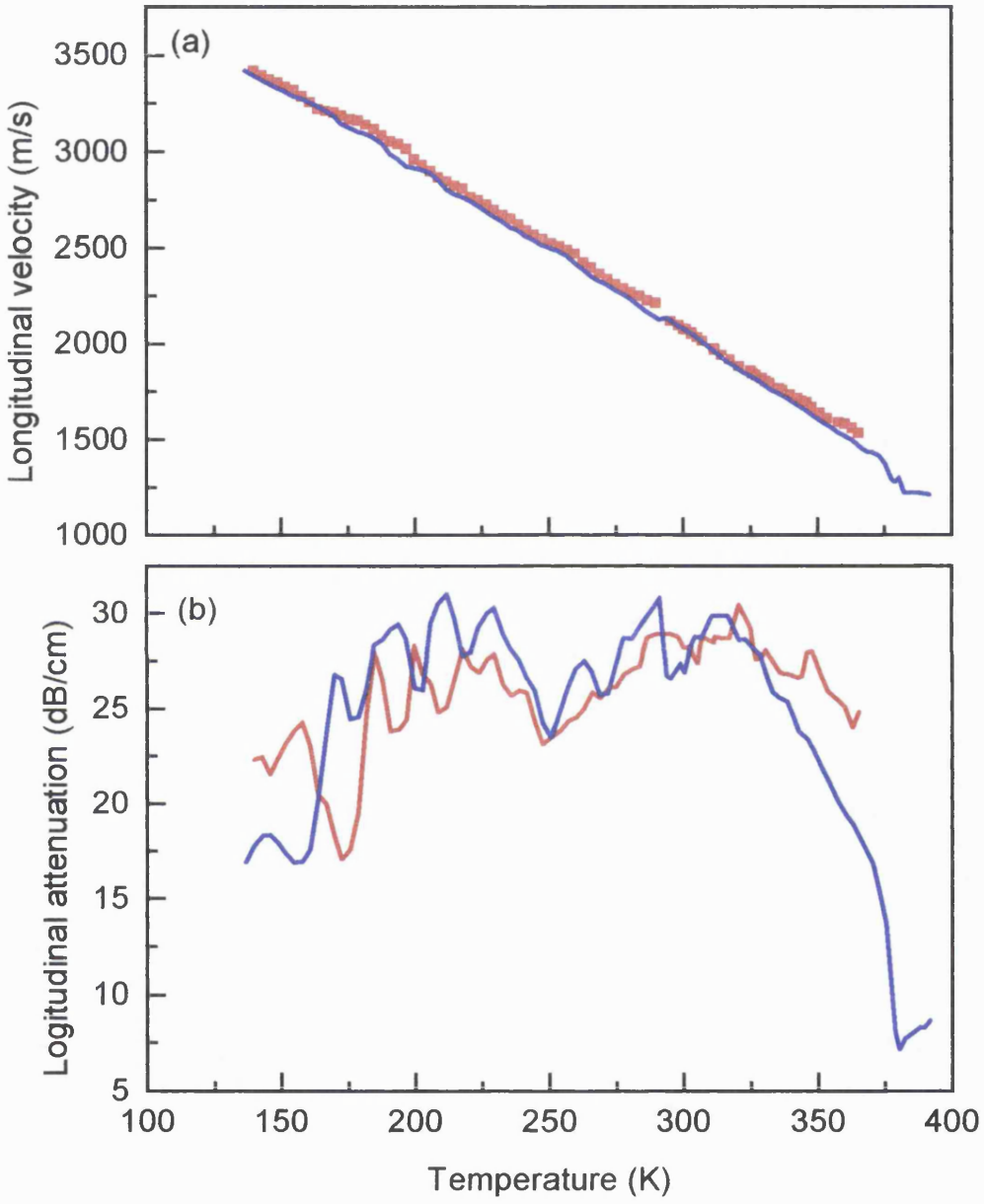

Figure 7.9 The temperature dependence of the velocity (a) and attenuation (b) of longitudinal ultrasonic waves propagated in low density polyethylene P61 (red) and crosslinked polyethylene P40 (blue).

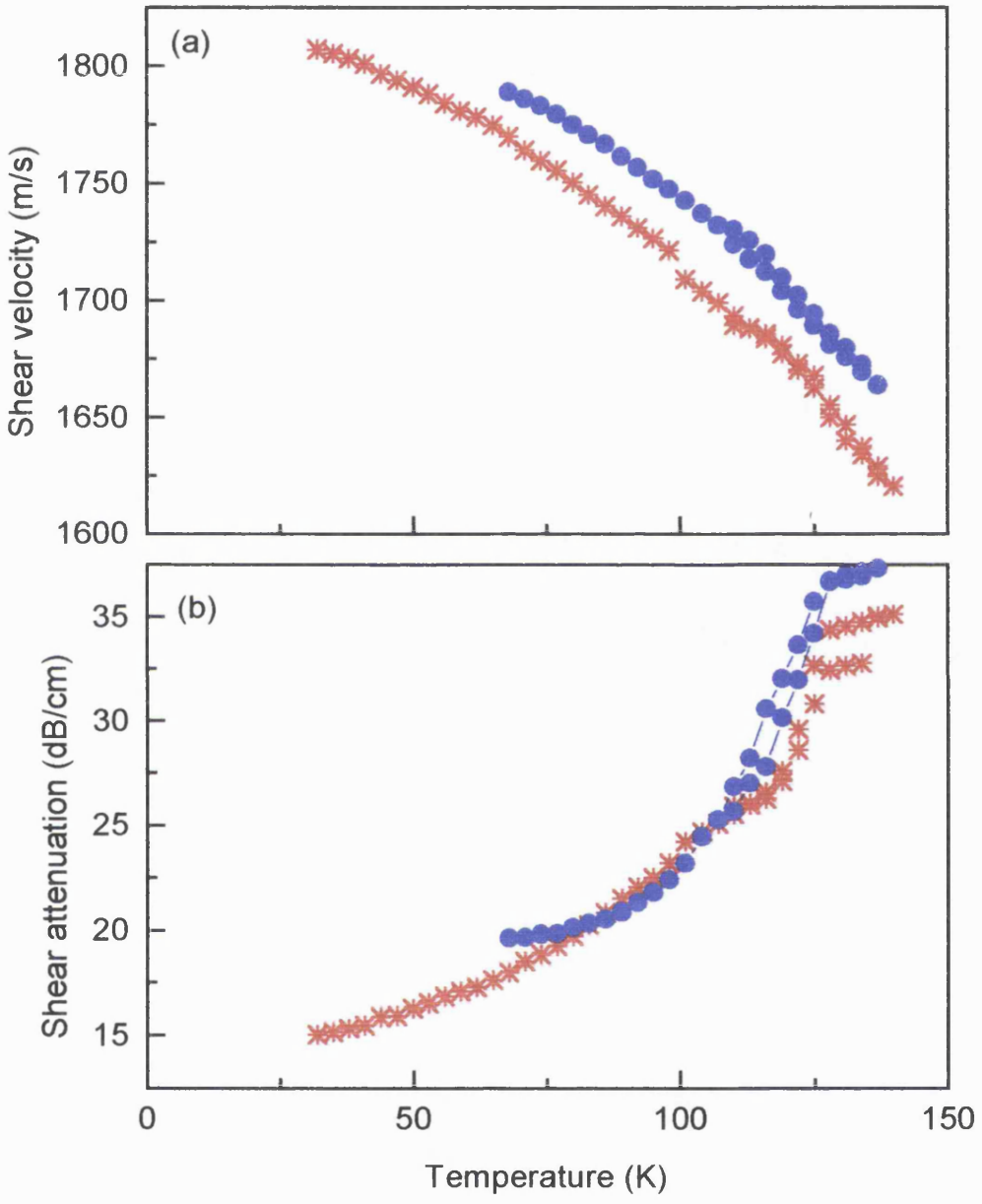

Figure 7.10 The temperature dependence of the velocity (a) and attenuation (b) of shear ultrasonic waves propagated in low density polyethylene P61 (red stars) and crosslinked polyethylene P40 (blue circles).

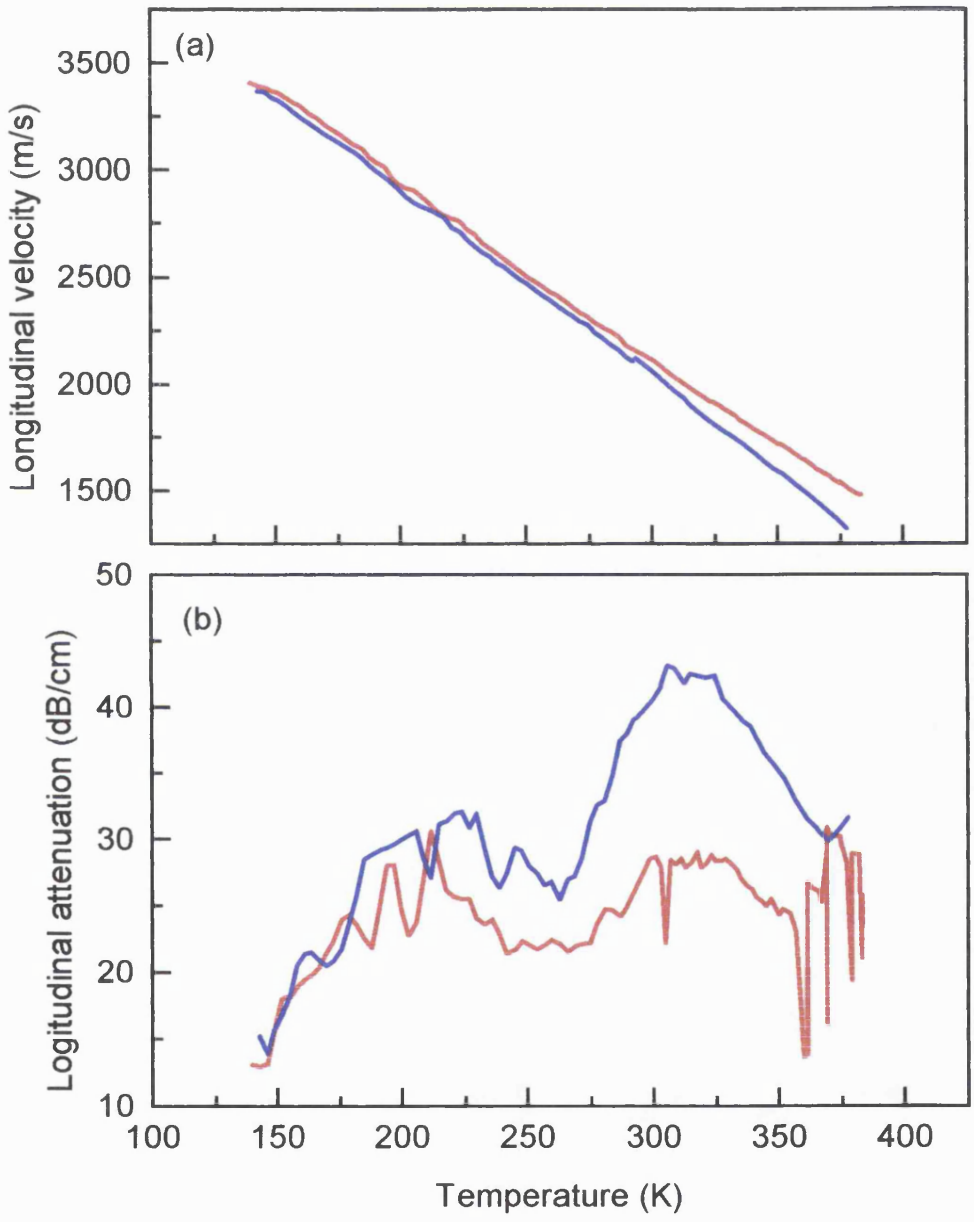

Figure 7.11 The temperature dependence of the velocity (a) and attenuation (b) of longitudinal ultrasonic waves propagated in low density polyethylene P64 (red) and crosslinked polyethylene P42 (blue).

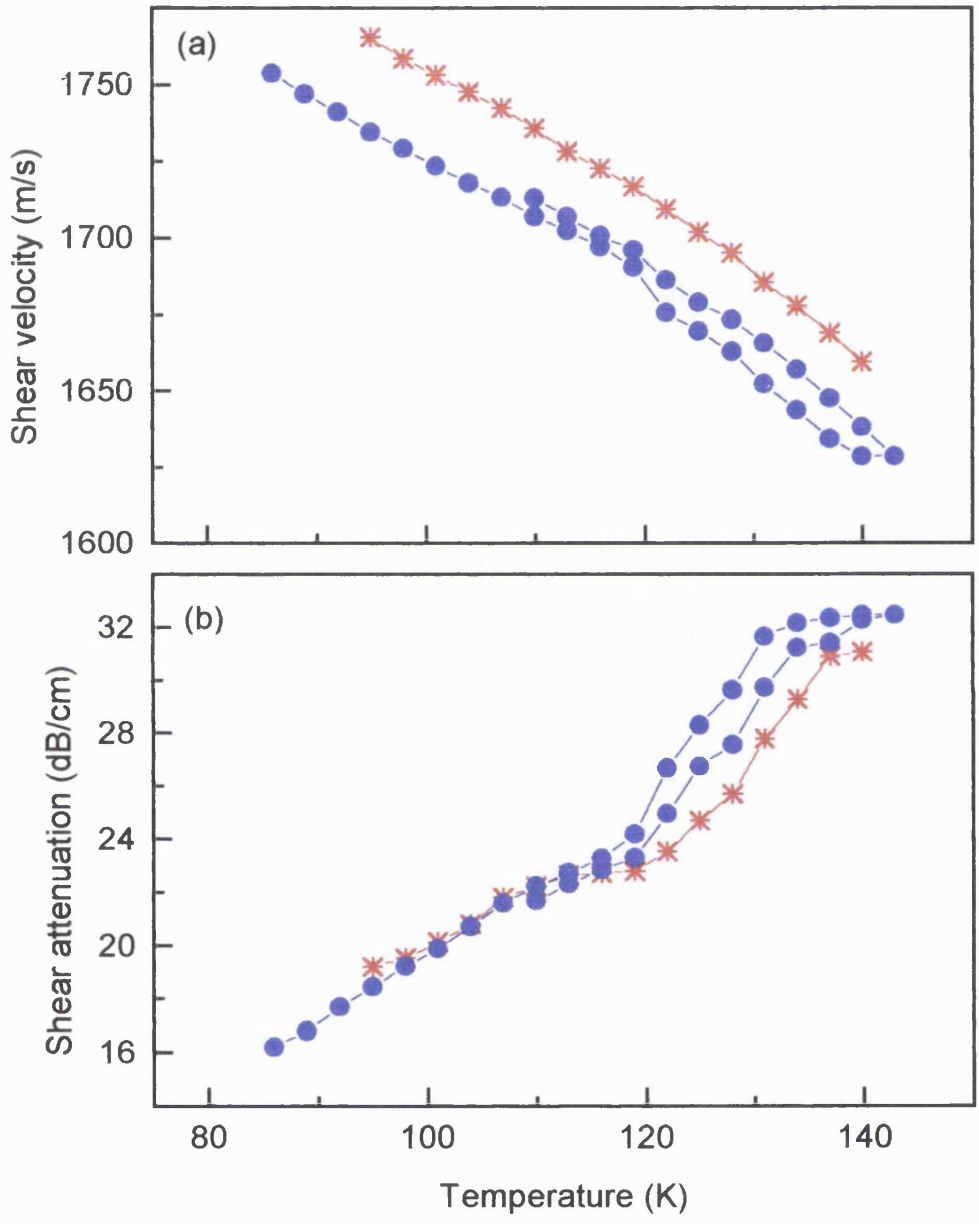

Figure 7.12 The temperature dependence of the velocity (a) and attenuation (b) of shear ultrasonic waves propagated in low density polyethylene P64 (red stars) and crosslinked polyethylene P42 (blue circles).

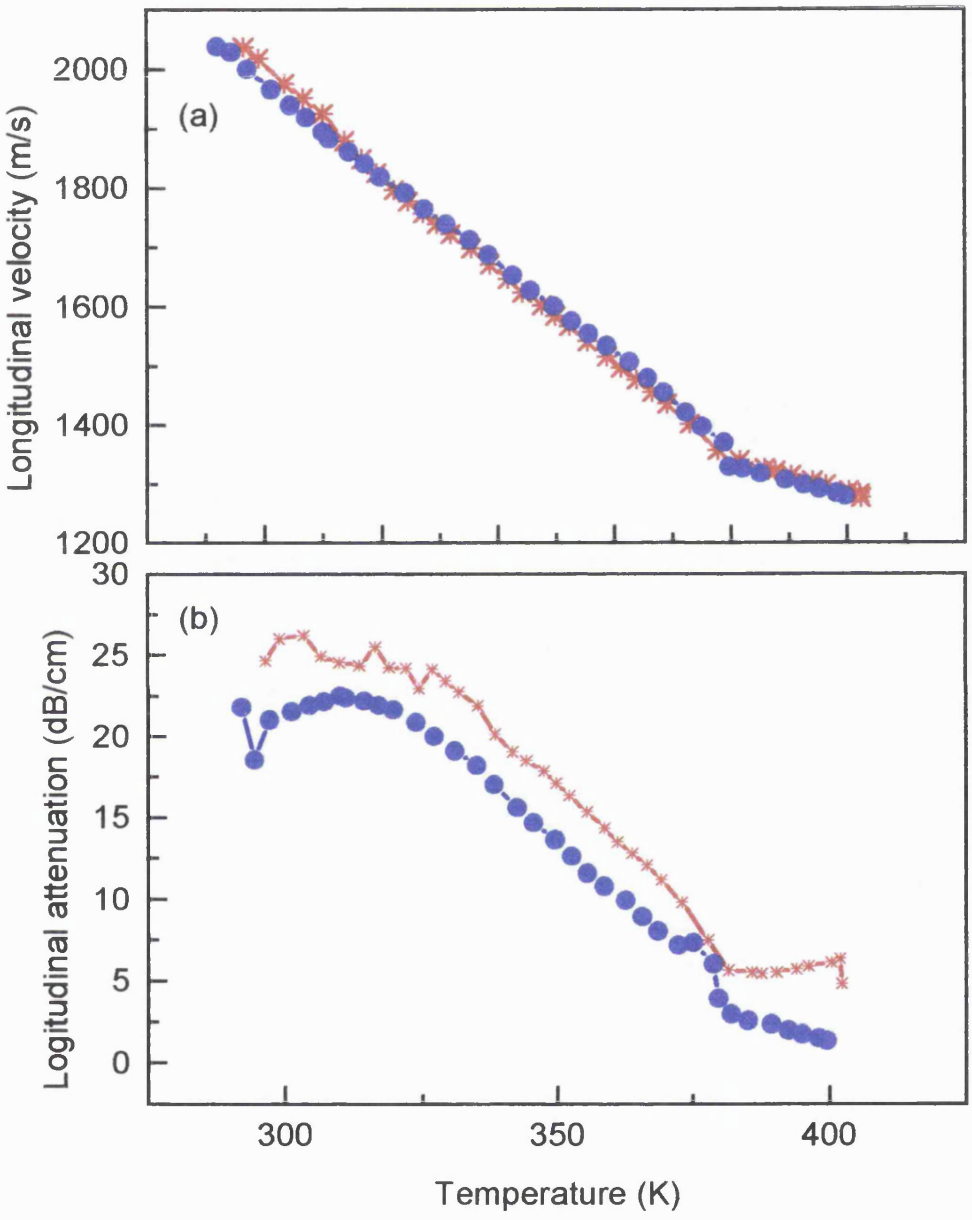

Figure 7.13 The temperature dependence of the velocity (a) and attenuation (b) of longitudinal ultrasonic waves propagated in cable sample C51 (red stars) and c56 (blue circles).

7.2.1. The ultrasonic properties of polyethylene 4201.

The temperature dependences of velocity and attenuation of 5MHz longitudinal ultrasonic waves propagated in low density polyethylene (LDPE) HFDQ 4201 (sample 1 in Table 7.1) are shown in Figure 7.1. There are two anomalous velocity kinks at about 130K and 180K, together with two corresponding attenuation peaks. It has been observed that in this temperature range, especially between 200K and 240K, the echoes were seriously distorted. For temperatures above 240K, the longitudinal ultrasonic wave velocity shows almost linear behaviour with two small kinks at 310K and 330K. Two attenuation peaks are found corresponding to these kinks (Figure 7.1(b)). Below 170K, the velocity increases non-linearly with decreasing temperature down to 40K, where it begins to drop down showing well defined structure (Figure 7.1(a)). This feature can hardly be seen in the longitudinal attenuation curve, which exhibits a small peak at about 130K. The temperature dependences of velocity and attenuation of 5MHz shear ultrasonic waves propagated in sample 1 are shown in Figure 7.2. A small hysteresis can be seen in both the velocity and attenuation data between cooling and warming cycles. The most noticeable feature in the shear ultrasonic wave velocity curve is the small drop at 32K which is similar to that in the longitudinal mode but shifted to a somewhat lower temperature. There is an attenuation peak at the same temperature corresponding to the velocity kink. The shear ultrasonic wave attenuation shows a shoulder at about 120K similar to that observed in the longitudinal wave attenuation.

To study the effects of crosslinking on the temperature dependence of the elastic properties, the procedure undertaken on sample 1 has been repeated with sample 2 (Table 7.1) which was crosslinked using electron beam irradiation. The results are shown in Figures 7.3 and 7.4. As for sample 1, there are anomalous velocity changes and corresponding attenuation peaks between 130K and 240K. The echoes were better than those obtained in sample 1 over this temperature range. The relaxation strength in the elastic modulus and the attenuation peak are increased substantially in the crosslinked polyethylene (compare Figures 7.1 with 7.3). At high temperatures, the velocity kinks are less pronounced and the attenuation is reduced significantly

compared with those of sample 1 (Figure 7.1(b) and Figure 7.3(b)). The shear ultrasonic wave velocity and attenuation in sample 2 show the same feature at 32K as those in sample 1, but the attenuation plateau at 110K is not present (Figure 7.4).

7.2.2. The ultrasonic properties of polyethylenes P3 and P16.

To study further the effect of peroxide crosslinking process, the temperature dependences of the velocity and attenuation of longitudinal and shear waves propagated in two low density polyethylenes in the form of base resin, base resin with additives (stabilisers) and crosslinked have been measured over a temperature range between 100 and 400K. The results for samples 3 to 8 (see Table 7.1) are shown in Figures 7.5 to 7.8.

The longitudinal wave velocity for thermoplastic polyethylene P3 (sample 3 in Table 7.1) shows almost linear behaviour above 220K and below 180K with a different slope in these two temperature regions (Figure 7.5(a)). It increases more rapidly at 220K, 190K and 183K, forming three velocity kinks which correspond to the attenuation peaks in Figure 7.5(b). The anomalous ultrasonic behaviour between 180K and 220K is believed to be a consequence of the glass transition of amorphous material in this polyethylene sample and provides further evidence for our speculation that the glass transition in polyethylene involves freezing of multiple molecular motions rather than only a single process. The attenuation is very high and often saturated in the vicinity of the peaks. The echo-train becomes distorted seriously while the polyethylene is undergoing the glass transition; this has an effect on the measurements in this temperature range.

Above the glass transition, the longitudinal wave velocity for pure polyethylene P3 decreases almost linearly with temperature except for a small change in slope between 305K and 320K (Figure 7.5(a)). At 380K, the amplitude of the echoes decreases rapidly and then disappears, indicating the melting point of the crystalline phase of the material. The longitudinal wave attenuation in this sample shows a broad maximum

around 320K, above which it decreases gradually with temperature along with small fluctuations until 380K, where the attenuation increases again (Figure 7.5(b)).

The shear wave velocity in polyethylene P3 increases smoothly below 140K down to 32K (Figure 7.6(a)). Corresponding to the velocity, the attenuation of the shear waves decreases as the temperature goes down (Figure 7.6(b)). At 38K it increases a little bit forming a small peak, which is similar to the attenuation peak observed in samples 1 and 2 around 40K but is much weaker.

Although the temperature dependence of the velocity of longitudinal ultrasonic waves propagated in sample P3+G16 (Table 7.1) shows some similarities to that for the pure sample (Figure 7.5(a)), the behaviour in the glass transition region is markedly different. The effect of the additives has been to shift the main glass transition temperature down to 175K and to reduce the complexity of the ultrasonic wave velocity signature. The longitudinal attenuation in this sample is larger than that in the pure sample (Figure 7.5(b)). While there is still an attenuation peak at 220K, the other two peaks are at 170K and 255K when the sample includes antioxidant, while they are at 185K and 245K in the pure sample. In addition, the attenuation becomes so high during the transition that it saturates in the neighbourhood of two of the peaks (Figure 7.5(b)). The antioxidant added to the sample has little effect on the high temperature ultrasonic behaviour. The shear wave velocity in sample P3+G16 is larger than that in pure polyethylene sample P3 and increases more rapidly as the temperature goes down (Figure 7.6(a)). While the general trend is similar to that for the pure polyethylene, the shear attenuation has a bigger value in this sample. The data above 134K are saturated, not real, values.

Normally, when crosslinks are introduced into a polymer, the interaction between polymer molecules is enhanced and the density of the sample is increased. However crosslinking also reduces the crystallinity of the polyethylene resulting in a decrease in density. As can be seen in Figure 7.5(a), the effect of peroxide crosslinking in polyethylene P3 below room temperature is to reduce the longitudinal ultrasonic velocity by about 3%, which is consistent with the lower density (by about 0.5%) of

the crosslinked sample (Table 7.1). However, no difference in the longitudinal wave velocity within the experimental error has been observed for pure P3, P3 with additives or peroxide crosslinked P3 above room temperature. For the crosslinked version of polyethylene P3, the longitudinal wave velocity drops just before the temperature reaches 380K, where it decreases again linearly with a much smaller slope (Figure 7.5(a)). There are two attenuation peaks at 310 and 320K, which are much stronger than the corresponding peaks for the thermoplastic sample. At higher temperatures, the attenuation in the crosslinked sample is much less, although it follows the same trend as it does in thermoplastic P3. There is a sudden jump in the longitudinal attenuation at 380K, which can be related to the melting of the crystalline region. The echoes remain reasonably well above 380K and the attenuation tends towards a constant value at higher temperatures. Thus it is possible to make ultrasonic studies of crosslinked polyethylene above its melting point.

The glass transition temperature has been increased to 190K from 175K for polyethylene P3 with additives by introducing crosslinks in the sample. A well defined step in the temperature dependence of longitudinal wave velocity curve for the crosslinked polyethylene P3 is very similar to that found for the polyethylene P3 with additives (Figure 7.5(a)) but occurs at a higher temperature. Corresponding to the velocity change, the two longitudinal attenuation peaks at 170K and 220K shift to 190K and 235K respectively (Figure 7.5(b)).

Our previous studies of polyethylenes established that individual materials had ultrasonic attenuation signatures, which differed markedly from those of other materials. However, comparing the data for P16 (Figures 7.7 and 7.8) with that for P3 (Figures 7.5 and 7.6), we found that the ultrasonic behaviour of these two polyethylenes is surprisingly similar. Not only the velocity kinks and the attenuation peaks occur at nearly the same temperature but also the details of the attenuation peaks are almost exactly coincident (compare Figure 7.5 with Figure 7.7). Measurements for sample P16 and P3 were made separately with different sample thickness, different bonding and different set up parameters for the ultrasonic equipment (gain, amplitude of the driving pulse, pulse width and R.F. pulse tuning); yet

the ultrasonic velocity and attenuation characteristics are essentially the same for both samples. It can be concluded, therefore, that:

1. These two samples, P3 and P16, are very similar in molecular structure, for example, degree of branches and distribution of molecular weights. From Table 7.2, we can see that P3 and P16 have nearly the same average molecular weight.
2. The measurements were made a number of times. The ultrasonic velocity and attenuation obtained are reproducible and reliable and the effect of bonding material is not important in processing the ultrasonic data.

It should be noted that the glass transition temperature T_g (206K) for crosslinked polyethylene P16 (Figure 7.7(a)) is higher than that (190K) for crosslinked P3 (Figure 7.5(a)), although the longitudinal wave velocity behaviour is similar. This feature, very likely, arises from the different number of crosslinks introduced in the two samples. In general, crosslinks tend to restrict molecular motions in a polymer. Therefore the effect of crosslinking is to increase the T_g. For low density crosslinks, T_g is found to increase linearly with number of crosslinks (Cowie 1991). The ultrasonic measurement indicates that the crosslink density in P16 is probably higher than that for P3.

The velocity and attenuation curves show nearly the same features for both polyethylene P3 and P16 as they are heated towards the melting point. The longitudinal wave velocity for thermoplastic polyethylene P16 (Figure 7.7(a)) is slightly greater than that for P3 (Figure 7.5(a)). The melting temperature (387K) (as indicated by the ultrasonic experiments) is also a little higher than that (380K) for P3. The addition of stabiliser has little effect on the longitudinal wave velocity but increases the value and complexity of the attenuation (Figures 7.5(b) and 7.7(b)). It is noted that the longitudinal wave attenuation in crosslinked polyethylene P16 is larger than that for crosslinked P3 below 380K and smaller above this temperature. This may again be due to the different crosslink density in these two samples.

7.2.3. The ultrasonic properties of polyethylene P61 and P64.

Figure 7.9 shows the temperature dependence of the velocity and attenuation of longitudinal ultrasonic waves propagated in thermoplastic polyethylene P61 and its crosslinked version P40. The longitudinal wave velocity for thermoplastic polyethylene P61 increases almost linearly as the temperature is reduced, with four small kinks appearing at 315K, 260K, 220K, 200K and 165K (Figure 7.9(a)). The attenuation curve shows several peaks in the corresponding temperature range (Figure 7.9(b)). The velocity kinks and attenuation peaks below room temperature can readily be related to the glass-rubber transition of the material (see section 7.4.3).

The temperature dependences of velocity and attenuation of longitudinal waves propagated in crosslinked polyethylene P40 are very similar to those of the pure thermoplastic polyethylene P61 (Figure 7.9(a) and (b)). This observation shows again that the results of the ultrasonic measurement are reliable and that the features found in the temperature dependence of attenuation and velocity are real characteristics of the polyethylenes. The velocity kinks and the corresponding attenuation peaks characterizing the glass transition are shifted to higher temperatures by crosslinking. Crosslinks between polymer molecules tend to restrict molecular motion, thus increasing the glass transition temperature of the polymer. The kink at 260K in the temperature dependence of the longitudinal wave velocity of polyethylene P61 remains at the same temperature for the crosslinked version P40 (Figure 7.9(a)). The strength of the attenuation peak corresponding to this velocity kink, however, has been increased by crosslinking (Figure 7.9(b)). The physical origin of this ultrasonic feature is unclear and may be associated with the molecular structure or the additives incorporated in the manufacturing process.

For thermoplastic polyethylene P64, four longitudinal wave velocity kinks have been observed at 315K, 220K, 200K and 185K (Figure 7.11(a)). The amplitudes of these kinks are relatively smaller than those for P61. The small kink found in the temperature dependence of longitudinal wave velocity of P61 at 260K has not been observed in P64. The glass transition seems to have a smaller effect on the ultrasonic properties of polyethylene P64 than it does on P61. The effect of crosslinking is to decrease the

longitudinal wave velocity (Figure 7.11(a)) and to increase the longitudinal wave attenuation (Figure 7.11(b)); this effect is enhanced at high temperatures.

The most remarkable features in the temperature dependence of the ultrasonic wave velocity are the glass transition at low temperatures and the melting at high temperatures; the behaviour of both transitions can be affected considerably by crosslinking as have been seen in the previous sections of this chapter. The physical origin of the small velocity kink and the corresponding attenuation peak at about 315K, which have consistently been observed in all the polyethylene samples studied so far no matter whether they are thermoplastic or crosslinked in type, will be discussed in section 7.4 and in Chapter 8 where the ultrasonic behaviour of polyethylene is interrelated with the low frequency data obtained using Dynamic Mechanical Thermal Analysis.

7.2.4. The ultrasonic behaviour of cable insulations above room temperature.

Figure 7.13 shows the temperature dependences of the velocity and attenuation of longitudinal ultrasonic waves propagated in cable samples C51 and C56. The ultrasonic behaviour of the cable insulations is similar to that of the plaque samples. The longitudinal ultrasonic wave velocity and attenuation decrease almost linearly with increasing temperature up to the melting point, where a change of slope is observed. The ultrasonic data obtained in both plaque and cable samples suggest that the melting of polyethylene cannot simply be regarded as a first order phase transition, which requires a volume discontinuity at melting temperature. For the two cable samples the velocity kink and the corresponding attenuation peak at about 315K are broadened as compared with plaque samples.

A new phenomenon observed in the measurements is that the quality of the echoes improves markedly as the cable insulations are heated all the way through the melting temperature, where a complete amorphous state is obtained. This observation indicates the possibility that the longitudinal ultrasonic wave velocity and attenuation can be measured accurately in the vicinity of the melting. These measurements have been

made and can be used to separate the mechanical properties arising from the crystalline and amorphous phase. This has enabled study of the effects of developing crystalline structure as the temperature decreases from that of melting.

To detect any difference in mechanical properties along the radius of a cable insulation, the velocity of longitudinal ultrasonic waves propagated in cable sample C23 at room temperature (293K) has been measured across the cable section. These measurements have been repeated five times and the results are shown in Table 7.6.

Table 7.6. The velocity in m/s of longitudinal ultrasonic waves propagated in different regions of the cross section area of cable C23 at 293K.

Inner	1943.9	1947.2	1946.9	1940.3	1941.9	$\overline{V}$ =1944
Outer	1949.5	1953.5	1953.2	1951.0	1947.9	$\overline{V}$ =1951

The accuracy of the velocity measurement is determined by the equation

$$\frac{\Delta V}{V} = \frac{\Delta f}{f} + \frac{\Delta l}{l} \tag{7.1}$$

where V is the velocity, f the overlap frequency and l the thickness of the sample. The first term is very small compared with the second term so that the error introduced in the velocity arises effectively from the thickness measurement. The accuracy of Δl in this work is better than 0.005mm, resulting in $\Delta V/V \sim 7\times10^{-4}$ which is much smaller than the velocity difference measured across the cable section $\Delta V/V \sim 3\times10^{-3}$).

The results in Table 7.6 show that the velocity of longitudinal ultrasonic waves propagated in the outer part is larger than that propagated in the inner part of the cable section. The ultrasonic velocity results, together with those obtained from the dielectric measurements, which have been discussed in Chapter 6, suggest that there may be a density difference across the cable section. The anisotropy, evidenced by ultrasonic and

dielectric measurements, may have important implications on the electrical properties, especially the breakdown behaviour of the cable insulation.

To summarize, the ultrasonic behaviour of polyethylene at low temperatures is dominated by a velocity decrease and an attenuation peak between 30K and 40K. There is an attenuation plateau at about 110K, which is less prominent in the crosslinked samples. A feature common to all samples is that there are anomalous changes in longitudinal ultrasonic wave velocity at about 200K, together with one or two attenuation peaks. The velocity tends to be linear at high temperatures although there are a number of small kinks associated with attenuation peaks. The ultrasonic behaviour of polyethylene at high temperatures is characterized by a broad attenuation peak, together with a velocity kink at about 315K and a change of slope in the velocity versus temperature curve at the melting point. The results show that the relaxation processes responsible for the kinks in the temperature dependence of the velocity of longitudinal ultrasonic waves also produce corresponding peaks in the attenuation. These will be discussed in detail in the following sections of this chapter.

7.3. Hydrostatic pressure dependence of longitudinal ultrasonic wave velocity of polyethylene and polyethylene cable insulation as a function of temperature

The relatively large intermolecular volume of polyethylene, arising from the long chain structure of the molecules bound together by van der Waals' intermolecular forces, determines the elastic as well as the electric properties of the polymer. To study the effect of hydrostatic pressure on the elastic properties of polyethylene, the velocities of 5MHz longitudinal waves propagated in thermoplastic polyethylenes P3, P16 and P61, crosslinked polyethylenes P3+G17, P16+G17, P40 and P42, and polyethylene cable insulations C51 and C56 have been measured as a function of hydrostatic pressure (up to 0.2GPa) at several temperatures between 290K and 360K. Results are presented in Figures 7.14 to 7.22.

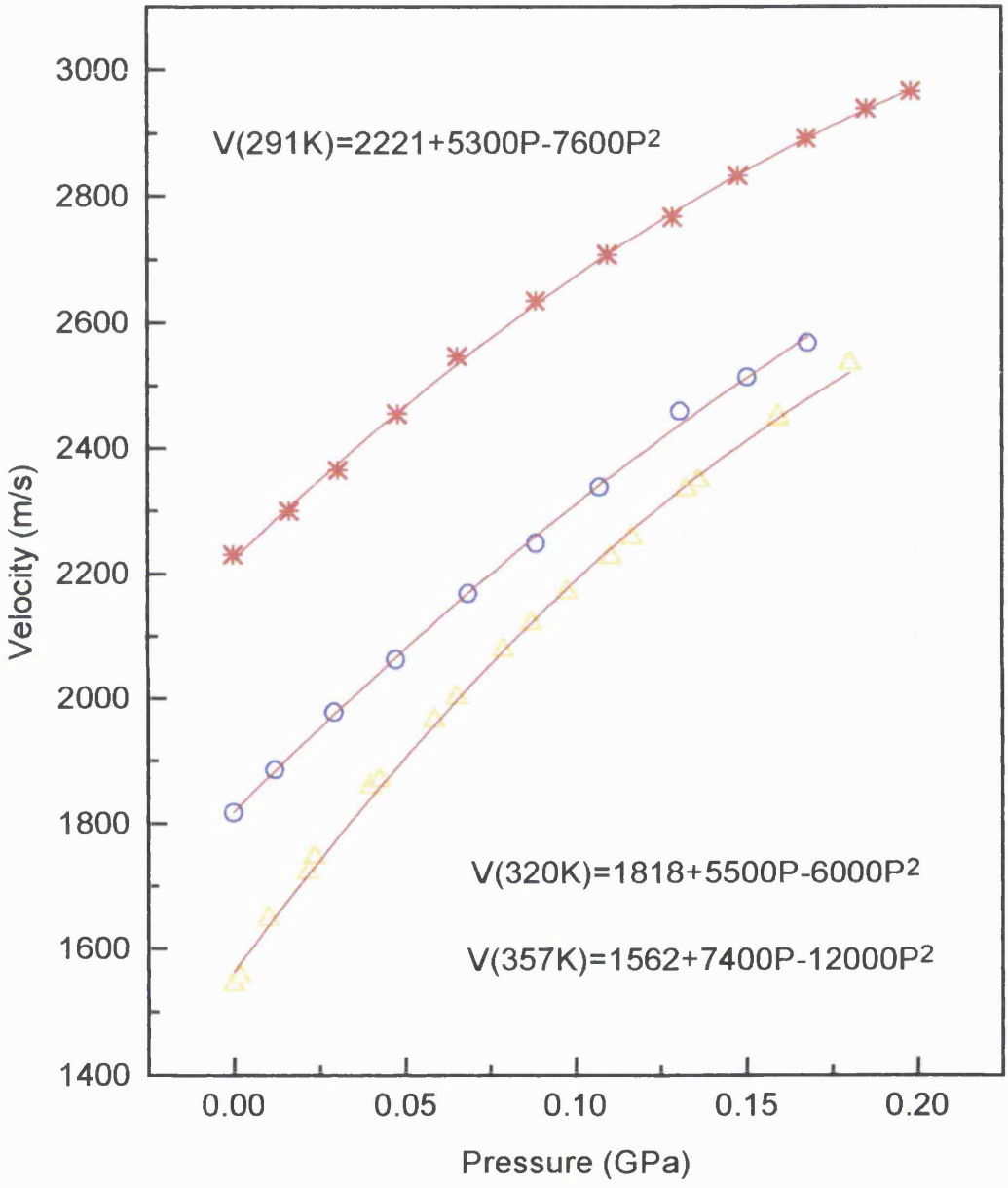

Figure 7.14 Pressure dependence of the velocity of 5MHz longitudinal ultrasonic waves propagated in LDPE P3 at 290K (stars), 320K (circles) and 357K (triangles).

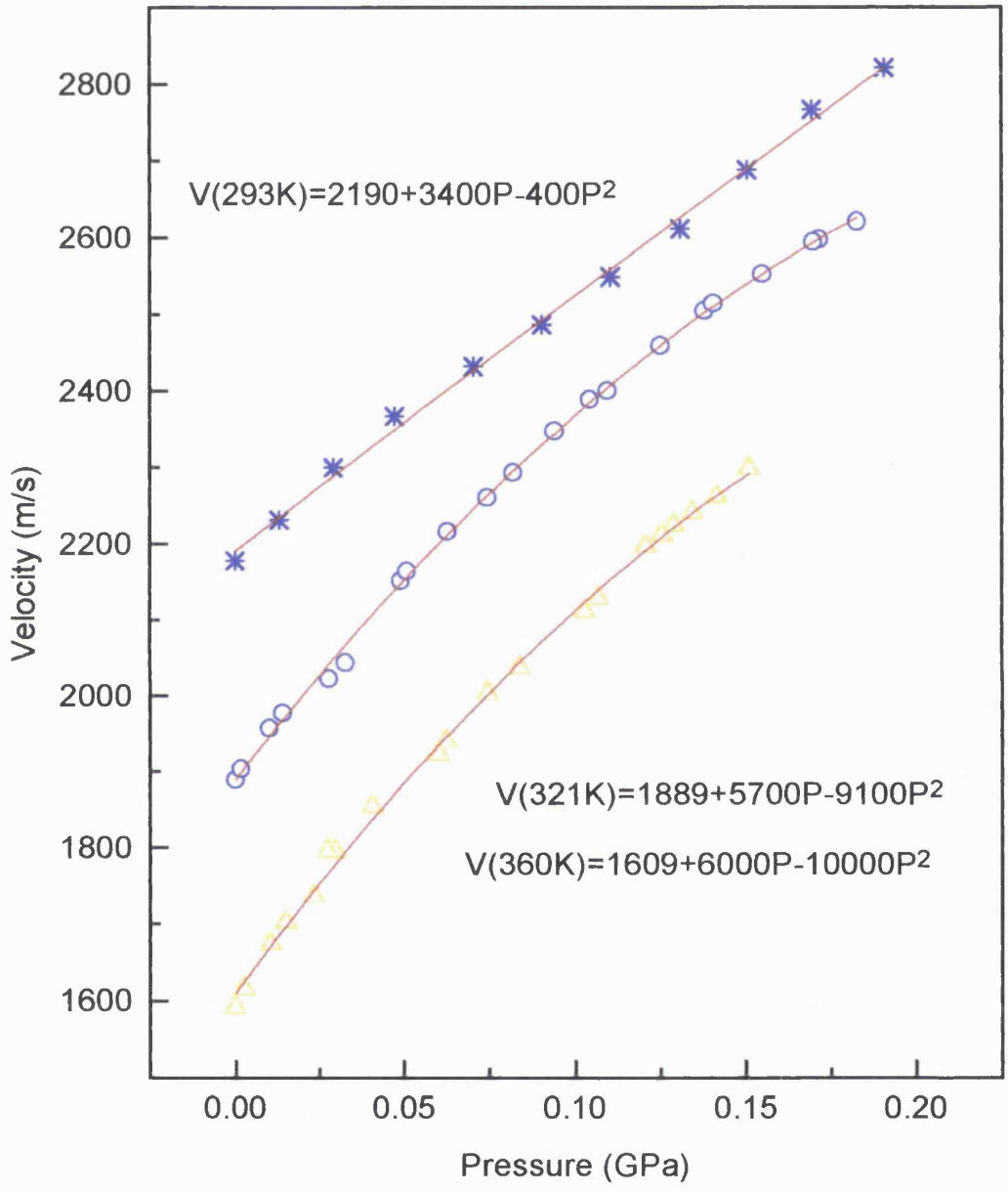

Figure 7.15 Pressure dependence of velocity of 5MHz longitudinal ultrasonic waves propagated in LDPE P16 at 290K (stars), 321K (circles) and 360K (triangles).

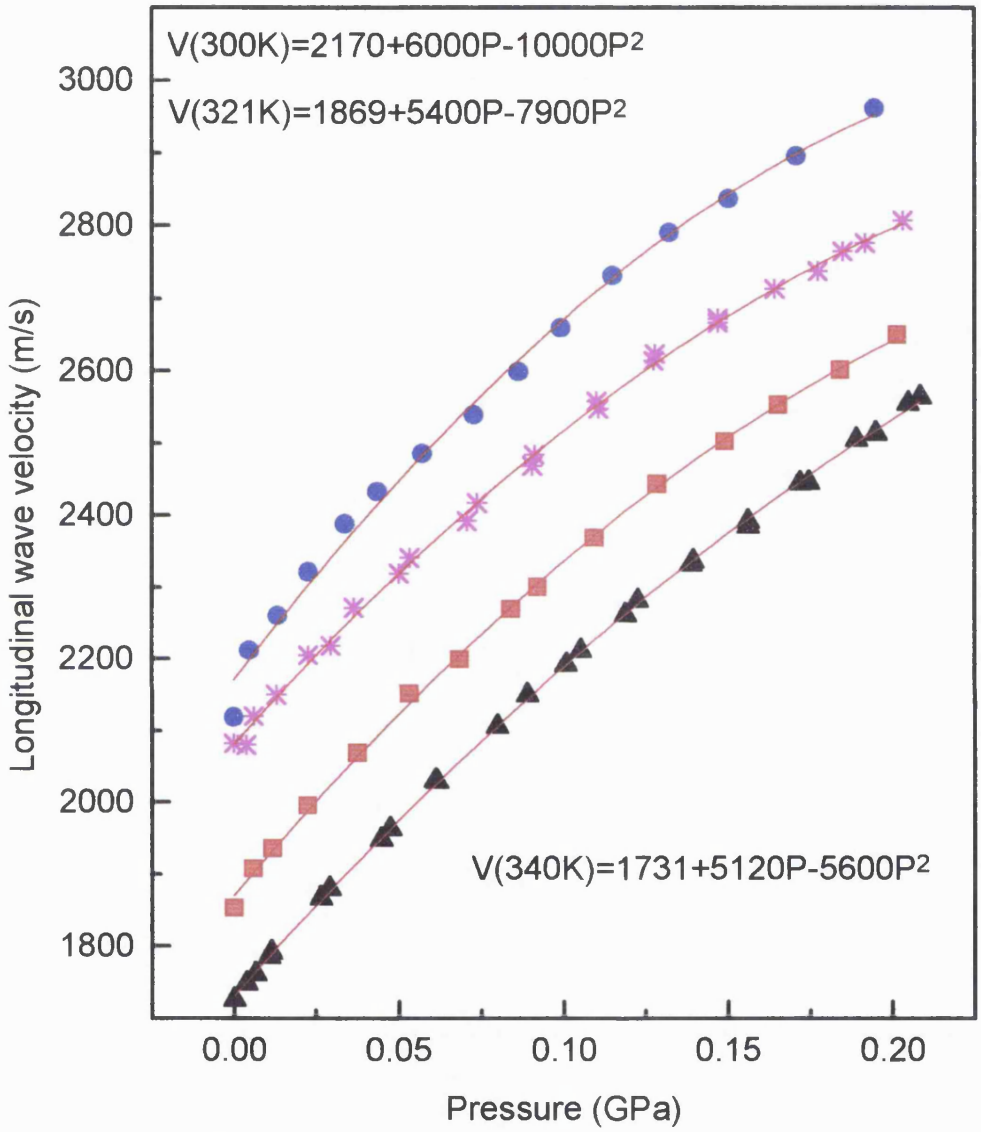

Figure 7.16 Pressure dependence of the velocity of the longitudinal ultrasonic waves propagated in low density polyethylene P61 at 300K (circles), 321K (squares) and 340K (triangles). The result measured again at 300K after pressure and temperature cycles is also given (stars).

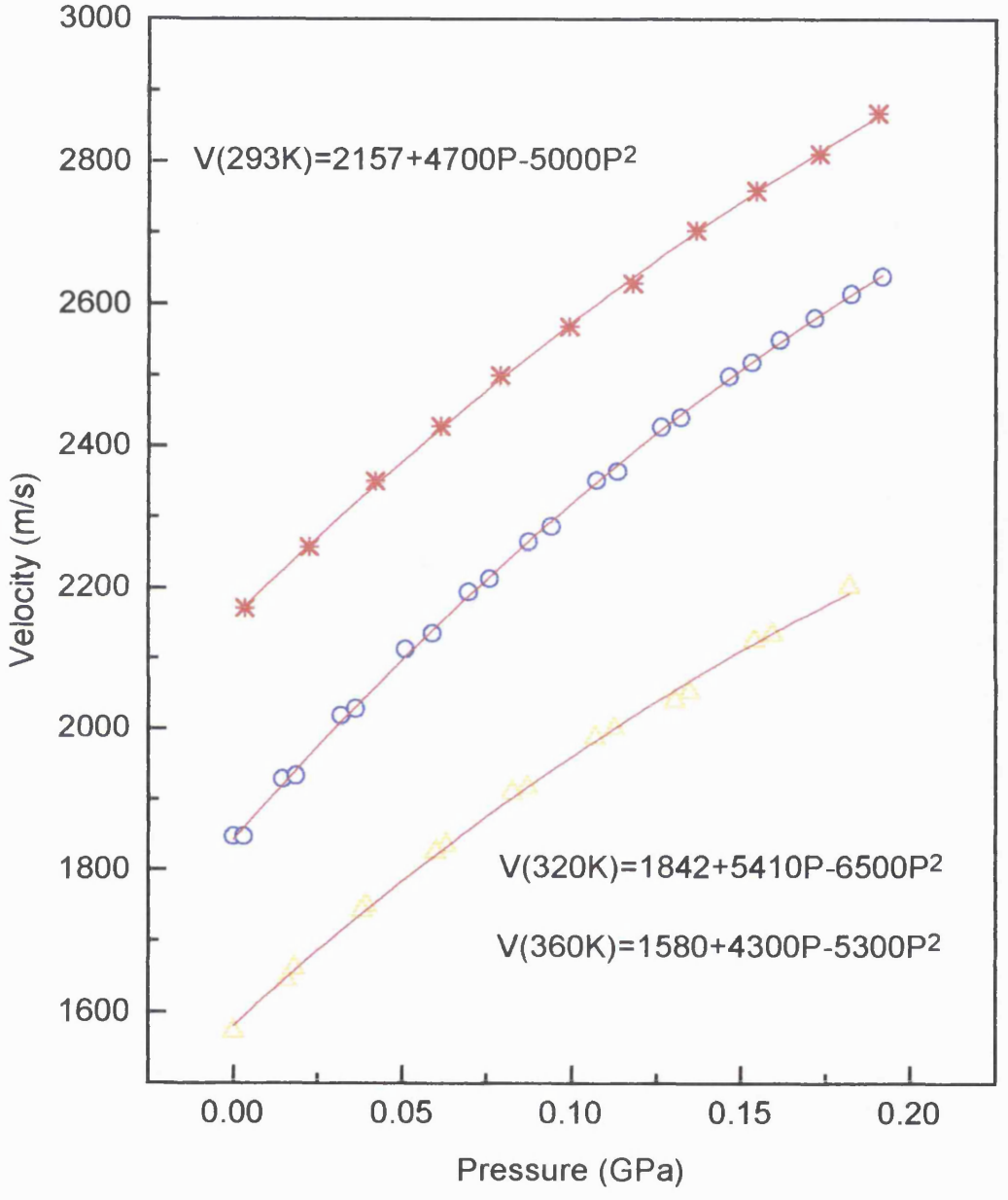

Figure 7.17 Pressure dependence of velocity of 5MHz longitudinal ultrasonic waves propagated in XLPE P3+G17 at 290K (stars), 320K (circles) and 360K (triangles).

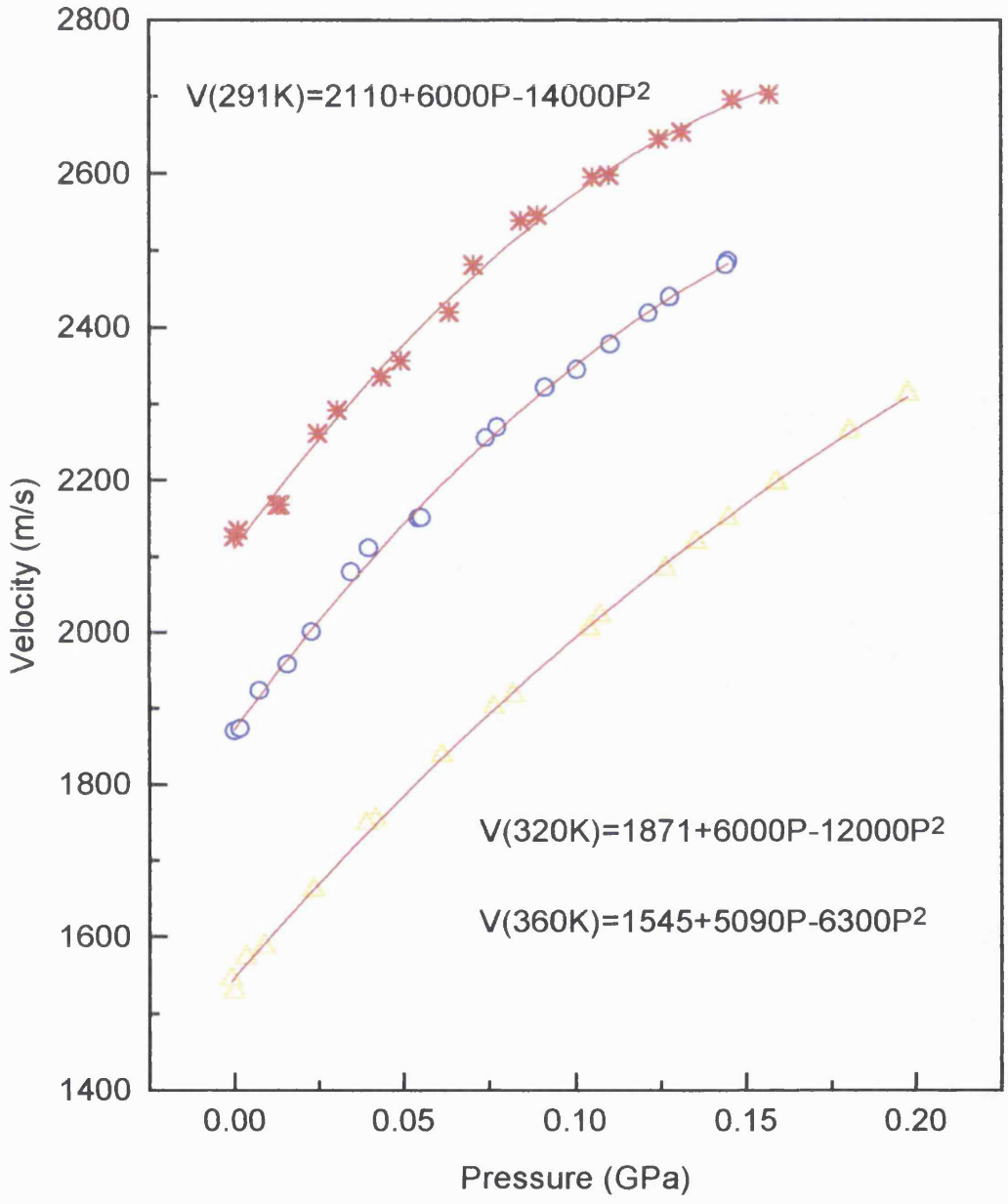

Figure 7.18 Pressure dependence of velocity of 5MHz longitudinal ultrasonic waves propagated in XLPE P16+G17 at 291K (stars), 320K (circles) and 360K (triangles).

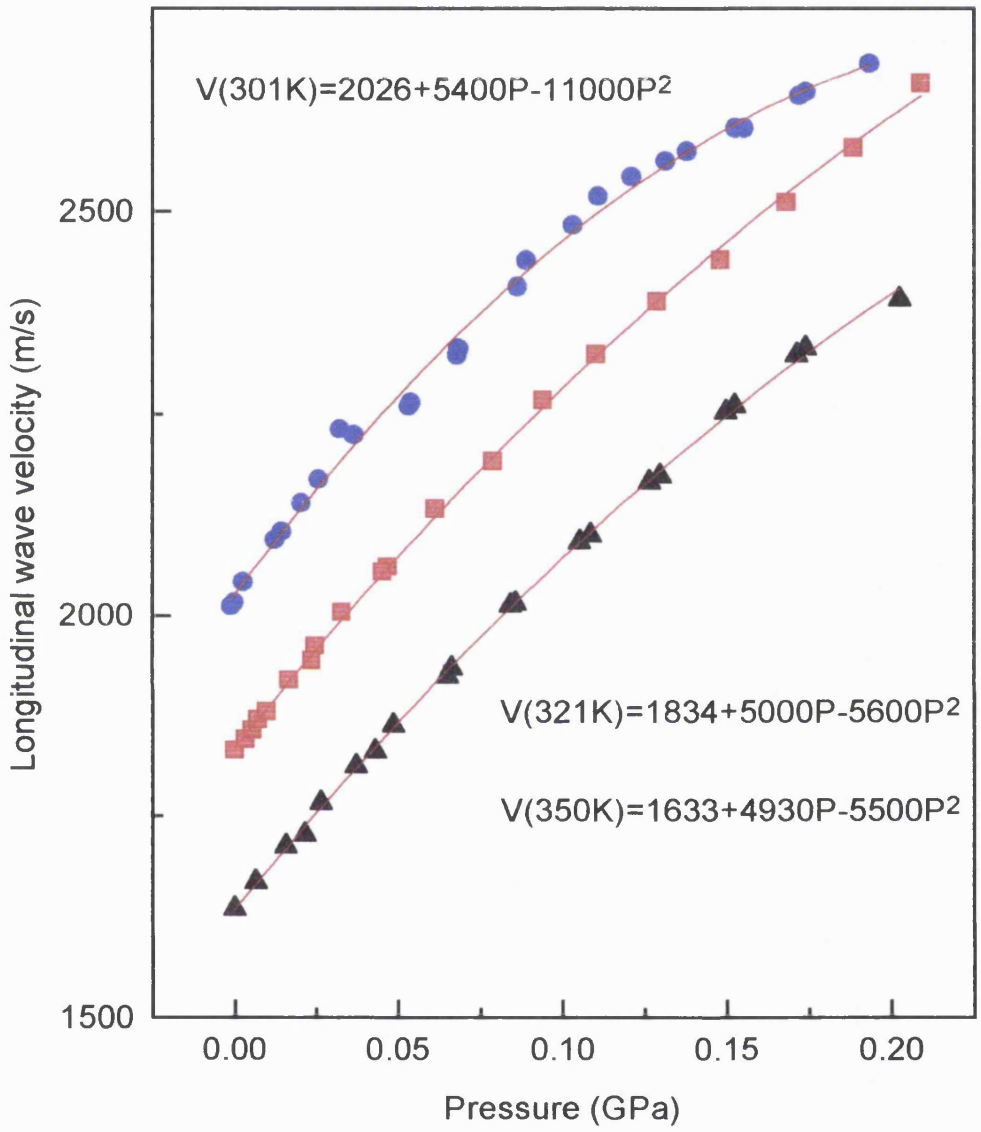

Figure 7.19 Pressure dependence of the velocity of the longitudinal ultrasonic waves propagated in crosslinked polyethylene P40 at 301K (circles), 321K (squares) and 350K (triangles).

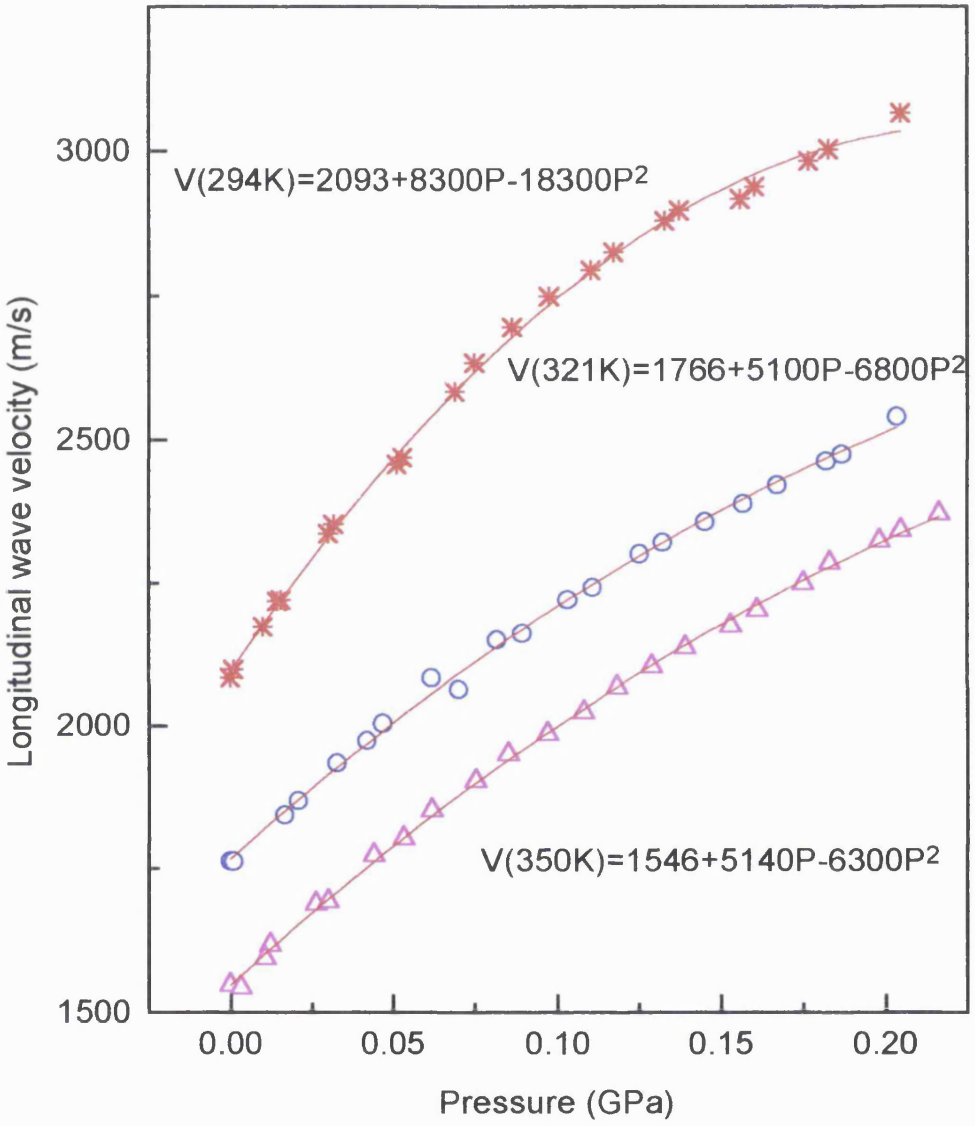

Figure 7.20 Pressure dependence of the velocity of 5MHz longitudinal ultrasonic waves propagated in crosslinked polyethylene P42 at 294K (stars), 321K (circles) and 350K (triangles).

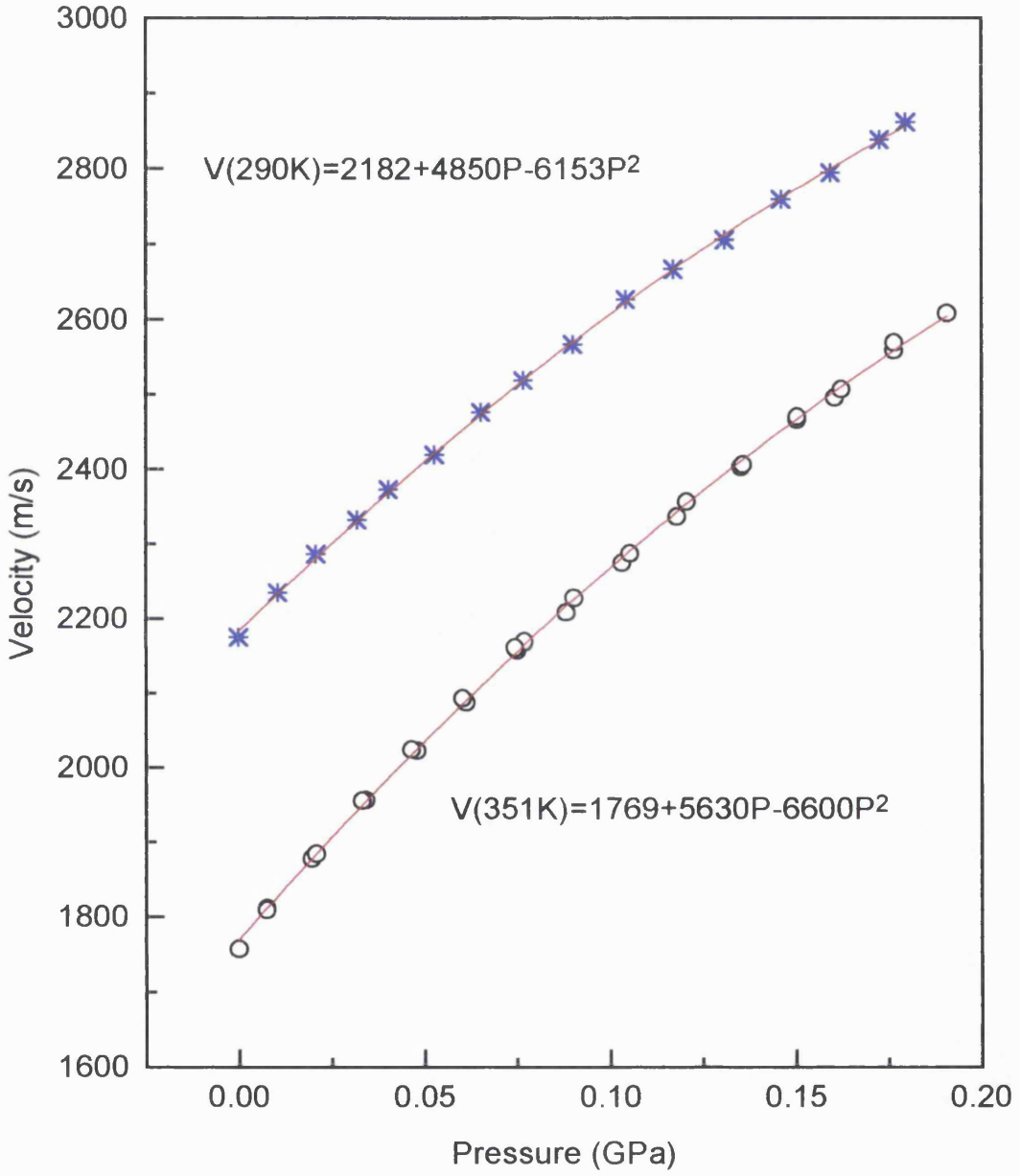

Figure 7.21 Pressure dependence of the velocity of 5MHz longitudinal ultrasonic waves propagated in polyethylene C51 at 290K (stars) and 351K (circles).

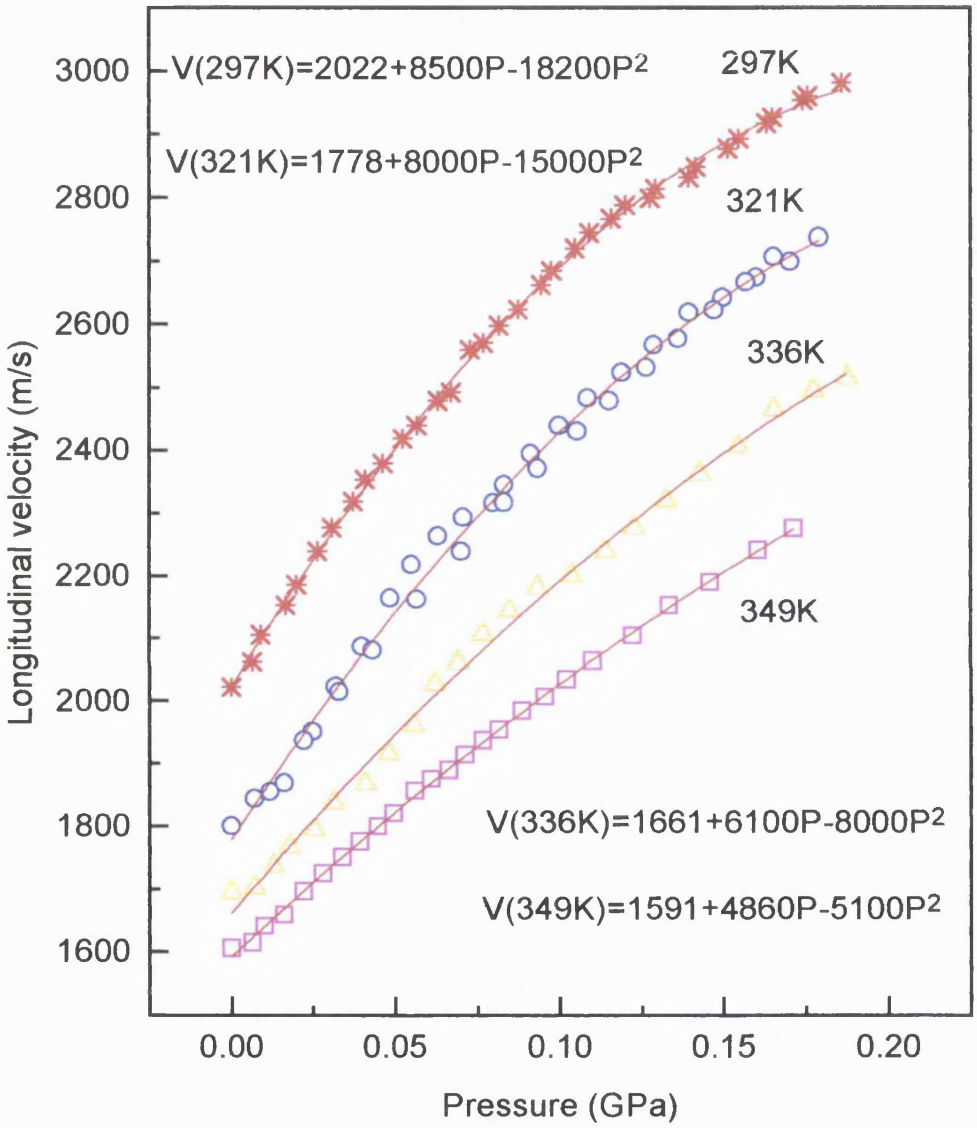

Figure 7.22 Pressure dependence of the velocity of longitudinal ultrasonic waves propagated in cable insulation C56 at selected temperatures.

The value of the wave velocity V at pressure P can be determined from the overlap frequency f and the thickness l_0 of the sample at normal pressure using

$$V = 2fl_0(1 - P\kappa / 3) \tag{7.2}$$

where κ is the volume compressibility. The compressibility of polyethylene at room temperature and atmospheric pressure is $\sim 3\times10^{-10}$/Pa (see following Chapters) and its value at higher pressures is expected to be less, so that equation (7.2) can be rewritten as

$$V = 2fl_0 \tag{7.3}$$

in a pressure range from 0 to 0.2 GPa to an accuracy better than 2%. The velocity calculated here using equation (7.3) is normally referred to as the *natural velocity* and it relates to the natural thickness (at atmospheric pressure) (Thurston and Brugger 1963).

The pressure dependence of the ultrasonic wave velocity shows that the velocity increases nonlinearly with increasing pressure for both thermoplastic and crosslinked polyethylenes as well as cable insulations (Figures 7.14 to 7.22), with the pressure gradient decreasing at higher pressures. The nonlinear effects are much larger for polyethylene than is usually found for crystalline solids or for PMMA (Ngope, Lambson and Saunders 1990) (the lines are usually straight in the pressure range available here). The solid lines shown are the least square fits of the data. The pressure derivative of the longitudinal wave velocity at atmospheric pressure is given in Table 7.7 for the nine samples at selected temperatures. The value of the pressure derivative $(\partial V_L/\partial P)_{P=0}$ for all the samples has the same order of magnitude, and varying temperature does not change this parameter significantly. For thermoplastic polyethylenes P3 and P16, $(\partial V_L/\partial P)_{P=0}$ at atmospheric pressure increases with temperature as expected: increasing temperature increases the inter-molecular volume and hence increases the compressibility of the polymer. For thermoplastic polyethylene P61, however, $(\partial V_L/\partial P)_{P=0}$ tends to decrease slightly with temperature.

Table 7.7. The longitudinal wave velocity V_L and the pressure derivatives of V_L and C_L for polyethylene samples at selected temperatures. R is the correlation parameter of the least-mean squares fit to the experimental data.

Sample	T (K)	$(V_L)_{P=0}$ (ms^{-1})	$(\partial V_L/\partial P)_{P=0}$ ($ms^{-1}Pa^{-1}$)	$\partial^2 V_L/\partial P^2$ ($ms^{-1}Pa^{-2}$)	R	$\partial C_L/\partial P$
P3 (LDPE)	291	2221	5.3×10^{-6}	-15.2×10^{-15}	0.9997	22.2
	320	1818	5.5×10^{-6}	-6×10^{-15}	0.9994	
	357	1562	7.4×10^{-6}	-12×10^{-15}	0.9993	
P16 (LDPE)	293	2190	3.4×10^{-6}	-0.4×10^{-15}	0.9987	14.3
	321	1889	5.7×10^{-6}	-9.1×10^{-15}	0.9995	
	360	1609	6.0×10^{-6}	-10×10^{-15}	0.9988	
P61 (LDPE)	300	2170	6.0×10^{-6}	-10×10^{-15}	0.9974	24.6
	321	1869	5.4×10^{-6}	-7.9×10^{-15}	0.9996	
	340	1731	5.1×10^{-6}	-5.6×10^{-15}	0.9998	
P3+G17 (XLPE)	293	2157	4.7×10^{-6}	-5.0×10^{-15}	0.9998	19.1
	320	1842	5.4×10^{-6}	-6.5×10^{-15}	0.9997	
	360	1580	4.3×10^{-6}	-5.3×10^{-15}	0.9992	
P16+G17 (XLPE)	291	2110	6.0×10^{-6}	-14×10^{-15}	0.9978	23.8
	320	1871	6.0×10^{-6}	-12×10^{-15}	0.9991	
	360	1545	5.1×10^{-6}	-6.3×10^{-15}	0.9997	
P40 (XLPE)	301	2026	5.4×10^{-6}	-11×10^{-15}	0.9977	20.6
	321	1834	5.0×10^{-6}	-5.6×10^{-15}	0.9996	
	350	1633	4.9×10^{-6}	-5.5×10^{-15}	0.9997	
P42 (XLPE)	294	2093	8.3×10^{-6}	-18.3×10^{-15}	0.9990	32.3
	321	1766	5.1×10^{-6}	-6.8×10^{-15}	0.9988	
	350	1546	5.1×10^{-6}	-6.3×10^{-15}	0.9996	
C51 (cable)	290	2182	4.9×10^{-6}	-6.15×10^{-15}	0.9998	20.3
	351	1769	5.6×10^{-6}	-6.6×10^{-15}	0.9998	
C56 (cable)	297	2022	8.5×10^{-6}	-18.2×10^{-15}	0.9995	32.0
	321	1778	8.0×10^{-6}	-15×10^{-15}	0.9977	
	336	1661	6.1×10^{-6}	-8×10^{-15}	0.9981	
	349	1591	4.9×10^{-6}	-5.1×10^{-15}	0.9997	

The pressure derivative $(\partial V_L/\partial P)_{P=0}$ of the longitudinal wave velocity for the crosslinked polyethylenes (Table 7.7) shows a tendency to decrease with temperature. At 360K, $(\partial V_L/\partial P)_{P=0}$ for polyethylene P3 and P16 at atmospheric pressure is decreased by crosslinking (Table 7.7). The crosslinks between the quasi-1D polymer molecules should enhance the inter-molecular force and restrict the molecular motion, resulting in lower compressibility. The decrease of the pressure gradient observed with increasing temperature for crosslinked polyethylene is not yet understood.

For the cable insulation C51, a very good echo-train has been obtained which enables a more accurate and reliable determination than for plaque material of the pressure effect on the ultrasonic behaviour. Data points obtained both with increasing and with decreasing pressure fall nicely on a smooth line: no hysteresis has been observed (Figure 7.21). The longitudinal velocity increases non-linearly with pressure and the value of $(\partial V_L/\partial P)_{P=0}$ is larger at a higher temperature (Table 7.7), similar to the observation for thermoplastic polyethylene but in contrast to that for the crosslinked version. In contrast, cable sample C56 made from the crosslinked polyethylene P16+G17, has a large $(\partial V_L/\partial P)_{P=0}$ at room temperature, which decreases as temperature is increased.

To highlight further the pressure effect on the elastic properties of polyethylene, we now calculate the pressure derivative of the longitudinal stiffness modulus $\partial C_L/\partial P$. It can be shown that for an isotropic material such as polyethylene

$$\frac{\partial C_L}{\partial P} = \rho V_L^2 \left(\frac{2}{f}\frac{\partial f}{\partial P} + \frac{1}{3}\kappa^T\right) \tag{7.4}$$

where $C_L = \rho V_L^2$ is the stiffness modulus, f is the overlap frequency and κ^T the isothermal compressibility, which can be related to adiabatic compressibility κ^S through

$$\frac{\kappa^T}{\kappa^S} = 1 + T\beta\gamma \tag{7.5}$$

where T is temperature, β is the volume thermal expansion coefficient and the thermal Grüneisen parameter γ is defined by

$$\gamma = \beta / \kappa^S \rho C_P = \beta / \kappa^T \rho C_v \tag{7.6}$$

For polyethylene at room temperature and atmospheric pressure γ~0.38 (Hartmann 1976/1977) , β~4.5×10^{-4}/K and the adiabatic compressibility can be obtained from ultrasonic measurements as κ^S~3.7×10^{-10}/Pa. According to equation (7.5), κ^T is equal to $1.05\times\kappa^S$~3.9×10^{-10}/Pa at room temperature (290K). It can be seen from Table 7.7 that the first term in the bracket of equation (7.4) has a typical value ~1.0×10^{-9}/Pa. Therefore the contribution from the compressibility cannot be neglected. Equation (7.4) is valid for isotropic materials at any temperatures and pressures. As the density and the compressibility of the polyethylene samples at high temperatures and pressures are not available, only the data at normal conditions can be processed. The pressure derivative of the longitudinal stiffness modulus for polyethylenes at room temperature and atmospheric pressure, calculated using equation (7.4), is also given in Table 7.7.

7.4. Discussion of the ultrasonic behaviour of polyethylene plaques and cable insulation

7.4.1. The large temperature dependence of the ultrasonic wave velocity.

While polyethylene follows the usual trend found for most materials in that the ultrasonic velocity decreases with temperature, the magnitude of the observed changes is much larger than might have been expected. In fact the differences between the velocities measured at high and low temperatures, and consequently the elastic stiffnesses (see Figures 7.1 to 7.13), are enormous: $\partial V_L/\partial T$ is typically -9.7ms^{-1}K^{-1} for thermoplastic polyethylenes at room temperature, which is much larger than that for aluminum (-0.917ms^{-1}K^{-1}), a typical metal, or even most liquids. Large values for $\partial V_L/\partial T$ obtained in the vicinity of room temperature from ultrasonic measurements using the immersion technique (Hartmann and Jarzynski 1974), indicate that a large

temperature dependence of the ultrasonic wave velocity is common to a number of polymers. This behaviour is not simply a property of materials in the amorphous state; a large increase in the ultrasonic wave velocity (and hence of elastic stiffness) as the temperature is reduced is not simply a characteristic of vitreous materials bound by weak van der Waals intermolecular forces. For example, the value of $\partial V_L/\partial T$ for polymethylmethacrylate (PMMA), a typical amorphous polymer, is -2.5ms^{-1}K^{-1} which is four times smaller in magnitude than that of polyethylene. One may argue that PMMA is still in its glassy state at room temperature, which is well above the glass transition for polyethylene; amorphous materials behave quite differently below and above the glass transition. Below the melting point, polyethylene includes crystalline regions as well as amorphous material. The situation can be clarified by examining the ultrasonic wave velocity behaviour above the melting temperature, where polyethylene is in a completely amorphous state. Figures 7.5(a), 7.7(a), 7.9(a), 7.11(a) and 7.13(a) show clearly that magnitude of $\partial V_L/\partial T$ of crosslinked polyethylene and cable insulations above the melting temperature (~380K) is, surprisingly, much smaller (~-2.85 ms^{-1}K^{-1}) than that below it (~-8.21 ms^{-1}K^{-1}). Therefore, the amorphous phase itself is not responsible for the large temperature dependence of the ultrasonic wave velocity in polyethylene below the melting point.

The large increase in the elastic stiffness with decreasing temperature is a crucial aspect of polyethylene behaviour, which seems to have gone almost without notice in the literature. An in-depth study of the way in which the elastic stiffness of polymers varies with temperature is needed to clarify fundamental understanding of these materials and to further practical applications at low temperature. For isotropic materials such as polyethylene, the value of $\partial V_L/\partial T$ can be related to the derivative of the longitudinal stiffness modulus $\partial C_L/\partial T$ through

$$\frac{1}{C_L}\frac{\partial C_L}{\partial T} = \frac{2}{V_L}\frac{\partial V_L}{\partial T} - \beta \qquad (7.7)$$

where β is volume thermal expansion coefficient, which has a typical value ~10^{-4} K^{-1} for polymers. For polyethylene at room temperature, V_L~2000 ms^{-1} and $\partial V_L/\partial T$~10 ms^{-1}K^{-1} so that the first term in the RHS of equation (7.7) can be estimated as the

comparatively large value of 0.01. Therefore the thermal expansion term can be omitted within an error of 1% and equation (7.7) then becomes

$$\frac{2}{V_L}\frac{\partial V_L}{\partial T}=\frac{1}{C_L}\frac{\partial C_L}{\partial T} \tag{7.8}$$

To separate the contribution of crystalline phase from that of the amorphous phase, we now consider the multiple scattering theory of Waterman and Truell (1961), which has been widely used to treat the ultrasonic propagation in two-phase materials with spherical scatterers of density ρ_2 and longitudinal velocity V_{L2}, distributed in a matrix with density ρ_1 and longitudinal velocity V_{L1}. Assuming the density and shear modulus of the scatterers are the same as those of the matrix, for small values of k_1a where a is the radius of the scatterers and $k_1=\omega/V_{L1}=\omega(\rho_1/C_{L1})^{1/2}$, the theory gives

$$\frac{1}{C_L}=\frac{1-\delta}{C_{L1}}+\frac{\delta}{C_{L2}}+\frac{2}{5}\delta\left(1+\frac{\delta}{2}\right)\omega^2\rho a^2\left[\frac{1}{C_{L1}}-\frac{1}{C_{L2}}\right]^2 \tag{7.9}$$

where ω is the angular frequency of the wave, and δ the volume fraction of scatterers. For polyethylene, a combination of X-ray, optical and electron microscopic evidence suggests that the crystalline regions extend for not more than a few hundred Ångström units in the chain direction, but probably for a much greater distance, though with distortion and branching, in a lateral direction (Bunn 1961). The wavelength of 5MHz longitudinal ultrasonic waves propagated in polyethylene is $\sim 10^{-4}$m, so that $k_1a<<1$. The last term on the right hand side of equation (7.9) is normally very small compared with the other two terms and can be neglected. The volume fraction of crystallinity ϕ_c, and the mass fraction of crystallinity χ_c can be determined using

$$\phi_c=\frac{\rho-\rho_a}{\rho_c-\rho_a} \tag{7.10}$$

and

$$\chi_c=\frac{\rho_c}{\rho}\bullet\frac{\rho-\rho_a}{\rho_c-\rho_a} \tag{7.11}$$

where ρ, ρ_a=855kg/m^3 and ρ_c=998kg/m^3 are the density of polyethylene, the amorphous and the crystalline polyethylene materials respectively. Table 7.8 shows that both the volume and the mass fraction of crystallinity for the polyethylenes studied

is near 0.5. To a good approximation, the volume fraction δ of crystalline phase in polyethylene can be taken as 0.5. Thus it follows from equation (7.9) that

$$\frac{1}{C_L} \approx \frac{1}{2}\left[\frac{1}{C_{L1}} + \frac{1}{C_{L2}}\right] \tag{7.12}$$

$$\frac{1}{C_L}\frac{\partial C_L}{\partial T} = \frac{C_L}{2}\left[\frac{1}{C_{L1}^2}\frac{\partial C_{L1}}{\partial T} + \frac{1}{C_{L2}^2}\frac{\partial C_{L2}}{\partial T}\right] \tag{7.13}$$

Substitution of equation (7.13) into equation (7.8) then gives

$$\frac{1}{V_L}\frac{\partial V_L}{\partial T} = \frac{C_L}{2}\left(\frac{1}{C_{L1}V_{L1}}\frac{\partial V_{L1}}{\partial T} + \frac{1}{C_{L2}V_{L2}}\frac{\partial V_{L2}}{\partial T}\right) \tag{7.14}$$

Table 7.8. The weight and number average molecular weight M_w and M_n, density ρ, volume ϕ_c and mass χ_c fractions of crystallinity at room temperature of the polyethylenes under study.

Sample	M_w	M_n	ρ (kg/m^3)	ϕ_c	χ_c
P3	101500	16850	919	0.448	0.486
P16	102550	15150	920	0.455	0.493
P61	92800	16400	924	0.483	0.521
P64	100900	15200	921	0.462	0.500
P2	80700	17050	930	0.524	0.563
P3+G16	101500	16850	915	0.420	0.458
P16+G16	102550	15150	920	0.455	0.493
P3+G17	101500	16850	914	0.413	0.451
P16+G17	102550	10150	914	0.413	0.451
P40	92800	16400	921	0.462	0.500
P42	100900	15200	916	0.427	0.465
C51	-	-	921	0.462	0.500
C56	102550	15150	917	0.434	0.472

For crosslinked polyethylene P16+G17 at 291K, V_L is equal to 2163m/s, $\partial V_L/\partial T$ = -9.31ms^{-1}K^{-1}; $\partial V_{L1}/\partial T$ and V_{L1} of the amorphous phase can be obtained from the data above melting temperature (Figure 7.7) and extrapolation of these data to the room temperature. We know the density of crystalline polyethylene is 998kg/m^3. The velocity of longitudinal ultrasonic waves propagated in crystalline polyethylene, however, is not available. To supply this and calculate the value of $\partial V_{L2}/\partial T$ of the crystalline polyethylene using equation (7.14), V_{L2} has been taken as 2430m/s, which is the longitudinal ultrasonic wave velocity obtained in a high density (ρ=957kg/m^3) polyethylene sample (Hartmann 1980). Eventually equation (7.14) gives

$$\partial V_{L2}/\partial T = -12.4 \text{ms}^{-1}\text{K}^{-1} \qquad (7.15)$$

for crystalline polyethylene. The same procedure has been applied on crosslinked polyethylene P3+G17 and cable insulations C51 and C56. The results are summarized in Table 7.9.

Table 7.9. The temperature derivatives of longitudinal ultrasonic wave velocity for semicrystalline ($\partial V_L/\partial T$), amorphous ($\partial V_{L1}/\partial T$) and crystalline ($\partial V_{L2}/\partial T$) polyethylenes at 291K. Here the volume crystallinity of these polyethylenes have been assumed to be temperature independent.

Sample	ρ (kg/m^3)	V_L (m/s)	$\partial V_L/\partial T$ (ms^{-1}K^{-1})	V_{L1} (m/s)	$\partial V_{L1}/\partial T$ (ms^{-1}K^{-1})	$\partial V_{L2}/\partial T$ (ms^{-1}K^{-1})
P3+G17	914	2169	-9.40	1540	-3.35	-13.6
P16+G17	914	2163	-9.31	1559	-3.70	-12.4
C51	921	2068	-8.21	1598	-2.85	-17.2
C56	917	1974	-7.61	1533	-2.53	-19.1

The large value of $\partial V_{L2}/\partial T$ obtained for the crystalline polyethylene is itself surprising and difficult to understand. $\partial V_{L2}/\partial T$ is three to eight times larger than the value of $\partial V_{L1}/\partial T$ found for the amorphous material (Table 7.9). X-ray measurements have shown (Bunn 1961) that the thermal expansion of the *a* axis of the unit cell of single

crystal polyethylene from 293K to 373K is ~3.5×10^{-4} K^{-1}, which has the same order of magnitude of the volume expansion for semicrystalline polyethylene. Therefore it might have been thought that the temperature dependences of the stiffness modulus and the corresponding sound wave velocity of the crystalline material should not be too far from those of the amorphous phase. In the following discussion, we will show that this unreasonably large value of $\partial V_{L2}/\partial T$ for the crystalline polyethylene results from the assumption that the crystallinity δ is invariant with temperature.

Polyethylene does not melt at a sharply defined temperature. Gradual melting is due primarily to the two-phase texture resulting from the crystallization in a tangle of very long molecules. Since the movements of molecular segments are more free in the amorphous than in the crystalline region, some strained molecular segments on the crystal boundaries would be expected to leave the crystalline region and become part of the amorphous fraction as temperature is increased. Small crystals will melt completely before the larger ones are dispersed. The melting point refers normally to the temperature at which the last crystals melt. Taking into account the changing of crystallinity δ, equation (7.12) should be rewritten as

$$\frac{1}{C_L}=\left[\frac{1-\delta}{C_{L1}}+\frac{\delta}{C_{L2}}\right] \tag{7.16}$$

and equation (7.14) becomes

$$\frac{2}{C_L V_L}\frac{\partial V_L}{\partial T}=\frac{\partial \delta}{\partial T}\left[\frac{1}{C_{L1}}-\frac{1}{C_{L2}}\right]+\left[\frac{1}{C_{L1}V_{L1}}\frac{\partial V_{L1}}{\partial T}+\frac{1}{C_{L2}V_{L2}}\frac{\partial V_{L2}}{\partial T}\right] \tag{7.17}$$

The temperature derivative of the crystallinity can be estimated using equation (7.10) as

$$\frac{\partial \delta}{\partial T}=\frac{1}{\rho_c-\rho_a}\frac{\partial \rho}{\partial T}=\frac{-\rho\beta}{\rho_c-\rho_a} \tag{7.18}$$

where β is the volume thermal expansion. Here it has been assumed, for simplicity, that the change in density is due to the crystal-amorphous phase transition alone and the contribution from the thermal expansion can be neglected. Equation (7.18) should give a upper limit value for $\partial\delta/\partial T$. Taking β as 4×10^{-4} K^{-1} for crosslinked plaque polyethylenes and 6×10^{-4} K^{-1} for cable insulations, the values of $\partial\delta/\partial T$ and $\partial V_{L2}/\partial T$ for the four samples have been calculated and the results are given in Table 7.10.

Table 7.10. The temperature derivative of crystallinity ($\partial\delta/\partial T$) and the temperature derivatives of longitudinal ultrasonic wave velocity for semicrystalline ($\partial V_L/\partial T$), amorphous ($\partial V_{L1}/\partial T$) and crystalline ($\partial V_{L2}/\partial T$) polyethylenes at 291K. In contrast to Table 7.9, the gradual change of crystallinity with temperature below the melting point has been taken into account.

Sample	ρ (kg/m^3)	$\partial\delta/\partial T$ $\times10^3$ K^{-1}	V_L (m/s)	$\partial V_L/\partial T$ (m/sK)	V_{L1} (m/s)	$\partial V_{L1}/\partial T$ (m/sK)	$\partial V_{L2}/\partial T$ (m/sK)
P3+G17	914	-2.56	2169	-9.40	1540	-3.35	-1.74
P16+G17	914	-2.56	2163	-9.31	1559	-3.70	-1.06
C51	921	-3.86	2068	-8.21	1598	-2.85	-1.23
C56	917	-3.85	1974	-7.61	1533	-2.53	-1.07

As can be seen from the results given in Table 7.10, the value of $\partial V_{L1}/\partial T$ for the amorphous polyethylene is near to that of liquids while the magnitude of the reassessed $\partial V_{L2}/\partial T$ of crystalline polyethylene is now similar to but slightly larger than that of aluminum (-0.9ms^{-1}K^{-1}). Although the temperature derivative of longitudinal ultrasonic wave velocity is small for both crystalline and amorphous phases, the overall $\partial V_L/\partial T$ of semicrystalline polyethylene still has a large value. The anomalous large temperature derivative of the longitudinal ultrasonic waves propagated in semicrystalline polyethylene arises mainly from the gradual crystalline-amorphous phase transition between the glass transition and the melting temperature, which is a characteristic of semicrystalline polymers. The mechanical and electrical properties, and most importantly, the breakdown behaviour of polyethylene in this temperature range must in some way be associated with this phase transition.

Superimposed on an approximately linear temperature dependence of the ultrasonic wave velocity, there are marked fluctuations consistent with a number of relaxation transitions in the thermoplastic polyethylene. The most remarkable feature observed between the glass transition and melting is the attenuation peak (or peaks) and a corresponding velocity kink at about 315K (Figure 7.7, 7.9, 7.11 and 7.13).

Comparison between the ultrasonic results and the DMTA data (see Chapter 8) shows that the attenuation peak and the velocity kink may be related to the loss peak observed at about 250K in low frequency DMTA measurements (see figures 8.1 to 8.4), which is normally referred to as the β transition. The Arrhenius plot of the DMTA data obtained at low frequencies (1 and 10Hz) extrapolates roughly up to the ultrasonic data, suggesting that both the DMTA loss peak and the ultrasonic attenuation peak arise from the same physical process: the motion of the side groups in the amorphous phase. In this temperature range, the crystalline areas in the polymer begin to melt. Along with the reduction of the crystallinity, more side groups get enough energy to move, which may be partly responsible for the β relaxation process. As peroxide crosslinking decreases the density and crystallinity of polyethylene, it increases the strength of the β transition. The effect of irradiation crosslinks, on the other hand, is to increase the density and crystallinity, resulting in a weaker β process (Figures 7.1 and 7.3). This will be discussed in more detail in Chapter 8.

7.4.2. Correlation between the velocity and attenuation of longitudinal ultrasonic waves.

An examination of the data shows that the relaxation processes responsible for the kinks in the temperature dependence of the velocity of longitudinal ultrasonic waves produce corresponding peaks in the attenuation (Figures 7.1, 7.3, 7.5, 7.7, 7.9, 7.11 and 7.13). To establish the correlation between the ultrasound wave velocity and attenuation, the velocity gradient (dV_L/dT) of the longitudinal ultrasonic waves propagated in the crosslinked polyethylene HFDQ 4201 is plotted against temperature in Figure 7.23. The attenuation curve in Figure 7.3(b) is also shown in Figure 7.23 for comparison.

The data in Figure 7.23 indicate that the attenuation α is proportional to the velocity gradient; the relation can be given as

$$\alpha = -A(dV_L / dT) + B \qquad (7.19)$$

where A and B are constants. It has been observed previously that an extremely good correlation exists between attenuation and the thermal coefficient of sound wave

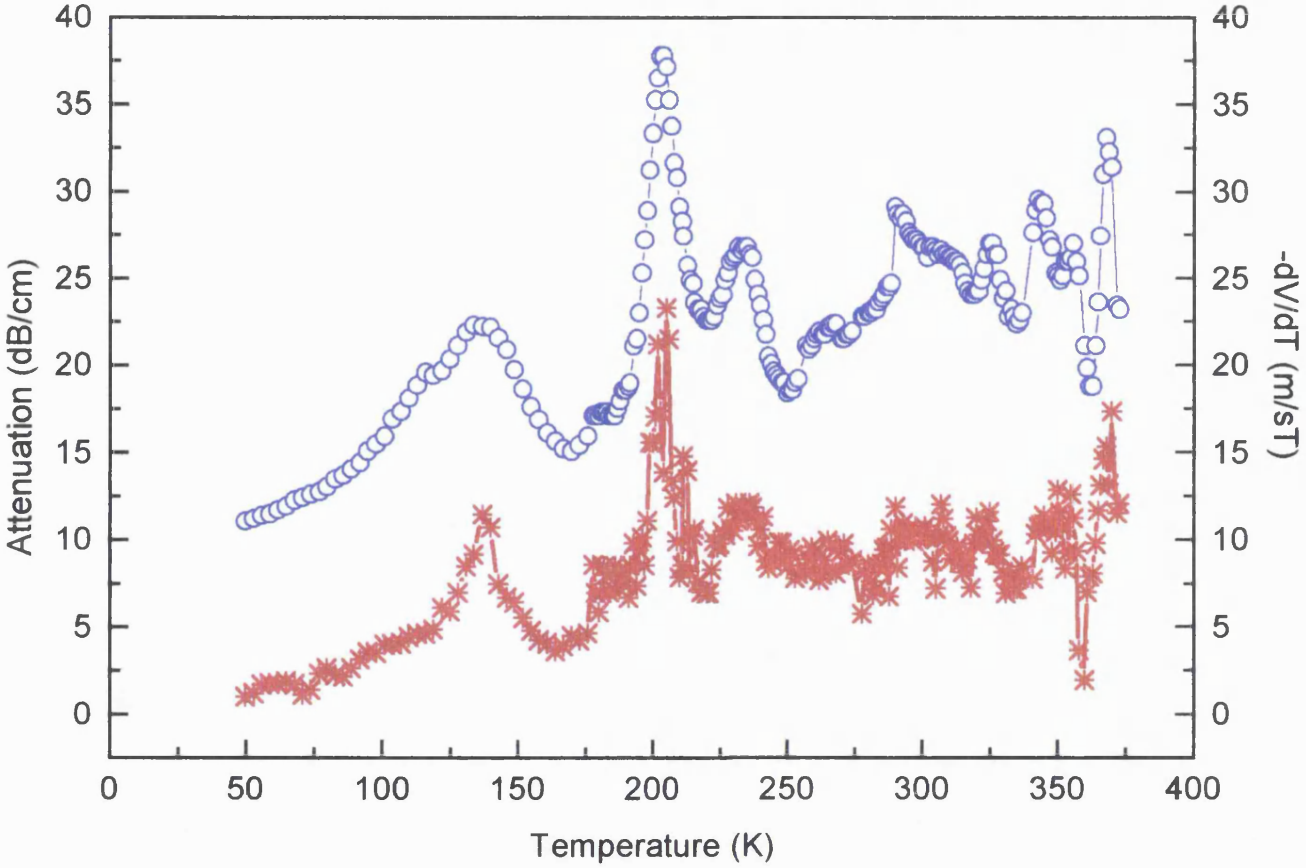

Figure 7.23 Comparison of the velocity gradient -dV/dT (stars) and attenuation of the longitudinal ultrasonic waves propagated in crosslinked polyethylene HFDQ 4201 (circles).

velocity for a number of polymers, although the attenuation coefficients for those polymers were not available at that time (Folds 1972).

Equation (7.19) can be understood in terms of linear viscoelasticity and hysteresis absorption. Ultrasonic attenuation measurements have shown that the ultrasonic absorption in polymers depends linearly on the frequency (Hartmann and Jarzynski 1972 and Nava, Pereira and Amorer 1991). This behaviour is referred to as hysteresis absorption because it occurs when the stress-strain relation exhibits hysteresis (Hartmann 1976/77). The hysteresis absorption is normally described in terms of the absorption per wavelength ($\alpha\lambda$) where λ is the wavelength (cm) and the absorption α is in neper per centimetre. Assuming linear viscoelasticity, $\alpha\lambda<<1$, and $\alpha\lambda$ approximately independent of frequency (i.e. hysteresis absorption), the relation between $\alpha\lambda$ longitudinal modulus C_{11} can be given as (Zener 1948)

$$\alpha\lambda = \frac{\pi^2}{2}\left(\frac{\partial \ln C_{11}}{\partial \ln \omega}\right)_{T,P} \tag{7.20}$$

where ω is the angular frequency and the derivative is evaluated at constant temperature T and hydrostatic pressure P.

Using the so called time-temperature superposition principle, Hartmann was able to convert the frequency derivative in equation (7.20) to a temperature derivative (Hartmann 1976/77). In general, the dynamic modulus of a viscoelastic material can be increased either by increasing the frequency or decreasing the temperature. In other words, increasing the frequency has the same effect as decreasing the temperature. Assuming that the longitudinal modulus is a function of temperature, pressure and frequency, the derivative in equation (7.20) can be written as

$$\left(\frac{\partial \ln C_{11}}{\partial \ln \omega}\right)_{T,P} = -\left(\frac{\partial T}{\partial \omega}\right)_{C_{11},P}\left(\frac{\partial \ln C_{11}}{\partial T}\right)_{P,\omega} \tag{7.21}$$

The key assumption which Hartmann has made is that, at least over a limited temperature range, the temperature dependence of the frequency at constant modulus and pressure is of the Arrhenius form

$$\omega = \omega_0 \exp(-\Delta H / RT) \tag{7.22}$$

where ω_0 is a constant, ΔH is the activation energy for the physical process responsible for the frequency dependence of the modulus and R is the gas constant. It follows from equation (7.22) that

$$\left(\frac{\partial T}{\partial \ln \omega}\right)_{C_{11},P} = \frac{RT^2}{\Delta H} \tag{7.23}$$

Substitution of equation (7.23) into equation (7.21) and then into equation (7.20) yields

$$\alpha\lambda = -\frac{\pi^2 RT^2}{2\Delta H}\left(\frac{\partial \ln C_{11}}{\partial T}\right)_{P,\omega} \tag{7.24}$$

To enable a comparison of the theory with the ultrasonic results shown in Figure 7.23, equation 7.24) can be rewritten as

$$\alpha = -\frac{\pi\omega RT^2}{2V_L \Delta H}\left(\frac{1}{V_L}\frac{\partial V_L}{\partial T} - \frac{\beta}{2}\right) \tag{7.25}$$

by using

$$\omega\lambda / 2\pi = V_L \tag{7.26}$$

and

$$\begin{aligned}\frac{\partial \ln C_{11}}{\partial T} &= \frac{1}{\rho V_L^2}\frac{\partial\left(\rho V_L^2\right)}{\partial T} \\ &= \frac{1}{\rho}\frac{\partial \rho}{\partial T} + \frac{2}{V_L}\frac{\partial V_L}{\partial T} \\ &= \frac{2}{V_L}\frac{\partial V_L}{\partial T} - \beta\end{aligned} \tag{7.27}$$

where ρ is the density and β is the volume thermal expansion coefficient. The subscripts P and ω are omitted for simplicity.

Although further quantitative discussion cannot be made for lack of information about the activation energy, the similarity between equations (7.25) and (7.19) indicates that the experimental result, equation (7.19), arises from the viscoelasticity of polyethylene.

7.4.3. Ultrasonic behaviour of polyethylene in the vicinity of glass transition.

The glass transition is the most important and best studied transition in polymers, although the basic physics, and the nature of the glassy state, remain unclear (Boyer 1989). In a semi-crystalline polymer such as polyethylene the glass transition arises from the amorphous material present. Ultrasonic measurements at the glass transition T_g assist in understanding the physical origin of this transition and for checking the theoretical models.

The ultrasonic behaviour of polyethylene during the glass transition is characterized with several velocity kinks and attenuation peaks. There are marked changes around 200K in both the velocity and attenuation of longitudinal ultrasonic waves (Figures 7.1, 7.3, 7.5, 7.7, 7.9, 7.11 and 7.13). Starting from 240K, the ultrasonic wave velocity increases more sharply with decreasing temperature and a well-defined kink has been observed below 200K. The echo-train deteriorates from the onset of the anomalous velocity change so that accurate measurements are not possible in this temperature range. The distorted echo-train begins to improve below 190K and becomes completely normal again at about 160K. Corresponding to the velocity changes, attenuation peaks have been observed over this temperature range.

Similar ultrasonic wave velocity and attenuation measurements on this polymer have been reported in the literature. Perepechko and Sorokin (1973) measured the velocity of 5 MHz ultrasonic waves propagated in a high density polyethylene and observed a slope change at 180K. It was suggested that this slope change in sound velocity corresponds to the glass transition. They also noticed that the largest temperature dependence of velocity occurs between 180K and 240K. Adachi et al. (1981) measured both velocity and attenuation of 5 MHz longitudinal ultrasonic waves in several polyethylene samples. A velocity kink and a broad attenuation peak were observed between 150K and 260K with the maximum at 220K. Although the ultrasonic behaviour obtained in the present work differs slightly from that found in former studies, there is little doubt about the existence of the glass transition in polyethylene in this temperature range. The effect of the glass transition on the ultrasonic behaviour of polyethylene observed in this work is much more evident, due

to enhanced sensitivity of our methods, than that reported (Perepechko and Sorokin 1973 and Adachi et al. 1981).

It should be noted that, instead of only one peak as observed in low frequency measurements (Schmieder and Wolf 1953, also see Chapter 8) and reported by Adachi et al. (1981) in the ultrasonic frequency range, there are three attenuation peaks corresponding to the glass transition (see Figures 7.1 and 7.5). These peaks can be understood qualitatively in terms of the "order parameter model", which assumes that a configurational equilibrium process, occurring at high temperatures, freezes out at T_g, leading to reduced thermal expansion, compressibility and heat capacity (Boyer 1989). Above T_g each segment is able to jump more or less freely between several inequivalent lattice positions in its neighbourhood. While the primary molecular motion freezes first, resulting in a principal attenuation peak, a number of segment motions may remain active down to lower temperatures. The freezing out of these sub-motions gives rise to the smaller attenuation peaks following the onset of the transition. This interpretation is equivalent to saying that the peaks in the attenuation of the longitudinal ultrasonic waves propagated in polyethylene arise from the wide distribution of the activation energy of the glass transition relaxation. In general, it has been found that the temperature dependence of the glass transition relaxation behaviour of amorphous and crystalline polymers does not fit a constant activation energy (Ward 1979). The morphological assignment of the Υ relaxation (see Chapter 8) has long been an open question and is still not completely resolved (Gray and McCRUM 1969 and Sayre, Swanson and Boyd 1978). The low frequency dynamic loss peak has a low temperature tail, which has led to speculation that the Υ process is a composite process with the high temperature portion originating in the amorphous phase and the low temperature tail being due to the crystalline phase. The present ultrasonic measurements suggest that the glass transition of polyethylene may contain several relaxation processes with different activation energies depending on the micro-structure of the sample. While at low frequencies the loss peaks overlap to form a broad maximum, these peaks separate from each other when a much higher frequency is applied. The higher the activation energy of relaxation, the higher the temperature of the relaxation peak. Depending on the measurement method and frequency used,

different values of the glass transition temperature can stem from the frequency dependence of the relaxation peaks. It is now clear why there are so many different values in the reported glass transition temperature of polyethylene (Hall 1989).

Crosslinking has marked effects on the ultrasonic behaviour of polyethylene at T_g. The echo-train of ultrasonic waves propagated in the cross-linked polyethylene is much better than that in the thermoplastic form. The attenuation is increased and the temperature dependence of the longitudinal velocity is enhanced by crosslinking, suggesting that the relaxation or relaxations in this temperature range have their origin in the amorphous material region. Normally, when crosslinks are introduced into a polymer, the density of the sample is increased proportionally. As the density increases, the molecular motion in the sample is restricted and T_g rises. For a high crosslink density the transition is broad and ill-defined, but at lower values, T_g is found to increase linearly with the number of crosslinks (Cowie 1991). It can be seen that the main peak corresponding to the glass transition, occurring at about 190K, in the attenuation of the longitudinal ultrasonic waves propagated in the thermoplastic polyethylene (Figure 7.1) does shift to a higher temperature with crosslinking (Figure 7.3). The peak at about 140K, however, does not shift much. The possibility cannot be excluded that the 140K peak has a different physical origin from the attenuation peak which is involved in the glass transition.

The distorted echo-train of longitudinal ultrasonic waves propagated in polyethylene at the glass transition may contain fundamental information about the microscopic mechanism of the process and should not be dismissed without examination. In general, the relaxation systems (see Chapter 8) absorb energy from the stress field, surmount the energy barrier, and relax to a new equilibrium state. The energy loss in the process gives rise to the high attenuation of the ultrasound waves, which in turn causes the poor echo-pattern at the transition. Another reason for the distortion of the echo-train is related to the two phases which may be present during the relaxation. According to the entropy model proposed by Gibbs and DiMarzio (Boyer 1989), the glass transition and its associated phenomena arise from the disappearance of configurational entropy as the temperature of the melt is lowered below the melting

point. The central idea of the model is that the amorphous liquid structure collapses to a hypothetical glass phase with zero (or relatively small) entropy during the second-order transition. The existence of the two phases and the continuous change of the magnitude of these two phases results in a instability in the elastic properties and may partly be responsible for the poor echo-train observed. Finally, the non-linear, nonexponential relaxation behaviour near T_g results in the properties of the polymer varying from point to point in the sample (Boyer 1989), and this may also make some contribution to the poor elastic behaviour in the vicinity of the glass transition.

7.4.4. The elastic constants and fractal model for polyethylene.

As shown in Chapter 2, the longitudinal and shear modulus C_{11} and C_{44}, Poisson's ratio P, Young's and bulk moduli Y and B of polyethylene can be determined by using the equations:

$$C_{11} = \rho V_L^2 \tag{7.28}$$

$$C_{44} = \rho V_S^2 \tag{7.29}$$

$$P = \frac{C_{11} - 2C_{44}}{2(C_{11} - C_{44})} \tag{7.30}$$

$$Y = \frac{C_{44}(3C_{11} - 4C_{44})}{C_{11} - C_{44}} \tag{7.31}$$

and

$$B = C_{11} - \frac{4C_{44}}{3} \tag{7.32}$$

The elastic constants of ten polyethylenes at 140K, below which both longitudinal and shear wave velocities are available, are given in Table 7.11. Due to the large attenuation of shear ultrasonic waves, it is not possible to obtain the shear wave velocity for polyethylene at high temperatures. To estimate the high temperature elastic constants, use has been made of the concept of the fractal dimension, which is probably best thought of as a fractal bond connectivity (Sauders et al. 1996).

It was first suggested by Mandelbrot that the elastic properties of polymers are related to fractal effects at the molecular level (Mandelbrot 1977). The simplest "polymer

system" is the standard self-avoiding walk (SAW) on a periodic lattice. The walk is a succession of N steps which can never intersect itself. This models a linear polymer in a good solvent. For large N, the quadratic average of displacement R is of the order of magnitude of N raised to a power which Mandelbrot denotes by 2/D, where D is fractal dimension. Computer simulations give value D=1 for a straight line, which happens to be identical to the Euclidean dimension, D=1.33 and 1.67 in the case of a plane and 3d-space. A fractal model has been widely used in polymer statistics and in studying the mechanism of dielectric breakdown of dielectrics. Computer simulation shows that dielectric breakdown has a fractal structure with a fractal dimension D~1.7 (Pietronero and Tosatti 1985). In what follows now, we intend to find the correlation between the longitudinal and shear modulus by using a fractal model so that the Young's modulus and the electromechanical dielectric breakdown strength of polyethylene at high temperatures can be estimated.

According to elastic theory, one needs two independent elastic constants, for example bulk and shear modulus B and C_{44}, to describe the elastic properties of isotropic solids. If there is only one microscopic "spring" constant, it should come as no surprise that the bulk and shear modulus B and C_{44} have a fixed ratio. By considering a 2D Sierpinski gasket with a fractal dimension D=1.5849, Bergman and Kantor (1984) were able to show this is holds for a random isotropic elastic medium. The bulk and shear modulus B and C_{44} have the universal ratio

$$\frac{B}{C_{44}} = \left(\frac{4}{d}\right) \tag{7.33}$$

Table 7.11. The density ρ, longitudinal wave velocity V_L, shear wave velocity V_S, second order elastic constants C_{11} and C_{44}, Poissen's ratio P, Young's and bulk modulus B and the effective fractal dimensionality $d=4C_{44}/B$ for polyethylene samples at 140K.

Sample	ρ (kg/m^3)	V_L (m/s)	V_s (m/s)	C_{11} (GPa)	C_{44} (GPa)	P	Y (GPa)	B (GPa)	$4C_{44}/B$
P3	919	3537	1637	11.49	2.463	0.364	6.717	8.206	1.201
P16	920	3352	1640	10.34	2.474	0.343	6.644	7.041	1.405
P61	924	3417	1620	10.79	2.425	0.355	6.572	7.557	1.284
P64	921	3402	1659	10.66	2.536	0.344	6.816	7.279	1.394
P3+G16	915	3502	1653	11.22	2.5	0.357	6.783	7.887	1.268
P16+G16	920	3489	1667	11.2	2.557	0.352	6.915	7.791	1.313
P3+G17	914	3420	1640	10.69	2.458	0.351	6.640	7.413	1.326
P16+G17	914	3374	1660	10.41	2.519	0.340	6.753	7.051	1.429
P40	921	3391	1653	10.59	2.517	0.344	6.766	7.234	1.392
P42	916	3400	1633	10.59	2.443	0.350	6.596	7.333	1.333

where d is a Euclidean dimensionality. They further showed that this relation holds even without the assumption of the single spring constant by constructing a slightly more realistic 2D elastic fractal network. One important advance in polymer physics has been to recognize the interests of discussing any statistical problem in arbitrary dimensions and to classify systems according to their behaviour as a function of d. Therefore we shall keep d as a parameter in our discussion. The above relation can be rewritten as

$$d = \frac{4C_{44}}{B} \qquad (7.34).$$

This formula has been applied to several glasses and some polymers (Bogue and Sladek 1990). Values of d range from 3.32 for tetrahedrally coordinated network glasses such as SiO_2 and GeO_2, through 2 for quasi-two-dimensional glasses (As_2S_3 and As_2Se_3), to ~0.84 for some polymer glasses. These results suggest that the structure of disordered systems such as glasses and polymers can be described approximately by the fractal network used in the deduction of the above formula. The parameter "d" which may better be called an effective dimensionality characterizes the dimensionality of the molecular structure. The values of d for the ten polyethylene samples are given in the last column of Table 7.11. In general, the d values are slightly larger for the crosslinked polyethylenes, which is consistent with the suggestion (Alexander et al. 1983) that the effect of the crosslinks is to restore the true three-dimensional Euclidean character of the vibrations.

A determination of the elastic constants of polyethylene at high temperatures, where the shear wave velocity data are not available, can be based on the assumption that the effective dimensionality d is independent of temperature. In fact, the elastic data for PMMA (Ngoepe, Lambson and Saunders 1990) show that the effective dimensionality d=1.3 for this amorphous polymer changes little over a temperature range from 10 to 290K. For semicrystalline polymers such as polyethylene, a difficulty arises from the fact that crystalline regions may have different d values from those of the amorphous phase, and the crystallinity changes with temperature. Nevertheless, the value of d should mainly be determined by the one dimensional polymer structure, which is

common in the crystalline phase as well as in the amorphous phase. Thus the shear modulus for polyethylene can be estimated using the measured longitudinal modulus and the effective dimensionality determined using the low temperature data:

$$C_{44} = \frac{dC_{11}}{4(1+d/3)} \qquad (7.35).$$

The Young's modulus can then be calculated from C_{11} and C_{44} using equation (7.31). The calculated elastic constants for polyethylenes at 300K are given in Table 7.12. The calculated shear wave velocity is also given for comparison.

Comparing Table 7.11 with Table 7.12, it is noted that Poisson's ratio at room temperature is exactly the same as those at low temperatures; of course it follows from the assumption of invariance of the effective dimensionality with temperature that a value of Poisson's ratio calculated from d must also be temperature independent. Due to the large acoustic damping in low density polyethylene, there are no measured shear wave velocity data available so far at room temperature. Although direct comparison is not possible, the calculated results in Table 7.12 can still be compared with those measured for high density polyethylene. The shear ultrasonic wave velocity measured at 5 MHz and the corresponding Young's modulus in high density polyethylene have been reported to be 1100m/s and 3.4GPa respectively (Perepechko and Sorokin 1973). These are in fairly good agreement with the values given in Table 7.12, if the difference in sample density is taken into account.

Table 7.12. The longitudinal velocity V_L and stiffness C_{11}, the shear wave velocity V_S and stiffness C_{44}, the Poisson's ratio P, the Young's modulus Y and the bulk modulus B for polyethylene samples at 300K.

Sample	V_L (m/s)	C_{11} (GPa)	V_S (m/s)	C_{44} (GPa)	P	Y (GPa)	B (GPa)
P3	2088	4.01	967	0.860	0.364	2.344	2.864
P16	2102	4.06	1028	0.971	0.343	2.609	2.765
P61	2075	3.98	984	0.894	0.355	2.424	2.787
P64	2110	4.11	1029	0.978	0.344	2.628	2.806
P3+G16	2122	4.12	1002	0.918	0.357	2.491	2.896
P16+G16	2123	4.15	1014	0.947	0.352	2.562	2.887
P3+G17	2099	4.03	1007	0.927	0.351	2.503	2.794
P16+G17	2076	3.94	1021	0.953	0.340	2.556	2.669
P40	2074	3.96	1011	0.941	0.344	2.530	2.705
P42	2059	3.88	989	0.895	0.350	2.417	2.687
C56	1974	3.57	971	0.864	0.340	2.316	2.418

7.4.5. Pressure derivative of longitudinal stiffness modulus.

The large hydrostatic pressure dependence of the longitudinal stiffness modulus, $\partial C_L/\partial P$, provides a characteristic non-linear acoustic property of polyethylene. As mentioned before, the very good echo-train obtained for the cable sample C51 has allowed a particularly accurate determination of $\partial C_L/\partial P$. Hence in the following discussion, the results for C51 will be taken as the example. The pressure derivative $\partial C_L/\partial P$ has a value of 20.3 for this sample C51 at 290K, which is much larger than that for $(Ag_2O)_y(B_2O_3)_{1-y}$ glasses (which ~3-4 for a number of values of y) (Saunders et al. 1987), a typical metal such as aluminum ($\partial B/\partial P$=5.5) (Bridgman 1958) and even a typical amorphous polymer PMMA (~10) (Ngoepe, Lambson and Saunders 1990). Most surprisingly, $\partial C_L/\partial P$ for polyethylene is also much greater than that of most of liquids; for example, $\partial C_L/\partial P = \partial B/\partial P$ is 10.0 for methyl alcohol and 8.9 for ethyl alcohol at 293K (Bridgman 1958). This larger $\partial C_L/\partial P$ may, at least qualitatively, be understood in terms of the two-phase texture structure of polyethylene.

Table 7.13. The pressure derivative of the longitudinal modulus for polyethylene compared with a $(Ag_2O)_y(B_2O_3)_{1-y}$ glass, aluminum, PMMA and two organic liquids.

Sample	C51	vitreous $(Ag_2O)_y(B_2O_3)_{1-y}$	Al	PMMA	methyl alcohol	ethyl alcohol
$\partial C_L/\partial P$	20.3	3-4	~5.5	10	10	8.9

It follows from the multiple scattering theory of Waterman and Truell (1961), equation (7.16), that

$$\frac{1}{C_L^2}\frac{\partial C_L}{\partial P} = \frac{\partial \delta}{\partial P}\left[\frac{1}{C_{L1}} - \frac{1}{C_{L2}}\right] + \left[\frac{1-\delta}{C_{L1}^2}\frac{\partial C_{L1}}{\partial P} + \frac{\delta}{C_{L2}^2}\frac{\partial C_{L2}}{\partial P}\right] \tag{7.36}$$

If we ignore the contribution from the pressure dependence of the crystallinity, and assume δ~0.5, equation (7.36) becomes

$$\frac{1}{C_L^2}\frac{\partial C_L}{\partial P} = \frac{1}{2}\left[\frac{1}{C_{L1}^2}\frac{\partial C_{L1}}{\partial P} + \frac{1}{C_{L2}^2}\frac{\partial C_{L2}}{\partial P}\right] \tag{7.37}$$

To calculate $\partial C_L/\partial P$ of polyethylene using equation (7.37), one needs to know the pressure derivative of the longitudinal stiffness modulus for the crystalline as well as the amorphous phase, which need to be found.

According to equation (7.32), the pressure derivative of the longitudinal stiffness modulus $\partial C_L/\partial P$ can be related to the pressure derivatives of the bulk $\partial B/\partial P$ and shear $\partial C_S/\partial P$ moduli using

$$\frac{\partial C_L}{\partial P} = \frac{\partial B}{\partial P} + \frac{4}{3}\frac{\partial C_S}{\partial P} \tag{7.38}$$

For normal liquids the shear modulus C_S is zero so that C_L equals the bulk modulus B and

$$\frac{\partial C_L}{\partial P} = \frac{\partial B}{\partial P} \tag{7.39}$$

Equation (7.39) can be used to describe approximately the mechanical properties of amorphous materials above the glass transition or semi-crystalline polymers above its melting temperature. For a rough estimation, the pressure derivative of the longitudinal stiffness modulus of amorphous polyethylene, $\partial C_{L1}/\partial P$ in equation (7.37), can be taken as 10, the value of $\partial B/\partial P$ of methyl alcohol (Table 7.13). In general, equation (7.39) does not hold for solids. However, the hydrostatic pressure derivative of the shear modulus is much smaller than that of the longitudinal stiffness modulus. For example, the value of $\partial C_L/\partial P$ is more than 12 times larger than that of $\partial C_S/\partial P$ for $AgPO_3$ glass (Saunders et al. 1996). The ratio of these two pressure derivatives is 4 for a typical amorphous polymer PMMA (Ngoepe, Lambson and Saunders 1990). Therefore equation (7.39) can be used to make a rough estimate of the value of $\partial C_{L2}/\partial P$ of crystalline polyethylene. If we take $\partial B/\partial P$=8.2 of a high density polyethylene (Hartmann 1976/77) as a value for $\partial C_{L2}/\partial P$ of the crystalline polyethylene, then, using equation (7.37), the value of $\partial C_L/\partial P$ for semicrystalline polyethylene at atmospheric pressure at 290K is estimated as 22.5, which is reasonably close to that (20.3) measured directly for polyethylene cable insulation C51 (see Table 7.13). This agreement indicates that the large $\partial C_L/\partial P$ of polyethylene can be attributed to its semicrystalline molecular structure; any effects of phase change due to application of

hydrostatic pressure are negligibly small compared with those due to changing the temperature.

7.4.6. Relationship between the effect of temperature and that of pressure.

The effect of increasing temperature is to decrease the ultrasonic wave velocity so that the parameter $(\partial V_L/\partial T)_P$ is negative, while applying pressure increases the velocity giving a positive $(\partial V_L/\partial P)_T$. Thus applying hydrostatic pressure induces effects in the same direction as those produced by reducing the temperature of the polymer. This feature is very useful in practice as applying pressure can shift the critical temperature of certain phase transitions, such as the melting and glass transitions, to a more convenient temperature range. Measurements of the temperature and hydrostatic pressure dependence of the longitudinal ultrasonic wave velocity enable estimation of a thermodynamic quantity $(\partial P/\partial T)_v$, which is a measure of the simultaneous changes in temperature and pressure required to keep the material volume fixed.

In general, the ultrasonic wave velocity V_L is a function of temperature T, pressure P and volume v, which itself is a function of T and P. The molecular interpretation of the sound velocity is based on the assumption that an important factor governing the sound velocity in a given polymer is the specific volume (or the free volume), so that the temperature and pressure derivatives of a physical quantity, such as ultrasonic wave velocity V_L, is given as

$$\left(\frac{\partial V_L}{\partial T}\right)_P = \left(\frac{\partial V_L}{\partial \mathrm{v}}\right)_{T,P}\left(\frac{\partial \mathrm{v}}{\partial T}\right)_P \tag{7.40}$$

$$\left(\frac{\partial V_L}{\partial P}\right)_T = \left(\frac{\partial V_L}{\partial \mathrm{v}}\right)_{P,T}\left(\frac{\partial \mathrm{v}}{\partial P}\right)_T \tag{7.41}$$

It follows that

$$-\left(\frac{\partial V_L}{\partial T}\right)_P \Big/ \left(\frac{\partial V_L}{\partial P}\right)_T = -\left(\frac{\partial \mathrm{v}}{\partial T}\right)_P \Big/ \left(\frac{\partial \mathrm{v}}{\partial P}\right)_T = \beta B = \left(\frac{\partial P}{\partial T}\right)_V \tag{7.42}$$

where β is the volume thermal expansion coefficient and B is isothermal bulk modulus. The quantity $(\partial P/\partial T)_v$ of the polyethylene samples, for which both the temperature and pressure data are available, calculated using equation (7.42), is given in Table 7.14. For

all the polyethylene samples studied at different temperatures, $(\partial T/\partial P)_v$ has the same order ($\sim 10^{-7}$ K/Pa) and is comparable with $(\partial T/\partial P)_f$ found for poly(ethylene oxide) using dielectric data ($\sim 10^{-7}$ K/Pa) (see Chapter 5).

Equation (7.42) enables a calculation of thermal expansion coefficient using values of $(\partial P/\partial T)_v$ and the bulk modulus B, which have been measured ultrasonically (Tables 7.11 and 7.12). The calculated (β_c) and the measured (β_m) thermal expansion coefficient for some polyethylenes at room temperature are given in Table 7.15. It can be seen that the calculated values agree fairly well with those measured directly, indicating that the bulk modulus estimated using the ultrasonic method is reliable.

The values of $(\partial P/\partial T)_v$ can also be used to obtain the Grüneisen parameter γ. It is known that

$$P = -\left(\frac{\partial F}{\partial V}\right)_T \tag{7.43}$$

where F is the Helmholtz free energy which can be written as

$$F = U + kT\sum_j \left[\frac{1}{2}\frac{h\nu_j}{kT} + \ln\left(1-\exp\left(-\frac{h\nu_j}{kT}\right)\right)\right] \tag{7.44}$$

where $U(V)$ is the temperature independent part of the internal energy. It follows from equations (7.43) and (7.44) that

$$P = -\frac{dU}{dV} + \sum_j \frac{\gamma_j E_j}{V} \tag{7.45}.$$

The summation is carried out over all the normal vibrational modes:

$$E_j = \frac{1}{2}h\nu_j + \frac{h\nu_j}{e^{h\nu_j/kT}-1} \tag{7.46}$$

is the energy of the jth linear oscillator, and the Grüneisen parameter γ_j is defined by

$$\gamma_j = -\frac{d\ln\nu_j}{d\ln V} \tag{7.47}$$

Table 7.14. Values of $(\partial V_L/\partial P)_T$, $(\partial V_L/\partial T)_P$ and $(\partial P/\partial T)_v$ of LDPE, XLPE and cable insulations determined from the dependences of ultrasonic wave velocity upon temperature and pressure at selected temperatures.

Sample	T (K)	$(\partial V_L/\partial T)_P$ (m/sK)	$(\partial V_L/\partial P)_T$ (m/sPa)	$(\partial P/\partial T)_v$ (Pa/K)
P3 (LDPE)	291	-9.7	5.3×10^{-6}	1.8×10^{6}
	320	-9.4	5.5×10^{-6}	1.7×10^{6}
	357	-9.4	7.4×10^{-6}	1.3×10^{6}
P16 (LDPE)	293	-9.7	3.4×10^{-6}	2.9×10^{6}
	321	-8.8	5.7×10^{-6}	1.5×10^{6}
	360	-8.8	6.0×10^{-6}	1.5×10^{6}
P61 (LDPE)	300	-8.9	6.0×10^{-6}	1.5×10^{6}
	321	-8.9	5.4×10^{-6}	1.6×10^{6}
	340	-8.9	5.1×10^{-6}	1.7×10^{6}
P3+G17 (XLPE)	293	-9.0	4.7×10^{-6}	1.9×10^{6}
	320	-9.0	5.4×10^{-6}	1.7×10^{6}
	360	-9.0	4.3×10^{-6}	2.1×10^{6}
P16+G17 (XLPE)	291	-9.3	6.0×10^{-6}	1.6×10^{6}
	320	-9.2	6.0×10^{-6}	1.5×10^{6}
	360	-9.2	5.1×10^{-6}	1.8×10^{6}
P40 (XLPE)	301	-9.3	5.4×10^{-6}	1.7×10^{6}
	321	-9.3	5.0×10^{-6}	1.9×10^{6}
	350	-9.3	4.9×10^{-6}	1.9×10^{6}
P42 (XLPE)	294	-9.9	8.3×10^{-6}	1.2×10^{6}
	321	-9.9	5.1×10^{-6}	1.9×10^{6}
	350	-9.5	5.1×10^{-6}	1.9×10^{6}
C51 (cable)	290	-8.4	4.9×10^{-6}	1.7×10^{6}
	351	-7.8	5.6×10^{-6}	1.4×10^{6}
C56 (cable)	297	-7.6	8.5×10^{-6}	0.89×10^{6}
	321	-7.6	8.0×10^{-6}	0.95×10^{6}
	336	-7.6	6.1×10^{-6}	1.2×10^{6}
	349	-7.6	4.9×10^{-6}	1.6×10^{6}

Table 7.15. The thermodynamic quantity $(\partial P/\partial T)_v$, the bulk modulus B, the Grüneisen parameter γ and the thermal expansion coefficient β_c calculated using equation (7.40) compared with that measured directly β_m for polyethylenes at room temperature.

Sample	$(\partial P/\partial T)_v$ (Pa/K)	B (GPa)	γ	β_c (/K)	β_m (/K)
P3	1.8×10^6	2.864	0.87	6.3×10^{-4}	
P16	2.9×10^6	2.765	1.39	10.5×10^{-4}	
P61	1.5×10^6	2.787	0.72	5.4×10^{-4}	
P3+G17	1.9×10^6	2.896	0.92	6.6×10^{-4}	
P16+G17	1.6×10^6	2.887	0.77	5.5×10^{-4}	
P40	1.7×10^6	2.705	0.82	6.3×10^{-4}	4.7×10^{-4}
P42	1.2×10^6	2.687	0.58	4.5×10^{-4}	4.5×10^{-4}
C56	0.89×10^6	2.418	0.43	3.7×10^{-4}	

which shows the relationship between the frequencies of normal vibrations and the volume of the solid. Grüneisen assumed that all the γ_j for different mode frequencies are equal, so that equation (7.45) becomes

$$P = -\frac{dU}{dV} + \frac{\gamma}{V}\sum_j E_j \tag{7.48}$$

Differentiating equation (7.48) with respect to temperature, we have

$$\left(\frac{\partial P}{\partial T}\right)_V = \frac{\gamma}{V}\sum_j \frac{dE_j}{dT} = \gamma\rho C_v \tag{7.49}.$$

Here ρ is the density and C_v is the constant volume specific heat. The constant pressure specific heat C_P for two polyethylenes (HFDQ 4201 EC and HFDA 4202 EC) have been measured as 2634 and 1890 $Jkg^{-1}K^{-1}$ respectively (Hampton 1989). The two specific heats are interrelated by

$$\frac{C_P}{C_v} = \frac{B_s}{B_T} \approx 1.03 \tag{7.50}$$

where B_s and B_T are the adiabatic and isothermal bulk moduli respectively. To calculate the Grüneisen parameter using equation (7.49), therefore, we can take $C_v \cong C_P = 2262$

$Jkg^{-1}K^{-1}$ without losing much accuracy. The Grüneisen parameters thus obtained are also given in Table 7.15.

The value of the Grüneisen parameters falls in a range of 0.43-1.39 for the polyethylenes studied. The relatively small Grüneisen constant of polyethylene suggests that the contribution from the vibrational anharmonicity on average is small. It is also noted that the value of $(\partial P/\partial T)_v$ obtained ultrasonically, is essentially the same as that determined dielectrically, which is consistent with work reported on other polymers (Baird 1972). This is compatible with the close association of the electrical, elastic and thermodynamic properties of polyethylene.

7.5. Concluding Summary

To conclude, the velocity and attenuation of longitudinal and shear ultrasonic waves propagated in polyethylene plaques and cable insulations have been measured as functions of temperature and hydrostatic pressure. The results show that the temperature and pressure derivatives of the longitudinal ultrasonic wave velocity are extremely large. It has been found that the large pressure dependence of the ultrasonic wave velocity arises mainly from the two-phase structure of polyethylene, while the gradual crystalline-amorphous phase transition has to be taken into account in order to explain the large temperature dependence of the velocity. A linear relation has been derived between the temperature derivative of the wave velocity and the ultrasonic attenuation. The effect of temperature has been correlated to the effect of pressure through a thermodynamic quantity of $(\partial P/\partial T)_v$ which enables an estimation of the Grüneisen parameter for polyethylene. The elastic constants of the polyethylene plaques and cable insulations have been calculated from the ultrasonic wave velocity data. These characteristic mechanical properties obtained in the ultrasonic measurements will further be discussed and related to the electrical breakdown behaviour of polyethylene in Chapter 9.

CHAPTER 8. THE RESULTS AND DISCUSSION OF THE DYNAMIC MECHANICAL THERMAL ANALYSIS (DMTA) MEASUREMENTS ON POLYETHYLENE: RELAXATION PROCESSES AND THEIR ACTIVATION ENERGY IN THERMOPLASTIC POLYETHYLENE

Details of the DMTA technique have been given in Chapter 4 for reference. Temperature dependences of the log storage modulus (or Young's modulus) E' and the loss tangent (tan δ) of thermoplastic polyethylene P3 and P16 measured at 1 and 10 Hz are given in Figures 8.1 to 8.4 respectively. These data were not obtained by the author but taken from Dr. Moody of BICC Cables Ltd. to provide complementary information at much lower frequencies to that obtained from ultrasonic studies and therefore help in understanding the nature of the relaxation processes which cause the high ultrasonic attenuation in polyethylene. For polyethylene P3, there are three peaks in the temperature dependence of tan δ measured at 1 Hz (Figure 8.1): the α-peak (at 351K), β-peak (at 262K) and γ-peak (at about 157K). The loss increases rapidly above 373K. Corresponding to these loss peaks, the modulus shows several kinks in the same temperature range. These results agree fairly well with those reported by Schmieder and Wolf (1953). The increase in tan δ above 373K corresponds to the crystal melting temperature. The γ-peak at 157K corresponds to the glass transition. Between the glass transition and the melting point, the loss tangent (tan δ) curve is dominated by the α and β relaxation peaks which shift 20K and 9K respectively over the frequency range from 1Hz to 10Hz (Figures 8.1 and 8.2). The log storage modulus is less sensitive to the relaxation processes, as expected: it represents the elastic response and corresponds to the completely recoverable energy. Not only do the loss peaks shift to higher temperatures, but also their heights, and the storage modulus, increase with increasing measurement frequency (Figures 8.1 and 8.2), indicating typical viscoelasticity of polymers in these polyethylenes. The temperature and frequency dependences of the log modulus and the loss tangent for thermoplastic polyethylene P16 are similar to those for P3 (compare Figures 8.1 and 8.2 with Figures 8.3 and 8.4).

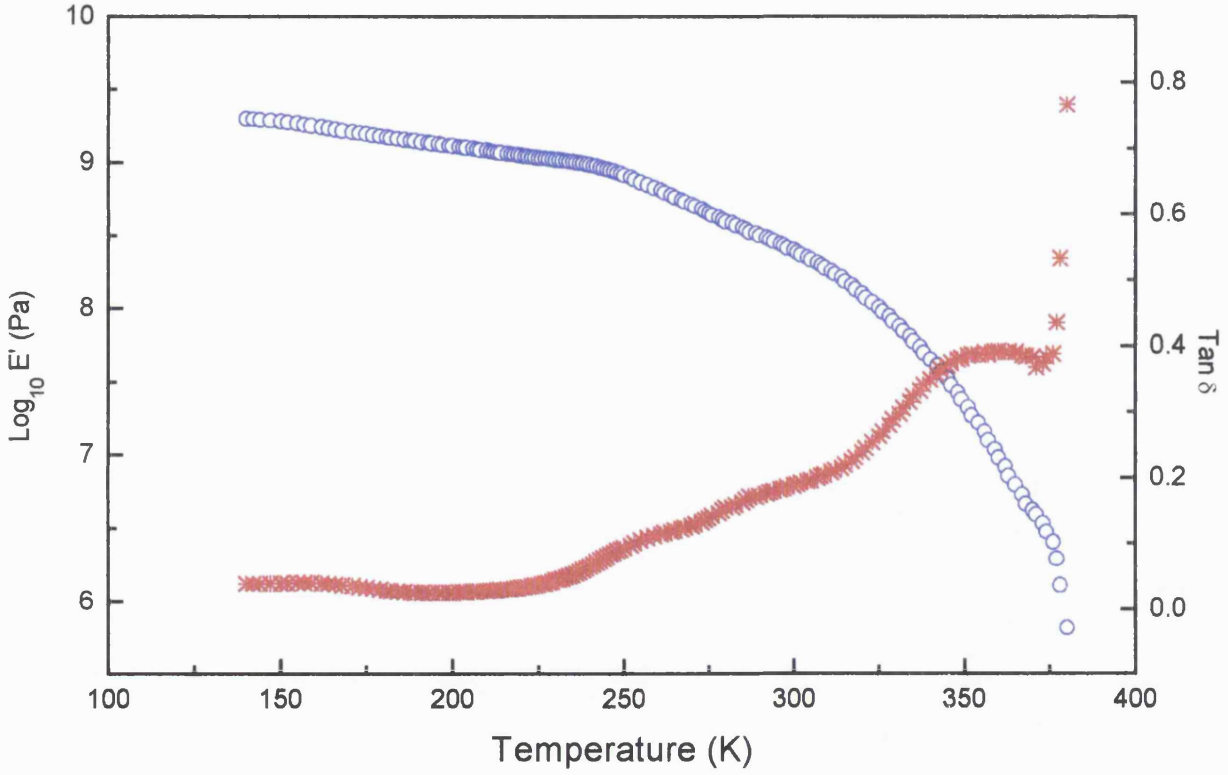

Figure 8.1. Temperature dependences of the log modulus, $\log_{10}$, (circles) and the loss tangent, tan δ, (stars) of thermoplastic polyethylene P3 measured at 1Hz.

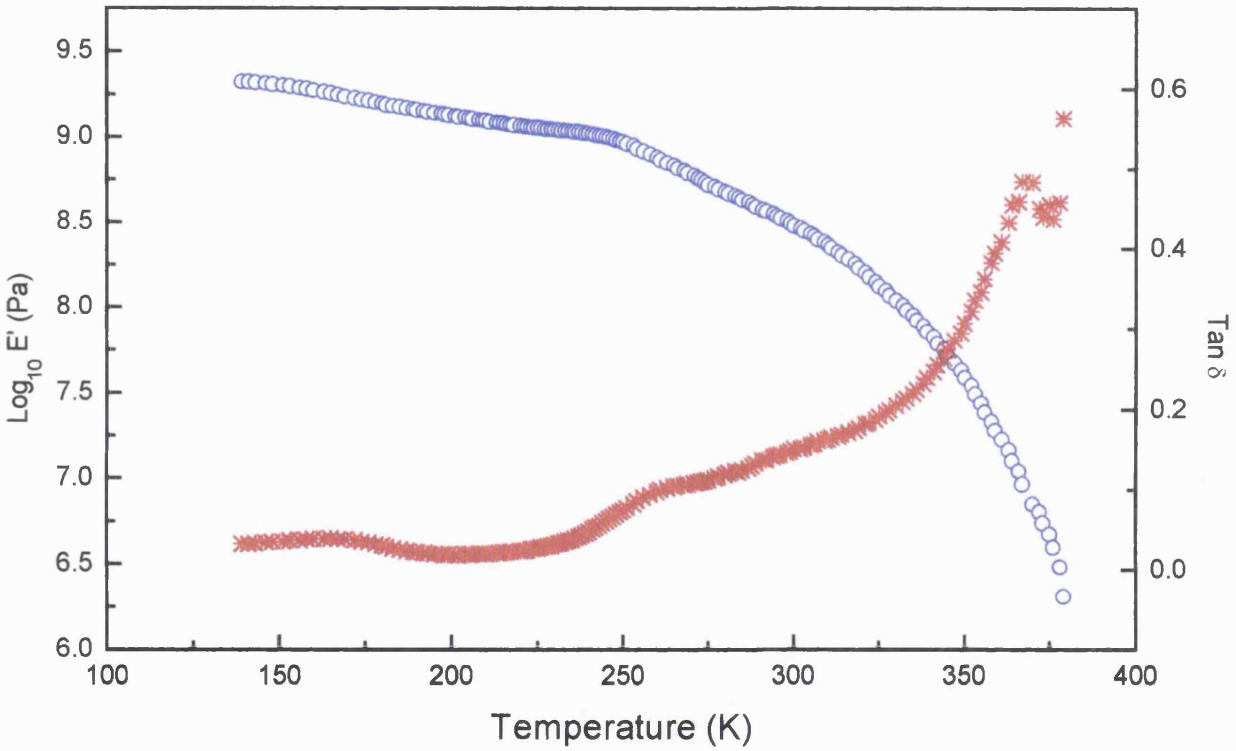

Figure 8.2. Temperature dependences of the log modulus, $\log_{10}E'$, (circles) and loss tangent, tan δ, (stars) of thermoplastic polyethylene P3 measured at 10 Hz.

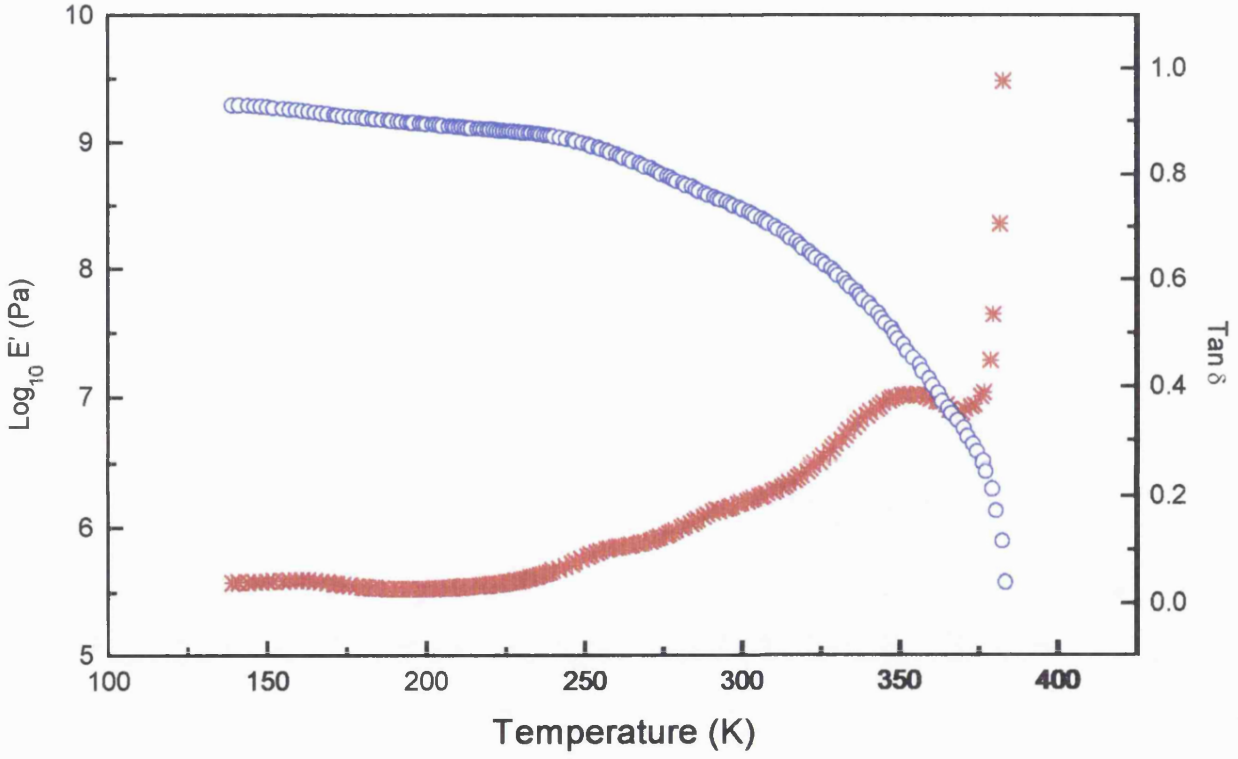

Figure 8.3. Temperature dependences of the log modulus, $\log_{10}E'$, (circles) and loss tangent, tan δ, (stars) of thermoplastic polyethylene P16 measured at 1 Hz.

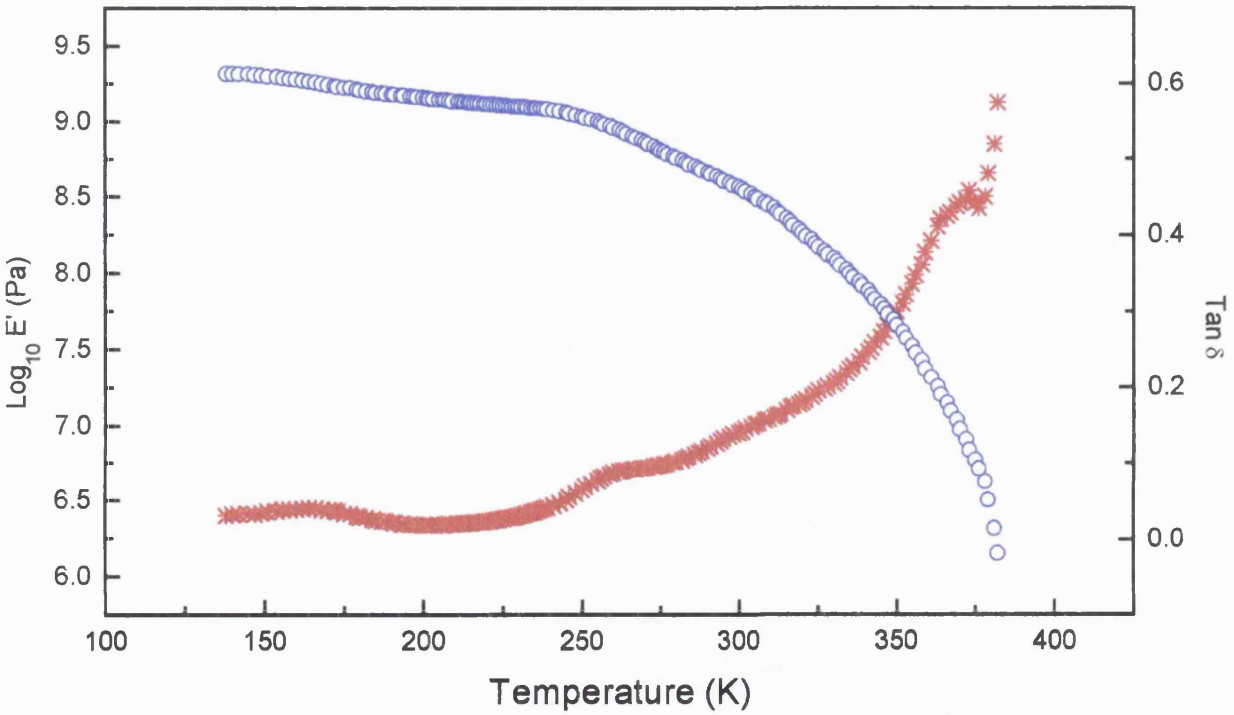

Figure 8.4. Temperature dependences of the log modulus, $\log_{10}E'$, (circles) and loss tangent, tan δ, (stars) of thermoplastic polyethylene P16 measured at 10 Hz.

In principle, the complex modulus or the internal friction, which is related to tan δ, can be associated with molecular motions by a simple relaxation model (Ward 1979), which assumes that certain molecular segments in the material can exist in two different conformational states, separated by an energy barrier ΔH, and that these molecular segments fluctuate between the two conformational states. These segmental movements can be characterized by a relaxation time, τ, which is expected to show an Arrhenius type temperature dependence:

$$\tau = \tau_o \exp(\Delta H / RT) \tag{8.1}$$

where τ_o is the natural relaxation time at a convenient reference temperature T_o. Under thermal equilibrium the average number of segments in each state remains unchanged and their distribution can be determined by Boltzmann statistics. If an external force is now applied to the material, so as to lower preferentially the energy of one conformational state with respect to the other, it disturbs the equilibrium, favouring a net conformational change towards the lower energy state. It is expected that the external oscillatory stress will be most effective in inducing these conformational changes when its frequency, ω, corresponds to the natural frequency (1/τ). The material shows a maximum in internal friction when

$$\omega\tau = 1 \tag{8.2}$$

where $\omega = 2\pi f$ and f being the measurement frequency. Therefore, the tanδ peak for the relaxation shifts by an amount that varies with frequency. Combining equations (8.1) and (8.2) gives

$$\ln f = -\Delta H / RT - \ln(2\pi\tau_o) \tag{8.3}$$

The activation energy can then be determined by measuring the temperature of the tan δ peak at several different frequencies.

Plots of *ln f* against *1/T* for the α, β and γ relaxation peaks are shown in Figures 8.5 and 8.6 for thermoplastic polyethylene P3 and P16 respectively. The straight lines are the least-mean-squares fits to the experimental data. An important result is that the Arrhenius plot of the DMTA data obtained at low frequencies extrapolates over several orders of magnitude of frequency up to the ultrasonic data (β and γ relaxation

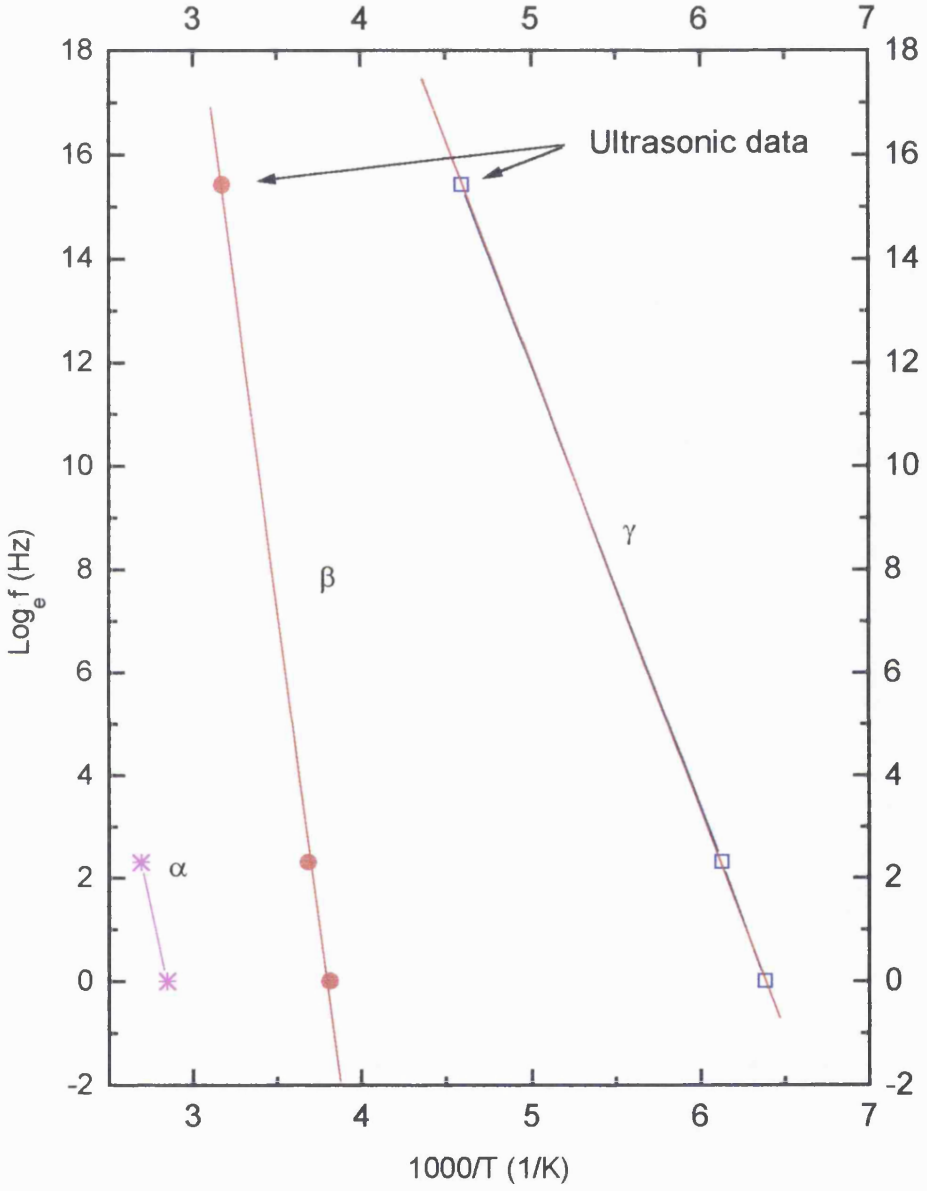

Figure 8.5. Log$_e$ f versus 1/T plot for α (stars), β (circles) and γ (squares) relaxation peaks in the temperature dependences of tan δ and ultrasonic wave attenuation for thermoplastic polyethylene P3.

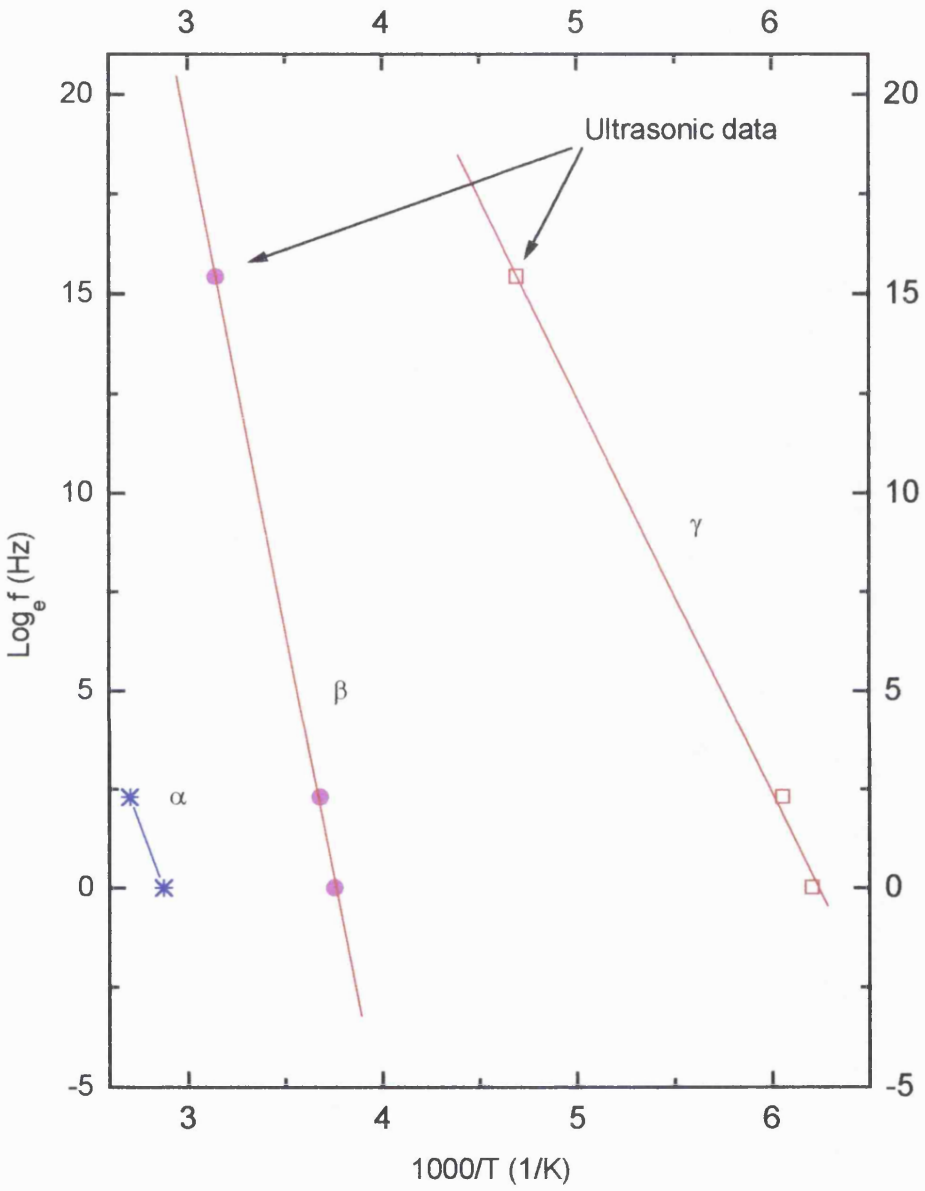

Figure 8.6. Log$_e$ f versus 1/T plot for α (stars), β (circles) and γ (squares) relaxation peaks in the temperature dependences of tan δ and ultrasonic wave attenuation for thermoplastic polyethylene P16.

in Figures 8.5 and 8.6), indicating that the particular peaks observed in ultrasonic attenuation experiments have the same physical origin as the corresponding peaks appearing in the DMTA measurements. If the data for the α peak is extrapolated up to the ultrasonic frequency range, the peak position is found to be above 400K which is above the melting temperature of polyethylene. That is why the α peak cannot be observed in the ultrasonic measurements carried out at 5 MHz. The values of the activation energy for the three relaxation processes in polyethylene P3 and P16 are shown in Table 8.1, together with those determined dielectrically (Sayre, Swanson and Boyd 1978) and mechanically (Hopkins and Kurkjian 1965) for comparison.

The α relaxation is believed (Sayre et al. 1978) to be due to a chain twist-rotation-translation mechanism that results in rotation-translation of a entire chain in the crystalline region. The position and intensity of the α-peak is therefore dependent on the crystallinity and the size of the crystallites.

Table 8.1. The activation energy in kJ/mole of α, β and γ relaxation in thermoplastic polyethylene P3 and P16.

Sample	α	β	γ
P3	124.3	207.2	71.6
P16	111.4	206.8	82.9
Polyethylene	104.2[(1)]	83.7-418.7[(2)]	72.4[(1)]

(1) Data for linear polyethylene, taken from Sayre et al. (1978).

(2) Data for branched polyethylene, taken from Hopkins and Kurkjian (1965)

The β relaxation is found (see Hedvig 1977) to be strongest in low density polyethylene. It becomes much weaker in high density polyethylene and is not visible in linear polyethylene. Therefore this peak is attributed to the motion of the side groups in the amorphous phase, which interacts with the crystallites of polyethylene (Table 8.2). Obviously the crystallites would restrict the motion of the side branches and therefore reduce the strength of the β relaxation. The movements of these side

groups when activated in an appropriate temperature range would "pull" out more polymer chains out of the crystalline region, resulting in a decrease in crystallinity with increasing temperature. As discussed in Chapter 7, this gradual crystalline -amorphous phase transition due to the molecular motion of side branches may be partly responsible for the extremely large temperature derivative of the ultrasonic wave velocity. The mechanical and perhaps electrical properties of low density polyethylene in the temperature range between glass transition and the melting region may depend strongly on the strength of the β relaxation. While the restrictions imposed on the β relaxation by the crystallites have been noticed (Nielson 1960), there seem to be no such studies on the effects of this relaxation on the crystallinity and hence the acoustic and mechanical behaviour of low density polyethylene reported in the literature. The large activation energy (Table 8.1) of β relaxation and the temperature and frequency ranges in which it occurs (~262K at 1 Hz and ~315K at 5 MHz) indicate that this relaxation process may be more important than conventionally thought for technical applications of polyethylene. The loss energy, which reaches its maximum value when the relaxation peak occurs, appears as heat which may produce an increase in temperature in a material subject to continuous cyclic stress at frequencies near to $(1/\tau)$. This could have implications for power cables in certain circumstances where the accumulation of heat may cause electrical breakdown and this will further be discussed in next chapter.

Table 8.2. The number of methyl groups per 1000 carbon atoms N_m, the number of ethyl groups per 1000 carbon atoms N_e, the density ρ, the crystallinity χ and the crystalline melting temperature T_m for low density polyethylene (LDPE), high density polyethylene (HDPE) and linear polyethylene (LPE).

Sample	N_m	N_e	ρ (kg/m^3)	χ	T_m (°C)
LDPE	21.5	14.4	910~920	~60%	105~120
HDPE	3	1	930~940	~87%	120~140
LPE	<1	<1	960	~93%	140

The γ relaxation is normally related to the glass transition and is attributed to a crankshaft-type local motion in the main chains of amorphous phase. However, the broad and anisotropic nature of the γ-peak (Figures 8.1 to 8.4) suggests that this transiton may include more than one molecular relaxation process, which is consistent with the ultrasonic results as discussed in Chapter 7. In fact, Matsui et al. (1971) have pointed out that the migration of defects such as screw dislocations in the crystalline region may make some contributions to the γ-peak.

It is interesting to note that an internal friction peak at 20K has been observed in a high density polyethylene (Papir and Baer 1971). The driving frequency used was about 3 Hz. If this internal peak arises from the same relaxation process as the ultrasonic attenuation peak at 40K, which has been observed in low density polyethylene in the present work (see Figures 7.1 to 7.4), the activation energy can be estimated to be 3.2 kJ/mole by using the Arrhenius relation. This value is very near the energy deference (3.3 kJ/mole) between the *gauche* position and the *trans* position of a polyethylene chain (see Figure 2.1 in Chapter 2). Therefore, the attenuation peak at 40K may be due to the rotation of the polymer chains between these two conformations. Because the potential barrier between these positions (about 10 kJ/mole, see Figure 2.1) is much larger than the activation energy calculated, classical thermal activation relaxation seems unlikely. The only possible mechanism is a quantum mechanical tunnelling relaxation which is dependent on the energy splitting of the two levels instead of the energy barrier between them (Hunklinger and Arnold 1976).

CHAPTER 9. THE ELASTIC AND DIELECTRIC PROPERTIES OF POLYETHYLENE IN RELATION TO ELECTRICAL BREAKDOWN

9.1. The electromechanical breakdown strength of polyethylene; the Stark-Garton approach

Electromechanical dielectric breakdown of polyethylene was first discussed by Stark and Garton (1955), who noted that the breakdown characteristics of irradiated polyethylene in the temperature range near the melting (or softening) point can be correlated with aspects of mechanical behaviour. This has resulted in the discovery of a form of breakdown caused by mechanical deformation.

Electrodes attached to the surface of a specimen during a dielectric breakdown test will exert a compressive force on the sample due to the mutual Coulombic attraction of the electrodes as the voltage V is imposed. If this is sufficient to cause appreciable deformation at an electric field below the intrinsic breakdown value, the dielectric strength will be reduced. The attractive force F is given by the differential of the energy U stored in the system with respect to the thickness d of the material at constant applied voltage:

$$F = \left(\frac{\partial U}{\partial d}\right)_V = \frac{\partial}{\partial d}\left(\frac{1}{2}CV^2\right)_V. \tag{9.1}$$

Substituting for the parallel-plate capacitance C of the specimen, Stark and Garton obtained an expression for the compressive force per unit area:

$$\frac{F}{A} = -\frac{1}{2}\varepsilon_0\varepsilon'\left(\frac{V}{d}\right)^2. \tag{9.2}$$

At equilibrium the electrical force causing compression is balanced by the elastic restoring force. Because the strains are large, a logarithmic form of strain (s) and stress (σ) relation:

$$\sigma = Y\log_e(1+s) = -Y\log_e\frac{d_0}{d} \tag{9.3}$$

can be found, where Y is Young's modulus and d_0 is the initial thickness. Hence the equilibrium thickness d can be determined from

$$\frac{1}{2}\varepsilon_0\varepsilon'\left(\frac{V}{d}\right)^2 = Y\log_e\left(\frac{d_0}{d}\right) \qquad (9.4).$$

Since $d^2\log_e(d_0/d)$ has a maximum value when $d/d_0 = \exp(-1/2) \approx 0.6$, no real value of V can produce a stable situation for values of d/d_0 less than 0.6. Further increase of V would result in mechanical collapse. Therefore the critical electric stress is

$$E_c = \left(\frac{Y}{\varepsilon_0\varepsilon'}\right)^{\frac{1}{2}} \qquad (9.5).$$

The highest apparent dielectric strength which can be observed is

$$E_a = \frac{V_c}{d_0} = \frac{d}{d_0}E_c \approx 0.6\left(\frac{Y}{\varepsilon_0\varepsilon'}\right)^{\frac{1}{2}} \qquad (9.6).$$

The intrinsic breakdown strength may be reached as the specimen thickness is reduced before the electromechanical breakdown takes place. Equation (9.6) allows the calculation of the electromechanical breakdown strength using the Young's modulus data.

The Young's modulus for four polyethylenes in the thermoplastic and crosslinked forms and for two cable insulations has been calculated using the characteristic dimension (see Chapter 7) and the longitudinal velocity data above room temperature up to the melting point. Values at selected temperatures are given in Table 9.1.

Table 9.1. The Young's modulus in GPa for polyethylene samples at selected temperatures.

Sample	300K	310K	320K	330K	340K	350K	360K	370K	380K
P3	2.34	2.12	1.88	1.69	1.50	1.35	1.24	1.07	0.93
P16	2.61	2.37	2.15	1.94	1.77	1.58	1.43	1.27	1.09
P61	2.42	2.23	2.00	1.84	1.69	1.52	1.40		
P64	2.63	2.41	2.22	2.06	1.90	1.74	1.60	1.45	1.31
P3+G17	2.50	2.23	2.02	1.83	1.66	1.48	1.32	1.15	0.89
P16+G17	2.56	2.31	2.12	1.92	1.73	1.54	1.35	1.20	0.96
P40	2.53	2.31	2.07	1.90	1.71	1.52	1.35	1.20	0.97
P42	2.42	2.19	1.96	1.79	1.61	1.44	1.28	1.12	1.03
C56	2.32	2.13	1.97	1.81	1.67	1.52	1.38	1.23	1.05

Table 9.2. The breakdown strength in MV/m calculated using Stark-Garton model equation (9.6) for polyethylene samples at selected temperatures.

Sample	300K	310K	320K	330K	340K	350K	360K	370K	380K
P3	6400	6100	5800	5500	5200	4900	4700	4300	4100
P16	6800	6500	6200	5900	5600	5300	5000	4700	4400
P61	6600	6300	6000	5700	5500	5200	5000		
P64	6800	6500	6200	6000	5800	5500	5300	5100	4800
P3+G17	6700	6300	6000	5700	5400	5100	4800	4500	4000
P16+G17	6700	6400	6100	5800	5500	5200	4900	4600	4100
P40	6700	6400	6000	5800	5500	5200	4900	4600	4100
P42	6500	6200	5900	5300	4800	4500			
C56	6400	6100	5900	5700	5400	5200	4900	4700	4300

Table 9.3. The mean a.c. breakdown strength E_b in MV/m measured at 50Hz electrically with a ramp rate of 2kV/s for thermoplastic polyethylene P3, P16, P61 and P64 above room temperature.

T (°C)	P3	P16	P61	P64
20	86.07	95.87	96.75	101.88
30	92.65	97.31	92.66	99.36
40	99.56	99.32	92.62	98.25
50	97.55	94.65	92.26	94.84
60	85.22	85.70	83.22	87.71
70	84.43	78.87	80.22	83.69
80	74.67	74.48	67.49	71.45
90	66.32	66.32	70.41	56.48
95	64.50	64.50	62.72	61.20

By substituting the Young's modulus determined from ultrasonic measurements and the dielectric constants $\varepsilon_0 = 8.845\times10^{-12} F/m$ and $\varepsilon' \approx 2.3$ into equation (9.6), the electromechanical breakdown strength has then been estimated for the polyethylenes and the results are presented in Table 9.2. To compare these results with those determined directly from electrical measurements, the mean electrical breakdown strength for thermoplastic P3, P16, P61 and P64 obtained electrically at BICC Cables Limited is given in Table 9.3. It is important to note that the breakdown data in Table 9.3 have been measured under a.c. conditions with a linear ramp rate of 2kV/s, the effect of which on the breakdown strength will be discussed in the following sections.

The dielectric strength calculated from ultrasonic data for polyethylene is one to two orders of magnitude larger than that measured electrically at 50Hz (compare Tables 9.2 and 9.3). It is also greater than the breakdown strength (0.58GV/m) calculated by

Stark and Garton (1955) using equation (9.6). This disagreement arises partly from the different values of Young's modulus used in the calculation. The Young's modulus Stark and Garton used was measured by a static method, which is carried out at much higher strains than that used in the ultrasonic technique, and results in a value of Young's modulus one to two orders of magnitude less than that obtained ultrasonically at a frequency of ~5MHz. The frequency dependence of the Young's modulus results directly from the viscoelastic properties of polyethylene. Physically, the amount of deformation produced in a polymer by a given stress depends on the length of time that the stress is applied. Correspondingly, the modulus will decrease with time. During the short time that the stress of a ultrasound wave is applied in one direction, only relatively small portions of the polymer can move; hence not as much strain is induced as in a low frequency or a typical static measurement, and the ultrasonic modulus is higher than the static modulus. According to the electromechanical breakdown model, stress-relaxation of the Young's modulus might be partly responsible for the electrical ageing process normally observed in polymeric insulations.

The effects of ageing have been completely ignored so far in the above discussion, which is normally applicable only to "ideal" insulating systems such as completely crystalline insulating materials and some very well made amorphous systems. An "ideal" insulating system has a Young's modulus which is not time dependent. Such a system will always breakdown when, and only when, a critical breakdown voltage is exceeded; below this critical voltage the system will never breakdown. The breakdown strength in this approach is time independent.

However, real insulating systems, especially polymers, are **not** ideal and it has been found experimentally that the breakdown strength E_b is related to the testing time t by (see, for example, Dissado and Fothergill 1992):

$$E_b^n \propto \frac{1}{t} \tag{9.7}$$

An insulation system may have a large breakdown strength in a short time scale and this breakdown strength would be much smaller as the time scale increases. The effect of ageing observed in breakdown testing is similar to the stress-relaxation process (or physical ageing) characterizing the mechanical properties of the viscoelastic materials. The relaxed breakdown strength E_b can be related to the relaxed Young's modulus using the electromechanical breakdown model, equation (9.6). This similarity suggests that the mechanical stress-relaxation may contribute to the ageing effects observed in polyethylene cable insulations under electrical load and provides further support to the electromechanical breakdown mechanism. The molecular structure of polyethylene, which is responsible for the mechanical relaxation process, may play an more important role in the electrical breakdown of this polymer than that conventionally thought.

The values of electromechanical breakdown strength of thermoplastic polyethylene P3 and P16 at selected temperatures, calculated from the Young's modulus measured at 1 and 10 Hz using DMTA method, are given in Tables 9.4 and 9.5. As a consequence of viscoelasticity, the Young's modulus and the corresponding breakdown strength are much smaller than those calculated from the 5 MHz ultrasonic data (Table 9.2); yet the values of E_b are still much larger than those of the a.c. breakdown strength measured at 50Hz (Table 9.3). The difference between the d.c. and a.c. breakdown strength, and that between the calculated and experimentally measured will be discussed further in following sections.

For all the polyethylene samples studied, the calculated breakdown strength decreases with increasing temperature, which is in agreement with that measured electrically. It

should be noted that both the Young's modulus and the dielectric constant ε′ in equation (9.6) are temperature dependent. Take P42 as an example; the Young's modulus (ultrasonic data) decreases ~50% between 300-360K, while ε′ reduces by ~10% over the same temperature range. Therefore the temperature dependence of the electromechanical breakdown strength would be smaller, if the decrease of ε′ is taken into account.

Table 9.4. The Young's modulus Y obtained from DMTA measurements at 1 Hz and the corresponding breakdown strength E_b calculated using equation (9.6) for thermoplastic polyethylene P3 and P16 at selected temperatures.

	P3		P16	
T (°C)	Y (GPa)	E_b (MV/m)	Y (GPa)	E_b (MV/m)
20	0.2985	2298	0.3516	2494
30	0.2289	2013	0.2729	2198
40	0.1684	1726	0.1950	1858
50	0.1104	1398	0.1213	1465
60	0.0680	1097	0.0771	1168
70	0.0374	814	0.0452	894
80	0.0179	563	0.0215	617
90	0.0073	359	0.0093	406
95	0.0047	288	0.0066	342

Table 9.5. The Young's modulus Y obtained from DMTA measurements at 10 Hz and the corresponding breakdown strength E_b calculated using equation (9.6) for thermoplastic polyethylene P3 and P16 at selected temperatures.

	P3		P16	
T (°C)	Y (GPa)	E_b (MV/m)	Y (GPa)	E_b (MV/m)
20	0.3594	2522	0.4295	2756
30	0.2818	2233	0.3351	2436
40	0.2109	1931	0.2415	2066
50	0.1448	1601	0.1648	1710
60	0.0955	1299	0.1087	1385
70	0.0590	1024	0.0673	1092
80	0.0311	740	0.0372	812
90	0.0146	510	0.0180	564
95	0.0087	392	0.0116	451

9.2. The electrofracture model

In Stark and Garton's (1955) electromechanical breakdown model, plastic flow was completely ignored. Plastic deformation prior to breakdown at localized regions of high electrical field was observed later by Blok and LeGrand (1969) using polarized light. This observation and further work followed in this direction not only verified electromechanical breakdown but also resulted in a new model, the electrofracture model, which takes into account of the plastic flow of dielectrics (Zeller et al. 1984).

The electrofracture model is based on the idea that in microscopic areas of stress concentration an instability may occur giving rise to a localized thinning and breakdown. It assumes a crack propagation mechanism travels with a maximum speed of that of sound waves. In order to form and propagate a filamentary crack in the dielectric, the sum of the electrostatic energy

$$W_{es} = \frac{1}{2}\varepsilon_o \varepsilon' E^2 \tag{9.8}$$

and the strain energy

$$W_{em} = \frac{1}{2}\sigma_m \varepsilon_m = \frac{\sigma_m^2}{2Y} = \frac{\varepsilon_o^2 \varepsilon'^2 E^4}{8Y} \tag{9.9}$$

induced by the enhanced electric field at the tip of the crack must be greater than the sum of the plastic deformation energy (required to push the material aside to form the crack) and the surface tension. Here σ_m, ε_m and Y are the mechanical stress, strain and Young's modulus respectively. That the surface tension is used in this approach implies that the crack is formed by displacing polymer chains without breaking bonds. In this model, the local field at the crack tip is assumed to be sufficiently low so that the strain energy (W_{em}) induced by the enhanced electrical field can be neglected compared with the electrostatic energy and, the plastic deformation energy is dominant over the surface tension. The electric field required at the end of the crack tip, according to electrofracture model, is then given by (Zeller et al. 1984)

$$E_{ef} = \left(\frac{2Y}{\varepsilon_0 \varepsilon_r} \right)^{1/2} \tag{9.10}$$

where Y is Young's modulus. Equation (9.10) is similar to equation (9.6): both E_a and E_{ef} have the same dependence on the Young's modulus.

9.3. The filamentary electromechanical breakdown model

The electrofracture is in fact an ageing process which operates at low electrical field without breaking the bonds between atoms. The filamentary electromechanical breakdown model is very similar to the electrofracture approach. In this model, the local electrical field at the crack tip is assumed to be sufficiently high so that the induced electromechanical stress energy (W_{em} in equation 9.9) is dominant over the electrostatic energy (W_{es} in equation 9.8). In addition the fracture toughness, instead of surface tension, has been used in the filamentary electromechanical breakdown model to characterize crack propagation. The filamentary electromechanical breakdown field can be written as (Dissado and Fothergill 1992)

$$E_{fem} = \left(\frac{8Y(2G + Yr_f)}{\varepsilon_0^2 \varepsilon_r^2 r_f} \right)^{1/4} \tag{9.11}$$

where G is toughness, r_f is the radius of the tubular crack. For polyethylene, the plastic deformation energy is small compared with the toughness (Dissado and Fothergill 1992): equation (9.11) can be simplified to

$$E_{fem} = \left(\frac{16GY}{\varepsilon_0^2 \varepsilon_r^2 r_f} \right)^{1/4} . \tag{9.12}$$

The filamentary electromechanical breakdown model, in the form of Equation (9.12), predicts a different Young's modulus dependence of the breakdown field at the tip of the crack from that of the electrofracture model.

All the three models presented here relate the breakdown field to the Young's modulus. However, the electromechanical breakdown field in equation (9.6) is the applied field, while for the other two approaches, the field is local field at the tip of the

crack. To compare the theories with the experimental results, it would be reasonable to assume that this local field is proportional to the applied field. If $\log(E_b)$ is now plotted against $\log(Y)$, one would expect a straight line with a slope of 1/2, according to the electrofracture model, or a slope of 1/4 if the filamentary electromechanical breakdown mechanism, equation (9.12), is correct.

Figures 9.1 and 9.2 show the $\log(E_b)$ versus $\log(Y)$ plot for thermoplastic polyethylenes P3, P16, P61 and P64. The breakdown fields of thermoplastic polyethylene P3 and P16 have similar Young's modulus dependence. As Young's modulus decreases with increasing temperature, the breakdown field increases slightly at first and then decreases linearly with decreasing Young's modulus; the slope of the least square fit to the linear part is 0.75 for P3 and 0.79 for P16. These results are not in agreement with predictions of either a gradient of 1/2, according to the electrofracture model, or 1/4 from the filamentary electromechanical breakdown mechanism. Thus although there is good correlation between the breakdown field and the Young's modulus, it seems that the present electromechanical breakdown theories cannot quantitatively describe the electrically measured breakdown strength. The relatively low breakdown strength for these two polyethylenes at room temperature and the small increase at higher temperatures (Figure 9.1 insets) may arise from the remanent stress frozen into the samples during the manufacturing process. A small increase in the X-ray crystallinity for these polyethylenes has also been observed as the sample is heated slightly above the room temperature (Figure 6.20(a)). Furthermore thermal expansion measurements on crosslinked polyethylene P16 show that there is anomalous contraction at about 300K (Figure 6.20(b)).

It is possible that different breakdown mechanisms dominate in different temperature ranges and more than one of them may be present simultaneously in appropriate conditions. It has been found that the log breakdown field versus log Young's modulus data for P61 and P64 cannot be fitted with confidence to a straight line (Figure 9.2(a) and (b)). By contrast these data can be fitted to a polynomial to a order of 2. This non-linear behaviour of the breakdown field does not necessarily mean that the

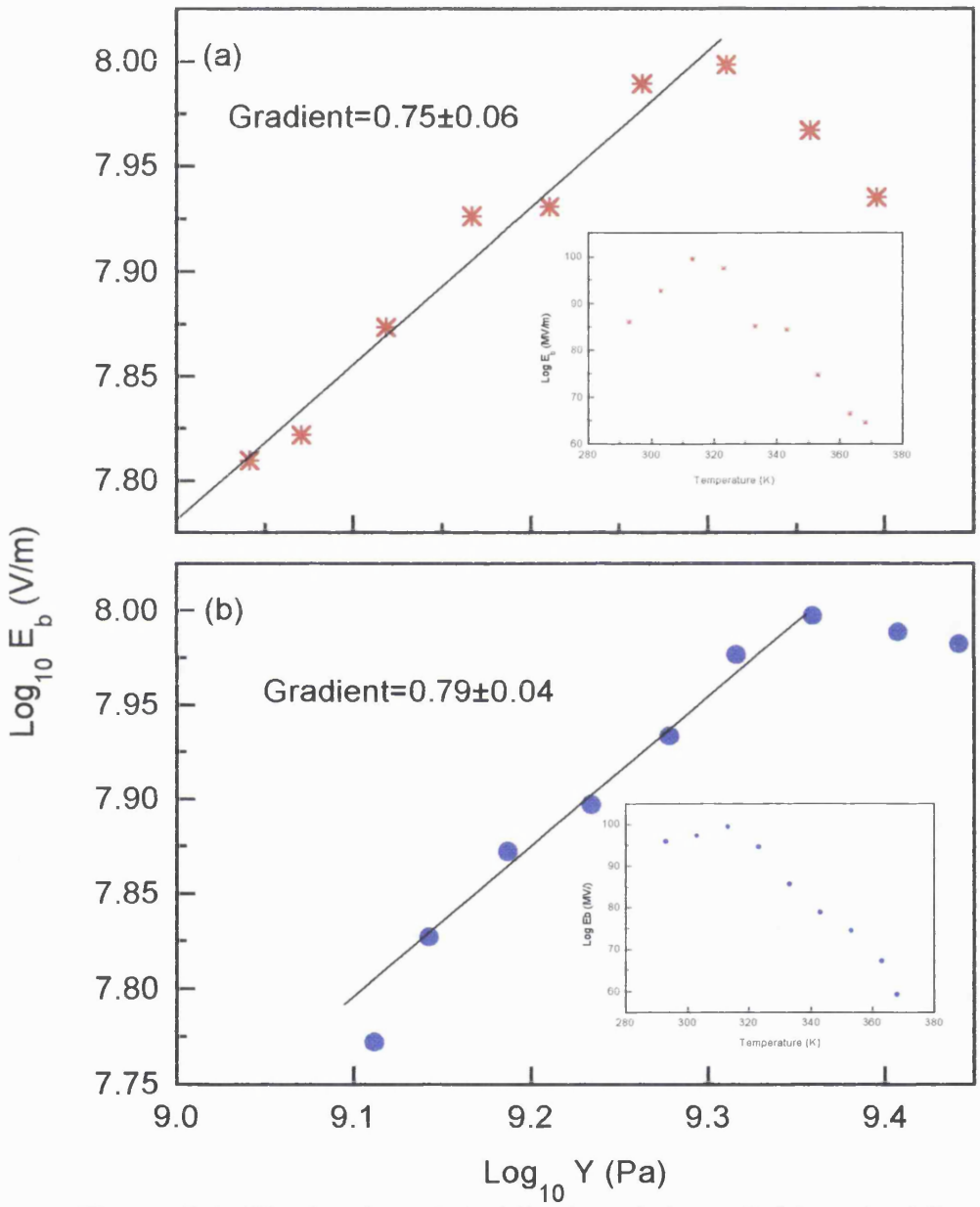

Figure 9.1. The log-log plot of the breakdown field against the Young's modulus for thermoplastic polyethylene (a) P3 and (b) P16. The insets are the temperature dependencies of breakdown fields.

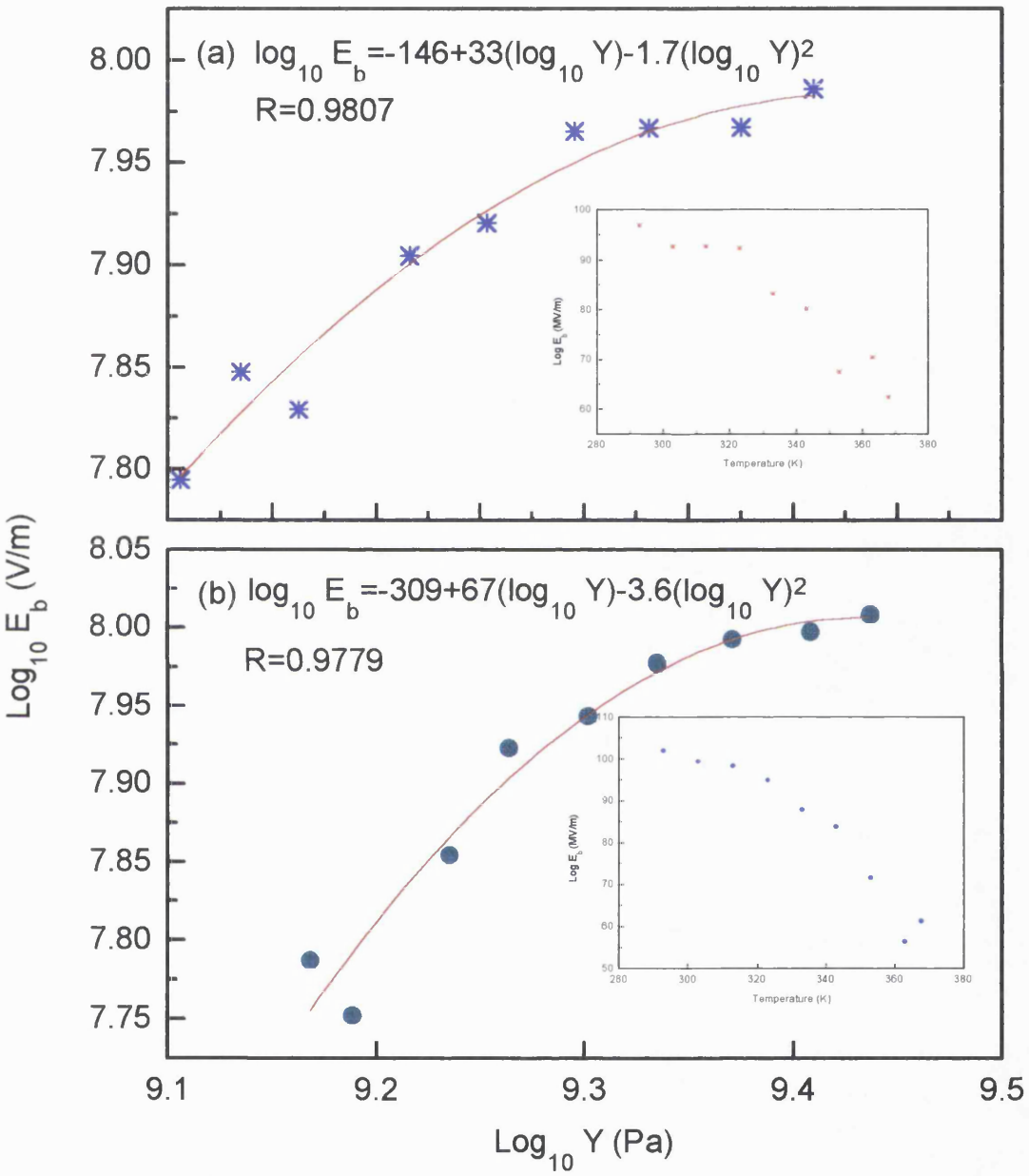

Figure 9.2. The log-log plot of the breakdown field against Young's modulus for thermoplastic polyethylene (a) P61 and (b) P64. The insets are the temperature dependencies of breakdown fields.

electromechanical breakdown mechanism is absent in these two cases. A slope of 1/4 has been observed in the log(E_b) versus log(Y) plot for both polyethylene P61 and P64 at about 300K (Figures 9.2(a) and (b)), suggesting that the dominant breakdown process is filamentary electromechanical breakdown. At higher temperatures (~325K), both curves show a gradient of 1/2, indicating a possible onset of the electrofracture mechanism in this temperature range. These observations are consistent with the basic assumptions of the theories. At high temperatures, the surface tension of the polymer is smaller, the molecules are more flexible and consequently a crack can form more easily without breaking the bonds of chains: this is a type of electrofracture. On the other hand, a brittle fracture involving bond breaks, predicted by the filamentary electromechanical breakdown model, is more likely to occur at lower temperatures.

9.4. The electronic breakdown model

The large difference between the calculated and measured breakdown strength and the non-linear Young's modulus dependence of the breakdown field also indicate the possibility that the electromechanical breakdown process might not be responsible for the observed electrical breakdown. According to the electronic breakdown theory proposed by Fröhlich (Fröhlich 1937, 1947, Dissado and Fothergill 1992), two ranges of temperature can be distinguished. Below a critical temperature T_c conduction electrons are present in low concentration and collisions between electrons may be neglected. The mean free path of the electrons may then be relatively long and an external field is able to accelerate the electrons to high energies. When a sufficient number of electrons have energies greater than the ionization energy of the atoms, breakdown can occur. The dielectric strength in this region can thus be increased by introducing more scattering centres or increasing temperature, which tend to reduce the mean free paths of the electrons and keep their energies low. Above T_c the concentration of electrons is sufficiently high so that collisions between conduction electrons predominate over electron-vibrational state collisions. The theory shows that log E_b is proportional to 1/T at high temperature range. The measured dielectric breakdown behaviour of polyethylene P3, P16, P61 and P64 is qualitatively consistent with Fröhlich's model. The dielectric strength of P3 and P16 increases with

temperature below 313K and decreases with temperature above this temperature, suggesting that T_c=313K for these two polyethylenes. The critical temperature for polyethylene P61 and P64 is expected to be equal or less than 293K. Figures 9.3 and 9.4 show the log E_b versus 1/T plots for the four thermoplastic polyethylenes. A nearly linear behaviour has been observed for P3 and P16 at high temperature range, while for P61 and P64, a polynomial fit is required to represent the data.

9.5. Correlation between a.c. breakdown and the dielectric behaviour of polyethylene

The mean a.c. breakdown strength E_b measured at 50Hz for thermoplastic polyethylene P3, P16, P61 and P64 (Table 9.3) is notably less than that obtained by the d.c. method. For example, the d.c. breakdown strength of a crosslinked polyethylene at 333K, reported by Stark and Garton (1955), is 500MV/m, which is ~6 times larger than the a.c. values given in Table 9.3. The d.c. breakdown strength for low density polyethylenes is reported as ~700 MV/m (Dissado and Fothergill 1992), which is essentially the same as that for crosslinked polyethylenes. The difference between the d.c. and a.c. breakdown strength of polyethylene can be attributed to the local internal heating at inclusions of impurities, which is closely related to the dielectric behaviour of the material.

In a.c. measurements, the applied electrical field alternates with circular frequency ω:

$$E = E_o \exp(j\omega t) \tag{9.13}$$

The phase lag between the polarization P and the applied field E leads to an absorption of energy in the dielectric:

$$\begin{aligned} P &= \varepsilon_o(\varepsilon' - j\varepsilon'' - 1)E_o \exp(j\omega t) \\ &= \varepsilon_o\left[(\varepsilon'-1)^2 + \varepsilon''^2\right]^{1/2} E_o \exp[j(\omega t - \phi)] \\ &= P_o \exp[j(\omega t - \phi)] \end{aligned} \tag{9.14}$$

where $\tan\phi = \varepsilon''/(\varepsilon'-1)$ and $P_o = \varepsilon_o\left[(\varepsilon'-1)^2 + \varepsilon''^2\right]^{1/2} E_o$. Any change in the polarization of the dielectric results in a displacement current of density

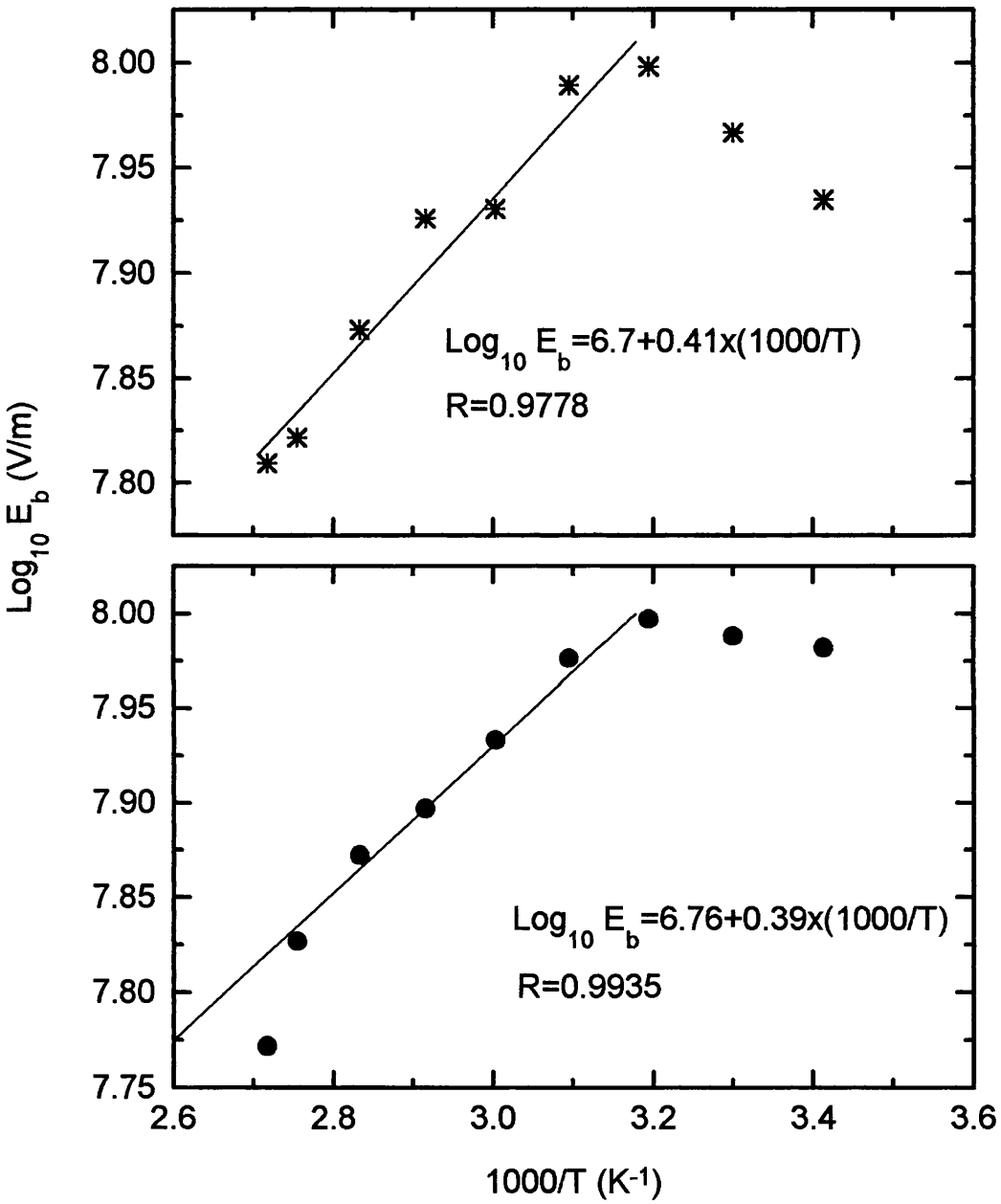

Figure 9.3. Log_{10} E_b versus 1/T plot for thermoplastic polyethylene (a) P3 and (b) P16.

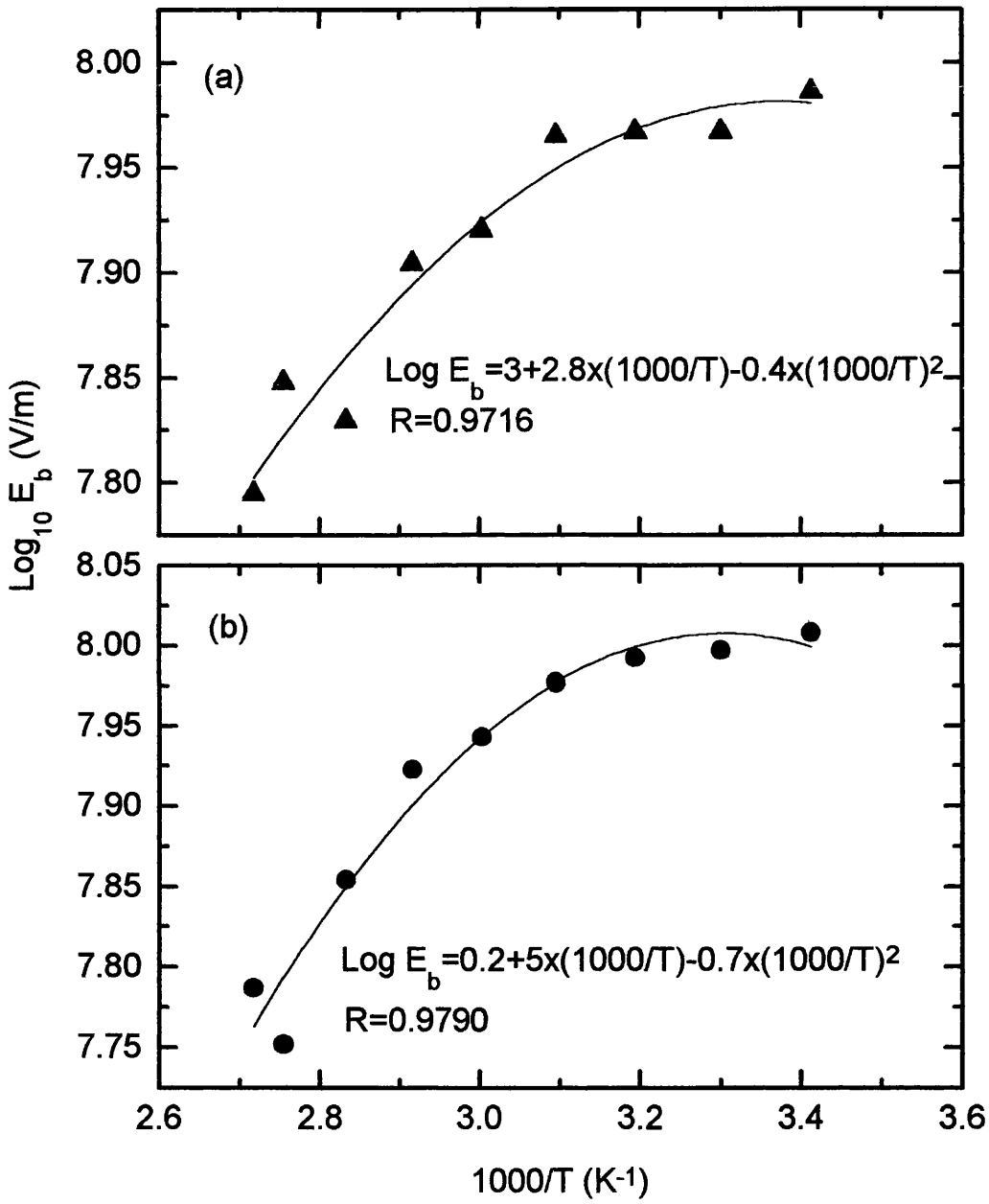

Figure 9.4. Log_{10} E_b versus 1/T plot for thermoplastic polyethylene (a) P61and (b) P64.

$$i = \frac{dP'}{dt} \tag{9.15}$$

and Joule heating

$$H = E'i = E'\frac{dP'}{dt} \tag{9.16}$$

per unit volume. E' and P' in equations (9.15) and (9.16) are real parts of the corresponding complex quantities:

$$\begin{aligned} E' &= E_o \cos\omega t \\ P' &= P_o \cos(\omega t - \phi) \end{aligned} \tag{9.17}$$

The displacement current according to equation (9.15) is

$$i = -P_o \omega \sin(\omega t - \phi) \tag{9.18}$$

and the rate of heating per unit volume is

$$\begin{aligned} H &= -E_o P_o \omega \cos\omega t \sin(\omega t - \phi) \\ &= -\frac{1}{2} E_o P_o \omega [\sin(2\omega t - \phi) - \sin\phi] \end{aligned} \tag{9.19}$$

When this rate of heating is averaged over a complete cycle, the first term, which is alternating with twice the frequency of the field, averages to zero. Therefore the average rate of Joule heating is equal to

$$\begin{aligned} \overline{H} &= \frac{1}{2} E_o P_o \omega \sin\phi \\ &= \frac{1}{2} E_o^2 \varepsilon_o \varepsilon'' \omega \end{aligned} \tag{9.20}$$

Although in general polyethylene is a non-polar material, the temperature and pressure dependences of the dielectric constant have shown that there are some dipolar impurities in the crosslinked versions of P3, P16, P61 and P64. It can be seen from equation (9.20) that the Joule heating is proportional to the dielectric loss and the frequency. In a high a.c. electrical field this Joule heating might be significant in areas which contain a high concentration of impurities, so that the local temperature is raised to a level at which either the local breakdown strength is lower than the applied field or thermal breakdown occurs. The characteristics of the frequency, temperature and pressure dependences of the dielectric constant of the four crosslinked polyethylenes indicate that a relatively large amount of impurities exist in samples P3+G17 and P16+G17. This is consistent with the lower a.c. breakdown strength observed for the corresponding low density polyethylenes (Table 9.3).

Let us now consider further the a.c. ramp breakdown test. Here the amplitude of the applied field is also time dependent, so that the overall field has the form

$$E = E_o(t)\exp(j\omega t) = \frac{dE}{dt} t \exp(j\omega t) \tag{9.21}$$

where $\frac{dE}{dt}$ is the ramp rate and $E_o(0)=0$ has been assumed. Using exactly the same procedure, it can be shown that the rate of Joule heating per unit volume in the case of an a.c ramp test is given by

$$\overline{H} = \frac{1}{2}\varepsilon_o \varepsilon'' \omega E_o^2(t) + \frac{1}{2}\varepsilon_o(\varepsilon' - 1)E_o(t)\frac{dE}{dt} \tag{9.22}$$

Now the average Joule heating depends not only on the dielectric loss but also on the dielectric constant. Equation (9.22) indicates that field ramp increases the Joule heating and hence would further reduce the breakdown strength. If this Joule heating makes a contribution to the observed breakdown behaviour, the features found in the temperature and pressure dependences of the dielectric constant must also play an important role in the breakdown process. From Figure 6.19 we see that the polarizability of P40 and P42 increases almost linearly with temperature below the melting region. The Joule heating would become larger as the orientation of the dipoles becomes easier and hence the breakdown strength would be smaller as the polarizability becomes bigger. The temperature dependence of the breakdown field for polyethylene P61 and P64 shown in the insets of Figure 9.2 is consistent with the temperature behaviour of the polarizability for their corresponding crosslinked versions (Figure 6.19). For crosslinked polyethylene P3 and P16, the polarizability decreases below about 310K and then increases with temperature towards the melting. Accordingly, the breakdown strength for the thermoplastic version of these two polyethylenes would increase first and then decrease with temperature as shown in the insets of Figure 9.1.

Thus Joule heating arising from the displacement current may be large enough to affect the breakdown behaviour in an a.c. ramp breakdown test. To analyze the a.c. breakdown data and study the mechanism of the breakdown process, the effect of

dissipative absorption of the dielectric needs to be taken into account. The large difference between the breakdown strength calculated using ultrasonic data and that measured electrically for thermoplastic polyethylenes P3, P16, P61 and P64, and that between the d.c. and a.c. breakdown strength can be understood, at least partly, in terms of the local Joule heating at impurities.

9.6. The thickness dependence of the breakdown strength and thermal breakdown

It can be shown (Dissado and Fothergill 1992) that the thermal breakdown strength of a thin slab of insulator is inversely proportional to the square root of the thickness, $d^{1/2}$:

$$E_b = T\left(\frac{2k_b\gamma}{d\sigma_o\phi\exp(1)}\right)^{1/2}\exp\left(\frac{\phi}{2k_bT}\right) \tag{9.23}$$

where T is temperature, γ is defined as the electrode thermal conductance per unit area and ϕ is activation energy. In section 9.5 we have shown that the Joule heating arising from the displacement current in an a.c. ramp test may lead to a thermal breakdown. If thermal breakdown process is responsible for the measured a.c. breakdown strength given in Table 9.3, one would expect that $E_b \propto d^{-1/2}$. Figure 9.5 shows the log-log plot of the thickness dependence of the breakdown strength for crosslinked cable insulations. The linear least square fit of the data gives a straight line with a slope of -0.416, which agrees reasonably well with the prediction of the thermal breakdown model, equation (9.23). The data in Figure 9.5 suggest strongly that the Joule heating assisted thermal breakdown is responsible for the relatively small values of the a.c. breakdown strength of the polyethylenes (Table 9.3). In addition, because all the breakdown data in Table 9.3 have been obtained on samples typically 0.2mm of thickness, the small values of the breakdown strength may be partly attributed to this relatively large thickness.

To summarize this discussion on the breakdown mechanism of polyethylene, it is concluded that the values of electromechanical breakdown strength calculated using

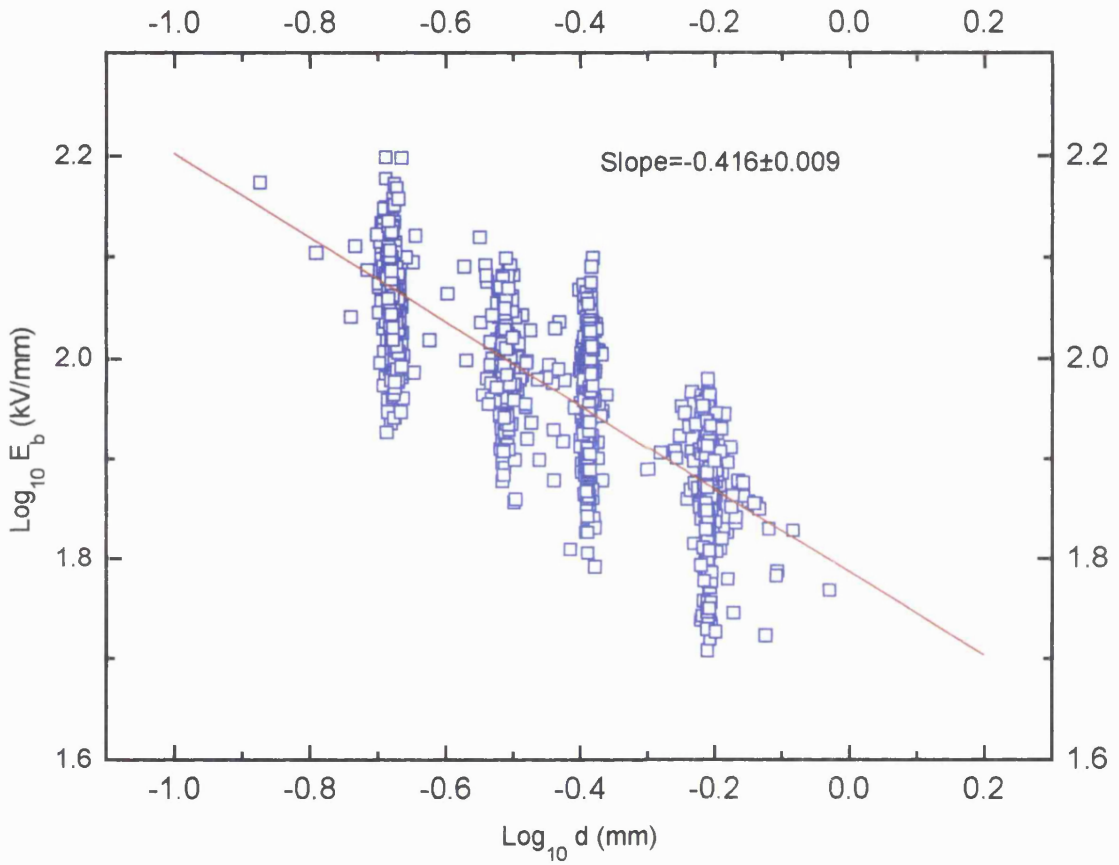

Figure 9.5. Log breakdown strength E_b versus log thichness d plot for crosslinked polyethylene cable insulations. The straight line is the least square fit to the data.

CHAPTER 10. SUMMARY AND CONCLUSIONS

The complex dielectric constants of crosslinked polyethylene plaques as well as polyethylene cable insulations have been measured as functions of frequency, temperature and hydrostatic pressure. The elastic and non-linear acoustic properties of thermoplastic and crosslinked polyethylenes as well as cable insulations have been obtained by measuring the temperature and pressure dependencies of the velocities and attenuation of 5 MHz longitudinal and shear ultrasonic waves propagated in these polymers. Efforts have been made to correlate the breakdown behaviour with the mechanical and the dielectric properties of polyethylene. The main conclusions are as follows:

(1) Measurements of the dielectric properties of the crosslinked polyethylenes and polyethylene cable insulations show that their dielectric constant decreases with frequency and temperature but increases with hydrostatic pressure. Analysis of the data evidences some impurities in the polyethylene samples, which result in non-zero temperature and pressure derivatives of the polarizability.

(2) Crosslinked polyethylene XLP3, XLP16 and cable insulation C56, among the samples studied, have similar dielectric behaviour. The dielectric properties of P40 are just like those measured for P42. It has been found that both $(\partial \ln\alpha/\partial T)_P$ and $(\partial \ln\alpha/\partial P)_T$ are negative for XLP3, XLP16 and C56 at room temperature and atmospheric pressure, in contrast to positive values obtained for P42. Moreover, the magnitude of $(\partial \ln\alpha/\partial T)_P$ and $(\partial \ln\alpha/\partial P)_T$ for P42 is much smaller than those for the other three samples, suggesting that there may be substantially less impurities in P42. The large dispersion at the low frequency end in the dielectric loss of XLP3 is consistent with this speculation.

(3) The value of $(\partial P/\partial T)_v$ obtained from the temperature and pressure dependencies of the dielectric constant agrees fairly well with that determined ultrasonically, which

implies that both the mechanical and dielectric properties of polyethylene are governed primarily by the specific volume (or free volume) of the polymer.

(4) Ultrasonic and dielectric measurements indicate that power cable insulations are not homogenous across the cable diameter in both mechanical and electrical properties: both the dielectric constant, and the velocity of longitudinal ultrasonic waves in the outer part are larger than those in the inner part of the cable section. These results suggest that there may be a density difference across the cable section: the outer part having a higher density than the inner part. This density gradient and the differences in electrical and mechanical properties across the cable section could have a large effect on the breakdown behaviour of the power cable. The ultrasonic measurement substantiates the dielectric data and is consistent with the correlation between the mechanical and electrical properties of the polymer.

(5). While the general trend is for the sound velocity to decrease linearly with temperature as expected, the magnitude of the temperature derivative of the longitudinal wave velocity, $-(\partial V_L/\partial T)$, is extremely large, especially in the temperature range between the melting and glass transitions. This ultrasonic behaviour can not simply be ascribed to the characteristics of either amorphous or the crystalline phases. It has been found that the gradual change in crystallinity below the melting point makes a large contribution to the observed temperature dependence of the sound velocity. The attenuation of longitudinal ultrasonic waves propagated in polyethylene has been found to be proportional to the temperature derivative of the ultrasonic wave velocity, which is consistent with the hysteresis absorption mechanism proposed by Hartmann (1976/77).

(6) The longitudinal stiffness modulus C_L of polyethylene increases non-linearly with hydrostatic pressure. The pressure derivative of C_L is much larger than that usually found for normal solids and organic liquids or even for amorphous polymers, indicating a large free volume effect in this semicrystalline polymer. Analysis of the pressure dependence data suggests that the crystalline-amorphous phase transition induced by

the application of pressure is negligible and the large value of $(\partial C_L/\partial P)$ is simply a consequence of the two-phase structure of polyethylene.

(7) Crosslinking has marked effects on the velocity and attenuation of ultrasonic waves. The mechanical properties of polyethylene are very variable, depending strongly on the different methods and conditions of the crosslinking. Ultrasonic wave velocity and attenuation measurements indicate that peroxide crosslinking increases the strength of the β relaxation. The effect of irradiation crosslinks, on the other hand, is to increase the density and crystallinity, resulting in a weaker β process. While crosslinking increases the glass transition temperature slightly, the effect of additives is to enhance the glass transition process and to shift the T_g to a lower temperature.

(8) The Young's modulus obtained from ultrasonic measurements has enabled an estimation, using the Stark-Garton model, of the electromechanical breakdown strength of polyethylene. Although the calculated breakdown strength is much larger than that measured electrically, the general trend is the same: the breakdown strength decreases with increasing temperature. The correlation established theoretically between the Young's modulus and the breakdown strength has been tested using both the ultrasonic and electrical data. The results suggest that different electromechanical breakdown mechanisms may dominate in different temperature ranges and more than one of them may be present simultaneously in appropriate conditions. The breakdown near room temperature can be attributed to the filamentary electromechanical breakdown mechanism, as the log breakdown field versus log Young's modulus plot has a slope of 1/4. At higher temperatures (~325K), this plot shows a gradient of 1/2, indicating the possible onset of the electrofracture mechanism in this temperature range.

The electromechanical breakdown mechanism leads to an electrical aging process which is directly related to the stress-relaxation of Young's modulus. Although models in this approach can describe the temperature dependence of the breakdown strength

qualitatively, it seems to be unlikely that this electromechanical process can initialize a breakdown with such a small value of breakdown strength as that given in Table 9.3. The large difference between the d.c. and a.c. breakdown strength suggests that the Joule heating driven thermal breakdown process may be responsible for the small values of a.c. breakdown strength measured at 50 Hz and this is further supported by measurements of the breakdown strength as a function of thickness of polyethylene cable insulations. An electromechanical or an electronic breakdown following a local increase of temperature due to Joule heating at impurities are plausible physical mechanisms.

(9) Measurements of the temperature and hydrostatic pressure dependence of the longitudinal ultrasonic wave velocity have enabled estimation of a thermodynamic quantity $(\partial P/\partial T)_v$, which is directly related with the thermal expansion and the bulk modulus of the polymer. The Grüneisen constant Υ characterizing the anharmonicity of the atomic vibrations has been obtained using the data of $(\partial P/\partial T)_v$ determined ultrasonically. The value of Υ falls in a range of 0.43-1.39 for the 8 polyethylenes studied. The relatively small Grüneisen constant suggests that the contribution from the vibrational anharmonicity is small, as far as the thermodynamic properties are concerned.

REFERENCES

Adachi K, Harrison G, Lamb J, North A M and Pethrick R A, Polymer **22** (1981)1032

Alers G A, in *Physical acoustics* **III-B** p 1, ed. Mason W P, (Academic Press, New York & London 1965)

Alexander S, Laermans C, Orbach R and Rosenberg H M, Phys. Rev. B **28** (1983) 4615

Anderson P W, Halperin B I and Varma C M, Phil. Mag. **25** (1972) 1

Arisawa K, Tsuge K and Wada Y, Jap. J. Appl. Phys. **4** (1965) 138

Arnold N D and Guenther A H, J. Appl. Polym. Sci. **10** (1966) 731

Asay J R and Guenther A H, J. Appl. Polym. Sci. **11** (1967) 1087

Auld B A, *Acoustic Fields and Waves in solids I*, (Wiley, New York 1973)

Baccaredda M and Butta E, J. Polym. Sci. **XXII** (1956) 217

Bailey F E and Koleske J V, *Poly(ethylene oxide)* (Academic Press, New York-San Francisco-London 1976)

Baird M E, in *Progres in Polymer Science* Volume 1, edited by A. D. Jenkins (Pergamon Press, Oxford-London-Edinburgh-New York-Toronto-Sydney-Paris-Braunschweig 1972)

Barker R E Jr, J. Appl. Phys. **38** (1967) 4234

Barlow A, IEEE Electrical Insulation Magazine **7** (1991) 8

Bartolotta A, Carini G, Marco G Di, Romeo C and Salvato G, J. Appl. Phys. **69** (1991) 704

Bergman D J and Kantor Y, Phys. Rev. Lett. **53** (1984) 511

Bhatia A B, *Ultrasonic Absorption: An Introduction To the Theory of Sound Absorption and Dispersion in Gases Liquids and Solids*, (Clarendon Press, Oxford 1967)

Blok J and LeGrand D G, J. Appl. Phys. **40** (1969) 288

Blythe A R, *Electrical Properties of Polymers* (Cambridge University Press, London-New York-Melbourne 1979)

Bogue R and Sladek R J, Phys. Rev. B **42** (1990) 5280

Bordelius N A and Semenchenko V K, Sov. Phys. Acoust. **16** (1971) 519

Boyd R H, Polymer **26** (1985) 323

Boyd R H, Polymer **26** (1985) 1123

Boyd R H, in *Methods of Experimental Physics* **16C** (1980) 379, edited by R.A. Fava, (Academic Press, New York-San Francisco-London 1980)

Boyer R F, Encyclopedia Polym. Sci. Engineering **17** (1989) 1

Bogue R and Sladek R J, Phys. Rev. B **42** (1990) 5280

Bosman A J and Havinga E E, Phys. Rev. **129** (1963) 1593

Bridgman P W, *The Physics of High Pressure*, (G. Bell and Sons LtD, London 1958)

Bruce P G and Vincent C A, J. Chem. Soc. Faraday Trans. **89** (1993) 3187

Bui Ai, Hoang-The-Giam and Destruel, in *Proc. Ann. Report Conf. Elect. Insulation and Dielectric Phenomena*, Claymont, USA, 21-25 Oct. 1984 (New York USA: IEEE 1984) 448

Bunn C W, The Structure of Polythene, in *Polythene*, edited by Renfrew A and Morgan P, (Iliffe & Sons Limited, London 1960)

Chadwick A V, Strange J H and Worboys M R, Solid State Ionics **9&10** (1983) 1155

Charlesby A, in *Polyethylene* p 307, ed. Renfrew A and Morgan P, (Iliffe & Sons Limited, London 1960)

Chen C K and Liepins R, *Electrical Properties of Polymers*, (Hanser Publishers, Munich-Vienna-New York 1987)

Choy C L, Hunt R G and Salinger G L, J. Chem. Phys. **52** (1970) 3629

Claytor T N and Sladek R J, Phys. Rev. B **18** (1978) 5842

Collins J G and White G K, Progress in Low Temperature Physics **4** (1964) 450, ed. Gorter C G

Connor T M, Read B E and Williams G, J. Appl. Chem. **14** (1964) 74

Cowie J M G, *Polymers: Chemistry and Physics of Modern Materials,* (Blackie, Glasgow and London 1991)

Crissman J M, Sauer J A and Woodward A E, J. Polym. Sci. **A2** (1964) 5075

Dainton F S, Evans D M, Hoare F E and Melia T P, Polymer **3** (1962) 277

Davidse P D, Waterman H I and Westerdijk J B, J. Polym. Sci. **59** (1962) 389

Dissado L A and Fothergill J C, *Electrical Degradation and Breakdown in Polymers*, (Peter Peregrinus LtD., London 1992)

Eby R K, J Acoust. Soc. Am. **36** (1964) 1485

Eisenberg A and Reich S, J. Chem. Phys. **51** (1969) 5706

Elliot S R, *Physics of Amorphous Material* (Longman Scientific &Technical, New York 1990)

Engeln I, Meissner M, and Pape H E, Polymer **26** (1985) 364

Fanggao C, Saunders G A, Lambson E F, Hampton R N, Carini G, Bartolotta A and Lanza M, J. Polymer Sci. B: Polymer Phys. **34** (1996) 425-33

Fanggao C and Saunders G A, Annual Report on the Work Carried Out in 1993 on the Contract: TO INVESTIGATE THE CORRELATION BETWEEN THE MECHANICAL AND ELECTRICAL PROPERTIES OF INSULATIONS USED IN POWER CABLES, 1994

Fanggao C and Saunders G A, Annual Report on the Work Carried Out in 1994 on the Contract: TO INVESTIGATE THE CORRELATION BETWEEN THE MECHANICAL AND ELECTRICAL PROPERTIES OF INSULATIONS USED IN POWER CABLES, 1995

Federle G and Hunklinger S, J. Phys. (France) Colloq. C9 **43** (1982) C9-505

Ferry J D, *Viscoelastic Properties of Polymers* p 1, (John Wiley and Sons, Inc., New York-London-Sydney- Toronto 1970)

Folds D L, J. Acoust. Soc. Am. **52** (1972) 426

Fontanella J J, Wintersgill M C, Calame J P, and Andeen C G, Solid State Ionics **8** (1983) 333

Fontanella J J, Wintersgill M C, Welcher P J, Calame J P and Andeen C G, IEEE Trans. Electr. Insul. **20**(6) (1985) 943

Fontanella J J, Wintersgill M C, Calame J P, Pursel F P and Figueroa D R, Solid State Ionics **9 & 10** (1983) 1139

Fröhlich H, Proc. Roy. Soc. (London), **A160** (1937) 230

Fröhlich H, Proc. Roy. Soc. (London), **A188** (1947) 521

Genensky S M and Newell G F, J. Chem. Phys. **26** (1957) 486

Gibbs D F and Jarman M, Phil. Mag. **7** (1963) 663

Gibbs D F and Hill G J, Phil. Mag. **9** (1964) 367

Gray R W and McCrum N G, J. Polym. Sci. A-2 **7** (1969) 1329

Haldon Robert A and Simha Robert, Macromolecules **1** (1968) 340

Haldon Robert A and Simha Robert, J. Appl. Phys. **3** (1968) 1890

Hall C, *Polymer Materials* p 51, (Macmillan, London 1989)

Hampton R N, Collier I T, Sidek H A A and Saunders G A, J. Non-crystalline Solids, **110** (1989) 213-222

Hampton R N 1989 Private Communication

Hartmann B and Jarzynski J, J. Appl. Phys. **43** (1972) 4304

Hartmann B, J. Acoust. Soc. Am. **56** (1974) 1469

Hartmann B, J. Appl. Polym. Sci. **19** (1975) 3241

Hartmann B, Acustica **36** (1976/77) 24

Hartmann B, Ultrasonic Measurements, in *Methods of Experimental Physics* **16-C** (1980) p 59, ed. Fava R A, (Academic Press: New York-San Francisco-London 1980)

Havinga E E, Phys. Chem. Solids **18** (1961) 253.

Hedvig P, *Dielectric Spectroscopy of Polymers* (Adam Hilger Ltd, Bristol 1977)

Hill N E, Vaughan W E, Price A H and Davies M, *Dielectric Properties and Molecular Behaviour* (Van Nostrand Reinhold Company, London 1969)

Holownia B P, Rubber Chem. Technol. **48** (1975) 246

Hopkins I L and Kurkjian C R, *Physical Acoustics **II-B*** p 91, ed. Mason W P, (Academic Press, New York & London 1965)

Huntington H B, *Solid State Physics **7*** ed. Seitz F and Turnbull D (Academic Press Inc., Publishers, New York 1958)

Hunklinger S and Arnold W, *Physical Acoustics* ***XII*** p 155, ed. Mason W P and Thurston R N, (Academic Press, New York, San Francisco & London 1976)

Ilisavskii Yu V, Kulakova L A and Tikhonov V V, Sov. Phys. Solid State **31** (1989) 1363

Inoue K, Kaji K, Kanaya T, Ikeda S, Shibata K, Misawa M and Kiyanagi Y, Phys. Rev. Lett., to be published.

Ishida Y, Matsuo M and Takayanagi M, Polymer Letters **3** (1965) 321

Jonscher A K, *Dielectric Relaxation in Solids* (Chelsea Dielectrics Press Ltd, London 1983)

Kanaya T, Kaji K, Ikeda S and Inoue K, Chem. Phys. Lett. (Netherlands) **150** (1988) 334

Khanarin V S, Gol'dman A Ya and Sysoev, Mech. Compos. Mater. (U.S.A.) **22** (1986) 7

Krupskaya N K, Sov. Phys. Acoust. **16** (1971) 519

Lamberson D L, Asay J R and Guenther A H, J. Appl. Phys. **43** (1972) 976

Laquer H L and Head E L, Low-temperature thermal expansion of plastics, Rept. A.E.C.D-2161. US Atomic Energy Commission, Oak Ridge (Tenn.) 1952

Levene A, Pullen W J and Roberts J, J. Polym. Sci. A **3** (1965) 697

Lyon K G, Salinger G L and Swenson C A, Phys. Rev. B **19** (1979) 4231

Macedo P B, Moynihan C T and Bose R, Phys. and Chem. of Glasses **13** (1972) 171

Mandelbrot B. B., *Fractals: Form, Chance and Dimension*, (W. H. Freeman & Company, San Francisco 1977)

Matsui M, Matsui R and Wada Y, Polym. J. **2** (1971) 134

May J E Jr., IRE Nat. Conv. Rec. **6** (1958) 134

McCrum N G, Read B E and Williams G, *Anelastic and Dielectric Effects in Polymeric Solids* (Wiley, New York 1967)

Naunton W J S, *The Applied Science of Rubbers* p563, (Edward Arnold Ltd. London 1961)

Nava R, Pereira D and Amorer L, J. Appl. Phys. **69** (1991) 99

Ngoepe P E, Lambson E F and Saunders G A, J. Material Sci. **25** (1990) 4654-4657

Nielsen L. E., *Mechanical Properties of Polymers,* (Reihold Publishing Corporation, Chapman & Hall Ltd., London & New York 1965)

North A M, Pethrick R A and Phillips D W, Macromolecules **10** (1977) 992

O'Reilly J M, J. Polymer Sci. **57** (1962) 429

Papadakis E P, J. Appl. Phys. **35** (1964) 1474

Papadakis E P, J. Acoust. Soc. Am. **42** (1967) 1045

Papir Yoram S and Baer Eric, J. Appl. Phys. **42** (1971) 4667

Perepechko I I and Sorokin V E, Sov. Phys. Acoust. **18** (1973) 485

Perepechko I I, *Low-Temperature Properties of Polymers* (Pergamon press, Oxford-New York-Toronto-Sydney-Paris-Frankfurt: 1980)

Pietronero L and Tosatti V. E., in *Fractals in Physics: Proc. of Sixth Trieste International Symposium on Fractals in Physics*, ICTP (Trieste, Italy 1985)

Phillips W A, J. Low Temp. Phys. **7** (1972) 351

Pich L, Polym. Engineering Sci. **24** (1984) 1354

Pich L, Massines F, Lessard G and Hamel, 1987 IEEE Proc. Ultrasonics Symposium 1125

Pich L, 1989 IEEE Ultrasonics Symposium Proc. **1** (New York, USA: IEEE 1989) 599

Pohl R O, *Amorphous Solids: Low-Temperature Properties* p 27, ed Phillips W A, (Springer Verlag, Berlin 1981)

Porter C H and Boyd R H, Macromolecules **4** (1971) 589

Rama Rao M, Indian J. Phys. **14** (1940) 109

Reddy G V, Chattopadhyay S, Singh Y P and Singh R P, Acustica **48** (1981) 347

Reese W, J. Appl. Phys. **37** (1966) 3959

Reese W, J. Appl. Phys. **37** (1966) 864

Reich S, Eisenberg A, J. Chem. Phys. 53 (1970) 2847

Rosenstock H B, J. Phys. Chem. Solids 23 (1962) 659

Saito S, Sasabe H, Nakajima T and Yada K, J. Polymer Sci. A-2 **6** (1968) 1297

Sauer J A and Kline D E, J. Polymer Sci. **18** (1955) 491

Saunders G A, Sidek H, Comins J D, Carini G and Federico M, Phil. Mag. B **56** (1987) 1-13

Saunders G A, Metcalfe R D, Cutroni M, Federico M and Piccolo A, Phys. Rev. B **53** (1996) 5287

Sayre John A, Swanson Stephen R and Boyd Richard H, J. Polym. Sci.: Polym. Phys. 16 (1978) 1739

Schmieder K and Wolf K, Kolloid-Z **134** (1953) 149

Schuyer J, J. Polym. Sci. **XXXVI** (1959) 475

Sinnott K M, J. Polym. Sci. **XXXV** (1959) 273

Slater J C, *Introduction To Chemical Physics* (McGraw-Hill Book Company, Inc., New York & London 1939)

Sochava I V, Vestnik LGU **10** (1961) 70

Sornette D, Acustica **67** (1989) 199

Sornette D, Acustica **67** (1989) 251

Sornette D, Acustica **68** (1989) 15

Stark K H and Garton C G, Nature **176** (1955) 1225

Sutherland H. J. and Lingle R, J. Appl. Phys. **43** (1972) 4022

Swan P R, J. Polym. Sci. **XLII** (1960) 525

Thurston R N and Brugger K, Phys. Rev. **133** (1963) A1604

Treloar L R G, *The Physics of Rubber Elasticity*, (Clarendon Press, Oxford 1975)

Tucker J E and Reese W, J. Chem. Phys. **46** (1967) 1388

Varley J H O, Nature **179** (1957) 686

Vincent C A, Prog. Solid St. Chem. **17** (1987) 145

Wada Yasaku, Itani Akira, Nishi Toshio and Nagai Satoshi, J Polym. Sci. A-2 **7** (1969) 201

Ward I M, *Mechanical Properties of Solid Polymers*, (John Wiley and Sons, Chichester-New York-Brisbane-Toronto-Singapore 1979)

Warfield R W, Cuevas J E and Barnet F R, Rheologica Acta, Band 9, Heft **3** (1970) 439

Wintersgill M C, Fontanella J J, Welcher P J and Andeen C G, J. Appl. Phys. **58** (1985) 2875

Woodward A E, *Transitions and Relaxations in Polymers* ed Boyer R (Interscience Publishers, Inc., New York 1966)

Waterman P. C. and Truell R., Multiple Scattering of Waves, J. Math Phys. **2** (1961) 512-537

Young R J and Lovell P A, *Introduction to Polymers,* (Chapman & Hall, London-New York-Tokyo-Melbourne-Madras 1991)

Zakin Jacques L, Simha Robert and Hershey Harry C, J. Appl. Phys. **10** (1966) 1455

Zeller R C and Pohl R O, Phys. Rev. B **4** (1971) 2029

Zener C, *Elasticity and Anelasticity of Metals* p 55, (University of Chicago Press, Chicago 1948)

Zeller H R and Schneider W R, J. Appl. Phys. **56** (1984) 455-459

APPENDIX 1. POLYETHYLENE SAMPLES STUDIED IN THE PRESENT WORK

No.	Plaque LDPE (Base resin)	Plaque XLPE (Crosslinked resin)	Plaque LDPE (Base resin with additives)	Cable sample
1	S112/P3/93	S316/P3+G17/93 S188/S299/94	S301/P16+G16/93	Not studied
2	S115/P16/93	S314/P16+G17/93 S185/P6/94	S313/P16+G17/93	C56 S260/C23/94
3	S402/P61/93	S404/P40/93 S186/P40/94	Not studied	Not studied
4	S403/P64/93	S405/P42/93 S187/P42/94	Not studied	Not studied
5	S401/P2/93	Not studied	Not studied	Not studied
6	Not Studied	BPH362	Not studied	C51